SIMULATION AND THERMODYNAMIC ANALYSIS OF HIGH PRESSURE LEAN BURN ENGINES

by

Sotirios Mamalis

A dissertation submitted in partial fulfillment
of the requirements for the degree of
Doctor of Philosophy
(Mechanical Engineering)
in The University of Michigan
2012

Doctoral Committee:

Associate Professor Claus Borgnakke, Co-Chair
Adjunct Professor Dionissios N. Assanis, Co-Chair
Professor Volker Sick
Assistant Professor Matthias Ihme
Research Scientist George A. Lavoie
Assistant Professor Aristotelis Babajimopoulos, Stony Brook University

To my Parents
Dimitris and Eirini

ACKNOWLEDGMENTS

The last five years have been marked by interaction and communication with intelligent, knowledgeable and wonderful people. Their guidance and support during my graduate student career at the University of Michigan have been essential and I am grateful to each one of them.

The research work presented in this document would not have been realized without the support of my advisor Professor Dennis Assanis, who gave me the chance to join his group at the W.E. Lay Automotive Laboratory of the University of Michigan in the fall of 2007. Meeting him in April of 2006 has been a significant point in my life. His expertise in the field of internal combustion engine research and his inspirational mentorship have been of catalytic importance for the shaping of my current and future endeavors in this field. I am really grateful for his guidance, friendship and generous support.

My competitive presence in the academic environment and research community would not have been made possible without the help of Professor Aris Babajimopoulos. His knowledge on modeling of internal combustion engines has played an important role in refining the research work conducted during the past five years. He has not only been an inspirational mentor but a great friend as well.

I would also like to express my gratitude to Professor Claus Borgnakke for accepting my invitation to serve as a co-chair in my doctoral committee and for his valuable input in the exergetic analysis presented in this document. His inspirational teaching has reinstated my interest in the field of thermodynamics.

Furthermore, I would like to thank Dr. George Lavoie for his guidance and interest in my work. Every discussion with him has been a learning experience and I greatly appreciate his willingness to share his wealth of knowledge with me.

My friends and colleagues at the University of Michigan W. E. Lay Automotive Laboratory have played an important role in helping me deliver this work. Everyone has contributed in their own way and I am grateful to all of them for generously sharing their time and knowledge.

Last but not least, I would like to thank my family for always believing in me. Their encouragement has played a key role in this work and my will to make them proud has proved to be one of my strongest motive forces.

TABLE OF CONTENTS

LIST OF FIGURES

LIST OF TABLES

ABSTRACT

High Pressure Lean Burn (HPLB) engines have the potential to achieve high load with high efficiency and low emissions compared to currently available powertrains. Various HPLB concepts have been experimentally studied in the literature, focusing on the combustion event but often neglecting the techniques required to provide appropriate cylinder boundary conditions. This dissertation investigates the interactions between the combustion event, in this case Homogeneous Charge Compression Ignition (HCCI), and engine processes occurring externally to the cylinder that are critical for HPLB operation. For that reason, multi-cylinder boosted HCCI engines were simulated and analyzed based on energy and exergy flow considerations.

The multi-cylinder engine model included several submodels the most critical of which were the HCCI combustion and heat transfer modules. Both of these were evaluated based on different experimental datasets and their capability to simulate wide range operation was assessed. The calibrated models were subsequently used to explore the synergies between boosting, Variable Valve Actuation (VVA), Exhaust Gas Recirculation (EGR) and different compression ratio levels for high load HCCI. It was found that utilizing hot intake air is highly beneficial for boosted operation. Hot air can reduce dependence on residual gas for mixture composition and temperature control; it also allows manipulation of the valve strategy so that boosting performance is optimized. In fact, it enables use of regular high lift valve events for improving engine efficiency and

suppressing pressure rise rates. It was found that the combination of advanced boosting systems with VVA strategies offers significant efficiency benefits and renders HCCI technology more accessible for future powertrain applications.

Energy and exergy analysis showed that advanced boosting and VVA enhanced dilution levels, suppressed cylinder temperatures and lowered pumping work. The outcome was high levels of thermal and gas exchange efficiencies. These benefits were enough to outweigh drawbacks from increased cylinder irreversibilities and reduced exhaust flow exergy, both resulting from low temperature combustion. Low heat rejection was also explored and was found to be very beneficial for HCCI. Overall, the engine simulation and analysis framework provides a useful tool for exploration and assessment of HPLB engines employing current or future technology.

CHAPTER 1

INTRODUCTION

Evolving emissions legislation and concerns for diminishing fuel reserves have prompted efforts from the global automotive industry to study advanced internal combustion engine concepts and investigate their potential for future automotive applications. The two well established engine concepts, the spark ignition engine and the diesel engine, have received significant development in the last decade, an outcome of efforts to satisfy stringent emissions regulations, with associated benefits in fuel economy and performance to satisfy customer needs. The spark-ignition engine (using port or direct fuel injection) has exhibited the potential for ultra-low emissions levels, while the diesel engine, based on its lean burn and high compression ratio, has provided higher efficiency in its applications, which range from light to heavy duty vehicles. Nevertheless, the spark-ignition engine has suffered from poor efficiency compared to lean burn engine concepts and the diesel engine suffers from the inevitability of engine-out NO_x and soot emissions, which in turn necessitates complex and expensive aftertreatment systems, including lean NO_x traps, particulate filters and urea SCR systems. Therefore, the need for lean burn engine concepts that can combine diesel-like efficiency with low NO_x and soot emissions has led to rigorous research of advanced Direct Injection Spark Ignition (DISI), Homogeneous Charge Compression Ignition (HCCI), and Spark Assisted Compression Ignition (SACI) engines.

DISI engines have gained significant momentum in the last few years and are currently being offered in a large range of vehicles in multiple markets around the world. The concept of downsizing and downspeeding, using boosted smaller displacement engines has offered efficiency benefits, but the NO_x emissions levels still pose the need for NO_x aftertreatment systems. The HCCI engine appears as a very promising concept since it has shown the potential to combine the advantages of SI and diesel engines, towards achieving high efficiency and low NO_x and soot emissions. However, there are some fundamental challenges associated with HCCI combustion. High rates of heat release and thus limited operating range are among the challenges emerging from the low-temperature combustion taking place in HCCI engines. The SACI concept promises to improve on some of the aforementioned challenges of the HCCI concept by retaining spark and flame propagation in the combustion process. However, there are still several technical hurdles that need to be overcome before automotive applications of HCCI and SACI engines can be realized.

1.1 Direct Injection Spark Ignition – Overview

Gasoline direct injection (GDI) was first used in 1925 as a means to allow a low compression ratio diesel engine to run on gasoline and heavy fuels. It was later used in aircraft engines during World War II and experimentally in automotive engines during the 1950's, 1960' and 1970's. However, the DISI concept in its current form was not introduced until 1996 when Mitsubishi started DISI engine production in an effort to comply with demanding European emissions regulations [1]. The authors reported that this engine had a compression ratio of 12.5, employed a "two-stage mixing" process in order to suppress knock at low engine speeds and added a lean NO_x catalyst to the aftertreatment system. They also reported that the outcome was a 20 % improvement in fuel economy compared to Port Fuel Injected engines (PFI), 10 % higher low-speed

torque and low emissions levels that could meet the standards of the time. Since then, DISI engines have been widely popular among the automotive manufacturers and a subject of rigorous research. Different configurations regarding the fuel injector placement have been proposed, thus introducing the piston-guided, wall guided and spray-guided concepts.

In recent years, the need for immediate improvements in fuel economy of DISI engines has led to engine downsizing and downspeeding. This method has allowed researchers to decrease engine displacement and improve their efficiency without compromising the high load and power density offered by larger naturally aspirated or boosted engines. Fraser et al. discussed the challenges associated with gasoline engine downsizing and highlighted the recently developed technologies that had major impact on improving DISI engine fuel economy [2]. These are Exhaust Gas Recirculation (EGR), Variable Valve Actuation (VVA), Controlled Auto-Ignition (CAI), downsizing and friction reduction. The authors claimed that spark ignition engines have more improvement potential than compression ignition engines and estimated that the relative efficiency advantage of diesel engines will be reduced in the future. It was also reported that Spray Guided Direct Injection (SGDI) can provide more accurate A/F ratio control, enables multiple injection and lean stratified operation. The authors discussed strategies to improve turbocharger performance, by employing scavenging during valve overlap and late injection events that increase exhaust enthalpy; however, they reached the conclusion that aggressive downsizing creates the need for additional boosting technology since the low speed torque and the transient response of the downsized engines required further improvements.

In 2010, Cruff et al. presented an experimental study on a fully flexible high load downsized DISI engine that could be optimized for selected vehicle applications [3]. It employed increased cylinder pressure capacity, cooled EGR, advanced two-stage turbocharging, variable valve timing and lift and E85 flex fuel capability. It was reported

that EGR dilution was an effective way to control exhaust temperature and knock, and by cooling it the authors were able to advance combustion and improve the engine's thermal efficiency. They also pointed out that while E85 offers higher octane number and higher latent heat of vaporization thus benefiting DISI engines, its combination with cooled EGR proved to be harmful for turbocharger performance. Boosting is an essential factor in the downsized engine concept since high load operation is enabled by increased air mass. Finally, the authors also reported that the 3.2 L V6 experimental engine was capable of 32 bar BMEP operating on 98 RON gasoline fuel.

1.2 Homogeneous Charge Compression Ignition - Overview

The HCCI combustion concept was first investigated in 1979 when Onishi et al. studied 2-stroke engine combustion and identified that compression ignition showed some benefits compared to spark ignition in the same gasoline engine [4]. That concept was called Active Thermo-Atmospheric Combustion (ATAC) at that time. Concurrently, Noguchi et al. investigated the same concept in an opposed piston engine concluding that there were some benefits in fuel consumption, NO_x and HC emissions [5].

In 1983, Najt and Foster performed 4-stroke HCCI experiments for the first time [6]. By employing cycle simulation with heat release analysis they showed that HCCI combustion is controlled by chemical kinetics and that physical parameters such as turbulence and fuel type affected ignition timing but not heat release. In this study, a semi-empirical ignition kinetics model was used in order to calculate heat release based on cylinder pressure, temperature and species concentration.

A few years later, Thring studied the effects of equivalence ratio (Φ), intake temperature and Exhaust Gas Recirculation (EGR) fraction on HCCI combustion using a single cylinder 4-stroke gasoline engine [7]. It was shown that the HCCI engine exhibited lower specific fuel consumption than a direct injected diesel engine.

These early studies and several subsequent ones referred to this new combustion mode using various terms such as ATAC (Active Thermo-Atmospheric Combustion - [4]), TS (Toyota Soken - [5]), CIHC (Compression-Ignited Homogeneous Charge - [6]), ARC (Active Radical Combustion - Honda), PCCI (Premixed Charge Compression Ignition), CAI (Controlled Auto-Ignition - Lotus), UNIBUS (Uniform Bulky Combustion System - Toyota), HCDC (Homogeneous Charge Diesel Combustion - Suzuki), MK (Modulated Kinetics - Nissan), OKP (Optimized Kinetic Process - Ford) and CCS (Combined Combustion System - Volkswagen). In recent years, HCCI and CAI have been the most prevalent terms used to describe this combustion mode.

The HCCI concept soon showed the potential for high efficiency combined with ultra-low emissions levels, but challenges associated with the combustion event limited the attainable load and power density of the engines. In order to overcome this obstacle, research efforts were initiated in the late 1990's towards investigating boosted HCCI engines. Christensen et al. were among the first to report that an experimental single-cylinder HCCI engine running on elevated intake pressure attained higher loads and exhibited higher combustion efficiency than naturally aspirated engines [13]. In the following years many experimental and modeling investigations on boosted HCCI engines were presented, including single cylinder experimental engines [15, 22, 23, 31], multi-cylinder turbocharged engines [25, 28], and lately a few modeling efforts of multi-cylinder boosted HCCI engines [30, 33, 38].

1.3 Spark Assisted Compression Ignition – Overview

DISI and HCCI engines are two distinct concepts that are based on spark and compression respectively to ignite the mixture. DISI engines rely on flame front propagation for the combustion event, while HCCI engines exhibit global autoignition and heat release from the bulk of the charge mass. The challenges associated with global

autoignition in HCCI engines, namely ensuring reliable autoignition while avoiding misfire or knock, have mainly been overcome by thermal management of the charge, through residual gas manipulation or intake air temperature control.

Spark assist is a method that has been used to supplement basic thermal control of HCCI and has formed a new combustion mode often called spark assisted compression ignition (SACI). The use of spark assist has been followed as a natural path, based on the physical existence of spark plugs in many experimental spark ignition engines that are operated in a dual SI/HCCI mode fashion. The concept behind spark assist includes the initiation of a reaction kernel before the main combustion event which burns only a portion of the charge. The energy released during that initial flame burn enables the autoignition of the rest of the charge, thus resulting in lower heat release rates compared to global autoignition in HCCI. During the last decade, numerous experimental studies have been presented that focused on spark assist and its potential to lower heat release rates compared to HCCI combustion [35, 36]. Results showed that varying spark assist can be used to phase the autoignition event during combustion and reduce cyclic variability phenomena. However, it has been reported that under certain operating conditions the spark might have very little or no effect on combustion. More importantly, it has been shown that the combustion mode can be varied from pure autoignition to pure flame propagation by adjusting the amount of residual gases in the cylinder.

Lavoie et al. recently compiled experimental and modeling results and proposed a conceptual multi-mode combustion diagram where HCCI, SACI and SI operating regions were represented [37]. This diagram was proposed in an attempt to promote understanding of the applicability range of spark assist and help separate the combustion event from the constraints posed by different engine setups. The authors concluded that SACI is most useful for ignition timing and burn rate control under medium to high loads that ensure adequate flame speeds.

1.4 Fundamentals of HCCI Engines

While HCCI is the focal point of this dissertation, it needs to be clarified that a lot of the major conclusions reached from this work and lot of the techniques proposed are applicable to all lean burn engine concepts whether they employ a spark event or not. The addition of boosting is another common element among these concepts that enables high efficiency operation. Therefore, it was considered useful to group all these concepts under the High Pressure Lean Burn (HPLB) characterization. This acronym is going to be used throughout this document when the text refers to this family of engine concepts. The current and following sections offer detailed descriptions of the fundamental characteristics and enabling technologies of HCCI combustion with a lot of them being common among all HPLB engine concepts.

The fundamentals of HCCI engines can be viewed effectively by comparing the HCCI engine concept to the two conventional and well known engine concepts: The spark ignition (SI) and the compression ignition (CI) engine. Starting from general engine characteristics, four points of comparison are worthy to be portrayed.

The first one compares the combustion processes in the engines. SI combustion is governed by flame propagation taking place in a premixed fuel and air mixture, while CI combustion is a process controlled by mixing of the injected fuel with air present in the cylinder. HCCI combustion starts with global autoignition of a homogeneous mixture of fuel and air, but homogeneity levels may vary according to injection strategies and other mixture preparation techniques.

The second point highlights the nature of heat release during the combustion process. In the SI and CI engines heat release is controlled by turbulent mixing, while it is widely accepted that HCCI heat release is controlled by chemical kinetics, with minimal effect of turbulence. This dependence on chemical kinetics means that there is no direct control of heat release during the combustion process.

Equivalence ratio is the focus of the third point. The SI engine operates under stoichiometric and lean conditions of $\Phi = 0.6 – 1$. This lower limit is usually posed by the flammability limits of the mixtures and the presence of an adequate flame front in lean burn SI engines. The CI engine operates globally under lean conditions, but locally and in specific where ignition occurs, equivalence ratio may range from 0.7 to 4. HCCI engines operate mostly under lean conditions with $\Phi = 0.1 – 1$ which is one of the reasons that enable low temperature combustion and result in low NO_x emissions. In addition, the absence of rich zones due to homogeneous charge prevents soot formation in the engine. Recent studies have suggested that the most efficient HCCI engine operation occurs for equivalence ratios between 0.4 and 0.6, especially when boosting is applied for high load operation [30].

The fourth and final point makes a comparison of Compression Ratio (CR) between the engines. SI engines operate on compression ratios of 8 – 14, CI engines on CR = 14 – 24 and HCCI engines on CR = 10 – 18, thus being somewhere between the first two. Note here that DISI engines employ compression ratios on the high side of the SI range and most modern diesel engines have moved towards the lower side of the diesel range.

1.5 Strengths and Challenges of HCCI

The aforementioned characteristics of HCCI engines are what define their strengths and weaknesses; both of these are going to be displayed in an effort to understand the challenges posed. From the previous comparative description the strengths of the HCCI concept form as follows:

- The relatively high compression ratio of HCCI results in a gain in thermal efficiency (η_{th}) compared to the SI engine, since these two quantities are directly related. The air standard Otto cycle gives us an approximate relation

between compression ratio and thermal efficiency: $\eta_{th} = 1 - \frac{1}{r^{\gamma-1}}$, where γ is the ratio of specific heats.

- The global autoignition of the homogeneous fuel and air mixture results in fast burn around TDC, thus maximizing expansion ratio and aiding indicated efficiency as well. As mentioned previously, homogeneity levels vary according to mixture preparation techniques used, thus resulting in different burn rates and effective expansion ratios.
- Lean mixtures exhibit higher ratios of specific heats γ, which in turn increase efficiency as well. The air standard Otto cycle provides an approximate relation between γ and thermal efficiency: $\eta_{th} = 1 - \frac{1}{r^{\gamma-1}}$
- HCCI (and all HPLB) engines operate unthrottled which helps them achieve lower pumping work, also resulting in increased indicated efficiency. Researchers have often characterized the pumping effectiveness of unthrottled engines by using the gas exchange efficiency metric.
- Absence of any rich zones due to largely homogeneous mixture results in very low soot formation during combustion.
- Excess air acting in parallel with residual gas (and potentially external EGR) in the cylinder, increase dilution levels of the mixture significantly. Increased dilution acts to lower pressure rise rates during heat release, peak cylinder temperatures and consequently prevent NO_x emissions formation.

The aforementioned strengths of the HCCI engine concept have led many researchers to consider it as a high efficiency alternative to SI combustion and as a low emissions alternative to CI combustion. The fact that HCCI combines the benefits of both SI and CI engines does not come without drawbacks though:

- There is a need for a well-mixed fuel, air and diluents mixture.
- The absence of spark means that the mixture needs sufficient energy to ignite by compression alone.

- The combustion process is controlled (and limited) by chemical kinetics, thus making Start of Combustion (SOC) difficult to control.
- The fast burn occurring around TDC results in high rates of heat release which often lead to ringing.
- Low cylinder temperatures may degrade combustion efficiency resulting in high levels of hydrocarbon (HC) and carbon monoxide (CO) emissions. These emissions are mainly products of unburned fuel trapped in piston crevices.

The challenges mentioned, result in the need for accurate control of burn rates across the entire speed and load range of the engine in order to achieve the desired operational characteristics. Inappropriate control can cause increased pressure rise rates and engine damage. It can be concluded that the HCCI combustion process is determined by the following five factors [8]:

- Initial mixture composition
- Initial mixture temperature
- Initial mixture pressure
- Rate and extent of compression work (engine speed and compression ratio)
- Rate and distribution of heat transfer (thermal stratification)

The dependence of HCCI combustion on the above set of parameters results in a complicated and challenging control problem. In order to face this problem and develop the HCCI concept, researchers have explored various enabling technologies coupled to scientific methods [8, 9, 10, 11]. The ultimate goal of this effort is to shape the HCCI engine into a credible and robust alternative to currently available powertrains.

1.6 Enabling Technologies

Variable Valve Actuation

Great importance lies in the fact that the first two governing factors mentioned above (initial mixture composition and temperature) are simultaneously affected by residual gas in the cylinder. Variable Valve Actuation (VVA) is an established technology that facilitates control of residual gas in the cylinder, thus allowing residual-effected HCCI combustion [9]. Variable valve actuation systems enable the implementation of valve strategies that allow the regulation of residual gas in the cylinder on a cycle basis. There are two widely accepted and well documented valve strategies that enable HCCI combustion. The first one is an exhaust gas retention strategy and is usually referred to as "recompression" or the "Negative Valve Overlap" (NVO) method; the second one is an exhaust gas reinduction strategy and is usually referred to as "rebreathing". The concept of recompression is based on early Exhaust Valve Closing (EVC) and late Intake Valve Opening (IVO) that form a negative valve overlap about gas exchange Top Dead Center (TDC). Early EVC means that the exhaust valve closes during the exhaust stroke and before gas exchange TDC, thus trapping burned gases in the cylinder and causing them to recompress (name origin). On the other hand, rebreathing is based on a secondary exhaust valve event taking place during (or overlapping with) the intake valve event, resulting in reinduction of exhaust gases which have escaped to the exhaust manifold. It should be noted that rebreathing has been used on naturally aspirated engines where intake and exhaust pressures allow reinduction of exhaust gas into the cylinder. Figure 1.1 shows plots of typical valve lifts for the two valve strategies described:

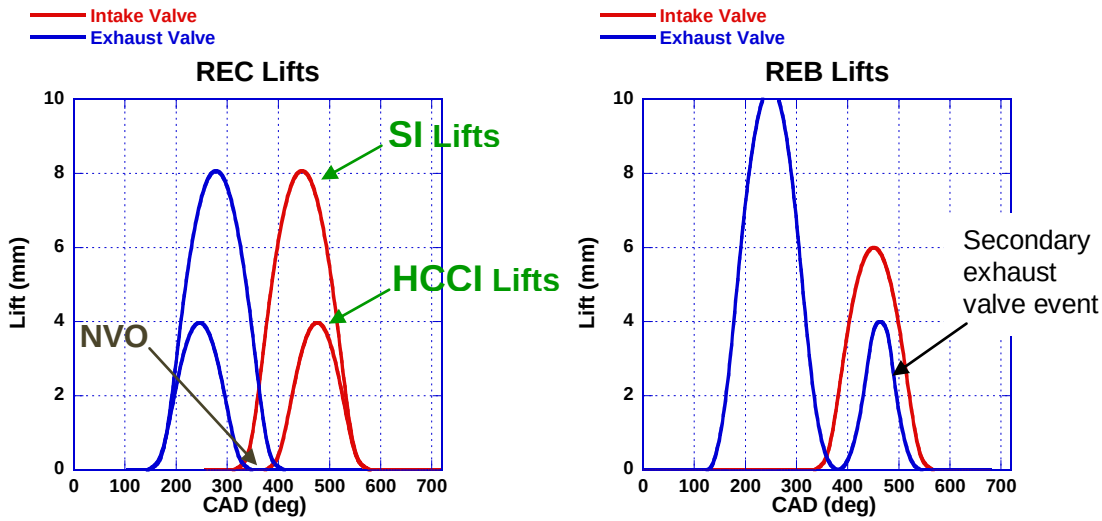

Figure 1.1 – Recompression and Rebreathing valve events

By observation of Figure 1.1 some useful information can be extracted. Starting from the recompression lift plot on the left, it can be seen that HCCI valve lifts can be scaled versions of SI valve lifts with the EVO and IVC points anchored. This is one of several variations of the recompression strategy presented in the literature. The cause of this scaled form is a practical constraint involving camshaft operation; in order to realize negative valve overlap, the duration of the exhaust and intake valve events must be reduced and therefore valve lifts must be reduced accordingly. The recompression strategy shown also points at one of the main challenges associated with HCCI when it comes to practical applications: The existence of NVO and lower than SI valve lifts, means that a large amount of fresh air that would be present in an SI engine cylinder is now substituted by exhaust gas. That would result in less fuel being able to be burned thus posing limits on the BMEP of the engine and limiting its operating range. From the rebreathing plot it can be seen that the secondary exhaust valve event takes place during the intake stroke, resulting in reinduction of hot exhaust gases into the cylinder caused by the pressure difference between the exhaust manifold and cylinder. In a similar manner to recompression, the reinduction of exhaust gases into the cylinder results in less fresh air

in the charge leading to similar load limitations for the engine. In both strategies, charge temperature can be controlled by regulating the amounts of cold intake air and hot residual gas that are mixed. Studies have shown that HCCI combustion can be realized with both of these strategies, and that rebreathing has the potential to help the engine achieve somewhat higher loads [10]. Rebreathing has also shown to help the engine achieve slightly better efficiency due to the absence of a recompression loop which increases pumping work [11]. The recompression strategy has proven to be more popular among research groups, possibly because of its simpler implementation in experimental setups and its resemblance to standard spark ignition lifts. Consequently, there have been various valve mechanisms proposed that can realize the recompression strategy, including variable duration camshafts, and scalable valve events that may change lift and duration simultaneously [30, 33].

Recompression and rebreathing are not the only valve strategies that have been used to enable HCCI combustion though. Regular spark ignition or diesel valve lifts forming a positive valve overlap (PVO) have been used in several experimental studies [13, 14, 31] where the experimental engine was a derivative of a production spark ignition or diesel engine respectively. In such cases, residual gas fraction was minimal (5 – 9 %) and the combustion mode was often referred to as “pure HCCI” by researchers. Mamalis et al. showed that full SI lifts (forming a PVO) can be used for boosted HCCI operation as long as the intake temperature can be brought to high levels from external compression. In that case, residual gas and mixture composition can be adequately adjusted by PVO or backpressure [38]. Results from this study showed that the use of higher valve lifts bring significant pumping work benefits, thus increasing net indicated efficiency of the engines. The key enabling technology involved in this study was boosting and it is going to be described later in this chapter.

Exhaust Gas Recirculation

Exhaust gas recirculation is an established technique that has been widely popular among diesel engine and SI engine manufacturers in the last decade. It allows control of ignition characteristics and cylinder temperatures by altering charge composition and properties. The dependence of HCCI combustion on residual gas for mixture preparation has lead researchers to explore EGR as an additional means to control ignition timing, combustion phasing and thus improve engine performance. Cairns and Blaxill [21] studied the effect of combined internal and external exhaust gas recirculation on gasoline HCCI operation and they reported that external EGR could help increase engine load through retarding ignition timing and prolonging burn duration. Both factors allowed for lower pressure rise rates and peak pressures as load increased. The authors noted that engine efficiency increased and the UHC emissions decreased but there was a need for increased intake temperature for ignition. Overall, they concluded that internal EGR can be used for lean HCCI at low loads and external EGR can be applied when higher load is needed, for an output increase of 20 to 65 %.

In 2002, John Dec presented a computational study on the effects of EGR on heat release rates and combustion limits in HCCI engines [15]. He identified the effects that EGR has on mixture preparation and he concluded that EGR increases the heat capacity of the mixture thus reducing temperature and reaction rates. The author also stated that EGR reduced oxygen concentration which also acted to reduce reaction rates and production rates of H_2O and CO_2. Furthermore, he noted that the largest effect of EGR is the reduced temperature after compression, but this effect and the fact that EGR slows chemical kinetics have a significant effect on combustion duration which can be increased by a factor of 2 or 3. This study displayed strong coupling between ignition timing and burn duration; the author reported that when ignition occurs around TDC, burn duration can be doubled with high EGR levels.

In 2003, Olsson et al. experimentally studied the effects of cooled EGR use on the emissions and performance of a boosted HCCI engine [16]. They reported that by using external EGR the engine CO, HC and NO_x emissions were reduced and the combustion efficiency was increased. The latter effect was observed in all cases but it was considered to be more important at low load cases. In agreement with the computational study presented by Dec [15], the authors reported that EGR slowed down combustion and that there was a need for increased intake temperature as the amount of EGR in the cylinder increased.

Another study from Cairns and Blaxill in 2005 explored the use of external EGR on a boosted experimental HCCI engine for expanding the high load potential [24]. The authors reported that the combination of internal and external EGR at naturally aspirated operation could lead to a stoichiometric mixture and could aid high load operation. They also reported that use of EGR aided combustion stability and lead to reduced HC and CO emissions.

In a later study, Sjoberg and Dec explored EGR and boost as means to manage low temperature heat release in HCCI combustion [17]. In this experimental study, EGR was seen as one of the ways to manage cool flame heat release which in turns controlled combustion phasing and allowed high load HCCI operation. The authors observed that low temperature heat release varied with boost, speed and load. It was also noted that EGR was an effective way to control combustion phasing when a fairly reactive fuel is used.

Intake Charge Boosting

The enabling technologies discussed so far aim at providing additional means of controlling ignition and heat release in HCCI combustion. Achieving ignition and lowering heat release rates are the key elements in expanding the operating range of HCCI engines and thus addressing the main problem that hinders practical applications of such engines. A very promising technology that has shown the potential to address this

problem is intake pressure boosting. Boosting affects HCCI combustion by introducing two major characteristics, increased dilution levels and increased mixture reactivity. On one hand, increased air mass increases mixture dilution which in turn lowers pressure rise rates during heat release. Lower pressure rise rates result in less knocking tendency, promote combustion control, allow more fuel to be injected and burned therefore increasing the attainable load of the engine. On the other hand, studies in the literature have shown that increased inlet pressure has an effect on combustion chemistry [17, 18]. It increases the reactivity of the mixture, thus shifting heat release earlier in the cycle, promoting high pressure rise rates but at the same time avoiding late partial burns and misfires. While earlier heat release through increased mixture reactivity might be seen as a process that leads to knock, its effect is overwhelmed by the increased dilution levels. Therefore, it should not be seen as a constraining factor but as an additional control knob for combustion phasing purposes.

Sjoberg et al. have shown that elevated intake pressure and dilution can be used to control low temperature heat release (LTHR) and thus control autoignition reactivity [17]. Particularly, it has been shown that boosting can help to mitigate the loss of LTHR as engine speed increases thus allowing operation across a wide engine speed range without the need for rapid intake temperature control. The effect of intake pressure boosting on low temperature combustion chemistry (LTC) has subsequently been investigated by Silke et al. [18]. It was found that increased intake pressure facilitates reactions that raise the concentration of radicals which lead to LTC chemistry and chain branching through the production of OH radicals, thus enhancing low temperature heat release. Recent experimental studies by Dec and Yang have shown that intake boost can facilitate high-load HCCI operation up to 16.3 bar IMEPg with 3.25 bar abs. intake pressure and high rates of EGR using 87 ON gasoline fuel [31]. The authors noted that a key factor for high load operation was the ability to substantially retard combustion with good stability and high efficiency, allowed by high intake boost and high EGR levels.

Prior to the aforementioned experimental studies that investigated fundamental aspects of boosted HCCI combustion, intake charge boosting for HCCI engines had been investigated for more than a decade and has since been shown that boost can help to extend the engines' upper load limit. One of the first studies by Christensen et al. used a diesel engine converted for HCCI operation and showed that boosting can help to increase the Indicated Mean Effective Pressure (IMEP) of the engine accompanied by a small decrease in NO_x and HC emissions [13]. The authors also showed that combustion efficiency improved as load increased and that boosting increased combustion duration because of the fact that there is more charge in the cylinder to be burned. Furthermore, they reported that the level of intake air preheating required was reduced as a result of boosting and that they applied up to 2 bar absolute intake pressure. A later experimental study by Olsson et al. utilized a turbocharged engine similar to the one used by Christensen et al. They suggested that a turbine for an HCCI engine be smaller and operate on a higher pressure ratio than a turbine in a similarly sized SI engine [14]. This study also identified a pumping problem in boosted HCCI since the exhaust backpressure was higher than the intake pressure and proposed the use of a Variable Geometry Turbine (VGT) for higher flexibility on boost control. The authors concluded that backpressure development was a result of the low exhaust temperature resulting from HCCI combustion. Two years later, another experimental study by the same group studied the effect of cooled EGR use on their turbocharged HCCI engine setup [16]. In this study, it was reported that NO_x was the limit for high load operation and the authors supported their earlier argument that a small turbine is required for boosted HCCI operation. One of the main conclusions of this study was that boosting and cooled EGR were two effective strategies for achieving high load HCCI.

In 2003, Hyvonen et al. studied a supercharged five cylinder 1.6L Saab Variable Compression Ratio (VCR) HCCI engine and showed that the operating range can be extended with boosting [19]. They also showed that the highly dilute mixture slowed

down the burn rate and reduced knock development. However, the supercharged engine suffered from low brake efficiency and it was calculated that using a turbocharger could result in a 32 to 97% load increase compared to supercharging. Turbocharger matching appeared to be a problem though, since the small turbine required for HCCI operation would be too small for SI operation and would hinder dual mode SI/HCCI operation. The authors concluded that in order to increase the operating range of the engine, increased dilution and lower octane fuel are necessary; they also reported that the maximum attainable load by their turbocharged HCCI was 10 bar BMEP. A subsequent study from Olsson et al. in 2004 confirmed the backpressure problem in turbocharged HCCI, but also showed an increase in engine efficiency with boosting despite the higher pumping work penalty [20]. The authors supported that ethanol is a very suitable fuel for boosted HCCI because of its low autoignition temperature and high octane rating. They also reported values of exhaust temperature which ranged between 250 and 450 ºC. Finally, it was suggested that two-stage boosting be used in order to increase gas exchange efficiency and reduce pumping work.

In 2005 Yap et al. applied boost to a single cylinder Port Fuel Injected (PFI) HCCI engine and concluded that there was substantial increase in load without the need for intake air preheating [22]. Specifically, the authors showed that with 1.4 bar intake pressure, 75 % of maximum SI engine load could be attained and that equivalence ratio was the main knob of combustion phasing control. In contrast to similar studies in the literature, the authors reported that boosting increased the pressure rise rates during combustion, but at the same time they reported that boost was their main knob of load control. In a different experimental study of the same year, the same researchers investigated the optimum valve timing strategy for boosted HCCI and they concluded that the exhaust event timing for boosted HCCI should be advanced compared to a naturally aspirated engine since it controlled residual gas fraction [23]. They also identified a maximum boost level until which intake air preheating was not required and

beyond that level it was. This observation appeared to be somewhat misleading since compression of the intake air would increase its temperature accordingly and increase the reactivity of the charge. Concurrently, Cairns and Blaxill worked on a boosted four cylinder HCCI engine; they showed that load can be increased with boosting and that heat release rates can be reduced resulting in greater stability, lower NO_x and HC but higher CO emissions [24]. The authors reported – similarly to other boosted HCCI studies – that while increasing load, boost increased peak cylinder pressure and reduced gas exchange efficiency due to backpressure development. Overall, they reported that most high load sites on the federal driving cycle could be obtained with boosting. It was shown that as turbocharger efficiency increased, the engine could be kept in HCCI mode longer, thus requiring less SI/HCCI mode transitions. The reported combined benefit of this operation was 12 % in fuel economy over an equivalent SI engine.

In 2007, Wilhelmsson et al. experimented on a 6-cylinder heavy duty Scania diesel engine equipped with VGT and converted to operate in HCCI mode, showing that the VGT helped to reduce pumping losses [25]. They also showed that early combustion increased backpressure through lowering exhaust temperature which also limited the benefits of turbocharging. The authors commented on the addition of n-heptane in the fuel as an ignition promoter through lowering the fuel octane rating. They supported n-heptane addition based on their observation that combustion efficiency was very sensitive to combustion phasing. In 2008, Yao et al. conducted an experimental study on the influence of boost pressure and fuel chemistry on HCCI combustion and performance [26]. They used four fuels with different octane ratings and two intake pressure levels; they concluded that intake boost can help to increase the operating range of the engine. The authors reported that boost advanced ignition timing, increased peak cylinder pressure but reduced pressure rise rate during combustion. They noted that dilution posed an upper limit on the amount of fuel that can be added to the mixture and they concluded that combustion efficiency of gasoline mixtures was lower than that of PRF fuel mixtures

when boosted. Another experimental study on boosted HCCI was published in 2008, where Martins and Zhao used a Ford four cylinder 1.6 L engine coupled to a small turbocharger and converted it to HCCI [28]. They verified that turbo matching was an issue since the turbocharger had to combine high load operation and high efficiency while operating at low mass flow rates. For that reason, they used a turbocharger sized for a 500 cc engine and concluded that boosting helped to extend the load range. However, they reported that gas exchange process was compromised as engine speeds rose and that there was need for a highly flexible valvetrain. The authors also noted that cooled external EGR helped to increase the upper load limit even more, and that the use of a wastegate valve to control boost pressure could help to extend the lower load limit.

The following year, Johansson et al. presented an experimental study of a modern turbocharged DISI engine converted to operate in HCCI mode [29]. The authors reported that the engine received modified and variable valve events, custom designed intake and exhaust manifolds and increased compression ratio in order to operate in HCCI mode. They also reported that boosting led to increased thermal efficiency compared to naturally aspirated operation; however, efficiency dropped quickly when combustion timing was phased away from maximum brake torque (MBT) timing. Split fuel injection was used in order to control cylinder to cylinder variations and an exhaust throttle was used in order to assist with driving EGR flow to the intake side. Spark assist was also used in this study and the authors noted that it improved combustion stability and enabled later combustion phasing. It was reported that the turbocharger was not appropriately sized for this HCCI engine. For that reason, the authors tried to improve its performance by phasing combustion later in the cycle so that they could maximize exhaust gas enthalpy. Overall, they reported only a modest increase in maximum load compared to the naturally aspirated operation and they attributed this result to the non-optimized turbocharger and valve strategy. In 2010, Mamalis et al. presented a multi-cylinder modeling study which attempted to compare different boosting strategies for HCCI

engines [30]. This study highlighted the operating differences between supercharging and turbocharging and concentrated on achieving the maximum possible load with different boost systems. The authors concluded that supercharging provided good control of the intake conditions but turbocharging was the most efficient boosting strategy since the main penalty came from pumping work. They also reported that two-stage turbocharging achieved the highest load but it suffered from poor gas exchange efficiency due to the high backpressure developed.

Concurrently, Dec and Yang experimented on boosting a single cylinder gasoline fueled engine for high power HCCI and they showed that by increasing intake pressure to 3.24 bar and adjusting the EGR content of the charge, a maximum load of 16.4 bar IMEPg could be achieved [31]. The engine used for the experiment employed high valve lifts thus the amount of residual gases trapped in the cylinders was minimal. Therefore, the authors reported that external EGR was essential for the extension of upper load limit above 9 bar IMEPg. The authors concluded that elevated pressure was the most important factor affecting intermediate temperature heat release (ITHR), which was the enabler of late combustion phasing while maintaining good stability. They also concluded that ITHR enhancement is fuel dependent and that combustion phasing is critical for high load HCCI.

Kulzer et al. investigated the potential of boosted HCCI application through a combined experimental and modeling study [32]. They highlighted that different breathing strategies resulted in different mixture enthalpies and homogeneity levels, thus affecting maximum load potential. The authors reported that EGR dilution increased equivalence ratio and reduced efficiency, but air dilution decreased Φ and increased engine efficiency. They also noted that combustion stability deteriorated at increased loads and that 9 bar NMEP was the borderline for boosted HCCI operation. Furthermore, they performed FTP 75 drive cycle simulations and they concluded that future engines

should be downsized boosted DISI engines which can also operate in boosted HCCI mode.

In the same year, Shingne et al. conducted a modeling investigation on turbocharger matching for a four cylinder boosted HCCI engine [33]. The study employed a two liter, four cylinder HCCI engine with variable duration valve events combined with single and two-stage turbocharging. The authors verified what was previously reported, that the turbochargers needed for boosted HCCI are smaller than those for similarly sized SI engines. They highlighted that the maximum attainable load was 12 bar NMEP with two-stage turbocharging, but in all cases the pumping work penalty was significant. As reported in a previous modeling investigation, the singe turbo system exhibited the best brake efficiency and the authors also noted that above 2000 rpm operation was limited by knock. Another modeling study by Mamalis et al. in 2010 discussed turbocharging requirements for boosting HCCI engines [34], and this study confirmed the maximum load values claimed by Dec and Yang in their experimental study [31]. The authors showed that by boosting intake pressure to 3 bar, loads as high as 17 bar NMEP can be achieved which are practically high load SI engine levels. The authors focused on the intake and exhaust conditions present at high load boosted HCCI and their respective requirements from the turbocharger. They reported that at maximum load Φ was 0.55 and peak cylinder pressures approached 145 bar. Finally, they concluded that a turbocharger suitable for high load boosted HCCI should combine high pressure ratios and high efficiency with lower than SI mass flow rates, and that turbine performance is crucial for the gas exchange efficiency of the engine. Recently, the same group conducted a study on optimal combinations of VVA strategies and boosting for high load HCCI [38]. The authors showed that a NVO/PVO cam switching strategy offered significant efficiency benefits at high load operation due to reduced pumping work. They also showed that by combining this VVA strategy with variable geometry boosting systems, a 5-12 bar NMEP load range can be realized. A major conclusion of

this study was that it is more efficient to heat the charge by using the intake system than to heat it by using the valve strategy.

The research studies of the past twelve years have clearly shown that intake pressure boosting is an essential technological step towards achieving high load HCCI. The fact that DISI engines are currently under downsizing development involving aggressive boosting, is another step towards developing multi-mode downsized gasoline engines. An engine that can combine SI, SACI and HCCI combustion modes, operate on a wide load range, achieve high efficiency and low emissions and probably be combined with mild hybridization subsystems appears to be the medium-term goal of powertrain research and a key towards building high efficiency vehicles.

1.7 1st and 2nd Law Analysis of Engine Concepts

The enabling technologies described in the previous section were mainly identified from experimental and modeling studies that attempted to improve HCCI engine operation in terms of efficiency, operating range, combustion stability and emissions. Efforts towards evaluating the same technologies from a more fundamental perspective have been put by different research groups using a combination of the first and second laws of thermodynamics. Examining the thermodynamics associated with improving engine efficiency provides valuable insight into the possible pathways toward next generation engines and allows a detailed investigation of the limits posed on different energy conversion techniques.

Exergy analysis of internal combustion engines has been used for a few decades to aid researchers with improving efficiency levels and gained momentum by efforts related to diesel engines. In 1984, Flynn et al. presented a 2nd law analysis study of a six cylinder experimental diesel engine [39]. The authors found that lean mixtures entailed 10 – 20 % greater irreversibilities compared to stoichiometric ones and that maximum

thermal efficiency would occur for mixtures that have a ratio of specific heats (γ) close to that of air. They concluded that the availability of the charge is a stronger function of temperature and pressure rise than γ variation. They also stated that in order to access the exergy associated with in-cylinder heat transfer, secondary heat recovery systems would be required. Concurrently, the same group published another study on 2nd law analysis which was based on the same experiment engine setup [40]. They investigated the application of five new techniques that would improve engine efficiency: turbocharging, turbocharging and aftercooling, turbocompounding, low heat rejection and the use of bottoming cycles. Some of these techniques are currently widely used in modern engines but the authors had managed to explain some of the trade-offs involved in their operation. They showed that by increasing mixture dilution levels, the amount of mixing in the cylinder increased and temperatures decreased thus increasing irreversibilities during combustion. In addition, the authors showed that aftercooling reduced the availability of intake air, creating the need for engine reoptimization to restore intake pressure and equivalence ratio levels. Turbocompounding was found to be beneficial for engine efficiency but the pressure ratio and efficiency of the turbine were deemed critical. Turbocharger efficiency was also very important since it affected the level of aftercooling and final exhaust gas availability levels. The authors stated that low heat rejection techniques were not beneficial because the exergy gained from reduced heat transfer was not converted into useful work but transferred out of the cylinder in the form of increased exhaust gas availability. Overall, they concluded that some heat recovery device is needed in the exhaust in order to aid engine efficiency.

A few years later, Alkidas performed a 2nd law analysis on a single-cylinder experimental diesel engine where he measured heat rejection to the coolant medium and lubricating oil [41]. In this study, a steady-state treatment of the engine was used with no storage terms in the control volume and all availability quantities were expressed in power terms. The author showed that brake power and available brake power varied

almost linearly with fuel input power. He also showed that combustion irreversibilities increased as load increased because the levels of friction, heat transfer and mixing were increasing. Results showed that the relative loss of heat transfer decreased with load and that exhaust availability was less than half of the exhaust energy. Exhaust availability that could be harnessed by the turbine was shown to be less that 30 % of the exhaust energy. Alkidas used the entropy equation to determine the irreversibilities during combustion and he showed that they increased as cylinder temperatures dropped.

A subsequent study by Van Gerpen and Shapiro performed a rigorous 2nd law analysis of diesel engine combustion [42]. The authors used a single-zone heat release model and they presented the development and solution of governing equations. They gave detailed descriptions of the thermomechanical and chemical availabilities and they also derived the availability balance equation. The authors showed the overall cylinder availability balance on crank angle basis and they explored effects of combustion timing, heat release curve and heat transfer correlation parameters on engine exergy flows.

In 1991, Bozza et al. presented a very interesting modeling study on 2nd law analysis of turbocharged diesel engine operation [43]. The authors used turbocharger performance maps and they explored the ways of reducing irreversibilities and exploiting the mechanical energy available. They performed exergy balances in the turbocharger and the engine system as well and they compared cylinder cumulative availability and energy terms. The authors claimed that the irreversibilities pattern depended primarily upon the magnitude of heat released and cylinder temperature; they also claimed that peak rate of change of irreversibilities occurred before that of fuel exergy. They noted that exergy destruction during combustion was mainly due to low temperatures and that exhaust stream exergy resulted mainly from the exhaust blowdown process. The last observation led them to conclude that high cylinder pressures would be beneficial to turbocharging. Results showed that turbocharging increased the second law efficiencies of the cylinder and engine system but they explained that the adiabatic process taking

place in a turbine did not lead to an effective availability recovery. The authors also commented on low heat rejection techniques and they reached a similar conclusion to the earlier study by Primus et al. [40]; exhaust flow availability increased which might be beneficial for turbocharging. Overall, they concluded that boosting may entail increased irreversibilities due to higher temperatures and mass flow rates, but the increased intake pressure is enough to compensate for these losses and offer efficiency benefits.

A few years later, Dunbar and Lior presented an investigation on the sources of combustion irreversibility [44]. It was a modeling study which targeted the theoretical processes of combustion in order to isolate phenomena that cause irreversibilities. They used hydrogen and methane as fuels and they showed that by increasing dilution levels, the temperature of the combustion products decreased thus leading to higher entropy generation. The authors categorized the processes that cause physical changes during combustion: (1) Reactant mixing, (2) fuel oxidation, (3) heat transfer and (4) product mixing. They also distinguished between the four physicochemical processes that contribute to global entropy generation: (1) Reactant diffusion, (2) fuel oxidation, (3) internal thermal energy exchange and (4) product mixing. By studying these processes, they concluded that the largest contributor to irreversibilities is internal energy exchange (60 – 80 %), second is fuel oxidation (10 – 25 %) and third is the mixing process (8 – 10 %). By comparing the two fuels, they showed that use of methane resulted in higher irreversibilities than use of hydrogen.

In 1998, Anderson et al. explored the use of Miller cycle in a naturally aspirated SI engine with late IVC from a 1st and 2nd law perspective [45]. Their goal behind the 2nd law analysis was to quantify the impact of various mechanisms that lead to exergy destruction. The authors compared a throttled version of the engine to an unthrottled one and they showed that the throttled design transferred more availability through heat loss to the surroundings. They claimed that 2nd law analysis recognized elevated pressure during blowdown as an increase in irreversibility. From the same point of view, the

increased intake pressure when late IVC was employed was found to offer an advantage in thermochemical availability.

In 2006, Farrell et al. presented a very interesting study on second law analysis of high efficiency gasoline engine concepts where they compared PFI, DISI and HCCI engine concepts from first and second law perspectives [47]. The authors reported that second law analysis can additionally describe losses during combustion while the first law analysis cannot. They concluded that low temperature combustion led to higher combustion irreversibility, but lean burn engines exhibited less irreversibility in other areas like heat transfer and fluid flow losses. These results led them to conclude that high temperature and pressure combustion is needed for maximum efficiency. However, low temperature is required for emissions control so high pressure by itself can be employed to improve engine efficiency. It was also reported that maximum thermal efficiency occurs when CA50 was 5 – 10 Crank Angle Degrees (CAD) after TDC and when burn duration was less the 35 CAD, conditions which apply to HCCI and SACI combustion. The authors commented on the ability to harness exergy and transfer its losses to different areas of the engine, which means that by reducing irreversibility in the combustion chamber, higher levels of exergy can be transferred to the exhaust and harnessed by turbines that produce useful work. That was an important finding since it showed that combustion manipulation can improve the efficiency of turbochargers which in turn increases intake pressure levels and thermal efficiency as well. It was also reported that elevated compression ratio is desired for high thermal efficiency, but friction losses limit it to a level of about 15. The authors also concluded that de-throttling, variable valve actuation and elimination of idling reduced the fluid flow losses significantly. Overall, the analysis showed that HCCI offered only modest efficiency improvements compared to an optimized DISI engine, but the reduced NO_x emissions was an added benefit of the system.

The study by Farrell et al. outlined above is one of the few studies on second law analysis of high pressure lean burn engines which take into account both combustion and hardware aspects of the system. There have been numerous other studies regarding second law analysis of internal combustion engines but the majority of them have been limited to SI or diesel engine applications.

In 2006 Rakopoulos and Giakoumis presented a review study of 2nd law analyses of internal combustion engine operation [48]. Their publication included a comprehensive review of previous studies on exergy analysis of engines, as well as their own modeling results for a medium duty marine diesel engine. The authors provided a detailed set of the equations involved in the 2nd law analysis of an engine cylinder and other engine subsystems, such as intake and exhaust manifolds, the turbocharger and the intercooler. They claimed that turbocharging is a very effective way to improve engine efficiency since part of the available exhaust energy is exploited. Similarly to the early study of Primus et al., they noted that intercooling decreased cylinder temperature and led to higher combustion irreversibilities. However, exergy destruction was somewhat counterbalanced by reduced cylinder heat transfer. The authors also commented on the fact that equivalence ratio and RGF greatly affected cylinder temperatures and combustion irreversibilities. The sources of irreversibilities across the engine system were examined and solutions to mitigate them were proposed; de-throttling, boosting, low heat rejection and rapid combustion events were some of them. The authors claimed that throttling in a conventional PFI engine can destroy up to 3 % of fuel availability. Engine speed was found not be an important factor, mainly affecting heat transfer availability. Insulation of the cylinder walls was found to be a favorable design choice since it can increase cylinder temperatures thus lowering combustion irreversibilities. The authors also considered alternative fuels use, oxygen enrichment and water addition techniques and studied their effect on combustion from a 2nd law perspective. Finally,

they included a detailed discussion on 2nd law efficiencies for the various engine subsystems.

A few years later, Lawand and Caton simulated turbocharged SI engines and presented a 2nd law analysis of them [49]. The authors did not use turbocharger maps but they prescribed the boundary conditions at the intake and exhaust according to engine speed. They found that as engine speed increased, the relative heat transfer decreased but friction increased, which are in agreement with the literature. The authors concluded that using a turbocharger does not significantly add to the overall irreversibilities. In addition, they observed a decrease in irreversibilities as load and speed increased which somewhat contradicts other results from the literature. Finally, they confirmed that combustion irreversibilities decreased as cylinder temperatures rose.

A recent study by Jerald Caton discussed the thermodynamics of high efficiency SI engines and justified several of the techniques currently used for improving their efficiency [50]. The author highlighted that lean burn engines exhibit lower relative heat transfer and that EGR use of up to 50 % increases γ during the expansion stroke. Both of these attributes were shown to improve thermal efficiency. He also noted that reducing burn duration from 60 to 30 CAD resulted in modest improvements in net indicated efficiency, and that increasing the wall temperature from 450 K to 550 K had a similar effect. Finally, the author identified the need for increased exhaust gas energy in order to aid turbocharger performance in a boosted lean burn engine.

In 2011, Edwards et al. presented a 2nd law analysis study which aimed at exploring practical efficiency limits of modern internal combustion engines [51]. The authors showed an overview of engine efficiency losses and they observed that energy distribution varies across the operating range. Exhaust energy was found to be highest at high load and speed while relative friction losses were highest at low load and speed. They also commented on the effect of engine size on efficiency, showing that larger engines exhibit higher efficiency levels due to a number of reasons related to heat transfer

losses, blow-by losses, combustion efficiency and engine speed. Furthermore, the authors stated that fuel selection affects irreversibilities during combustion and that the effect is more pronounced in lean burn engines. They noted that state of the art engines destroy 20 – 25 % of the fuel exergy during combustion but that cannot be reduced below 20 % with the known combustion systems. It was observed that major availability benefits can occur by manipulating cylinder heat transfer. The options for reducing heat transfer include advanced LTC strategies, low heat rejection techniques and higher engine coolant temperatures. The authors claimed that the combination of these features could reduce heat loss from about 25 % of the fuel exergy down to 5 %. Reduction in friction and pumping losses could offer some efficiency gains, and improved harvesting of exhaust exergy could also offer a 5 % of fuel exergy benefit. The authors concluded that a combination of all these techniques could lead to a 60 % efficient transportation engine, but that would be cost-prohibitive with currently available technology.

The investigations outlined above examined the problem of improving engine efficiency from a fundamental perspective and showed that there are various technical pathways that can lead to high efficiency engines and quantified the potential gains. However, these studies are limited in number, thus the next generation downsized multi-mode engine concept – as described previously – and its peripheral components may need further analysis and investigation. This fact leaves room and gives the opportunity for original contributions in this field.

1.8 Objective and Document Organization

This dissertation and the research work behind it are parts of a broader synergistic effort which aims at exploring high pressure lean burn engines from both experimental and computational aspects, in order to promote fundamental understanding of these engines and guide future development activities. The objective of the present doctoral

work is to combine advanced combustion, boosting and variable valve actuation in efficient simulation tools, that will enable quantification and analysis of the trade-offs involved in HPLB engines. The primary goals of this dissertation are to:

- Evaluate the performance of available combustion and heat transfer models using different sets of experimental data; to assess their capability of modeling high pressure lean burn engine operation and reveal potential drawbacks.
- Integrate advanced combustion, boosting and VVA strategies in detailed multi-cylinder engine models; utilize these models to quantify the trade-offs involved in HPLB operation introducing parameters such as compression ratio and EGR use.
- Investigate HPLB engine operation from a 2^{nd} law perspective in order to identify practical efficiency limits, assess the effectiveness of different operating strategies and propose solutions that can improve overall engine efficiency.

The remaining document is organized in five chapters which will present this doctoral research work in detail. Chapter 2 will discuss the motivation behind this work and describe the combustion and heat transfer models employed. The governing equations of 2^{nd} law analysis will also be presented and analyzed. Particular emphasis will be given in the underlying methodology of the multi-cylinder engine simulations. In Chapter 3, the performance evaluation process of the available combustion and heat transfer models will be described. Three different sets of experimental data are going to be introduced and the models will be assessed based on their ability to simulate the experiments. Subsequently, Chapter 4 will present multi-cylinder engine models and it will display the results of detailed simulations. Different mixture preparation techniques are going to be examined and the effect of parameters such as intake temperature, compression ratio, EGR use, boosting system and VVA to engine operating range and efficiency are going to be investigated and explained. The trade-offs involved in the

combination of these techniques are going to be quantified and analyzed on the basis of thermodynamics. 2nd law analysis of HPLB engine will be presented in Chapter 5. The results obtained from multi-cylinder engine simulations are going to be used in order to extract useful information about the thermodynamic processes taking place in an HPLB engine system. Existing operating techniques will be evaluated and new ones will be proposed based on optimal exergy manipulation principles. Finally, the document will be concluded with a synopsis of the findings and contributions, as well as with recommendations for future work in Chapter 6.

The original contributions presented in this dissertation have also been reported in the following publications:

Mamalis, S., Nair, V., Andruskiewicz, P., Assanis, D., Babajimopoulos, A., Wermuth, N., and Najt, P. M. "Comparison of Different Boosting Strategies for Homogeneous Charge Compression Ignition Engines – A Modeling Study", SAE Int. J. Engines 3(1): 296-308, 2010 [30]

Mamalis, S. and Babajimopoulos A., "Model-based Estimation of Turbocharger Requirement for Boosting an HCCI engine", *Proceedings of the ASME Internal Combustion Engine Fall Technical Conference*, ASME Paper ICEF2010-35122, 2010 [34]

Mamalis, S., Babajimopoulos, A., Guralp, O. and Najt, P. M., "Optimal use of Boosting Configuration and Valve Strategies for High Load HCCI - A Modeling Study", SAE Paper 2012-01-1101, 2012 [38]

Mamalis, S., Babajimopoulos, A., Guralp, O., Najt, P. M., and Assanis, D. N., "The Interaction between Compression Ratio, Boosting and Variable Valve Actuation for High Load HCCI – A Modeling Study", to be submitted to International Journal of Engine Research

1.9 References

1. Ando, H., Noma, K., Iida, K., Nakayama, O. and Yamauchi, T., "Mitsubishi GDI engine – Strategies to meet the European requirements", SAE Paper 1997-29-0017

2. Fraser, N., Blaxill, H., Lumsden, G. and Bassett, M., "Challenges for Increased Efficiency through Gasoline Engine Downsizing", SAE Paper 2009-01-1053

3. Cruff, L., Kaiser, M., Krause, S., Harris, R., Krueger, U. and Williams, M., "EBDI® - Application of a Fully Flexible High BMEP Downsized Spark Ignited Engine", SAE paper 2010-01-0587

4. Onishi, S., Hong Jo, S. Shoda, K., Do Jo, P. and Kato, S., "Active Thermo-Atmosphere Combustion (ATAC) – A New Combustion Process for Internal Combustion Engines", SAE Paper 790501, 1979

5. Noguchi, M., Tanaka, Y., Tanaka, T., and Takeuchi, Y., "A Study on Gasoline Engine Combustion by Observation of Intermediate Reactive Products during Combustion", SAE Paper 790840, 1979

6. Najt P. M. and Foster D. E., "Compression Ignited Homogeneous Charge Combustion", SAE Paper 830264, 1983

7. Thring R. H., "Homogeneous-Charge Compression-Ignition (HCCI) Engines", SAE Paper 892068, 1989

8. Caton P.A., Song H.H., Kaahaaina N.B. and Edwards C.F., Residual-effected homogeneous charge compression ignition with delayed intake-valve closing at elevated compression ratio, *Int. J. Engine Res.* 2005 Vol.6, No.4, p.399-219

9. Milovanovic N., Chen R. and Turner J., "Influence of the Variable Valve Timing Strategy on the Control of a Homogeneous Charge Compression Ignition Engine", SAE Paper 2004-01-1899

10. Kuo T.-W., 2006, "Valve and Fueling Strategy for Operating a Controlled Auto-Ignition Combustion Engine", SAE 2006 HCCI Symposium, September 25-26, 2006, San Ramon, CA

11. Chesa Rocafort J. L., Andreae M. M., Green W. H., Cheng W. K. and Cowart J. S., "A Modeling Investigation into the Optimal Intake and Exhaust Valve Event Duration and Timing for a Homogeneous Charge Compression Ignition Engine", SAE Paper 2005-01-3746

12. Olsson J., Tunestal P., Haraldsson G., and Johansson B., "A Turbo Charged Dual Fuel HCCI Engine", SAE Paper 2001-01-1896, 2001

13. Christensen M., Johansson B., Amneus P., and Mauss F., "Supercharged Homogeneous Charge Compression Ignition", SAE Paper 980787, 1998

14. Olsson J., Tunestal P., Haraldsson G., and Johansson B., "A Turbo Charged Dual Fuel HCCI Engine", SAE Paper 2001-01-1896, 2001

15. Dec, J. "A Computational Study of the Effects of Low Fuel Loading and EGR an Heat Release Rates and Combustion Limits in HCCI Engines, SAE Paper 2002-01-1309, 2002

16. Olsson, J., Tunestal, P., Ulfvik, J. and Johansson, B., "The Effect of Cooled EGR on Emissions and Performance of a Turbocharged HCCI Engine", SAE Paper 2003-01-0743, 2003

17. Sjoberg M. and Dec J., "EGR and Intake Boost for Managing HCCI Low Temperature Heat Release over Wide Ranges of Engine Speed", SAE Paper 2007-01-0051, 2007

18. Silke E., Pitz W., Westbrook C., Sjoberg M. and Dec J., "Understanding the Chemical Effects of Increased Boost Pressure under HCCI Conditions", SAE Paper 2008-01-0019, 2008

19. Hyvonen J., Haraldsson G. and Johansson B., “Supercharging HCCI to Extend the Operating Range in a Multi-Cylinder VCR-HCCI Engine”, SAE Paper 2003-01-3214, 2003

20. Olsson, J., Tunestal, P., and Johansson, B., “Boosting for High Load HCCI”, SAE Paper 2004-01-0940, 2004

21. Cairns, A. and Blaxill, H., “The Effects of Combined Internal and External Exhaust Gas Recirculation on Gasoline Controlled Auto-Ignition”, SAE Paper 2005-01-0133, 2005

22. Yap D., Wyszynski M., Megaritis A., Xu H., “Applying boosting to gasoline HCCI operation with residual trapping”, SAE Paper 2005-01-2121, 2005

23. Yap D., Wyszynski M., Megaritis A., Xu H., “Effect of inlet valve timing on boosted gasoline HCCI with residual gas trapping”, SAE Paper 2005-01-2136, 2005

24. Cairns A. and Blaxill H., “Lean Boost and External Exhaust Gas Recirculation for High Load Controlled Auto-Ignition”, SAE Paper 2005-01-3744, 2007

25. Wilhelmsson C., Tunestal P., and Johansson B., “Operation Strategy of a Dual Fuel HCCI Engine with VGT”, SAE Paper 2007-01-1855, 2007

26. Yao M., Liu H., Zhang B. and Zheng Z., “The Influence of Boost Pressure and Fuel Chemistry on Combustion and Performance of a HCCI Engine”, SAE Paper 2008-01-0051, 2008

27. Cairns A., Fraser N. and Blaxill H., “Pre Versus Post Compressor Supply of Cooled EGR for Full Load Fuel Economy in Turbocharged Gasoline Engines”, SAE Paper 2008-01-0425, 2008

28. Martins M. and Zhao H., “4-Stroke Multi-Cylinder Gasoline Engine with Controlled Auto-Ignition (CAI) Combustion: a comparison between Naturally Aspirated and Turbocharged Operation”, SAE Paper 2008-36-0305, 2008

29. Johansson, T., Johansson, B., Tunestal, P. and Aulin, H., "HCCI Operating Range in a Turbocharged Multi Cylinder Engine with VVT and Spray-Guided DI", SAE Paper 2009-01-0494, 2009

30. Mamalis, S., Nair, V., Andruskiewicz, P., Assanis, D., Babajimopoulos, A., Wermuth, N., and Najt, P. M. "Comparison of Different Boosting Strategies for Homogeneous Charge Compression Ignition Engines – A Modeling Study", SAE Int. J. Engines 3(1): 296-308, 2010

31. Dec. J. and Yang. Y., "Boosted HCCI for High Power without Engine Knock and Ultra-Low NO_x Emissions using a Conventional Fuel", SAE Paper 2010-01-1086, 2010

32. Kulzer, A., Lejsek, D. and Nier, T., "A Thermodynamic Study on Boosted HCCI: Motivation, Analysis and Potential", SAE Paper 2010-01-1082, 2010

33. Shingne, P., Assanis, D., Babajimopoulos, A., Keller, P., Roth, D. and Becker, M., "Turbocharger Matching for a 4-Cylinder Gasoline HCCI Engine Using a 1D Engine Simulation", SAE Paper 2010-01-2143, 2010

34. Mamalis, S. and Babajimopoulos A., "Model-based Estimation of Turbocharger Requirement for Boosting an HCCI engine", *Proceedings of the ASME Internal Combustion Engine Fall Technical Conference*, ASME Paper ICEF2010-35122, 2010

35. Hyvonen, J., Haraldsson, G. and Johansson, B., "Operating Conditions Using Spark Assisted HCCI Combustion During Combustion Mode Transfer to SI in a Multi-Cylinder VCD-HCCI Engine", SAE Paper 2005-01-0109, 2005

36. Daw, C. S., Edwards, K. D., Wagner, R. M. and Green, J.J.B Jr., "Modeling Cyclic Variability in Spark-Assisted HCCI", *J. Eng. Gas Turb. Power*, 130 (2008) 052801, 2008

37. Lavoie, G. A., Martz, J., Wooldridge, M. and Assanis, D., "A Multi-mode Combustion Diagram for Spark Assisted Compression Ignition", *Combustion and Flame*, 157 (2010) 1106-1110, 2010

38. Mamalis, S., Babajimopoulos, A., Guralp, O. and Najt, P. M., "Optimal use of Boosting Configuration and Valve Strategies for High Load HCCI - A Modeling Study", SAE Paper 2012-01-1101, 2012

39. Flynn, P. F., Hoag, K. L., Kamel, M. M. and Primus, R. J., "A New Perspective on Diesel Engine Evaluation Based on Second Law Analysis", SAE Paper 840032, 1984

40. Primus, R. J., Hoag, K. L., Flynn, P. F. and Brands, M. C., "An Appraisal of Advanced Engine Concepts Using Second Law Analysis Techniques", SAE Paper 841287, 1984

41. Alkidas, A. C., "The Application of Availability and Energy Balances to a Diesel Engine", *J. Eng. Gas Turb. Power,* 110 (1988) 462-469, 1988

42. Van Gerpen, J. H. and Shapiro, H. N., "Second-Law Analysis of Diesel Engine Combustion", *J. Eng. Gas Turb. Power,* 112 (1990) 129-137, 1990

43. Bozza, F., Nocera, R., Senatore, A. and Tuccillo, R., "Second Law Analysis of Turbocharged Engine Operation", SAE Paper 910418, 1991

44. Dunbar, W. R. and Lior, N., "Sources of Combustion Irreversibility", Combust. Sci. and Tech., 1994, Vol. 103, pp. 41-61

45. Anderson, M. K., Assanis, D. N. and Filipi, Z. S., "First and Second Law Analyses of a Naturally-Aspirated, Miller Cycle, SI Engine with Late Intake Valve Closure", SAE Paper 980889, 1998

46. Caton, J., "Operating Characteristics of a Spark-Ignition Engine Using the Second Law of Thermodynamics: Effects of Speed and Load", SAE Paper 2000-01-0952, 2000

47. Farrell, J. T., Stevens, J. G. and Weissman, W., "A Second Law Analysis of High Efficiency Low Emission Gasoline Engine Concepts", SAE Paper 2006-01-0491, 2006

48. Rakopoulos, C. D. and Giakoumis, E. G., "Second-law analyses applied to internal combustion engines operation", *Progress in Energy and Combustion Science*, 32 (2006) 2-47, 2006

49. Lawand, V. J. and Caton, J. A., "A Turbocharged, Spark-Ignition Engine: Results from an Engine Cycle Simulation Including the Second Law of Thermodynamics", *Proceedings of the ASME Internal Combustion Engine Spring Technical Conference*, ASME Paper ICES2009-76023, 2009

50. Caton, J., "An Assessment of the Thermodynamics Associated with High-Efficiency Engine", *Proceedings of the ASME Internal Combustion Engine Fall Technical Conference*, ASME Paper ICEF2010-35037, 2010

51. Edwards, K. D., Wagner, R. M., and Theiss, T. J., "Exploring Practical Efficiency Limits for Goal Setting," AEC/HCCI Working Group Meeting, 23 – 25 August 2011, Southfield, MI, USA

CHAPTER 2

MOTIVATION AND RESEARCH METHODS

The introduction and literature review presented in Chapter 1 aimed at detailing the fundamentals of DISI, HCCI and SACI engines and building the foundation for a more elaborate discussion on modeling and simulation of advanced engine concepts. The current chapter will proceed to this discussion by portraying the motivation behind the present research work, stating its objective and displaying the tools that will be used to complete this effort.

2.1 Motivation

Many of the studies outlined in Chapter 1 have led numerous researchers to believe that the future of internal combustion engines relies heavily on downsizing and boosting concepts. Such engines will need to employ multi-mode combustion systems in order to achieve high efficiency and low emissions while not neglecting performance. The majority of the studies related to these concepts have been experimental investigations which focused primarily on the combustion event without accounting for engine system interactions and requirements. At the same time, modeling efforts have been limited, often including gross assumptions and always pertaining to a specific combustion mode.

Recent modeling efforts at the University of Michigan W. E. Lay Automotive Engineering Laboratory focused on the thermodynamics of HPLB engines and were

presented by Lavoie et al. [1]. The authors investigated the thermodynamics of highly dilute and boosted gasoline engine applications, in an effort to assess the benefits of combining dilution and boosting to achieve high efficiency. Commercial engine simulation software was used to model a single cylinder engine based on certain assumptions regarding the combustion event and the engine system. Their assumptions included optimal combustion at all conditions having a Wiebe-shaped burn curve, fixed combustion timing at CA50 = 10° after TDC and combustion duration of 25°. They also used standard Woschni heat transfer and fixed valve events. The authors implemented a turbocharger phenomenological model which made use of thermodynamic equations of compressors and turbines to calculate backpressure, given intake pressure requirements, charge dilution levels and constant isentropic efficiencies for the turbomachines. They also set the compression ratio to 12 and kept the engine speed constant at 2400 RPM with the intake temperature being 333 K. Several parameters were swept such as engine load, intake pressure, equivalence ratio and EGR levels resulting in interesting findings. Some of them are displayed in Figure 2.1 below, where brake efficiency and intake pressure are shown as functions of engine BMEP. On the left plot, the efficiency advantage of lean burn engines compared to stoichiometric SI engines is shown and it occurs across the entire load range. The authors divided the plot region into three colored areas which represent the three different combustion mode regimes; HCCI, SACI and SI. They claimed that every combustion mode can cover a different engine operating area depending on required load and equivalence ratio. On the right plot, intake pressure and effective equivalence ratio ($\Phi' = \Phi(1 - RGF)$) are shown as functions of BMEP in an effort to visualize optimal boost strategies for lean burn engines. It was shown that the operating curve can sweep through different combustion mode regimes and that different Overall Turbocharger Efficiency (OTE) results in different intake pressures across the load range.

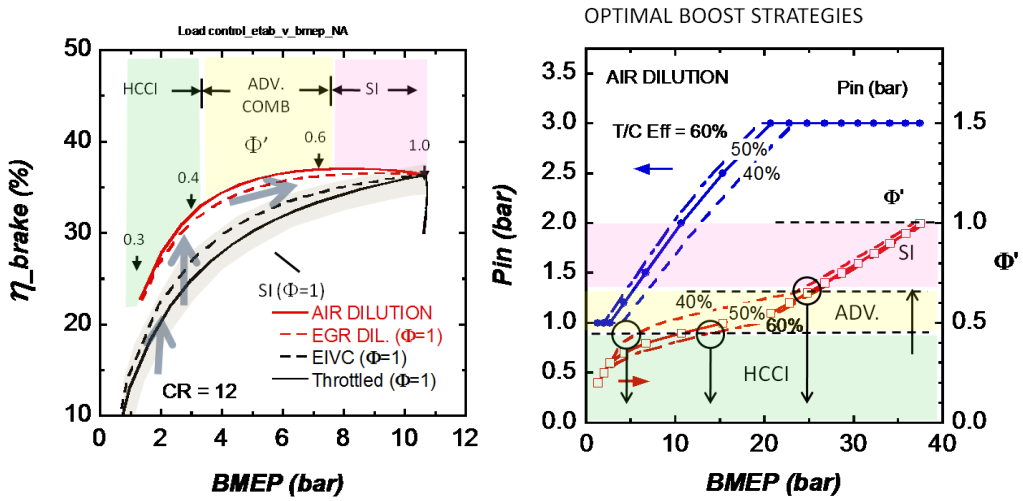

Figure 2.1 – Brake efficiency and intake pressure as functions of BMEP for the single cylinder engine model of Lavoie et al. [1].

The authors reached some very interesting conclusions that paved the way for further investigation into this topic. They found that spark assist and stratification can link the HCCI and SI regions, which would allow additional efficiency gains. They compared EGR versus air dilution and they concluded that EGR dilution is superior for NO_x suppression, but is inferior when it comes to engine thermal efficiency. That was attributed to a higher ratio of specific heats for the air dilute mixture. It was also noted that there is essentially no point in boosting at low equivalence ratios, since exhaust gas enthalpy was reduced and pumping work was increased. In addition, they commented on the use of constant overall turbocharger efficiency, stating that increased OTE allowed for wider HCCI and SACI combustion ranges and that transition points between HCCI, SACI and SI depend largely on OTE. Finally, they estimated that an optimized combination of downsizing, boosting and advanced combustion can lead to a potential 50% efficiency gain compared to current engine concepts.

The experimental and modeling studies presented in the literature have indicated that there is significant room for original contributions in the field of high pressure lean burn engine modeling and simulation. Coupling low temperature combustion modeling to

system level analysis can significantly help researchers to gain insight into the fundamentals of HPLB engines and provide the framework for understanding the challenges involved in the design and development of future powertrains. Such a framework has the ability to capture all system level aspects of downsized boosted engines such as turbocharging, variable valve actuation, EGR and other potentially used technologies. It would also serve as a powerful tool in the hands of anyone that wishes to simulate high efficiency engine concepts and draw conclusions regarding their performance, emissions and fuel economy. In specific, for those that wish to examine the interactions of high pressure, low or high temperature combustion modes with variable valve actuation strategies and boosting systems, such a framework can be a valuable design tool as well.

2.2 Research objective

Since the motivation behind this doctoral work has been displayed, its objective can be stated as to investigate the interactions between advanced combustion, boosting and variable valve actuation for high pressure lean burn engines.

The objective was met in three steps; first, the tools that were used for the system level analysis were assessed against experimental results. The performance evaluation process primarily involved the University of Michigan HCCI and heat transfer models. Once the tools had been verified for use in system level models, extensive four-cylinder engine simulations were performed. These simulations aimed at assessing the feasibility of boosted HCCI operation through use of actual turbomachine performance maps. They also aimed at exploring the requirements and benefits associated with use of advanced valve strategies and mixture preparation techniques such as external EGR. The third part of the research work put emphasis on thermodynamics and performed second law analysis of HPLB engines. In order to achieve that, an exergy analysis framework was

introduced to system level simulations, which allowed for a more theoretical approach of advanced engine concepts.

The keen reader would have already realized that the presented research work followed an inverse approach compared to what is usually performed. Instead of starting from a theoretical level of study and proceeding to the practical application of it, this dissertation will present performance evaluation of existing combustion and heat transfer models, use them together with a variety of well-established models for engine system simulations, and finally investigate the potential for future advancements in high efficiency engine technology.

The theoretical component of the research work resulted in a framework which can help one to determine the highest achievable efficiency with currently available technology and potential drawbacks of currently used solutions. The combination of 1^{st} and 2^{nd} law analyses or the exploration of energy view versus exergy view of an engine system, proved to be highly instructive. It enabled the identification and quantification of engine efficiency losses, such as fluid flow, mechanical, combustion, heat transfer and exhaust losses. Through quantification, one can propose solutions that have the potential to mitigate these losses based on enabling technologies for different engine concepts. The preceding hardware related analysis part, described the realistic processes and components that enable high efficiency engine concepts. It also identified critical areas for future technological development and can be used to calculate potential efficiency improvements through technological advancements in relevant engine components.

After presenting the motivation behind this doctoral research work and stating its research objective, this chapter will proceed by displaying the framework and tools that were developed and used in order to meet the stated goals.

2.3 Tools

As stated earlier, the primary goal of the present work was to investigate the interactions between the combustion event and various engine subsystems for high pressure lean burn engines. The following sections will present the framework and modeling tools used to achieve the desired goals. System level and combustion modeling will be described first, followed by second law analysis.

2.3.1 System Level Modeling

Engine system level analysis was a major part of the present work. In order to perform it, extensive use of GT-Power was made. GT-Power is part of commercial software package GT-Suite (distributed by Gamma Technologies, Inc.) which is an engine cycle simulation tool capable of steady-state and transient simulations [2]. It is well suited for analyzing powertrain systems and it provides a user-friendly graphical interface which enables modeling of different engine concepts.

The simulation is based on one-dimensional (1-D) gas dynamics, representing fluid flow, mechanical and heat transfer processes through the pipes, valves, ports, cylinders and other components of engine systems such as turbochargers and intercoolers [2]. The tool features object-oriented code design that provides a model building facility and enables managing of object libraries as well as building, editing, executing and post-processing models. A key feature for this research work was its option to implement individual models that describe in-cylinder processes through user subroutines.

Homogeneous charge compression ignition was the combustion mode of focus in this work. As detailed in chapter one, its combination of high efficiency potential and minimal emissions formation render it as a very attractive alternative to conventional SI combustion. The following section gives a description of the University of Michigan

HCCI combustion and heat transfer models and their implementation in GT-Power through user subroutines.

2.3.2 UM HCCI Combustion and Heat Transfer Correlations

During the last decade, research efforts at the University of Michigan have largely focused on investigating the fundamentals of HCCI combustion. A critical point of that work has been the development of robust combustion models that can be used for system level simulations. In addition, a new heat transfer model was proposed that could describe heat loss processes in low temperature combustion engines. Both of these models have been presented by Babajimopoulos et al. [3] and will be described in detail here as well. They feature correlations for ignition, fuel burn rate, combustion efficiency and heat transfer rate. As seen in Chapter 1, operational limits of HCCI engines are commonly determined by NO_x emissions and ringing intensity levels. In order to extend the model capabilities, the authors included appropriate expressions for NO_x and ringing intensity calculations. By exploiting the flexibility offered through GT-Suite, the UM HCCI combustion and heat transfer models were implemented through user subroutines. The basic equations used in these models are described in the following.

Ignition

Ignition timing was calculated using an autoignition integral approach proposed by Livengood and Wu in 1955 [4]. The expression for ignition delay time τ is typically given in Arrhenius form:

$$\tau = AP^{-a} \exp\left(\frac{E_A}{R^0 T}\right) \tag{2.1}$$

where A is a pre-exponential factor that is a function of composition and temperature, P is cylinder pressure, T is cylinder temperature, E_A is activation energy, R is the universal gas

constant and α is the reaction order. Ignition time, t_{IGN}, was defined as the time when the auto-ignition integral reaches the value of 1:

$$\int_0^{t_{IGN}} \frac{1}{\tau} d\tau = 1 \tag{2.2}$$

The ignition delay correlation itself was proposed by He et al. in 2005 [5] based on experiments in a rapid compression machine with iso-octane/N_2/O_2 mixtures:

$$\tau = 1.3E-7 \cdot P^{-1.05} \cdot \phi_{FO}^{-0.77} \cdot \chi_{O_2}^{-1.41} \exp\left(\frac{33700}{R^0 T}\right) \tag{2.3}$$

where P is chamber pressure (atm), T is chamber temperature (K), Φ_{FO} is the fuel/oxygen equivalence ratio, χ_{O2} is the oxygen mole fraction (%), R is the universal gas constant (cal/mol/K), and τ is the ignition delay time (ms). The units of the pre-exponential factor are $ms \cdot atm^{1.05}$.

Combustion

After ignition timing had been determined, the heat release curve and combustion efficiency were calculated using correlations developed at the University of Michigan. They are based on studies carried out by Babajimopoulos et al. using a CFD model coupled with a multi-zone detailed chemical kinetics solver (KIVA-3v-MZ) [6]. Chemical kinetics in this study were represented by a 197 species skeletal mechanism for isooctane fuel [7]. The authors reported that extensive parametric sweeps were performed using KIVA-3v-MZ, allowing several parameters to be varied, such as equivalence ratio, residual gas fraction level, engine speed and compression ratio. It was claimed that the effect of residual gas could be included by introducing a modified definition of equivalence ratio, Φ i.e.

$$\Phi' = \Phi(1 - RGF) \tag{2.4}$$

where *RGF* is the residual gas fraction. The new parameter Φ' represented the energy content of the charge. The parameters varied in the CFD simulations were Φ' (0.2 - 0.4), RGF (0 – 40%), fueling rate (7 – 14 mg/cycle) and engine speed (750 – 2000 RPM). The CFD results were analyzed and correlations were developed that capture HCCI combustion characteristics as functions of ignition timing, composition, engine speed and geometry. A summary of the correlations is given below.

Results from this study indicated that the most important factors determining burn rate characteristics were ignition timing θ_{IGN}, equivalence ratio Φ and engine speed. Despite the wide range of parameters, the authors found that data could be scaled by engine speed and equivalence ratio to generate well defined relationships suitable for curve fitting.

The following relationship defined the 0 – 50 % burn interval ($\theta_{0\text{-}50}$) vs. ignition timing (θ_{IGN}), scaled by *RPM* and Φ':

$$\theta_{0-50} = f_1(\theta_{IGN})\left(\frac{RPM}{2000}\right)^{0.3}\left(\frac{\phi'}{0.3}\right)^{-1.5} \tag{2.5}$$

The following relationship defined the 0 – 90 % burn interval ($\theta_{0\text{-}90}$) vs. location of 50 % heat release (θ_{50}), scaled by Φ':

$$\theta_{0-90} = f_2(\theta_{50})\left(\frac{\phi'}{0.3}\right)^{-1.1} \tag{2.6}$$

Once the ignition timing (θ_{IGN}) was determined by the auto ignition integral, the two previous relationships completely defined the mass fraction burned curve.

The last quantity required in order to define the energy release on an absolute basis was combustion efficiency. Babajimopoulos et al. showed that a very good correlation for combustion efficiency could be based on peak mean cylinder temperature. They reported that combustion efficiency decreased rapidly when peak temperature

dropped below 1500 K. They also observed similar behavior to that reported by Sjoberg and Dec [8]; the deteriorating combustion efficiency appeared to be strongly affected by poor CO to CO_2 conversion at low temperatures. They concluded that combustion efficiency can be represented by:

$$\eta_{comb} = f_3\left(T_{peak}\right) \tag{2.7}$$

In addition, they showed that the fuel mass fraction burned x_b can be represented by a Wiebe function:

$$x_b = \eta_{comb}\left[1 - e^{\left(-\left(\frac{\theta-\theta_{IGN}}{\Delta\theta}\right)^{W+1}\right)}\right] \tag{2.8}$$

where the coefficients W and $\Delta\theta$ are determined by fitting the burn curve through the 50 % and 90 % burn points.

Equations (2.2) to (2.8) define the burn curve, with the exception that at start of combustion, peak temperature and combustion efficiency in the cylinder are not known. That would be the case in an actual engine as well, since peak temperature and combustion efficiency can be measured after the combustion event has been completed. In order to resolve this, the authors used an efficient method, based on an approximate correlation of GT-Power which supplies peak temperature as a function of equivalence ratio, residual gas fraction, ignition temperature, location of 90 % heat release, and combustion efficiency:

$$T_{peak} = f_4\left(\phi, RGF, T_{ign}, \theta_{90}, \eta_{comb}\right) \tag{2.9}$$

They reported that equations (2.7) and (2.9) form a system of two equations and two unknowns that can be solved iteratively without going through the cycle calculation.

Heat Transfer

Babajimopoulos et al. reported that the sensitivity of HCCI combustion to temperature enhances the need for a reliable heat transfer model to calculate heat loss characteristics [3]. Chang et al. developed a heat transfer model at the University of Michigan specifically to describe heat transfer in HCCI engines [9]. The model is based on the known Woschni correlation, but its parameters were modified to better match the heat transfer characteristics observed in HCCI engine experiments. Modifications included use of the instantaneous cylinder height as the lengthscale, reduced temperature exponent and reduced characteristic velocity. The instantaneous heat transfer coefficient was given by:

$$h_m = a_{scaling} L^{-0.2} \cdot P^{0.8} \cdot T^{-0.73} \cdot w_m{}^{0.8} \tag{2.10}$$

where L is a characteristic lengthscale equal to the instantaneous cylinder height (m), P (kPa) and T (K) are instantaneous pressure and mean in-cylinder temperature respectively, and $\alpha_{scaling}$ is a constant between 10 and 12 which can be adjusted to describe specific engines.

In the same study, characteristic velocity w_m (m/s) was given by:

$$w_m = C_1 S_P + \frac{C_2}{6} \frac{V_d T_r}{P_r V_r} \left(P - P_{mot} \right) \tag{2.11}$$

where S_P is the mean piston speed (m/s), T_r (K), P_r (kPa) and V_r (m^3) are reference temperature, pressure and volume respectively, taken at a point just after intake valve closing, V_d (m^3) is the displaced volume and P_{mot} (kPa) is the motoring pressure. Chang et al. assumed that there is no swirl effect on characteristic velocity and they reported values of C_1 and C_2 to be 2.28 and 0.00324 respectively, which are identical to the original correlation by Woschni. Although the modified Woschni correlation originated from in-cylinder heat flux measurements, it was found that it underpredicted heat transfer. The result was overprediction of gross indicated efficiency values as will be shown in the

following chapters. Therefore, the classic Woschni heat transfer correlation was used in the simulations presented in this dissertation.

The research community has shown that ringing is the primary constraint when it comes to upper load limit of HCCI engines. Ringing phenomena result directly from fundamental characteristics of HCCI combustion. Compression ignition of a homogeneous charge results in very high heat release rates from the bulk of the cylinder charge. Pressure rise rates increase significantly, resulting in ringing combustion which is similar in nature to end gas knock observed in SI engines. In order to quantify knock during HCCI combustion, Eng [10] introduced in 2002 a measure of the cylinder pressure acoustic intensity which he called Ringing Intensity (R.I.):

$$R.I. = \frac{1}{2\gamma} \frac{\left(\beta \left. \frac{dP}{dt} \right|_{\max} \right)^2}{P_{\max}} \sqrt{\gamma R T_{\max}} \tag{2.12}$$

where $\left. \frac{dP}{dt} \right|_{\max}$ is the maximum pressure rise rate (kPa/ms), P_{max} (Pa) is the maximum cylinder pressure, T_{max} (K) is the maximum cylinder temperature, γ is the ratio of specific heats, R (J/kg/K) is the gas constant and β is an empirical coefficient that relates the pressure pulsation amplitude to the maximum rate of pressure rise. In this study, the value of β is recommended to be 0.05 [10]. The units of R.I. resulting from equation (2.12) are MW/m^2. R.I. was used throughout the studies presented in this dissertation in order to characterize ringing limit during HCCI combustion. The upper limit was set at 6 MW/m^2, which is a value widely accepted by the research community based on actual acoustic testing.

NO_x emissions calculations were performed by a submodel implemented in the GT-Power user subroutines and was described by Babajimopoulos et al. [3]. This model employed the widely used Zeldovich mechanism as described by Heywood [11] and includes the reactions:

$$O + N_2 \leftrightarrow NO + N$$

$$N + O_2 \leftrightarrow NO + O$$

$$N + OH \leftrightarrow NO + H$$

By applying partial equilibrium approximation, the molar rate of formation of NO can be calculated as:

$$\frac{dn_{NO}}{dt} = 2V_b\left(1 - a^2\right)\frac{R_1}{1 + a\dfrac{R_1}{R_2 + R_3}} \tag{2.13}$$

Where

$$R_1 = 1.6E7 \cdot [NO] \cdot [N] \tag{2.14}$$

$$R_2 = 1.5E3 \cdot T_b \exp\left(\frac{-19500}{T_b}\right) \cdot [NO] \cdot [O] \tag{2.15}$$

$$R_3 = 2.0E8 \cdot T_b \exp\left(\frac{-23650}{T_b}\right) \cdot [NO] \cdot [H] \tag{2.16}$$

$$a = \frac{[NO]}{[NO]_{eq}} \tag{2.17}$$

The terms in square brackets represent concentration of species (mol/m^3), V_b is the volume of the burned zone (m^3) and T_b is the temperature of the burned zone, which is calculated by GT-Power based on a 2-zone representation of the combustion chamber. NO_x emissions in this text are presented as NO_x emissions index ($EINO_x$ in g NO/kg fuel). They were calculated by integration of NO production in the cylinder and reported per amount of fuel injected in the cylinder.

Combining the models described above provided a very powerful tool for system level simulations. It captured the key characteristics of HCCI combustion such as ignition timing, burn duration and combustion efficiency while being computationally

inexpensive and robust. The following section will describe the framework used for second law analysis which was also combined with the HCCI models presented.

2.4 Second-law Analysis

Internal combustion engine modeling is generally based on traditional first law analysis and this is the case with the models described in the previous section. However, it has long been understood that first law analysis has limitations that do not allow engineers to gain absolute insight into the fundamentals of engine operation. Second law analysis can provide a solution to that challenge by providing the means to evaluate inefficiencies associated with various engine processes, and it has been applied to internal combustion engine studies for more than four decades.

2.4.1 Availability Concept

Second law analysis is based on the concept of availability or exergy. These two terms will be used interchangeably in this dissertation. Also, the letter A will be used to represent availability or exergy so that here is no confusion with Φ used for equivalence ratio. Availability represents the potential of a system to produce useful work. It is defined as the maximum theoretical work output that can be produced by bringing a system into equilibrium with a reference environment. This is a general statement and it includes work that can be obtained by exploiting differences in velocity, potential energy, temperature, pressure and composition between the system and the environment.

For a closed system undergoing only heat and work transfers with the environment, the thermomechanical availability can be defined as:

$$A_{tm} = (E - U_0) + p_0(V - V_0) - T_0(S - S_0) \tag{2.18}$$

where $E = E_K + E_p + U$ is the sum of kinetic, potential and internal energies, p_0 and T_0 are the pressure and temperature of the environment and U_0, V_0 and S_0 are the internal energy, volume and entropy of the system at p_0 and T_0 respectively.

From the definition of availability, we can conclude that it is an extensive property [13]. Availability depends on both the state of the system and the state of the environment; it is a measure of a system's thermodynamic potential relative to the chosen environment [17]. From the definition, one can also deduce that the availability of a system is zero when thermal, mechanical and chemical equilibrium exist with the chosen environment. Thermal equilibrium exists when the temperature of the system and the environment are equal; mechanical equilibrium exists when the pressure of the system and the environment are equal. Chemical equilibrium exists when the composition of the system and the environment are equal. Equivalently, when there are no species in the system that can interact with others in the environment to produce useful work. Several studies have suggested that chemical availability should not be taken into account when studying internal combustion engines, since its recovery cannot be realized in practical systems [14, 15, 16, 18]. Flynn et al. even suggested that the thermal availability term not be included, since it could only be recovered in stationary applications [14]. Some of these studies were presented a few decades ago and have proposed solutions based on the available technology of the time. However, technology has progressed and novel solutions can now be applied for the recovery of exhaust gas thermal availability. For that reason, the thermal component was included in availability calculations in this dissertation. However, the chemical component was not included, since the composition of exhaust gas cannot be used to produce useful work. It should be noted that the working fluid was not considered to be of uniform composition; however, its potential to produce useful work due to compositional differences with the environment was neglected.

2.4.2 Dead or Reference State

When thermal, mechanical and chemical equilibria are attained and the system is at rest and zero elevation relative to the reference environment, no further potential exists for work production. At these conditions, the system is considered to be at the dead state [17]. For the purposes of internal combustion engine studies, the dead state is defined to have the same composition as the given state; therefore no work potential exists due to compositional differences. Strictly, this is a restricted dead state since composition is assigned to be the same as the given state, but it will be referred to as dead state in this text [23]. In the availability calculations performed in this dissertation, pressure and temperature at the dead state where p_0 = 1.01325 bar and T_0 = 298.15 K. In case that the dead state undergoes any changes, these changes will be reflected in the value of system availability.

2.4.3 General Availability Balance Equation

For an open system (control volume) exchanging mass with the surrounding environment, the rate of change of total availability can be expressed as [13]:

$$\frac{dA_{CV}}{dt} = \sum\left(1-\frac{T_0}{T}\right)\dot{Q}_{CV} - \dot{W}_{CV} + p_0\frac{dV}{dt} + \sum \dot{m}_i b_i - \sum \dot{m}_e b_e - \dot{I} \qquad (2.19)$$

where:

- $\frac{dA_{CV}}{dt}$ is the rate of change of total control volume exergy,
- $\sum\left(1-\frac{T_0}{T}\right)\dot{Q}_{CV}$ is the availability transfer associated with heat transfer from the working fluid to the surroundings, where T is the temperature at the system boundary and $\dot{Q}_{CV}$ is the heat transfer rate at the system boundaries,

- $-\dot{W}_{CV} + p_0 \frac{dV}{dt}$ are the availability terms associated with shaft or boundary work,
- $\sum \dot{m}_i b_i$ and $\sum \dot{m}_e b_e$ are the availability terms associated with influx and efflux respectively. The terms b_i and b_e are the specific flow exergies and are given by:

$$b_j = h_j - h_0 - T_0(s_j - s_0) \tag{2.20}$$

where h_j and s_j are the system specific enthalpy and entropy respectively,

- and $\dot{I}$ it the rate of exergy destruction (irreversibility) in the control volume.

Equation (2.19) states that the rate of exergy storage is equal to the rate of transfer by heat plus the rate of transfer by shaft or boundary work plus the rate of transfer by flow minus the exergy destruction.

2.4.4 Fuel Availability

Chemical availability of the fuel on a molar basis can be defined as [23]:

$$\bar{a}_{fch}(T_0, p_0) = \bar{g}_f(T_0, p_0) - \left(\sum_P x_P \bar{\mu}_P^0 - \sum_R x_R \bar{\mu}_R^0 \right) \tag{2.21}$$

where index *P* denotes product species, index *R* denotes reactant species and the overbar denotes molar properties. For liquid hydrocarbon fuels of the type C_zH_y that are pertinent to internal combustion engine studies the above expression can be approximated by:

$$a_{fch} = LHV\left(1.04224 + 0.011925\frac{y}{z} - \frac{0.042}{z}\right) \tag{2.22}$$

where LHV is the fuel lower heating value [23]. The latter expression has been used for availability calculations in this dissertation and it assumes no oxygen and sulfur content in the fuel.

2.4.5 Engine Cylinder Availability Balance

By considering the engine cylinder as the control volume, the general availability balance equation (2.19) can be written on a crank angle basis as:

$$\frac{dA_{cyl}}{d\theta} = \frac{d\dot{m}_{in}}{d\theta} b_{in} - \frac{d\dot{m}_{exh}}{d\theta} b_{exh} - \frac{dA_W}{d\theta} - \frac{dA_Q}{d\theta} + \frac{dA_f}{d\theta} - \frac{dI}{d\theta} \tag{2.23}$$

where $\dot{m}_{in}$ is the intake mass flow rate, $\dot{m}_{exh}$ is the exhaust mass flow rate, b_{in} is the intake flow availability and b_{exh} is the exhaust flow availability.

The rest of the terms on equation (2.23) are described in the following:

$$\frac{dA_W}{d\theta} = \left(p_{cyl} - p_0\right)\frac{dV}{d\theta} \tag{2.24}$$

is the net rate of availability transfer to the piston associated with indicated work, where $\frac{dV}{d\theta}$ is the rate of change of cylinder volume and p_{cyl} is the instantaneous cylinder pressure.

$$\frac{dA_Q}{d\theta} = \left(1 - \frac{T_0}{T_{cyl}}\right)\frac{dQ}{d\theta} \tag{2.25}$$

is the rate of availability transfer associated with heat transfer from the working fluid to the cylinder walls, where T_{cyl} is the instantaneous cylinder temperature. It should be noted that in the current formulation, the system is considered to be the entire cylinder with its boundaries being the cylinder walls. Therefore, heat is considered to be transferred from a mean temperature working fluid to the cylinder walls. A few studies in the literature have followed different approaches, where heat loss was considered part of the irreversibilities and was added to the combustion irreversibilities [16]. In that case, the cylinder was considered an open thermodynamic system at steady state. It should be noted that the exergy transferred to the walls through heat transfer is a large part of the fuel exergy. However, it is almost completely destroyed once it is transferred to the cooling medium, since its recovery potential is minimal.

$$\frac{dA_f}{d\theta} = \frac{dm_{fb}}{d\theta}\alpha_{fch} \tag{2.26}$$

is the rate of availability input to the cylinder through burned fuel, where α_{fch} is the fuel chemical availability as defined in equation (2.22). This expression includes the availability input associated with flow work and the thermomechanical and chemical availabilities of the fuel.

The last term that needs to be defined is the rate of change of total cylinder availability and it can be derived from the definition of exergy as the maximum available work at a given state of a system:

$$A = ma = m(e - e_0) + p_0 m(v - v_0) - T_0 m(s - s_0) \tag{2.27}$$

The rate of change of A on a crank angle basis becomes:

$$\frac{dA}{d\theta} = \frac{dme}{d\theta} - e_0\frac{dm}{dt} + p_0\frac{dV}{d\theta} - p_0 v_0\frac{dm}{d\theta} - T_0\frac{dms}{d\theta} + T_0 s_0\frac{dm}{d\theta} \tag{2.28}$$

or

$$\frac{dA}{d\theta} = \frac{dme}{d\theta} + p_0\frac{dV}{d\theta} - T_0\frac{dms}{d\theta} - (h_0 - T_0 s_0)\frac{dm}{d\theta} \tag{2.29}$$

where the dead state enthalpy is $h_0 = e_0 + p_0 v_0$.

The last term in equation (2.29) can be expressed by making use of the chemical potential expression for every species in the mixture:

$$\mu_i = g_i(T, p_i) \tag{2.30}$$

where the Gibbs function is $g = h - Ts$.

By combining the above expressions we can express the rate of change of total cylinder exergy as:

$$\frac{dA_{cyl}}{d\theta} = \frac{dU}{d\theta} + p_0 \frac{dV}{d\theta} - T_0 \frac{dS}{d\theta} - \sum_i \frac{dm_i}{d\theta} \mu_{i,0} \tag{2.31}$$

In the above equations, the Gibbs function was used to calculate the chemical potential of species i at the dead state. Use of the species chemical potential was essential for cylinder availability calculations during the combustion event. However, the chemical availability of the charge was neglected as explained in the previous sections. By using the Gibbs function and not the exact definition of availability ($a = u - T_0 s$), an assumption is introduced, which is the use of fuel lower heating value at T_0 instead of T for all exergy calculations.

2.4.6 Cylinder Irreversibilities

After all the availability transfer and storage terms in equation (2.31) had been explicitly expressed, it could be solved to calculate the rate of change of exergy destruction in the cylinder $\frac{dI}{d\theta}$. Cylinder irreversibilities resulted primarily from the combustion process. Other physical processes such as viscous dissipation, throttling through the valves and mixing contributed to availability destruction as well. Dunbar and Lior showed that there are four physicochemical processes that take place during combustion and are the primary contributors to global entropy generation [19]: Reactant diffusion, fuel oxidation, internal thermal energy exchange and product mixing. The vast majority of second law analysis studies in the literature have treated friction irreversibilities separately from the rest of the irreversibilities. In these cases, friction irreversibilities were computed as the difference between indicated and brake work.

Van Gerpen and Shapiro presented a rigorous development of availability balance equations and used the entropy equation to calculate entropy generation and the irreversibilities [17]:

$$\frac{dS}{d\theta} = \dot{m}_{in} s_{in} - \dot{m}_{exh} s_{exh} + \frac{\dot{Q}}{T_{cyl}} + \dot{S}_{GEN} \tag{2.32}$$

where $\dot{S}_{GEN}$ is the rate of total entropy generation. A similar approach was followed by several other research groups as well. It should be noted that the nature of the combustion model used in this dissertation hindered the use of the entropy equation. Therefore cylinder irreversibilities were calculated through the cylinder availability balance equation (2.23).

2.4.7 First-law Analysis Dependency

The fact that the second law analysis presented in this dissertation was performed as post-processing of engine simulation results meant that it was based on traditional first law analysis of engine and cylinder processes. First law analysis was performed within the GT-Power framework aided by the University of Michigan combustion and heat transfer models.

By examining the availability terms that appear in the cylinder availability balance equation (2.23), we can identify quantities that needed to be derived from the first law analysis. Equation (2.24) expressed the net rate of availability transfer to the piston associated with indicated work, where instantaneous cylinder pressure p_{cyl} was an output from the first law analysis. The same holds for instantaneous cylinder temperature T_{cyl} and the rate of heat transfer $dQ/d\theta$ in equation (2.25). Specifically, the rate of heat transfer was supplied by the University of Michigan HCCI heat transfer model that was described in the previous sections. The last quantity that was supplied by the first law analysis was the burn rate that appeared in equation (2.26) and was needed to calculate the rate of availability input to the cylinder through burned fuel. Burn rate was a direct result of the UM HCCI combustion model that was described in the previous sections as well.

2.4.8 Engine Subsystems Availability Balance

Complete multi-cylinder engine modeling using the GT-Power framework allowed extension of the exergy analysis to other engine subsystems such as intake and exhaust manifolds, turbocharger and aftercooler. By following a similar approach to the one presented in equation (2.19) for cylinder availability balance, similar equations for the engine subsystems can be derived.

Intake Manifold

The exergy balance for the intake manifold can be described as:

$$\frac{dA_{IM}}{d\theta} = \frac{dm_{in}}{d\theta} b_{in} - \frac{dm_{out}}{d\theta} b_{out} - \frac{dI_{IM}}{d\theta} \tag{2.33}$$

where b_{in} and b_{out} are the flow exergies downstream of the aftercooler and at the intake ports respectively. I_{IM} are the irreversibilities at the intake manifold which result from mixing of hot and cold gases and viscous dissipation. The literature has shown that inlet manifold irreversibilities are very low and account for less that 1 % of fuel chemical exergy [23]. Heat losses are generally neglected for intake manifold flows since the gas temperature is similar to that of the manifold walls.

Exhaust Manifold

The exergy balance for the exhaust manifold can be described in a similar manner:

$$\frac{dA_{EM}}{d\theta} = \frac{dm_{in}}{d\theta} b_{in} - \frac{dm_{out}}{d\theta} b_{out} + \frac{dA_{Q,EM}}{d\theta} - \frac{dI_{EM}}{d\theta} \tag{2.34}$$

where b_{in} and b_{out} are the flow exergies at the exhaust ports and at the turbine inlet respectively. $A_{Q,EM}$ is the exergy transfer in the exhaust manifold associated with heat

transfer from the hot exhaust gases to the manifold walls. They can be calculated in the same manner as that of cylinder heat transfer:

$$\frac{dA_{Q,EM}}{d\theta} = \left(1 - \frac{T_0}{T_{EM}}\right)\frac{dQ_{EM}}{d\theta} \tag{2.35}$$

where $dQ_{EM}/d\theta$ is the rate of heat transfer in the exhaust manifold and T_{EM} is the temperature of the exhaust gas in the manifold. I_{EM} in equation (2.34) are the irreversibilities in the exhaust manifold and they were calculated from the balance equation. Several second law analysis studies have shown that exergy destruction results from throttling across the exhaust valves, mixing between hot and cold gases in the manifold and fluid friction with the walls. Rakopoulos and Giakoumis modeled a medium-duty diesel engine and showed that exhaust manifold irreversibilities accounted for 1.5 – 3 % of fuel chemical exergy [23]. They also noted that turbocharged engines exhibited increased irreversibilities compared to naturally aspirated ones since exhaust backpressure increased and fluid motion was more vigorous. The present research work showed that low temperature combustion engines may suffer less exhaust manifold irreversibilities; exhaust temperatures are lower than those of high temperature combustion engines thus reducing heat losses to the manifold walls. However, in the case of boosted LTC engines, backpressure development may act to increase exhaust irreversibilities.

Turbocharger

In order to study the exergy balance of the turbocharger it is useful to distinguish between the compressor and turbine as control volumes. Starting from the compressor, the exergy balance can be expressed as:

$$-\frac{dW_C}{d\theta} = \frac{dm_{in}}{d\theta}b_{in} - \frac{dm_{out}}{d\theta}b_{out} - \frac{dI_C}{d\theta} \tag{2.36}$$

where W_C is the compressor work, b_{in} and b_{out} are the flow exergies at the inlet and outlet of the compressor respectively and I_C are the compressor irreversibilities. The negative sign of the compressor work in the above equation expresses the fact that work is an input to the compressor.

The exergy balance for the turbine can be expressed in a similar fashion:

$$\frac{dW_T}{d\theta} = \frac{dm_{in}}{d\theta} b_{in} - \frac{dm_{out}}{d\theta} b_{out} - \frac{dI_T}{d\theta} \tag{2.37}$$

where W_T is the compressor work, b_{in} and b_{out} are the flow exergies at the inlet and outlet of the turbine respectively and I_T are the turbine irreversibilities. The positive sign of the turbine work in the above equation expresses the fact that work is an output from the turbine. The exergy balance equations presented above implicitly assume adiabatic treatment of turbomachines; therefore heat losses within the devices are neglected. The literature has shown that irreversibilities result primarily from fluid friction within the impellers. Bozza et al. presented exergy balance for the entire turbocharger including transient effects which described the kinetic energy variation of the rotors and the connecting shaft. Transient analysis was out of the scope of the present research work though.

Intercooler/Aftercooler

The last engine subsystem that can be of interest in an exergy analysis is the intercooler of aftercooler depending on the boosting system setup. The availability balance for an aftercooler can be expressed as [23]:

$$\Delta A_w = \frac{dm_{in}}{d\theta} b_{in} - \frac{dm_{out}}{d\theta} b_{out} - \frac{dI_{AC}}{d\theta} \tag{2.38}$$

where b_{in} and b_{out} are flow exergies at the aftercooler inlet and outlet respectively and I_{AC} are the irreversibilities. The term ΔA_w represents the exergy difference of the cooling

medium as it is used to cool the compressed gas flowing through the aftercooler. It can be calculated as:

$$\Delta A_w = \frac{dm_w}{d\theta}\left(b_{w,out} - b_{w,in}\right) \tag{2.39}$$

where $dm_w/d\theta$ is the mass flow rate of cooling medium through the aftercooler and $b_{w,out}$ and $b_{w,in}$ are the flow exergies of the cooling medium at the inlet and outlet sides of the cooler. The exergy loss observed in an aftercooler is primarily a result of heat transfer from the compressed gas to the wall of the cooler. Naturally, exergy loss increases as the difference between compressed gas temperature and cooling medium increases. As mentioned earlier in the discussion on cylinder heat transfer, availability transfer from a hot gas to a cooling medium is not desirable since it cannot be recovered. Therefore, cooling the hot air that will be used for work production does not make sense from a second law perspective. This argument is going to be augmented by other factors affecting engine performance when multi-cylinder HCCI results will be discussed in the following chapters. However, cooling the intake air can be often necessary, especially when it is involved in boosted stoichiometric SI engine operation.

2.4.9 Second-law efficiency

Second law efficiency can be used to compare different engine systems from a second law perspective. It can be generally defined as the availability output versus the availability input and it shows how effectively the fuel availability is converted into useful work. A few studies in the literature have used the Greek letter ε (epsilon) for the second law efficiency. The same letter is going to be used throughout this dissertation in order to avoid any confusion with the first law efficiency η (eta).

By considering the concept of availability, a fundamental difference between first and second law efficiency can be identified [23]; first law efficiency takes into account

energy losses while second law efficiency includes exergy losses and exergy destruction (irreversibilities). The fact that energy is conserved means that first law efficiencies do not indicate internal irreversibilities of the system.

Cylinder

For an engine cylinder, second law efficiency on an indicated basis can be defined as:

$$\varepsilon_{cyl,d} = \frac{W_{i,d}}{A_f} \tag{2.40}$$

where $W_{i,d}$ is indicated work and A_f is total fuel availability [23]:

$$A_f = m_f a_{fch} = a_{fch} \int_0^{720} \frac{dm_{f,b}}{d\theta} d\theta \tag{2.41}$$

where m_f is the amount of fuel mass injected per cycle and $dm_{f,b}/d\theta$ is the burn rate.
On a brake basis the cylinder second law efficiency would be:

$$\varepsilon_{cyl,b} = \frac{W_b}{A_f} \tag{2.42}$$

where W_b is brake work. The equivalent first law efficiency would be:

$$\eta_b = \frac{W_b}{m_f Q_{LHV}} \tag{2.43}$$

where Q_{LHV} is the fuel lower heating value. By using equation (2.22), one can calculate the ratio of fuel chemical exergy to fuel lower heating value. For the isooctane fuel used in this dissertation that ratio is 1.0638. The fact that chemical exergy is about 6 % higher than the fuel LHV means that second law efficiencies are always somewhat lower that their first law equivalents.

Engine system

The brake second law efficiency shown in equation (2.42) can be also used to describe the whole engine system. In that case, total brake work and total fuel mass would be accounted for:

$$\varepsilon_{eng} = \frac{W_{b,eng}}{A_{f,eng}} \tag{2.44}$$

where $W_{b,end}$ is engine brake work and $A_{f,eng}$ is total fuel availability.

Additional total engine exergy efficiency can be defined in a similar way by taking into account the availability of the exhaust gases:

$$\varepsilon_{eng,tot} = \frac{W_{b,eng} + A_{exh,tot}}{A_{f,eng}} \tag{2.45}$$

where $A_{exh,tot}$ is total availability of the exhaust gases exiting the turbine and it can be defined as:

$$A_{exh,tot} = \int_{0}^{720} \frac{dm_{exh}}{d\theta} b_{T,exh} d\theta \tag{2.46}$$

where $b_{T,exh}$ is flow availability of the exhaust gases downstream of the turbine. Rakopoulos et al. studied a medium duty IDI diesel engine operating at 1500 rpm and they reported 40.31 % cylinder exergy efficiency but 42.9 % net indicated (first-law) efficiency [23]. The authors also reported that the engine exergy efficiency was 40.31 %, but that climbed to 53.76 % when availability of the post-turbine exhaust gases was taken into account. Farrell et al. showed engine exergy efficiencies around 40 % for an ultra-lean burn DISI engine operating at 20 % to 60 % load [22]. It was shown that exergy efficiency reduced as load increased above 60 %, as a result of increasing fractions of fuel availability being transferred out of the cylinder with exhaust gases. Alkidas studied a single-cylinder diesel engine under steady-state operation and reported brake exergy efficiency of 38 % when operating at 1200 rpm and 10.83 bar BMEP [16].

Turbocharger

Exergy efficiencies can also be defined for the turbocharger by taking into account inlet and discharge flow availabilities as well as work involved in the compression or expansion processes. Starting from the compressor, its exergy efficiency can be defined as:

$$\varepsilon_C = \frac{\dot{m}_C \left(b_{C,out} - b_{C,in} \right)}{\left| \dot{W}_C \right|} \tag{2.47}$$

where $b_{C,out}$ and $b_{C,in}$ are the flow exergies at the discharge and inlet of the compressor respectively. Compressor power that appears on the denominator in equation (2.47), is negative since it is an input to the compressor; therefore its absolute value can be used for the exergy efficiency calculation.

A similar definition can be used for turbine exergy efficiency:

$$\varepsilon_T = \frac{\dot{W}_T}{\dot{m}_T \left(b_{T,in} - b_{T,out} \right)} \tag{2.48}$$

where $b_{T,out}$ and $b_{T,in}$ are flow exergies at the discharge and inlet of the turbine respectively. Turbine power that appears on the numerator in equation (2.48) is positive since it is an output from the turbine. As mentioned previously, adiabatic treatment of turbomachines is an underlying assumption for the formulation of the above set of equations. In addition, the kinetic and potential energy of the gas were neglected.

A question that is commonly raised is how the isentropic and exergy efficiencies of turbomachines differ. Both can be classified as second law efficiencies but they describe different processes. Isentropic efficiency describes how close the actual compression or expansion process is to the isentropic compression or expansion. The turbine exergy efficiency describes how well the exhaust gas exergy is converted to useful work. In the compressor case, exergy efficiency describes how well the compressor work is converted to inlet air exergy. In the turbine case, exergy efficiency

describes how well the exhaust gas exergy is converted to useful work at the turbine shaft. Despite the fact that isentropic and exergy efficiencies are different metrics, they are connected. Increasing isentropic efficiencies lead to increased exergy efficiencies since the actual compression or expansion processes approach the ideal processes more. That would lead to increasing exploitation of the shaft work or exhaust exergy respectively. The diesel engine study by Rakopoulos et al. showed compressor and turbine exergy efficiencies of 76.4 % and 87.4 % respectively [23].

Exhaust manifold

In his diesel engine availability study, Alkidas also defined an exhaust efficiency metric as [16]:

$$\varepsilon_{exh} = \frac{W_{exh,\max}}{E_{exh}} \tag{2.49}$$

where $W_{exh,max}$ is the availability (or maximum extractable work) of the exhaust gases and $E_{exh} = m_{exh}(h_{exh} - h_0)$ is the thermal energy of the exhaust gases. The author showed that exhaust efficiency was always lower than 50 % which meant that less than 50 % of the exhaust gas energy could be recovered as useful work by any means.

The UM combustion and heat transfer models coupled to the availability analysis equations described in this section, created a framework for second-law analysis of LTC engines. The fact that exergy analysis literature has focused on traditional engine concepts (mainly diesel engines) allows for original contributions in the field of LTC engine simulation and analysis. The following section will describe the methodology followed for model performance evaluation, multi-cylinder engine simulation and second law analysis.

2.5 Methodology

The present research work will be displayed in three steps: the first one is combustion and heat transfer model performance evaluation. The second one is multi-cylinder engine simulation using the calibrated combustion model and the third one is second law analysis of LTC engines. Accomplishing these tasks would not be possible without the appropriate research methodology and use of the tools that were described in previous sections. The current section will attempt to display the individual methodology behind the three steps in order to facilitate understanding of the results that will be presented in the following chapters.

2.5.1 Combustion Model Performance evaluation

Calibrating the UM HCCI combustion and heat transfer models was crucial for the present research work since they form the basis for any single-cylinder or multi-cylinder engine simulation. It is also a highly instructive task since it gives the researcher the chance to consolidate experimental and modeling results and through that, to identify critical phenomena that take place in LTC engines which need to be accurately simulated.

The experimental datasets that were used to evaluate the performance of the UM HCCI models were sourced from three different engine setups. The first one was a single cylinder SI research engine that was modified in order to operate in naturally aspirated and boosted HCCI modes. The specifications of that engine are shown in Table 2.1. This engine is present at the University of Michigan W. E. Lay Automotive Laboratory and has been primarily used to investigate boosted high load HCCI operation. It is going to be referred to as GM boosted engine in this dissertation. For performance evaluation purposes, intake pressure and load sweeps were performed; the sweeps were subsequently simulated in order to assess model performance at high intake pressure HCCI combustion.

Table 2.1 – GM boosted engine specifications

Cylinder displacement (L)	0.55
Bore/Stroke (mm)	86/94.6
Connecting Rod Length (mm)	152.2
Compression Ratio	12.5:1
Number of valves	4
Fuel Type	87 ON Gasoline
Valve Profiles	4 mm lift/ 120 CAD duration
Symmetric NVO	72 – 178 CAD
Fueling Method	Direct Injection

The second dataset used for model performance evaluation originated from a similar single cylinder SI research engine that was also modified to operate on HCCI mode [27]. This engine is also present at the W. E. Lay Automotive Laboratory and it features a unique Fully Flexible Valve Actuation (FFVA) system that allows electrohydraulic control of the valve events. It is going to be referred to as FFVA engine in this dissertation and its specifications can be seen in Table 2.2. Additional information on the valve events and the gas exchange process will be provided in the following chapter.

Results from the FFVA engine consisted of an HCCI combustion phasing sweep at naturally aspirated conditions and at a load level of around 3.5 bar IMEPn. Simulating that kind of operation allowed the assessment of model performance when combustion occurred early or late in the cycle.

Table 2.2 – FFVA engine specifications

Cylinder displacement (L)	0.55
Bore/Stroke (mm)	86/94.6
Connecting Rod Length (mm)	152.2
Compression Ratio	12.41:1
Number of valves	4
Fuel Type	87 ON Gasoline
Valve Profiles	Variable lift/ variable duration
Head Design	Pent-roof
Fueling Method	Direct Injection

The third dataset that was used for model performance evaluation and calibration was generated at Sandia National Laboratories using a single-cylinder medium-duty diesel engine that was modified to operate on HCCI mode. It is going to be referred to as Sandia engine in this dissertation and its specifications are shown in the following table:

Dec et al. have published several studies using this specific engine setup, but the one being especially interesting for model performance evaluation purposes was presented by that group in 2010 [26]. The authors investigated high load boosted HCCI operation on conventional gasoline fuel and made use of external EGR to achieve high load and high efficiency levels. Its importance lies in the fact that mixture preparation was performed in a different way compared to the GM boosted and FFVA engines. Instead of trapping residual gas for charge heating on a cycle basis, the authors used intake preheating and introduced external EGR when ignition needed to be phased later in the cycle. Their method of mixture preparation appeared particularly interesting for modeling purposes because the errors in estimating residual gas fraction were much

smaller than for the NVO engines. Therefore, it was deemed necessary that the UM HCCI combustion model be evaluated against the Sandia engine data.

The performance evaluation process was the same for all three datasets and it was initiated by Three Pressure Analysis (TPA). TPA utilized instantaneous intake, exhaust and cylinder pressures which were measured in the respective experiments, in order to assess the gas exchange description capability of the models. After the gas exchange processes had been assessed, the performance of the heat transfer models was evaluated based on comparison of closed cycle parameters between the experiments and the simulations. By calibrating the gas exchange and heat transfer models, good agreement on charge mass and heat transfer rates between the experiment and simulation could be achieved. The final step in the performance evaluation and calibration process was associated with HCCI ignition timing and burn rates. The forward calculation HCCI model was assessed by making use of all the calibration parameters that appeared in the previous steps of the process. Experimental results were compared to forward calculations so that potential differences in ignition timing and burn rates could be identified. The findings of the performance evaluation process will be presented in detail in chapter 3 and details about modeling of critical phenomena will be discussed.

Table 2.3 – Sandia engine specifications

Cylinder displacement (L)	0.981
Bore/Stroke (mm)	102/120
Connecting Rod Length (mm)	192
Compression Ratio	14:1
Number of valves	4
IVO/IVC	0 CAD/202 CAD
EVO/EVC	482 CAD/8 CAD
Swirl Ratio	0.9
Fueling System	Fully premixed
Engine Speed (RPM)	1200
Intake Temperature (° C)	45 – 146
Intake Pressure (bar abs.)	1 – 3.25
Coolant Temperature (° C)	100

2.5.2 Multi Cylinder Engine Simulations

After the performance evaluation process had been completed, the calibrated combustion and heat transfer models were used to perform multi-cylinder engine simulations. The goal behind these simulations was to integrate advanced combustion, boosting, VVA strategies and EGR in order to investigate HPLB engines as systems and characterize the trade-offs involved in their operation. That goal was achieved by making extensive use of multi-cylinder engine models that featured different boosting systems, VVA strategies, different methods of mixture preparation and different compression ratio levels. All of these models were operated using a unique setup that allowed the user to interactively change various engine parameters during runtime. This setup is going to be

referred to as virtual dyno in this dissertation. The term virtual dyno was established because the interactive way of operating the engine models resembled the operation of actual engine dynamometers.

Chapter 4 will present and analyze a collection of multi-cylinder engine studies that were performed using the virtual dyno tool. These studies were focused on investigating and understanding the effects of intake temperature on high load HCCI operation, the combination of VVA and boosting and the trade-offs involved, the differences between negative and positive valve overlap strategies for mixture preparation and combustion control, the effects of compression ratio level on high load HCCI operation and the effects of external EGR use on combustion and engine system behavior.

2.5.3 Second Law Analysis

Second law analysis of LTC engines will be presented in Chapter 5 and it was based on the multi cylinder engine simulations described above. The availability analysis framework presented in section 2.4 was implemented in MATLAB as post-processing of the results generated by GT-Power simulations. Coupling multi-cylinder engine simulations to the availability analysis framework enabled investigation of multiple engine systems from a second law perspective and assessment of different techniques associated with boosting, VVA and EGR use.

This chapter presented the motivation behind the proposed research work, set the research objectives, gave a detailed description of the tools used and outlined the methodology employed to reach the research goals. The following chapter will present the HCCI combustion model performance evaluation and calibration effort and analyze the results obtained.

2.6 References

1. Assanis, D.N., Lavoie, G. L. and Ortiz-Soto, E., "Thermodynamic Sweet Spot Under Highly Dilute and Boosted Gasoline Engine Conditions", SAE 2011 High Efficiency IC Engines Symposium, April 10-11, 2011, Detroit, MI

2. Gamma Technologies, Inc., http://www.gtisoft.com

3. Babajimopoulos, A., Challa, V.S.S.P., Lavoie, G.A. and Assanis, D.N., 2009, "Model-Based Assessment of Two Variable Cam Timing Strategies for HCCI Engines: Recompression vs. Rebreathing," ICES2009-76103, Proceedings of the ASME Internal Combustion Engine Division, Milwaukee, WI

4. Livengood, J.C. and Wu, P.C. 1955, "Correlation of Autoignition Phenomena in Internal Combustion Engines and Rapid Compression Machines," *Proceedings of the Combustion Institute*, **5**, pp. 347-356.

5. He, X., Donovan, M.T., Zigler, B.T., Palmer, T.R., Walton, S.M., Wooldridge, M.S. and Atreya, A., 2005, "An Experimental and Modeling Study of Iso-octane Ignition Delay Times at Homogeneous Charge Compression Ignition Conditions," *Combustion and Flame*, **142**(3), pp. 266-275

6. Babajimopoulos, A., Assanis, D.N., Flowers, D.L., Aceves, S.M. and Hessel, R.P., 2005, "A fully coupled computational fluid dynamics and multi-zone model with detailed chemical kinetics for the simulation of premixed charge compression ignition engines," *International Journal of Engine Research*, **6**(5), pp. 497-512.

7. Aceves, S.M., Martinez-Frias, J., Flowers, D., Smith, J.R., Dibble, R., and Chen, J.Y., 2002, "A Computer Generated Reduced Iso-Octane Chemical Kinetic Mechanism Applied to Simulation of HCCI Combustion," SAE 2002-01-2870

8. Sjoberg, M. and Dec, J.E., 2005, "An investigation into lowest acceptable combustion temperatures for hydrocarbon fuels in HCCI engines," *Proceedings of the Combustion Institute*, Livermore, CA

9. Chang, J., Guralp, O., Filipi, Z., Assanis, D., Kuo, T., Najt, P. and Rask, R., "New Heat Transfer Correlation for an HCCI Engine Derived from Measurements of Instantaneous Surface Heat Flux", SAE Paper 2004-01-2996, 2004

10. Eng, J.A., "Characterization of Pressure Waves in HCCI Combustion", SAE 2002-01-2859

11. Heywood, J.B., 1988, *Internal Combustion Engine Fundamentals*, McGraw-Hill Inc.

12. Lavoie, G. A., Martz, J., Wooldridge, M. and Assanis, D., "A Multi-mode Combustion Diagram for Spark Assisted Compression Ignition", *Combustion and Flame*, 157 (2010) 1106-1110, 2010

13. Sonntag, R. E., Borgnakke, C. and Van Wylen, G. J., *Fundamentals of Thermodynamics*, 6th edition, Wiley, 2003

14. Flynn, P. F., Hoag, K. L., Kamel, M. M. and Primus, R. J., "A New Perspective on Diesel Engine Evaluation Based on Second Law Analysis", SAE Paper 840032, 1984

15. Primus, R. J., Hoag, K. L., Flynn, P. F. and Brands, M. C., "An Appraisal of Advanced Engine Concepts Using Second Law Analysis Techniques", SAE Paper 841287, 1984

16. Alkidas, A. C., "The Application of Availability and Energy Balances to a Diesel Engine", *J. Eng. Gas Turb. Power*, 110 (1988) 462-469, 1988

17. Van Gerpen, J. H. and Shapiro, H. N., "Second-Law Analysis of Diesel Engine Combustion", *J. Eng. Gas Turb. Power*, 112 (1990) 129-137, 1990

18. Bozza, F., Nocera, R., Senatore, A. and Tuccillo, R., "Second Law Analysis of Turbocharged Engine Operation", SAE Paper 910418, 1991

19. Dunbar, W. R. and Lior, N., "Sources of Combustion Irreversibility", Combust. Sci. and Tech., 1994, Vol. 103, pp. 41-61

20. Anderson, M. K., Assanis, D. N. and Filipi, Z. S., "First and Second Law Analyses of a Naturally-Aspirated, Miller Cycle, SI Engine with Late Intake Valve Closure", SAE Paper 980889, 1998

21. Caton, J., "Operating Characteristics of a Spark-Ignition Engine Using the Second Law of Thermodynamics: Effects of Speed and Load", SAE Paper 2000-01-0952, 2000

22. Farrell, J. T., Stevens, J. G. and Weissman, W., "A Second Law Analysis of High Efficiency Low Emission Gasoline Engine Concepts", SAE Paper 2006-01-0491, 2006

23. Rakopoulos, C. D. and Giakoumis, E. G., "Second-law analyses applied to internal combustion engines operation", *Progress in Energy and Combustion Science*, 32 (2006) 2-47, 2006

24. Lawand, V. J. and Caton, J. A., "A Turbocharged, Spark-Ignition Engine: Results from an Engine Cycle Simulation Including the Second Law of Thermodynamics", *Proceedings of the ASME Internal Combustion Engine Spring Technical Conference*, ASME Paper ICES2009-76023, 2009

25. Caton, J., "An Assessment of the Thermodynamics Associated with High-Efficiency Engine", *Proceedings of the ASME Internal Combustion Engine Fall Technical Conference*, ASME Paper ICEF2010-35037, 2010

26. Dec. J. and Yang. Y., "Boosted HCCI for High Power without Engine Knock and Ultra-Low NO_x Emissions using a Conventional Fuel", SAE Paper 2010-01-1086, 2010

27. Manofsky, L., Vavra, J., Assanis, D. and Babajimopoulos, A., "Bridging the Gap between HCCI and SI: Spark-Assisted Compression Ignition", SAE Paper 2011-01-1179, 2011

CHAPTER 3

HCCI COMBUSTION MODEL PERFORMANCE EVALUATION

Following the literature review presented in Chapter 1 and the motivation, research objectives, tools and methodology presented in Chapter 2, the current chapter will present the HCCI combustion model performance evaluation effort. As described in chapter 2, the performance evaluation process was based on three distinct sets of experimental data that originated from three different engines and formed a complete set of results representing different operating techniques for HCCI operation.

The FFVA engine results were used to investigate combustion model behavior at naturally aspirated conditions, NVO operation and variable combustion phasing; the GM boosted engine results were used to examine model behavior at boosted conditions, NVO operation and high load; finally, the Sandia engine results were utilized to investigate model behavior at boosted conditions with positive valve overlap and EGR use at elevated compression ratio. These three datasets will be presented individually in the following sections. Assessment of the gas exchange and heat transfer process will follow and the chapter will conclude with the assessment of the combustion model and a summary of the findings. The importance of accurately describing HCCI combustion phenomena is going to be demonstrated by examining cases where the combustion model did not perform adequately.

3.1 Model Performance Evaluation against FFVA Engine Results

3.1.1 Three Pressure Analysis

The first experimental dataset used in the performance evaluation process was generated from the FFVA engine at the University of Michigan W. E. Lay Automotive Lab. The engine was run in HCCI mode at naturally aspirated conditions and combustion was phased in the cycle through a sweep of negative valve overlap. The engine features an innovative electrohydraulic valve actuation system that allows variable duration and lift valve events [1]. Figure 2.1 shows the valve events for the most advanced operating point which corresponded to NVO = 181.4 CAD and almost 60% residual gas trapped in the cylinder. It should be noted that the end points of the valve events (EVO and IVC) were anchored during the NVO sweep. As displayed in Figure 2.1, EVO was located before expansion BDC, IVC was located after compression BDC while EVC and IVO were varied by changing the exhaust and intake duration respectively. The trapezoidal profile of the valve lifts offered increased effective flow area compared to traditional lobe-shaped events.

Model performance evaluation aimed at assessing the description of the gas exchange, heat transfer and combustion events. For that reason, the evaluation was accomplished in two steps; the first one was Three Pressure Analysis (TPA). The concept behind TPA suggests that by using instantaneous values of intake, exhaust and cylinder pressures, the actual gas exchange process can be simulated, allowing for assessment of the valve discharge coefficients and valve events in the model. In addition, by prescribing the combustion event, the heat transfer correlations can be isolated from the burn rate correlations and thus assessed as well. After gas exchange and heat transfer had been assessed, the UM HCCI combustion model was activated in order to perform forward combustion simulations and compare the calculated burn rates to those experimentally observed.

It should be noted that there are certain engine variables that could not be directly measured in the experiments. Therefore, they were subsequently calculated by heat release analysis of the experimental measurements. One of these variables was cylinder Residual Gas Fraction (RGF) and is particularly important for HCCI engines. In the case of these variables, results from the TPA model were compared against another model that was employed in the heat release analysis, thus rendering these variables inappropriate for model calibration. The model employed was proposed by Fitzgerald et al. [3].

Inputs to TPA included instantaneous intake, exhaust and cylinder pressures, intake temperature, valve events, fueling rate and combustion efficiency for the combustion phasing sweep examined. Table 3.1 shows the input conditions for the six operating points of the NVO sweep. Intake pressure, exhaust pressure and intake temperature were held constant while NVO was gradually reduced in order to phase combustion later in the cycle.

The engine simulation software used prescribed intake and exhaust conditions and valve events in order to simulate the gas exchange process through the cylinder. The cylinder pressure was used to generate a burn rate curve which was subsequently applied to the energy equation and a new pressure trace was calculated.

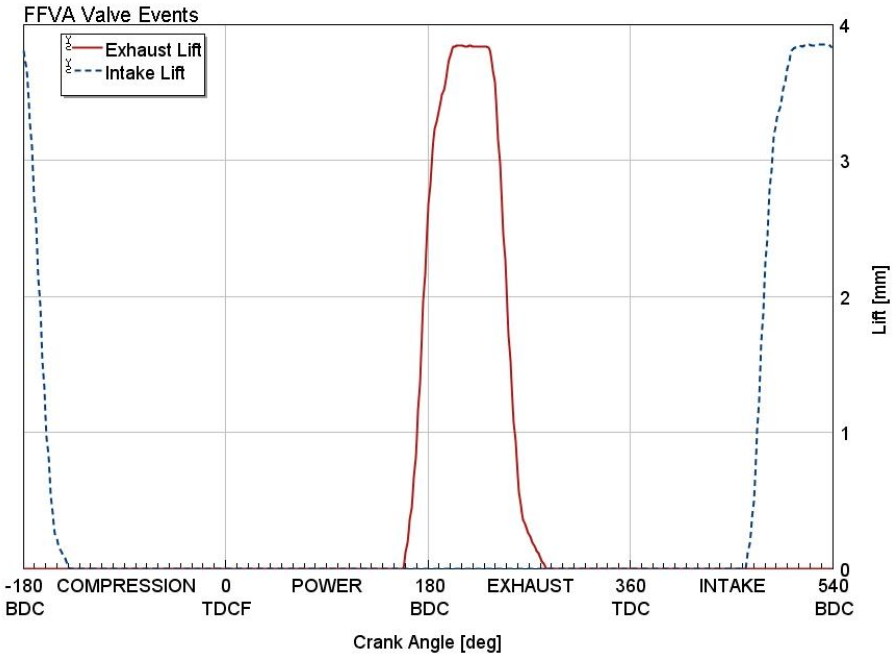

Figure 3.1 – Valve events for the FFVA engine at NVO = 181.4 CAD.

Table 3.1 – FFVA combustion phasing sweep operating conditions

Intake Pressure (bar)	1.01	1.00	1.00	1.00	1.00	0.99
Exhaust Pressure (bar)	1.05	1.05	1.04	1.05	1.04	1.04
Intake Temperature (K)	318.25	318.25	318.45	318.45	318.25	318.25
NVO (CAD)	181.4	178.5	174.7	171.3	167.0	162.1
Fuel (mg/cycle)	9.53	9.58	9.58	9.55	9.5	9.5
η_{comb} (%)	97.1	96.5	95.7	94.6	93.2	91.2

The NVO values shown in Table 3.1 were measured during the experiments from the data acquisition system of the fully flexible valvetrain. However, analysis of TPA results revealed that in order to match the slope of the pressure traces after intake valve closing, NVO had to be reduced in all cases. Figure 3.2 shows NVO as a function of CA50 for both the experiment and the three pressure analysis. It appeared that NVO had to be consistently lower in the TPA and the difference increased as combustion was phased later in the cycle. The discrepancies observed may have occurred due to

inaccurate valve position reading of the FFVA valvetrain. With the NVO correction, TPA was able to match the pressure trace of the experiment to less than 1% error. In addition, it allowed accurate calculation of RGF which is shown in Figure 3.3 as a function of CA50 as well. The experimental results that will be displayed hereafter include errors bars, which are based on measurement error. Experimental error and uncertainty are discussed in section 3.4 of this chapter and methods for uncertainty calculation are outlined.

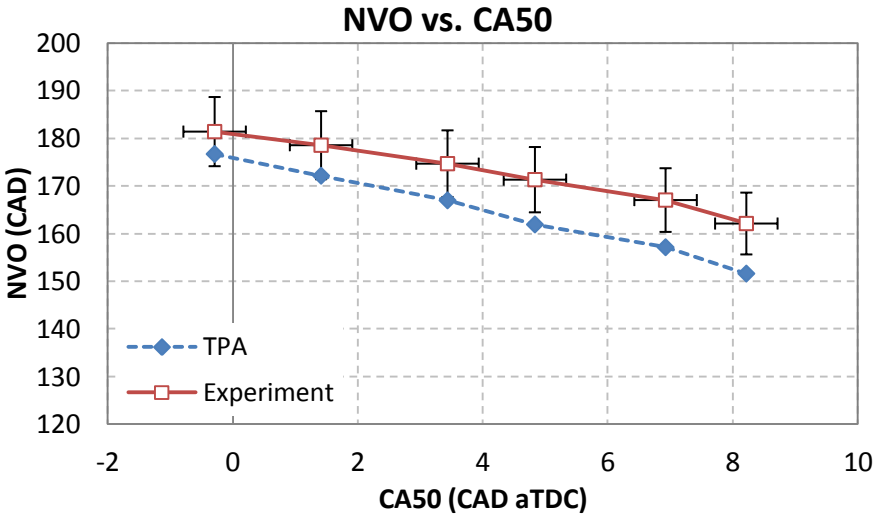

Figure 3.2 – NVO as a function of CA50 for the six cases of the FFVA combustion phasing experiment.

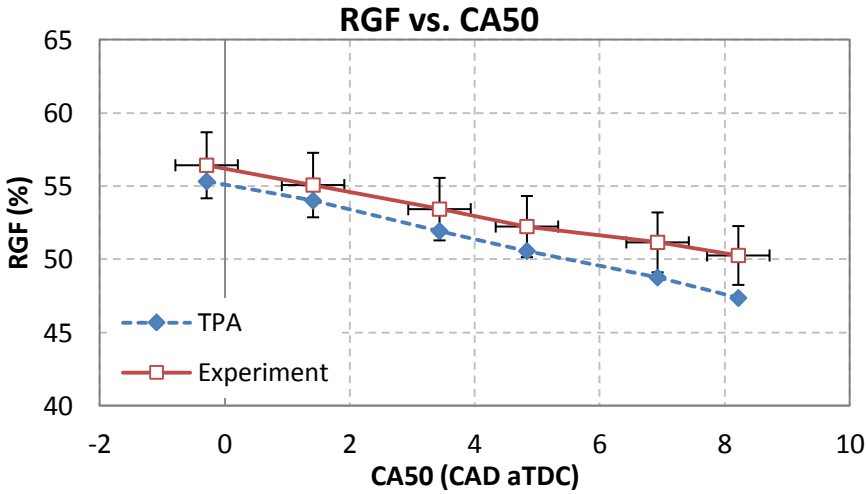

Figure 3.3 – Residual Gas Fraction as a function of CA50 for the six cases of the FFVA combustion phasing experiment.

Figure 3.4 shows the pressure traces of the experiment and TPA for compression, combustion and expansion after the NVO was calibrated. It should be noted that NVO had to be consistently lower in the TPA, so it was calibrated once for the entire sweep. The pressure traces shown below represent the operating point where CA50 was 4.8 CAD aTDC but the agreement was very good for all operating points. It can be observed that the experimental pressure trace is less than 1 % higher before ignition (around -15 CAD) which can be attributed to potential pre-ignition reactions.

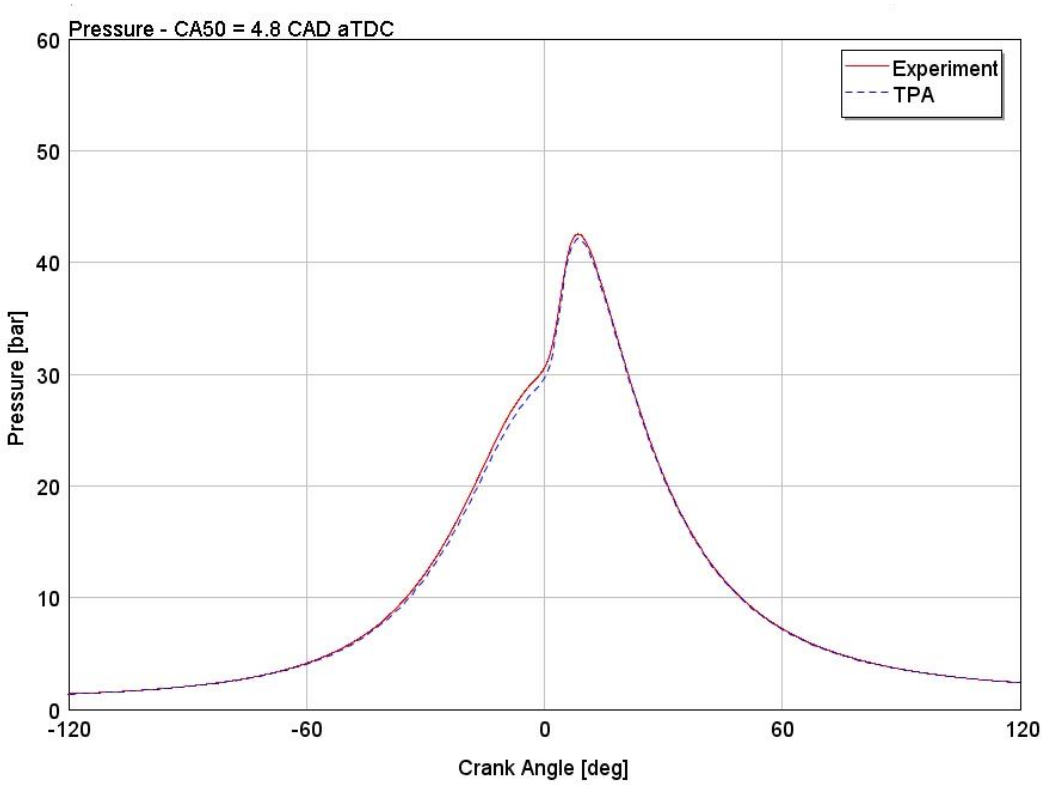

Figure 3.4 – Comparison of pressure traces between the experiment and TPA during compression, combustion and expansion for the case of CA50 = 4.8 CAD aTDC.

Similar discrepancies can be observed in the pressure traces during recompression that are shown in Figure 3.5. Since the valve events were calibrated, the two pressure traces are identical until 355 CAD, just before recompression TDC. In a similar manner during the expansion part of recompression, the experimental pressure was less than 1 % higher than that of TPA, which indicated that heat release may have occurred during the

recompression event. The same effect was observed for all the operating points examined with TPA. It should be noted that using the pressure traces to calibrate the gas exchange process seemed to be the most robust method, since the cylinder pressure trace is a direct measurement of the engine high-speed data acquisition system. On the other hand, RGF did not seem as a robust metric since it was calculated through heat release analysis of the experimental results albeit using established methods shown in the literature [2, 3, 4].

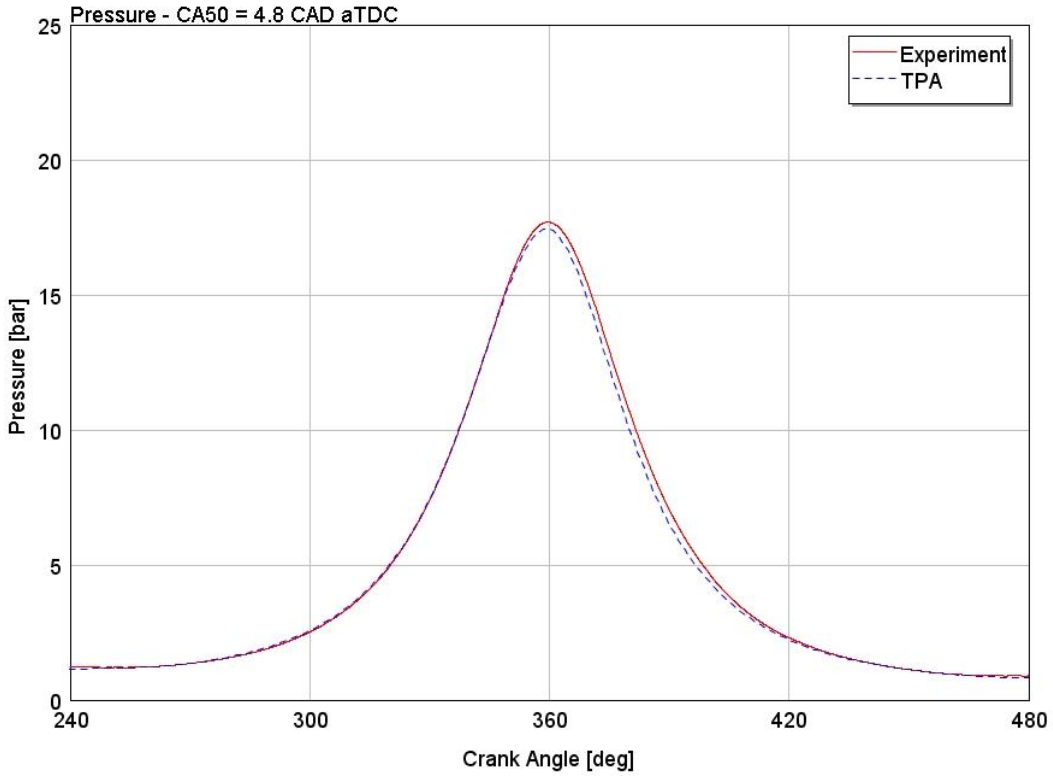

Figure 3.5 – Comparison of pressure traces between the experiment and TPA during recompression for the case of CA50 = 4.8 CAD aTDC.

Results of the three pressure analysis revealed very good agreement in the closed portion of the cycle between experiment and TPA. Gross IMEP and indicated efficiency are shown in Figure 3.6 and Figure 3.7 respectively displaying very good agreement overall. Late combustion phasing seemed to have a more pronounced effect on the experiment that in the TPA. Both IMEPg and $\eta_{i,g}$ decreased faster in the experiment.

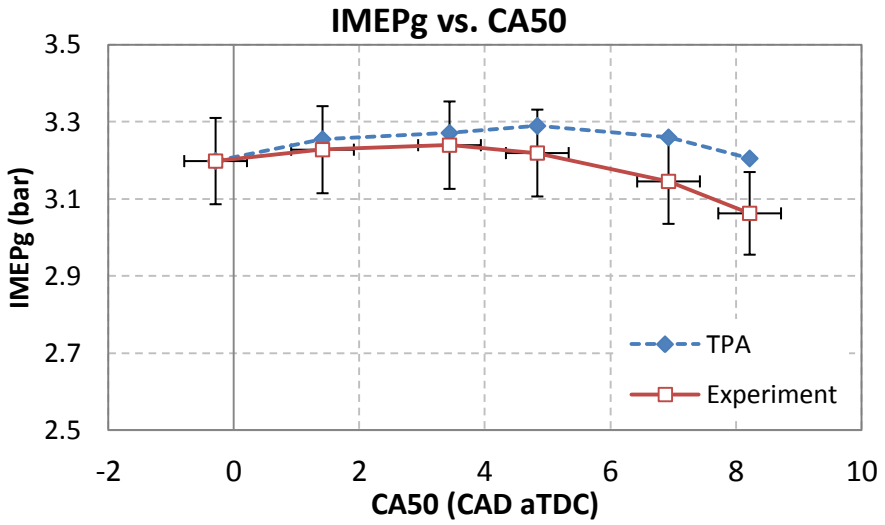

Figure 3.6 – IMEPg as a function of CA50 for the six cases of the FFVA combustion phasing experiment.

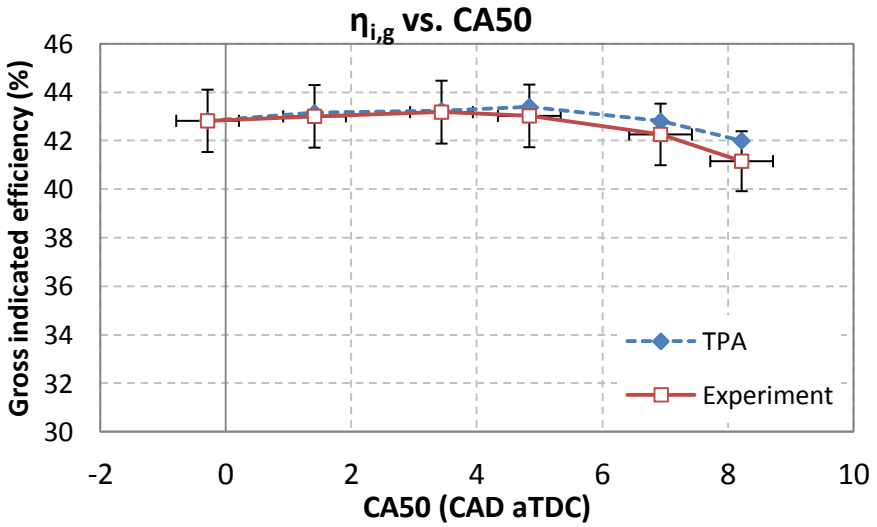

Figure 3.7 – Gross indicated efficiency as a function of CA50 for the six cases of the FFVA combustion phasing experiment.

Despite the fact that TPA matched closely the experiments during the closed portion of the cycle, some differences appeared in the gas exchange process. Figure 3.8 shows net IMEP as a function of CA50. IMEPn calculated by TPA was lower than the experimental one with the reason being increased PMEP which is shown in Figure 3.9. PMEP values calculated by TPA were about two times higher compared to those

obtained from the experiment. This effect can be attributed to the valve discharge coefficients (C_D) used in the engine model, which were initially generated for lobe-shaped valve events. Effort was put into calibrating the discharge coefficients in order to match cylinder air trapped mass for the entire phasing sweep. However, the trapezoidal nature of the valve events prevented accurate representation of the mass flow through the valves. As a result, PMEP could not be accurately matched to the experimental values.

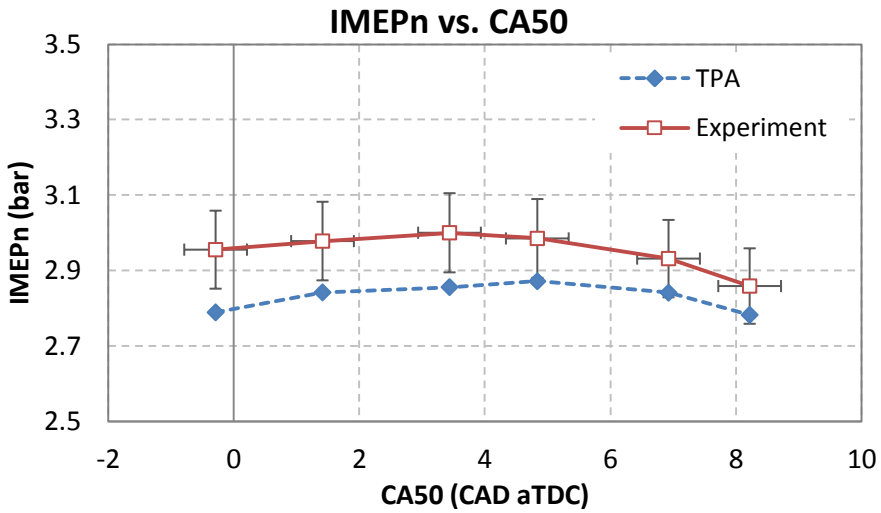

Figure 3.8 – IMEPn as a function of CA50 for the six cases of the FFVA combustion phasing experiment.

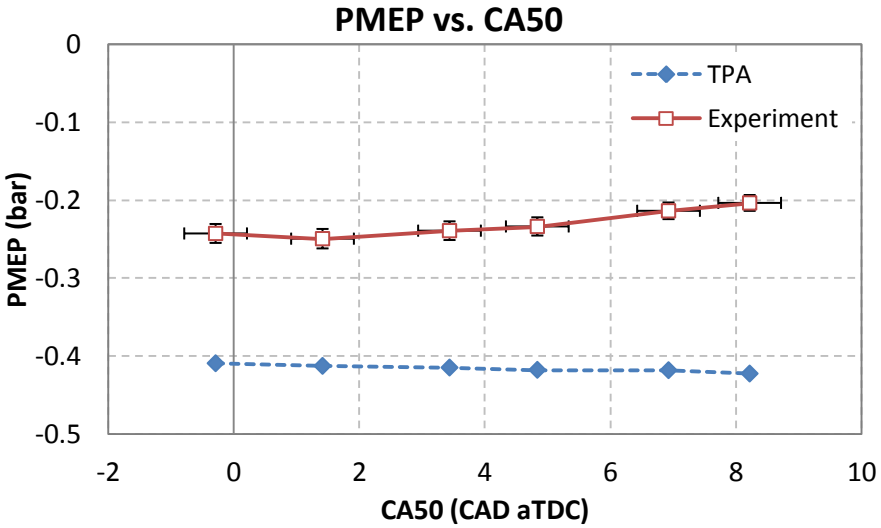

Figure 3.9 – PMEP as a function of CA50 for the six cases of the FFVA combustion phasing experiment.

The agreement between experiment and TPA on trapped air and total masses is displayed on Figure 3.10 and Figure 3.11 respectively. The maximum difference between measured and calculated air mass was 5.7 % which was considered satisfactory. As shown in Figure 3.3, RGF was constantly lower in the TPA which explained the trend of total trapped mass. The maximum difference in total trapped mass was 2.4 % which was also considered satisfactory. As explained earlier, the discharge coefficients obtained for lobe-shaped valve events were inappropriate for the trapezoidal valve lifts of the FFVA engine. The resulting discrepancies in the gas exchange process skewed the calculations of trapped masses and pumping work in the model.

The importance of achieving good agreement in the trapped air and total masses lies in the fact that they directly affect dilution levels and work production, both of which play key roles to simulating LTC engines. Figure 3.12 displays equivalence ratio as a function of CA50 and shows that the mixture in TPA was consistently richer than in the experiment. The discrepancies in Φ can be explained by the differences in trapped air and total mass discussed previously. Effective equivalence ratio is of greater importance for the combustion model and it is shown in Figure 3.13 as a function of combustion phasing as well. Effective equivalence ratio was defined in chapter 2 as $\Phi' = \Phi(1 - RGF)$ and is one of the parameters that appear in the burn rate correlation (the other one is RPM). The combination of higher equivalence ratio and lower RGF in the TPA resulted in Φ' that was very close to that of the experiment. Equivalence ratio decreased with CA50 since NVO and RGF were reduced in order to phase ignition timing later in the cycle. That was not the case with Φ' though; as commented in Chapter 2, effective equivalence ratio is a metric of the energy content of the charge. Φ' was constant during that combustion phasing sweep indicating that the charge was roughly equally potent across the phasing range.

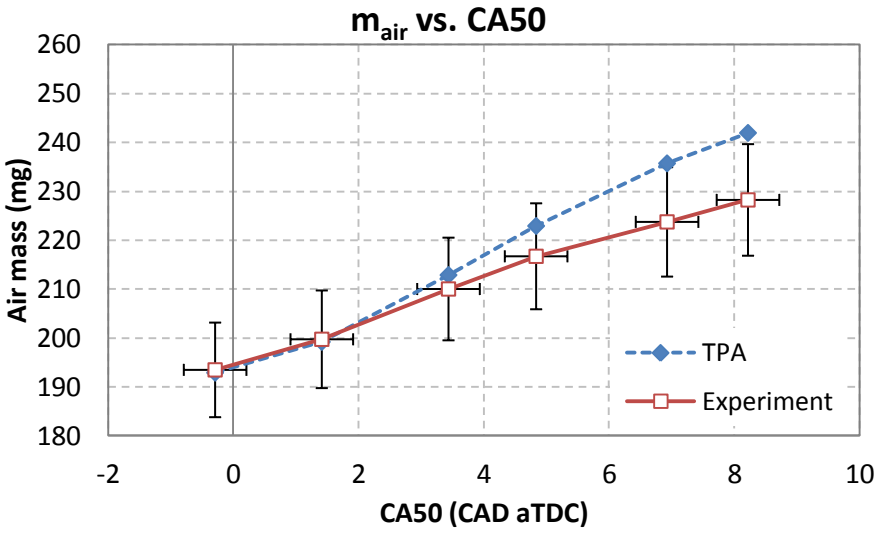

Figure 3.10 – Cylinder air trapped mass as a function of CA50 for the six cases of the FFVA combustion phasing experiment.

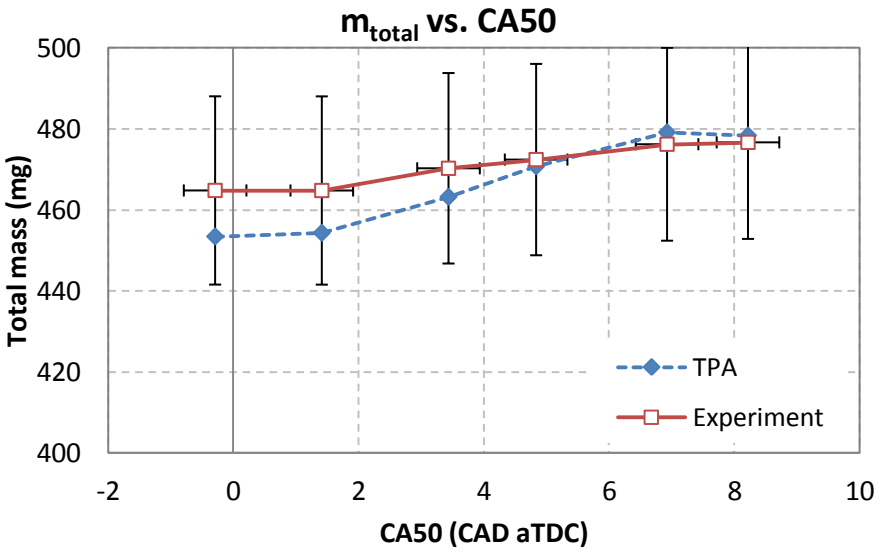

Figure 3.11 – Cylinder total trapped mass as a function of CA50 for the six cases of the FFVA combustion phasing experiment.

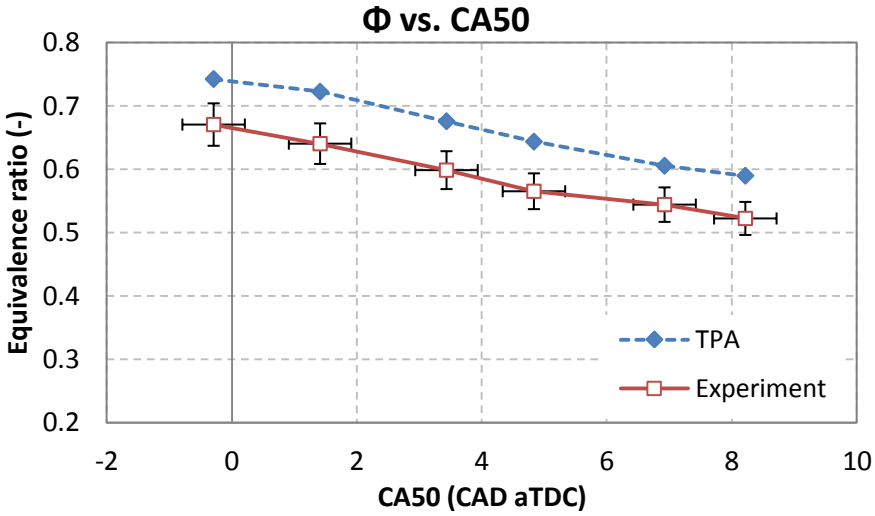

Figure 3.12 – Equivalence ratio as a function of CA50 for the six cases of the FFVA combustion phasing experiment.

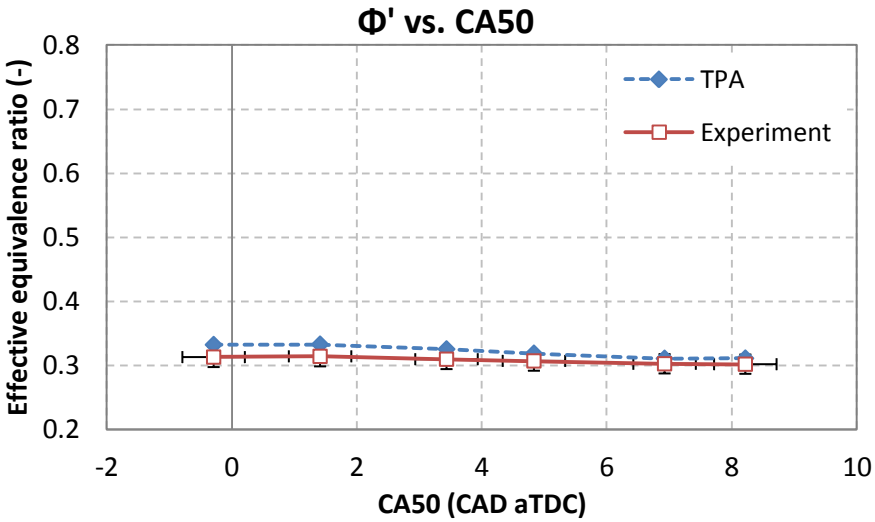

Figure 3.13 – Effective equivalence ratio as a function of CA50 for the six cases of the FFVA combustion phasing experiment.

Overall, TPA results showed good agreement in air and total trapped masses and closed cycle performance parameters with the experiment. TPA indicated that in order to achieve good agreement in the pressure traces, NVO had to be reduced compared to the experiment. Pumping work appeared to be overpredicted in TPA which was attributed to the valve discharge coefficients used for the fully flexible valvetrain.

3.1.2 FFVA Forward Simulation

After TPA was completed, the mean intake and exhaust pressures, mean intake temperature, fueling rate and calibrated valve events were used to perform forward calculations of the combustion phasing experiment. This section will describe the results obtained from the UM combustion model and explain the effects of the key parameters involved.

Figure 3.14 shows negative valve overlap as a function of CA50 for the forward simulation. NVO values are similar to those seen previously in Figure 3.2 but the simulation curve appears to be shifted to the right (about 0.5 CAD at low loads). The reason is that the combustion model calculated later CA50 values compared to those obtained from the experiment, which will be discussed in the following. The resulting residual gas fraction is shown in Figure 3.15 which displays a better agreement in RGF compared to what was observed in the TPA results. In spite of the good agreement between model and experiment, RGF was not considered as a robust metric for performance evaluation purposes for the reasons discussed earlier.

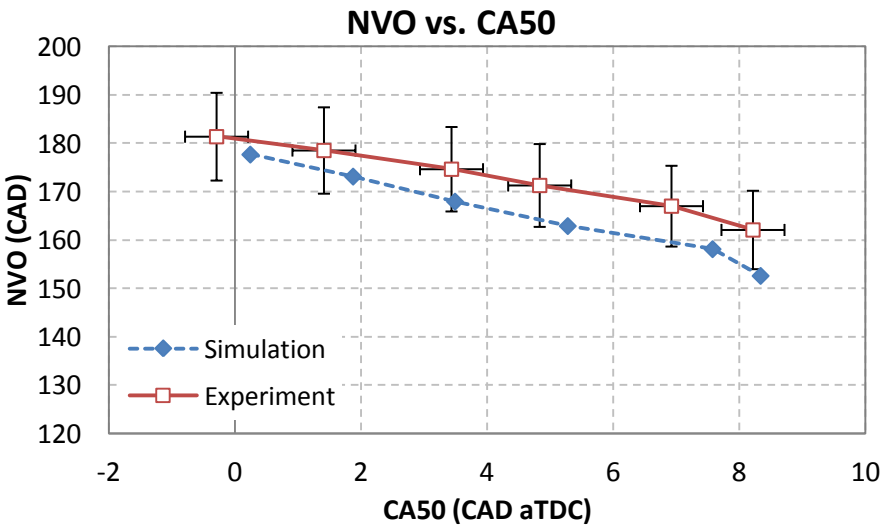

Figure 3.14 – NVO as a function of CA50 in the forward simulation of the FFVA combustion phasing experiment.

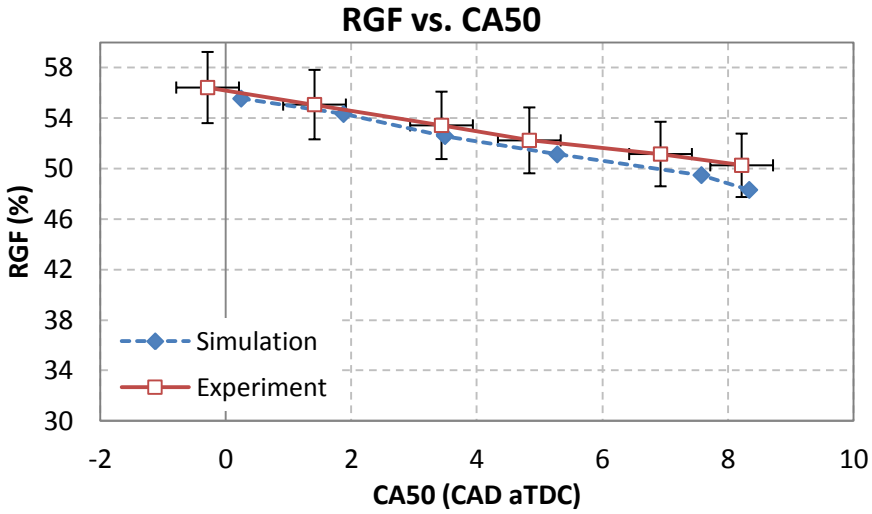

Figure 3.15 – RGF as a function of CA50 in the forward simulation of the FFVA combustion phasing experiment.

TPA results revealed very good agreement with the experiment for the closed portion of the cycle. However, Figure 3.16 shows that this was not necessarily the case for the forward simulation as well. TPA utilized the instantaneous cylinder pressure supplied from the experiment which resulted in an exact representation of the actual combustion event. On the other hand, the forward simulation was based on the autoignition integral expression and burn rate correlations presented in Chapter 2. As expected, there were some discrepancies during the closed portion of the cycle and they are shown in the following figures. The ignition delay correlation accurately calculated ignition timings. The burn rate correlation calculated later CA50 values compared to the experiment; the difference though was less than 0.5 CAD which is insignificant. Overall, the agreement on ignition timing and burn duration was good. Figure 3.16 and Figure 3.17 display one of the drawbacks of the forward simulation which is gross efficiency and is directly related to heat transfer description. As stated in Chapter 2, the heat transfer model used in this study was the classic Woschni model and not the modified version [7]. The reasons will be analyzed in the following sections where the GM boosted engine experiment will be discussed. IMEPg and gross indicated efficiency were consistently

higher than the experiment by up to 9 %, which indicated that heat transfer was underpredicted compared to the experiment.

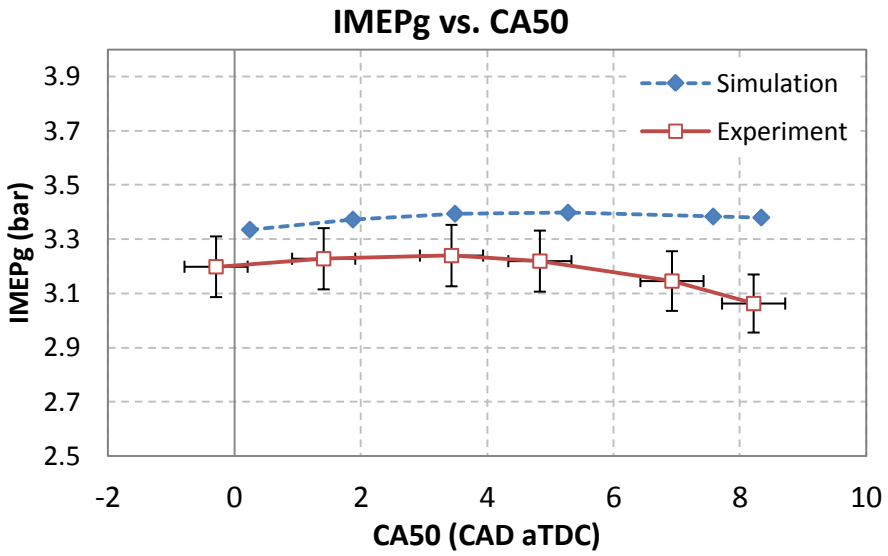

Figure 3.16 – Gross IMEP as a function of CA50 in the forward simulation of the FFVA combustion phasing experiment.

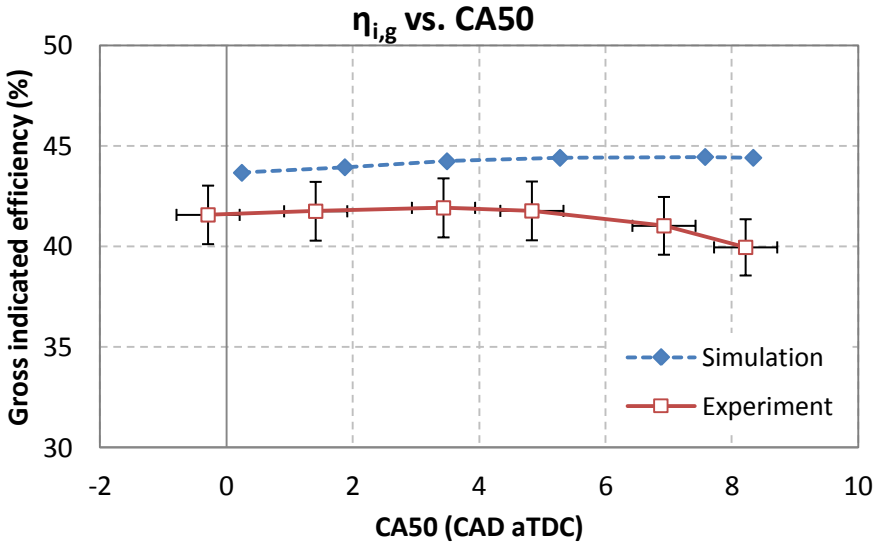

Figure 3.17 – Gross indicated efficiency as a function of CA50 in the forward simulation of the FFVA combustion phasing experiment.

As observed in the three pressure analysis results of the previous section, the model calculated higher pumping work compared to the experiment. This is clearly

shown in Figure 3.18 where IMEPn is shown as a function of CA50 and in Figure 3.19 which displays PMEP as a function of CA50 as well. IMEPg in the simulation was somewhat higher than the experiment; however, IMEPn was somewhat lower in the simulation due to higher calculated pumping losses. PMEP in the model was constantly higher than the experiment by a factor of two which impacted the net indicated efficiency of the simulation. The higher PMEP calculated by the model is attributable primarily to the discharge coefficients involved in the simulation of mass flow through the valves. These discharge coefficients were not available for the FFVA engine and they were approached by values pertinent to lobe-shaped valve events. The difference in net indicated efficiency between the experiment and the simulation is also displayed in Figure 3.20 which shows NSFC as a function of CA50. The simulation calculated 6 % higher specific fuel consumption than the measured one for most operating points. In addition, it could not capture the reducing efficiency of the latest combustion phasing cases, even though combustion phasing was calculated well.

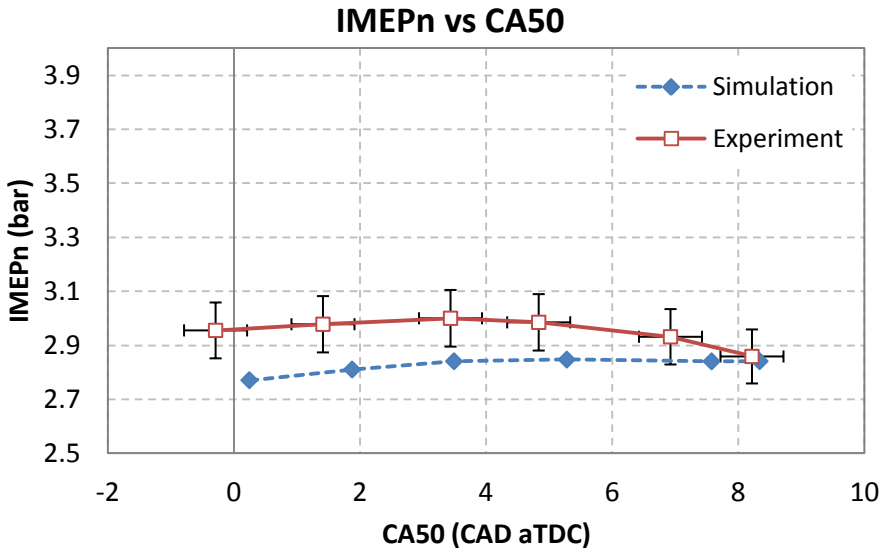

Figure 3.18 – Net IMEP as a function of CA50 in the forward simulation of the FFVA combustion phasing experiment.

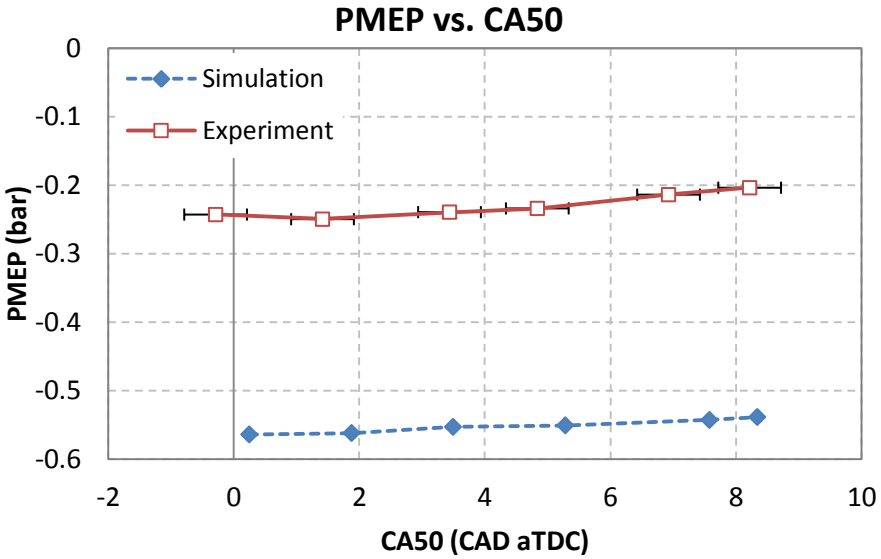

Figure 3.19 – PMEP as a function of CA50 in the forward simulation of the FFVA combustion phasing experiment.

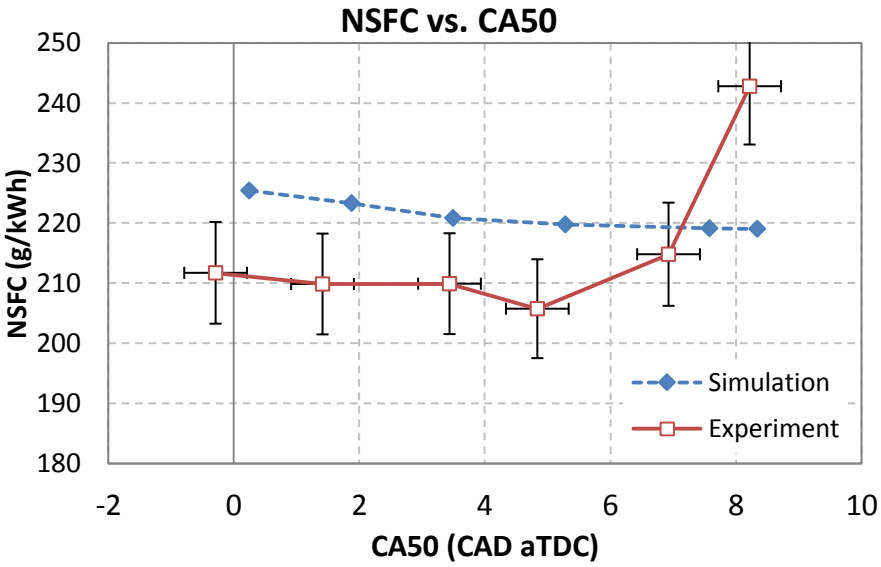

Figure 3.20 – Net Specific Fuel Consumption as a function of CA50 in the forward simulation of the FFVA combustion phasing experiment.

As commented in the three pressure analysis section, achieving agreement in air and total masses was essential for the accurate calculation of engine performance parameters. Figure 3.21 shows trapped air mass as a function of CA50 and exhibits very good agreement between the model and the experiment. The pumping work problem identified above can be largely explained by the need to accurately calculate trapped air

mass in the simulation. Discharge coefficients in the model were adjusted according to trapped air mass agreement with the experiment, but the resulting pumping work was higher. Figure 3.22 displays trapped total mass as a function of CA50 and one can see that agreement deteriorated as combustion was phased later in the cycle; however, it was considered very good since it did not exceed 4 %. This difference in trapped total mass can be explained by the RGF calculation shown in Figure 3.15. Simulation of the recompression and blowdown phases was affected by discharge coefficients and resulted in calculating lower RGF than what was extracted from the experiment, resulting in lower trapped total mass as combustion was retarded.

The fact that trapped air and total masses agreed well with the experiment was another indication that heat transfer description was primarily responsible for the difference in gross indicated efficiency observed in Figure 3.17. Other factors that may contribute to the $\eta_{i,g}$ difference are blowby and potentially stratification, or turbulence variation with NVO that cannot be described by the combustion model.

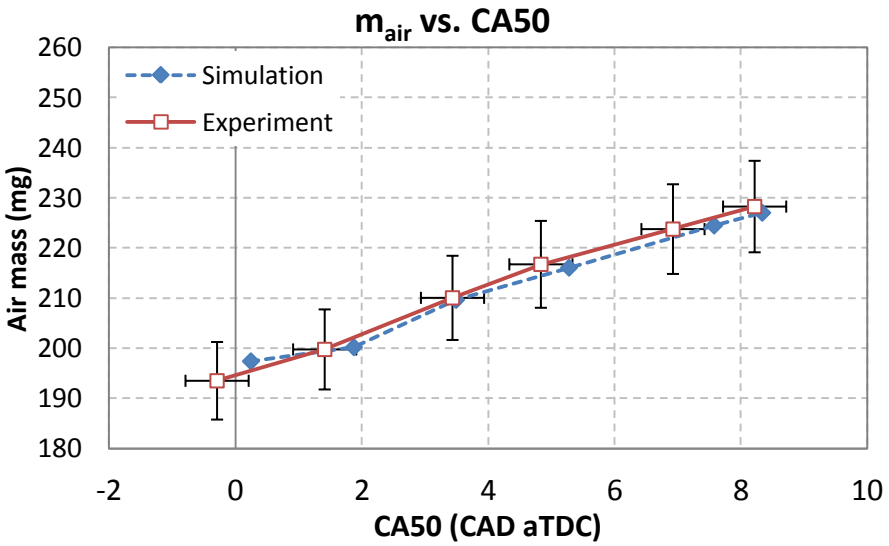

Figure 3.21 – Trapped air mass as a function of CA50 in the forward simulation of the FFVA combustion phasing experiment.

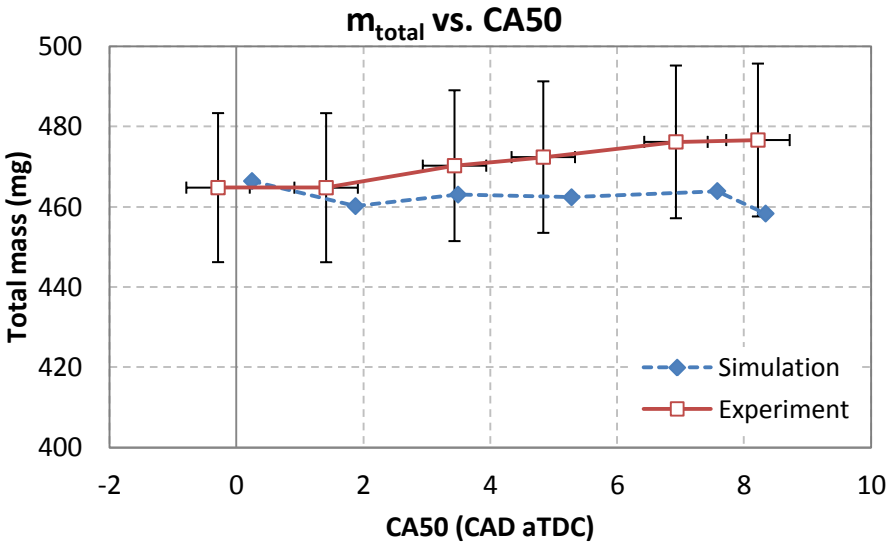

Figure 3.22 – Trapped total mass as a function of CA50 in the forward simulation of the FFVA combustion phasing experiment.

The values of trapped air mass, trapped total mass and residual gas fraction examined in the previous figures, directly affected charge dilution levels which are critical for HCCI operation. Figure 3.23 shows equivalence ratio as a function of CA50 and one can see that the simulation constantly calculates higher Φ than the experiment. The fueling rate in the simulation was exactly the same as in the experiment, therefore the Φ difference can be explained by the lower trapped total mass calculated in the simulation.

Figure 3.24 displays effective equivalence ratio as a function of CA50. As commented in the TPA section, Φ' is a metric of the energy content of the charge. As expected, it was approximately constant during the combustion phasing sweep experiment. Despite the difference observed in Φ, the agreement on Φ' was very good. The reason stems from the difference in calculated RGF, since residual gas was taken into account in the calculation of effective equivalence ratio. As presented in chapter 2, the burn rate correlation is dependent upon Φ' and RPM. Therefore, the very good agreement observed on Φ' was a factor that contributed to the successful representation of the FFVA experiment.

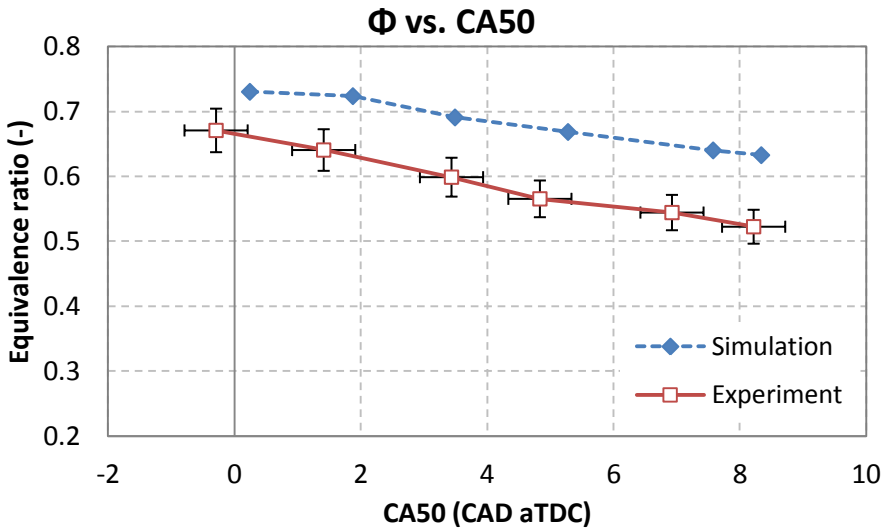

Figure 3.23 – Equivalence ratio as a function of CA50 in the forward simulation of the FFVA combustion phasing experiment.

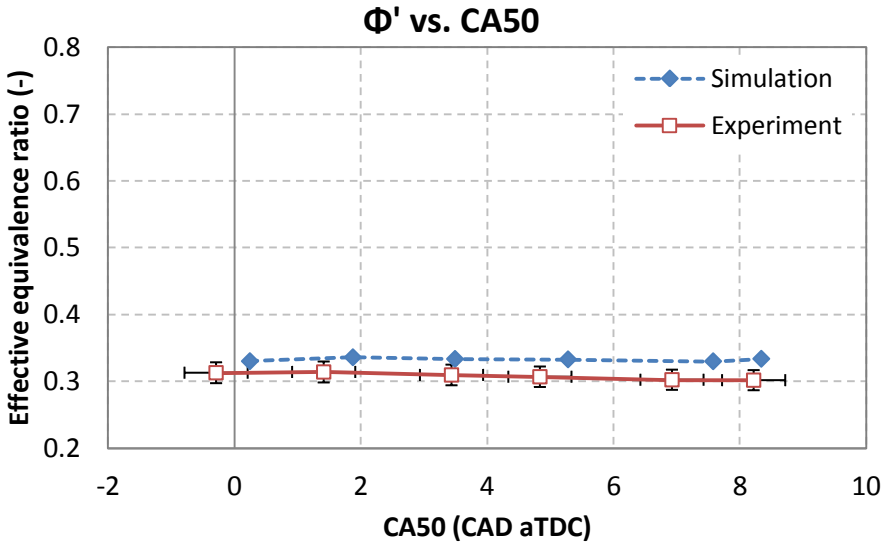

Figure 3.24 – Effective equivalence ratio as a function of CA50 in the forward simulation of the FFVA combustion phasing experiment.

The nature of the forward simulation allowed for the calculation of two additional metrics, the ringing intensity which is shown in Figure 3.25, and the NO_x emissions index which is shown in Figure 3.26. Ringing intensity decreased as combustion was phased later in the cycle since pressure rise rates during heat release were lower. The model was able to capture the reducing trend of R.I. but the slope was not as steep as that observed in the experiment. Nevertheless, the agreement was considered very good. However, that

was not the case for the NO_x emissions index which was constantly underpredicted in the simulation by a factor of three or more. NO_x emissions were never a problem during the FFVA experiment since they were always well below the 1 g/kg fuel limit imposed by US-2010 regulations. That fact reduced the importance of accurate calculations from the extended Zeldovich mechanism that was implemented in the combustion model.

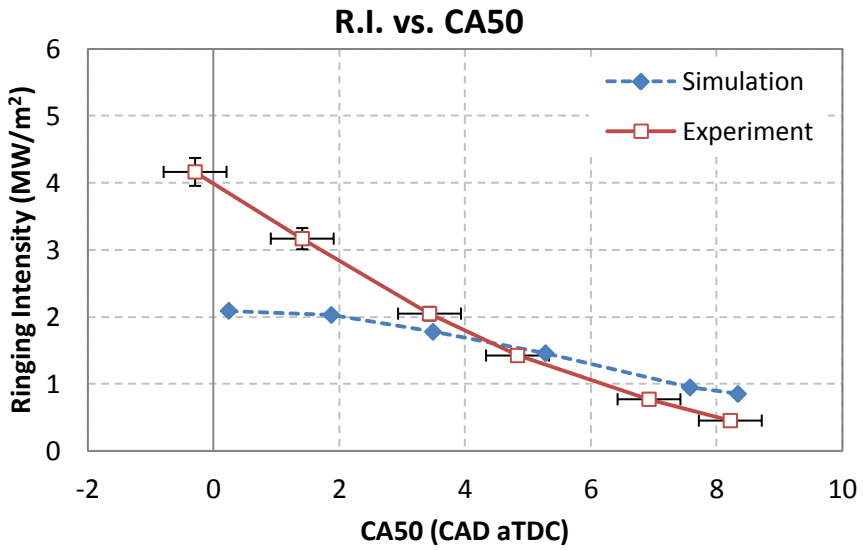

Figure 3.25 – Ringing intensity as a function of CA50 in the forward simulation of the FFVA combustion phasing experiment.

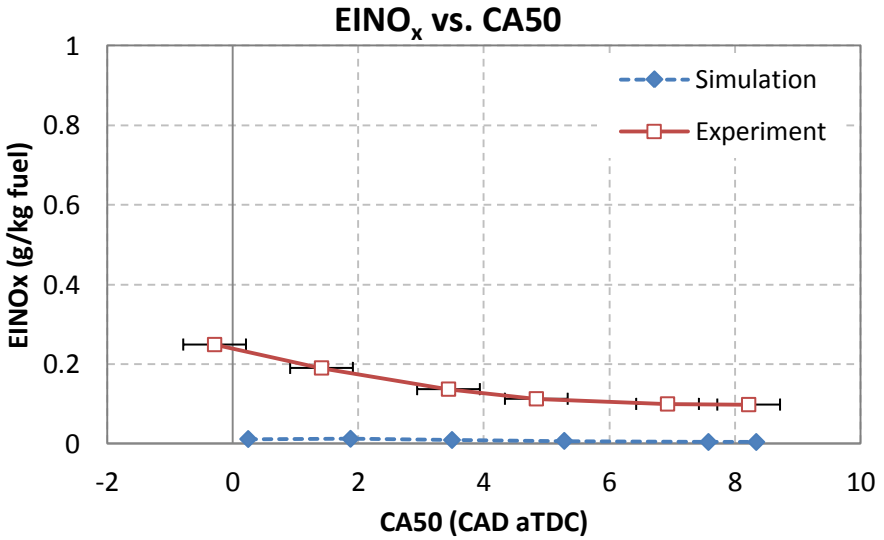

Figure 3.26 – NO_x emissions index as a function of CA50 in the forward simulation of the FFVA combustion phasing experiment.

The following four figures show a comparison of pressure traces between the experiment and simulation for two operating points of the sweep (CA50 = - 0.3 and 4.8 CAD aTDC) during the combustion and recompression events. As observed in the figures shown so far, the agreement between experiment and simulation was better when combustion was phased early in the cycle. This observation can be verified from Figure 3.27; the pressure traces were very close to each other which indicated that the model was very good at calculating ignition timing and burn rate. Figure 3.29 shows the same pressure traces for the case of CA50 = 4.8 CAD aTDC. The agreement was very good at that point as well, albeit with some discrepancies in post-compression pressures. Figure 3.28 and Figure 3.30 compare pressure traces for these two operating points during the recompression phase. It was observed that the experimental pressure was always higher than the simulated one. The reason behind the difference was heat release during recompression that could not be captured by the model.

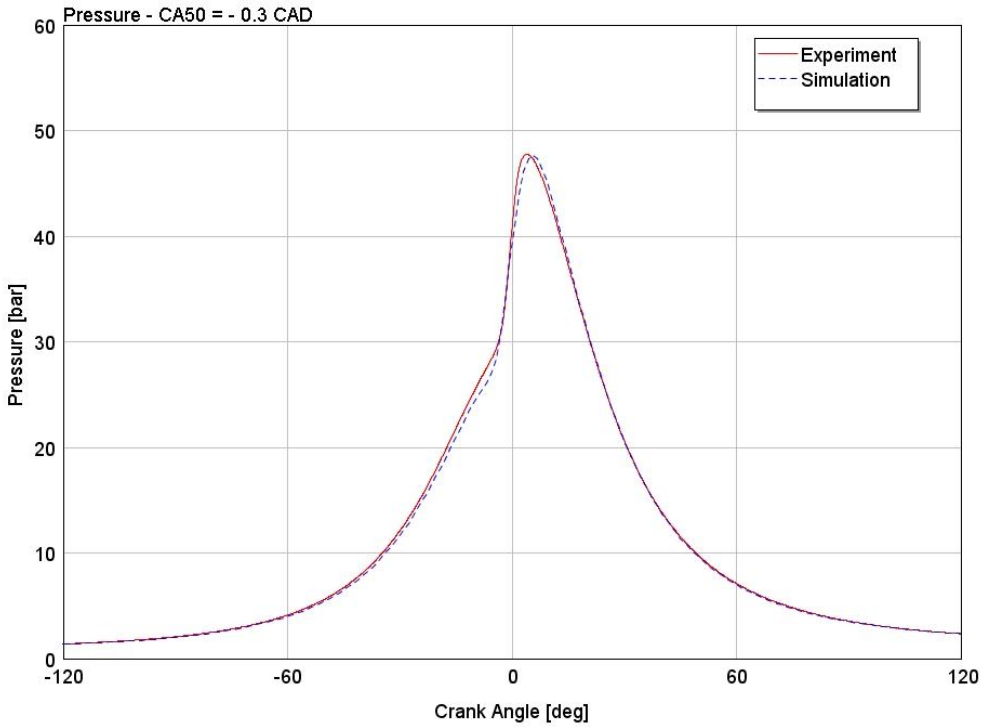

Figure 3.27 – Comparison of pressure traces during the main compression and combustion event for the operating point of CA50 = - 0.3 CAD aTDC.

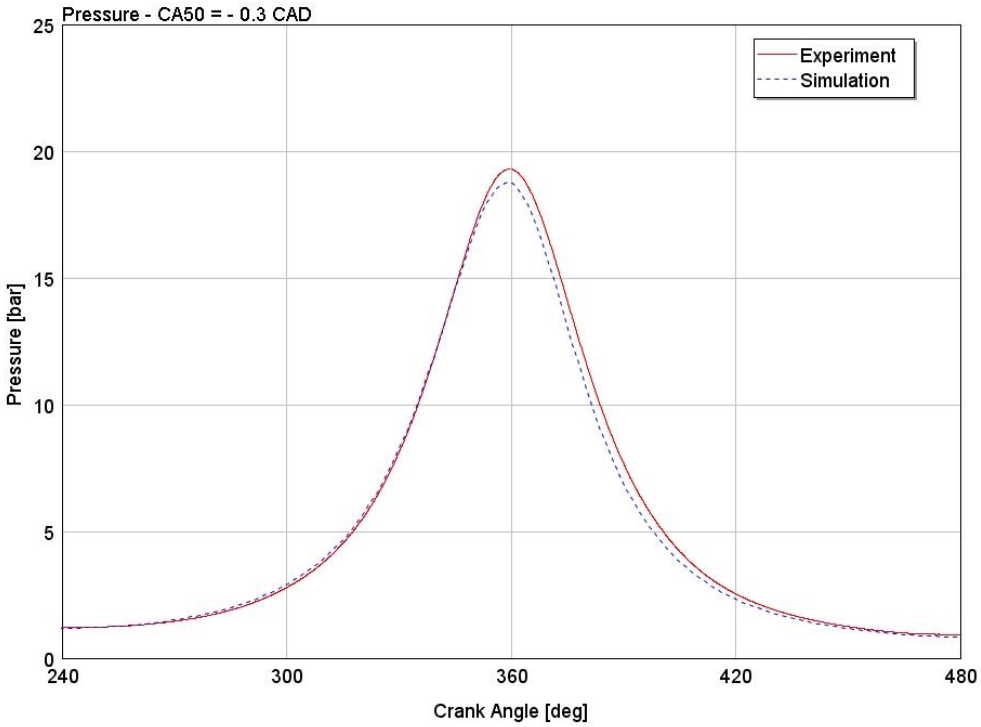

Figure 3.28 – Comparison of pressure traces during the recompression event for the operating point of CA50 = - 0.3 CAD aTDC.

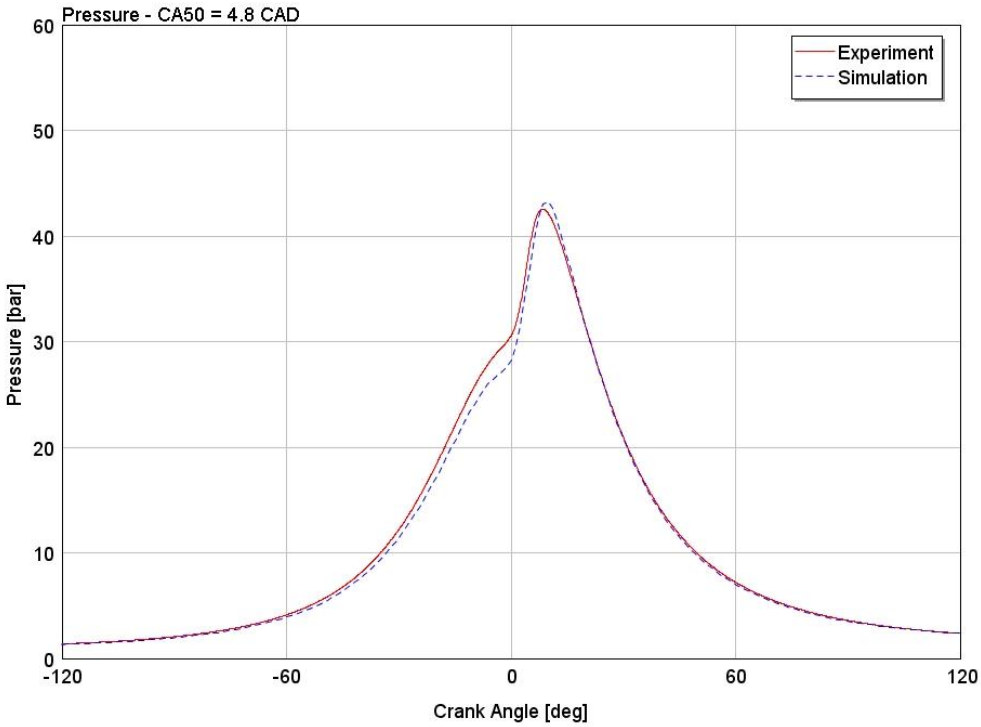

Figure 3.29 – Comparison of pressure traces during the main compression and combustion event for the operating point of CA50 = 4.8 CAD aTDC.

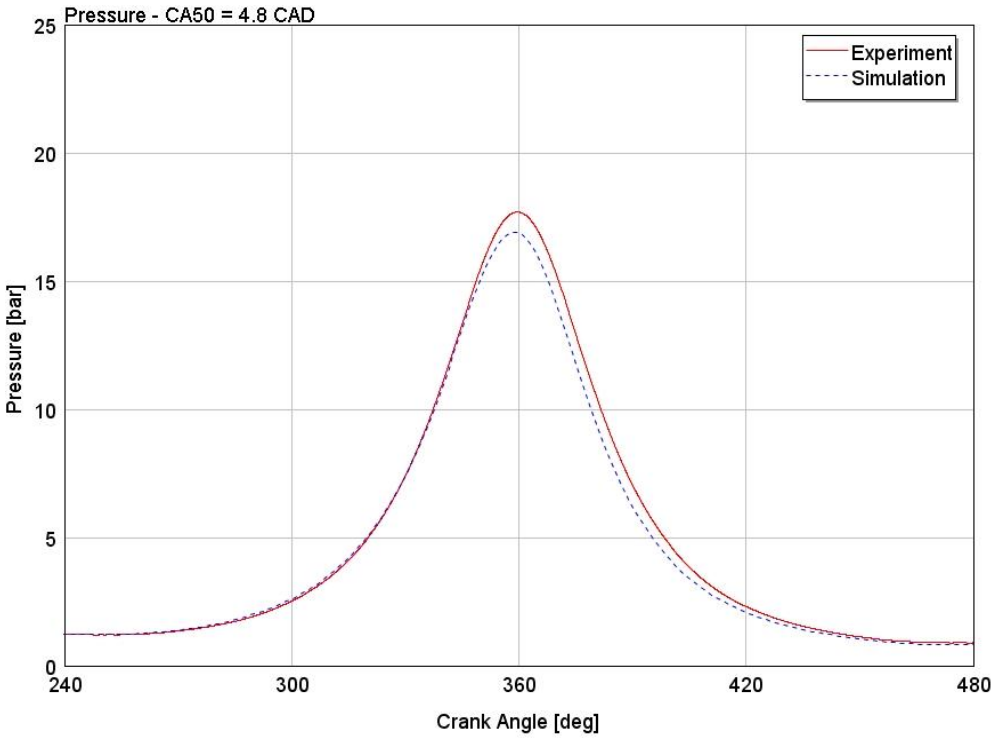

Figure 3.30 – Comparison of pressure traces during the recompression event for the operating point of CA50 = 4.8 CAD aTDC.

The comparison between experimental and modeling results presented in this section demonstrated that the UM HCCI combustion model is very good at calculating ignition and burn rate for naturally aspirated conditions. The engine model exhibited higher pumping work than the measured one which was attributed to the non-representative discharge coefficients used for describing flow through the valves of the FFVA engine. Despite higher pumping work, calculation of performance parameters, trapped masses and ringing intensity was successful with minimal model calibration. The next section will present a similar set of results for the GM boosted engine experiment and discuss the implications of modeling high pressure HCCI combustion.

3.2 Model Performance Evaluation against GM Boosted Engine Results

3.2.1 Three Pressure Analysis

Approach of the GM boosted engine experiment was initiated by a three pressure analysis (TPA) study, in the same way as that presented for the FFVA engine in the previous sections. Similarly, the goal of TPA was to isolate the gas exchange and heat transfer processes before examining the performance of the combustion model. In order to reach that goal, measured instantaneous intake, exhaust and cylinder pressures were used as inputs to the TPA model along with negative valve overlap, fueling rate and combustion efficiency. The experiment consisted of simultaneous intake pressure and load sweeps and Table 3.2 shows the operating conditions for the seven points measured and simulated. While conducting the experiment, intake pressure was gradually increased in order to offer the dilution levels required for increased fueling rates without ringing. Exhaust pressure was calculated and imposed by assuming constant Overall Turbocharger Efficiency (OTE) across the load range. Assuming constant OTE across a wide range of operating conditions did not necessarily reflect actual turbocharger operation, but it allowed for calculation of appropriate backpressure values that were verified by multi-cylinder engine simulations.

In contrast to the FFVA engine presented in the previous sections, the GM boosted engine employed a production-derived cylinder head with low lift 4 mm camshafts and variable cam phasing. The valve events are shown in Figure 3.31 and were of constant duration (125 CAD); therefore there were no anchored endpoints as those seen in the FFVA engine. Phasing of the valve events resulted in phasing of EVO and IVC, thus compression and blowdown were affected by valve timings.

Table 3.2 – GM boosted engine intake pressure and load sweep operating conditions

Intake Pressure (bar)	1	1.21	1.41	1.72	1.92	2.33	2.65
Exhaust Pressure (bar)	1.05	1.22	1.44	1.89	2.12	2.78	3.44
Intake Temperature (K)	308.1	307.5	307.1	306.5	306.5	306	305.8
NVO (CAD)	128.8	128.9	120.9	103.8	97.3	83.8	72.4
Fuel (mg/cycle)	12.2	13.4	14.7	17.9	19.6	22.3	24
η_{comb} (%)	96.9	96.5	96.3	96.6	96.5	96.4	96.3

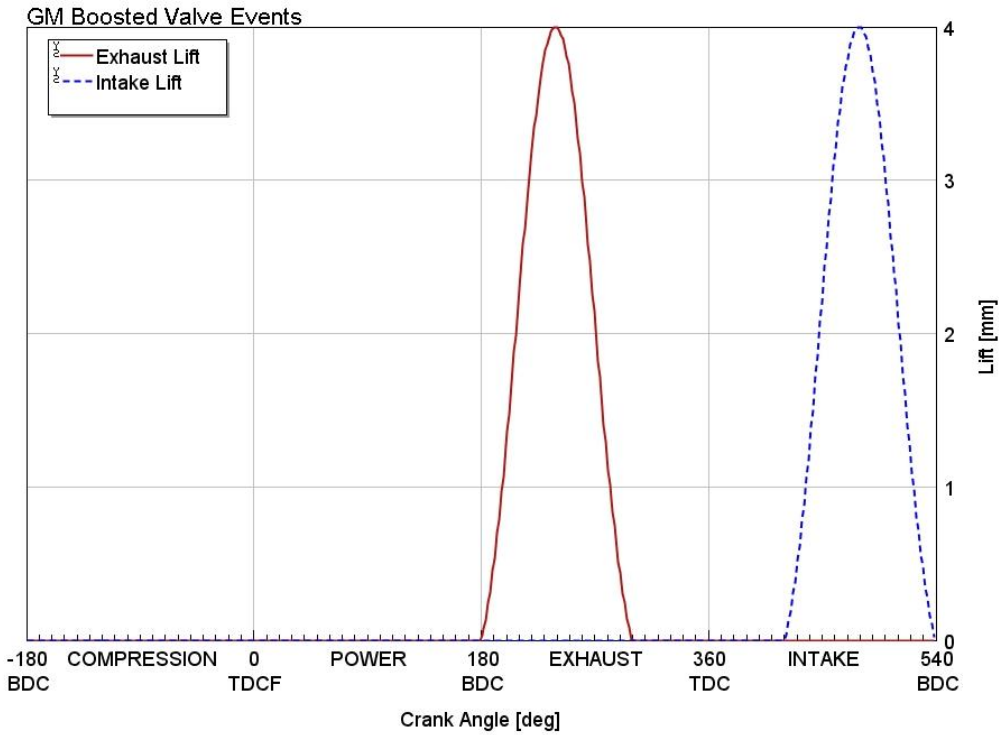

Figure 3.31 – GM boosted engine valve lifts for NVO = 120.9 CAD.

Heat Transfer Description

Results from the FFVA engine suggested that heat transfer played a critical role in successfully simulating the closed part of the cycle. The modified Woschni correlation that was proposed in 2004 did not help in achieving good agreement on gross indicated

efficiencies and it was replaced by the standard Woschni correlation [6]. TPA for the GM boosted engine confirmed the need for accurate heat transfer description and prompted a short comparison of available heat transfer correlations.

The classic Woschni correlation was developed for diesel engines and it proposed the following expression for the heat transfer coefficient:

$$h = 3.26 \cdot B^{-0.2} \cdot P^{0.8} \cdot T^{-0.53} \cdot w^{0.8} \tag{3.1}$$

where B is cylinder bore (m), P (kPa) and T (K) are instantaneous pressure and mean in-cylinder temperature respectively and w (m/s) is the characteristic velocity given by:

$$w = C_1 S_P + \frac{C_2}{6} \frac{V_d T_r}{P_r V_r} \left(P - P_{mot} \right) \tag{3.2}$$

With c_1 = 2.28 and c_2 = 3.24E-3. The rest of the parameters in equation (3.2) have been described in Chapter 2. The second term in equation (3.2) is referred to as pressure-velocity term and was introduced to capture the effect of a flame-affected boundary layer and the corresponding increase in heat loss to the walls. The modified Woschni correlation proposed a reduction in the pressure-velocity term by a factor of 6, based on the absence of propagating flame fronts in HCCI engines. In addition, the expression for heat transfer coefficient replaced the cylinder bore with instantaneous cylinder height and employed an increased exponent on the cylinder temperature.

Despite the fact that the modified Woschni expression was developed based on experimental HCCI measurements, it was observed that it overpredicted heat transfer in the simulations. For that reason, it was deemed appropriate to compare it to the classic Woschni and further modify it if needed. Figure 3.32 and Figure 3.33 show a comparison of the two correlations and display that the modified Woschni consistently calculated high heat flux before combustion and during recompression. A third correlation is also shown which is a hybrid between the first two and was named HCCI Woschni. The HCCI Woschni correlation utilized the pressure-velocity term reduction suggested in the

modified Woschni but kept the heat transfer coefficient expression of the original Woschni. TPA revealed that use of the HCCI Woschni correlation gave the most accurate description of the closed portion of the cycle and the best agreement in gross indicated efficiency.

It should be noted that the HCCI Woschni correlation was not developed using any kind of experimental results since that was out of the scope of the present research work; it was merely a product of combining features from different correlations in a way pertinent to HCCI engine operation. In addition, the author does not claim that the HCCI Woschni correlation is capable of capturing heat transfer phenomena in boosted HCCI engines. It was only derived based on post-processing of experimental and modeling results. In order to devise a heat transfer correlation capable of capturing boosted HCCI phenomena, further fundamental work would be required. The TPA and forward results that will be presented in the following have made use of the HCCI Woschni correlation.

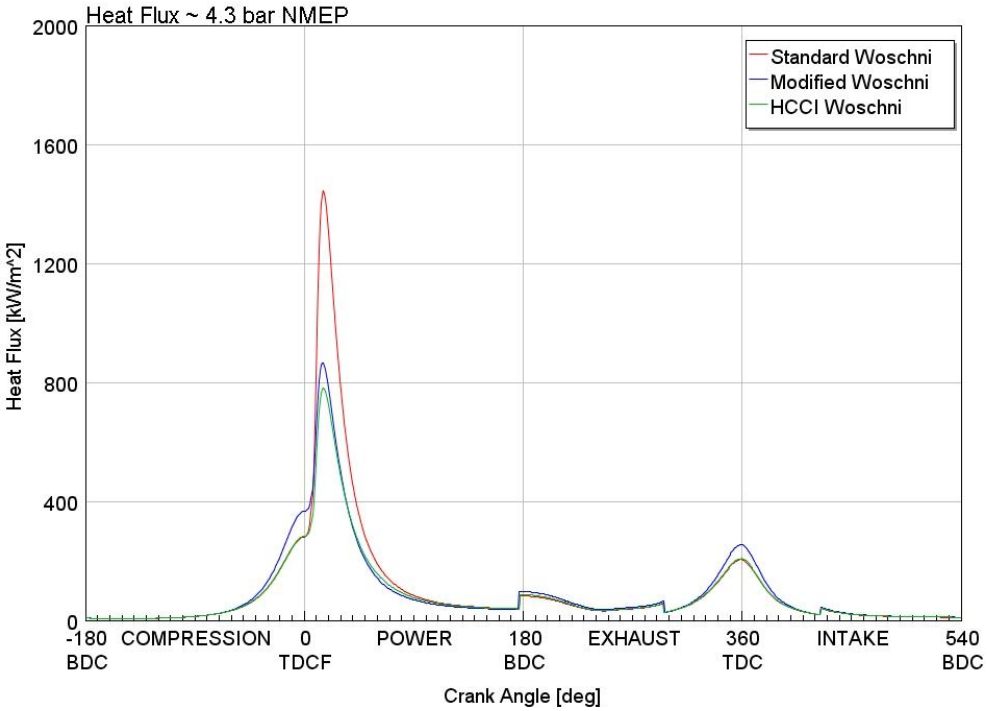

Figure 3.32 – Heat flux for the GM boosted HCCI engine at 4.3 bar NMEP – comparison of three heat transfer correlations.

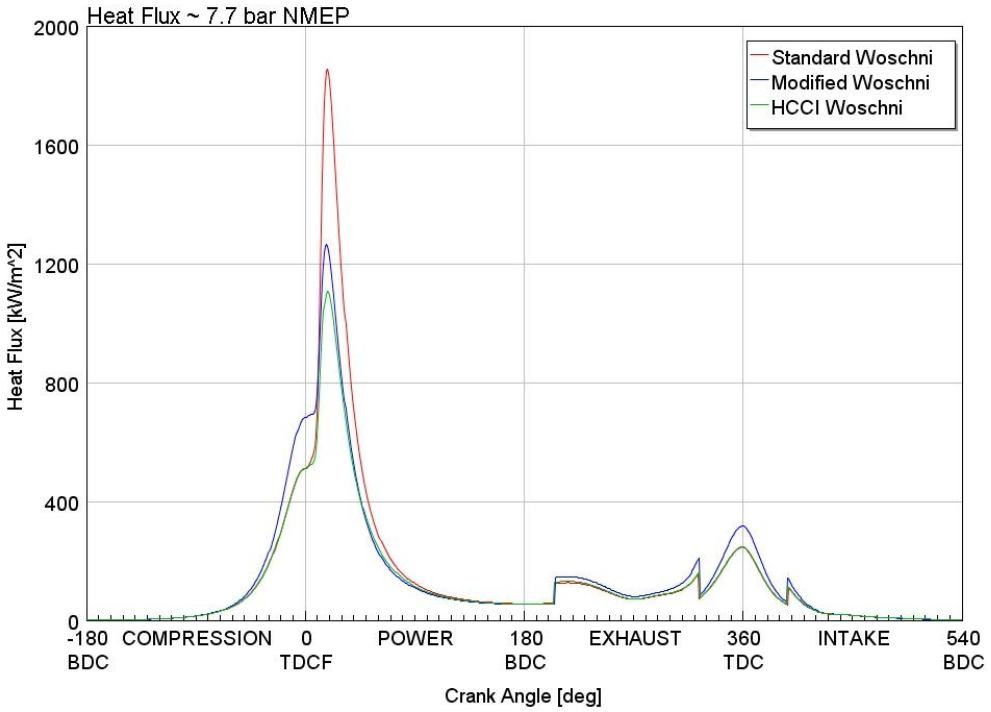

Figure 3.33 – Heat flux for the GM boosted HCCI engine at 7.7 bar NMEP – comparison of three heat transfer correlations.

Three Pressure Analysis Results

The following figures present the TPA results for the intake pressure and load sweep experiment. As explained above, the heat transfer correlation used was the HCCI Woschni. Figure 3.34 and Figure 3.35 display IMEPg and gross indicated efficiency as functions of fueling rate respectively. These performance parameters of the closed portion of the cycle reflect the importance of accurate heat transfer description. One can observe that agreement between experiment and simulation was excellent at medium loads and very good overall, although the model could not capture the exact slope of IMEPg or efficiency.

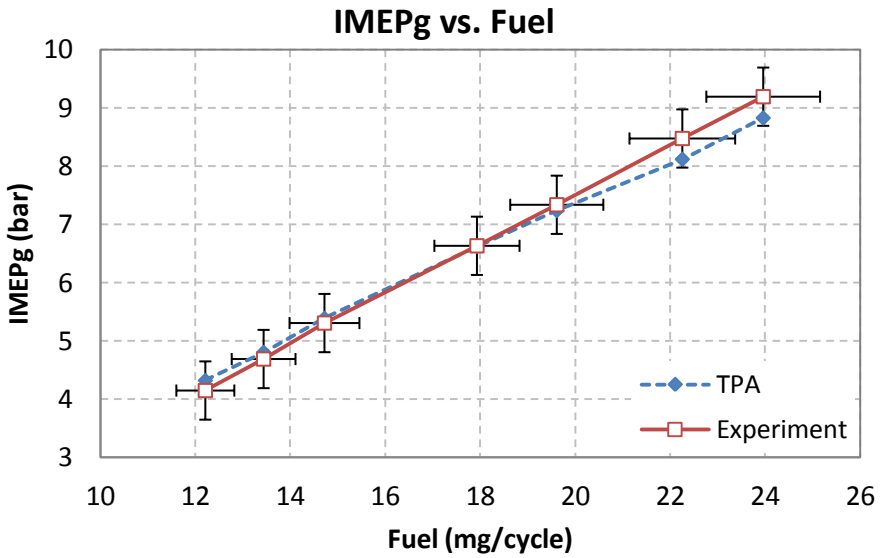

Figure 3.34 – Gross IMEP as a function of fueling rate from TPA of the GM boosted engine experiment.

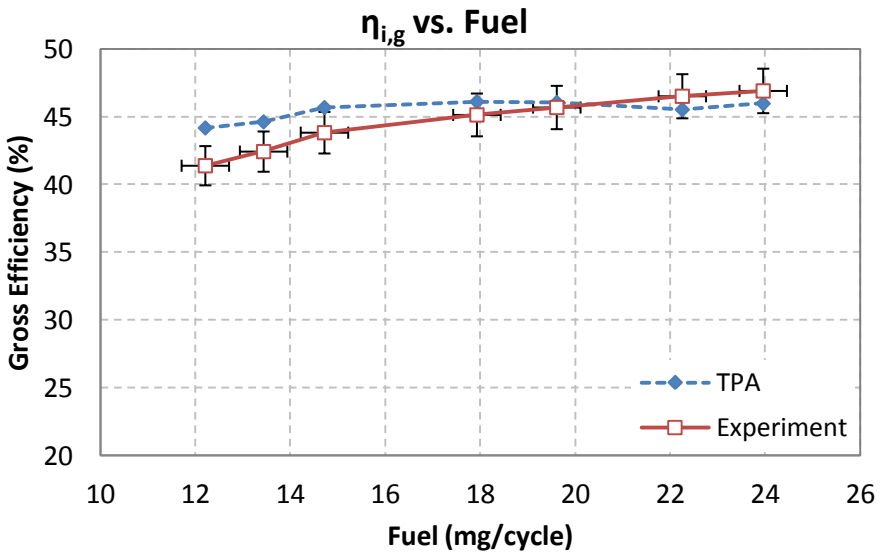

Figure 3.35 – Gross indicated efficiency as a function of fueling rate from TPA of the GM boosted engine experiment.

Figure 3.36 shows net IMEP as a function of fueling rate for the boosted experiment and it displays very good agreement between experiment and TPA across the load range. In contrast to what was observed for the FFVA experiment in the previous sections, pumping work was calculated satisfactorily in the simulation. Figure 3.37 shows PMEP as a function of fueling rate and reveals that the simulated PMEP was constantly

higher (more negative) than the one measured, but the difference was minimal at 0.1 bar or less. The very good agreement on PMEP can be attributed to use of appropriate discharge coefficients for simulating flows through the valves which were experimentally obtained.

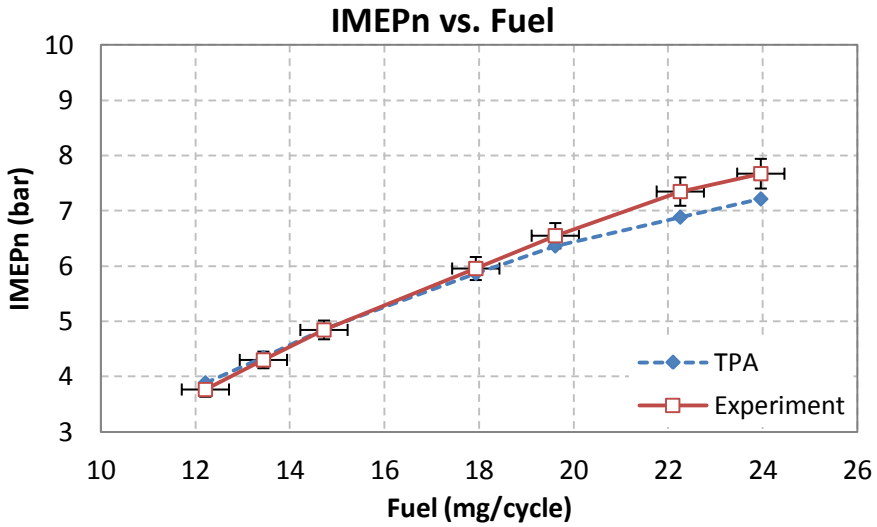

Figure 3.36 – Net IMEP as a function of fueling rate from TPA of the GM boosted engine experiment.

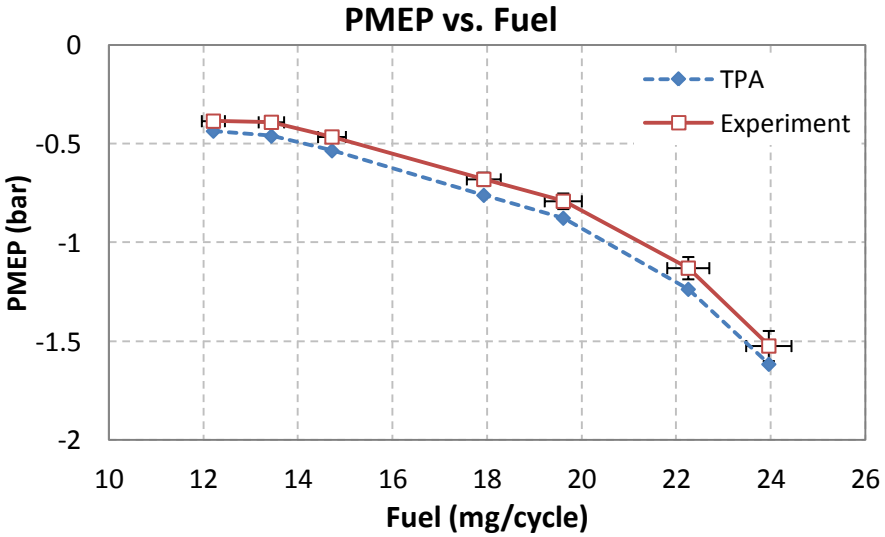

Figure 3.37 – PMEP as a function of fueling rate from TPA of the GM boosted engine experiment.

Figure 3.38 and Figure 3.39 show air and total trapped masses as functions of fueling rate and verify the very good agreement between experiment and TPA. Accurate calculation of the trapped masses was essential for composition and work calculations and TPA showed that the engine model was very good at calculating mass flows into and out of the cylinder. Some discrepancies remain at low and high loads but they were always lower than 4 % which was considered very good. Residual gas fraction also played an important role in the accurate representation of the experiment and it is shown in Figure 3.40 as a function of fueling rate. TPA was successful at calculating air and total trapped mass in the cylinder, therefore good calculations of RGF followed naturally. RGF was used to simultaneously control charge temperature and composition on a cycle basis, and had a direct effect on ignition timing. The latter was a critical factor in the assessment of the model that will be discussed in the following section. As noted previously for the FFVA engine results, RGF was not a direct measurement but a result of heat release analysis; as such, it could not be used as a metric for model calibration purposes.

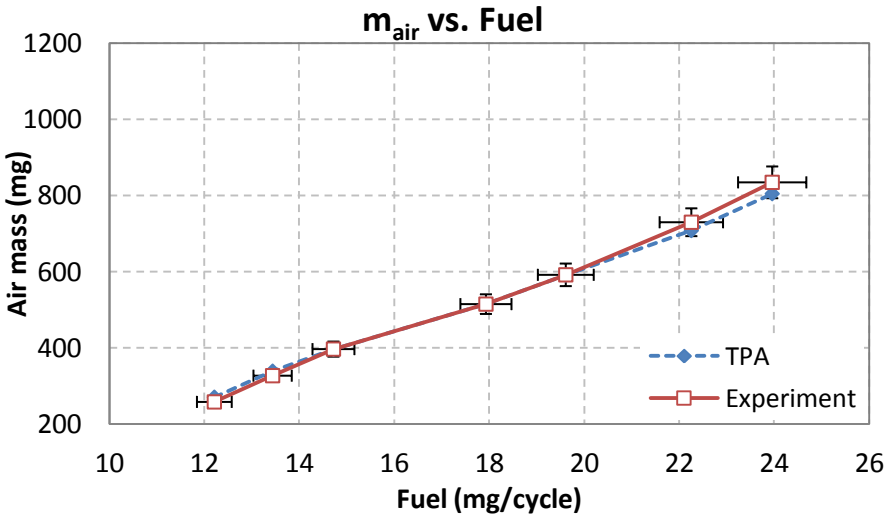

Figure 3.38 – Trapped air mass as a function of fueling rate from TPA of the GM boosted engine experiment.

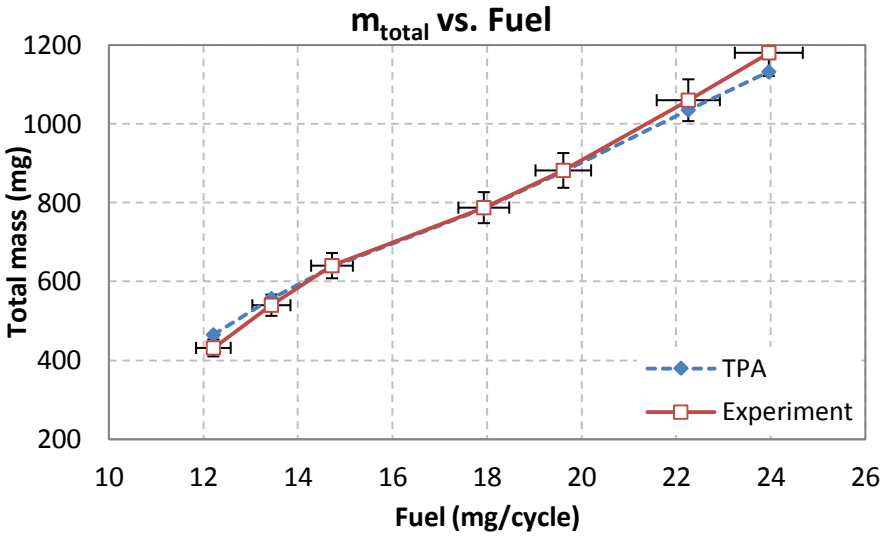

Figure 3.39 – Trapped total mass as a function of fueling rate from TPA of the GM boosted engine experiment.

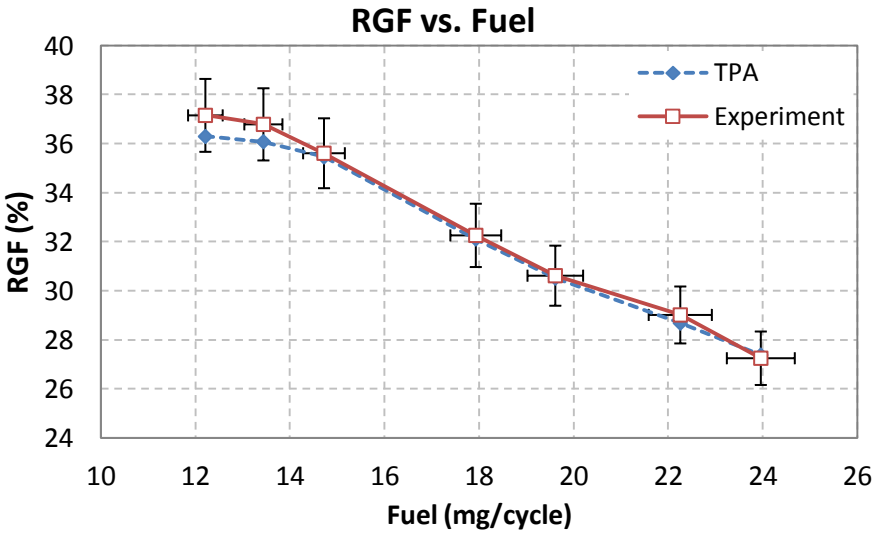

Figure 3.40 – Trapped total mass as a function of fueling rate from TPA of the GM boosted engine experiment.

The composition parameters that were calculated from TPA are shown in Figure 3.41 and Figure 3.42 and confirm the successful simulation of the gas exchange process. Equivalence ratio was affected by trapped air mass and fueling rate; effective equivalence ratio was additionally affected by residual gas in the cylinder. The excellent agreement observed in previous plots justified the agreement in equivalence ratios between experiment and TPA. As discussed in Chapter 2, Φ' was one of the factors that control

burn duration in the HCCI combustion correlation; therefore, its accurate calculation was critical for successful forward simulations.

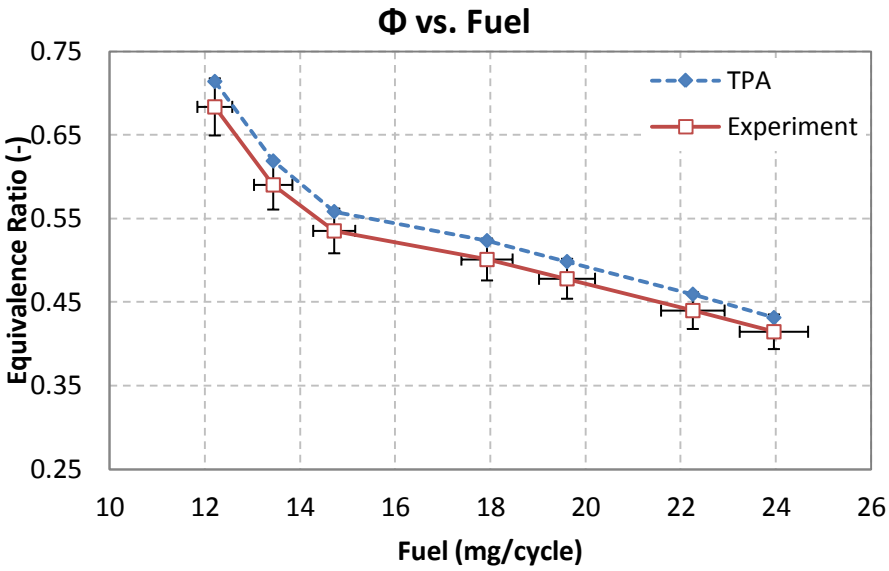

Figure 3.41 – Equivalence ratio as a function of fueling rate from TPA of the GM boosted engine experiment.

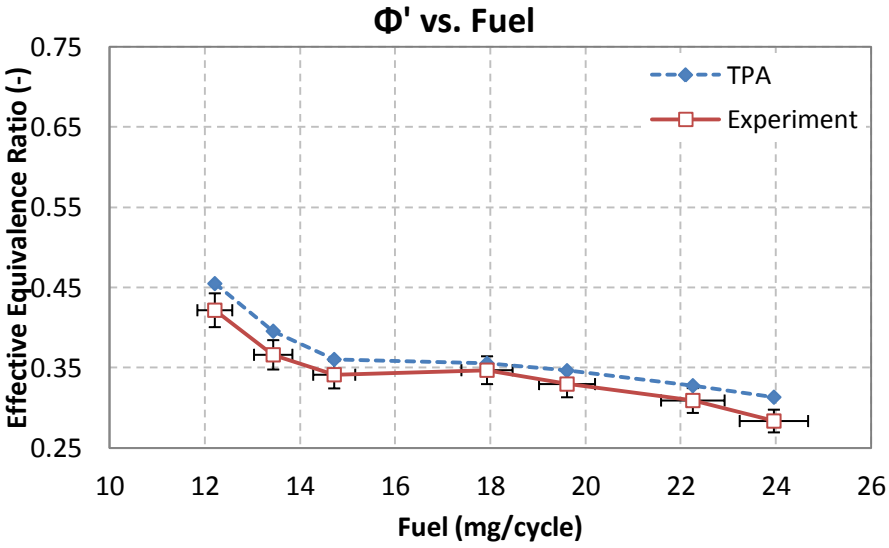

Figure 3.42 – Effective equivalence ratio as a function of fueling rate from TPA of the GM boosted engine experiment.

3.2.2 GM Boosted Forward Simulation

After three pressure analysis had been completed and its results had been examined, the boosted HCCI experiment was replicated using the UM combustion model. The accurate representation of the gas exchange process achieved with TPA, along with use of the HCCI Woschni heat transfer correlation provided a solid ground for successful forward simulation of the boosted experiment. The following set of plots display similar results to those presented earlier for the FFVA forward simulation and compare modeling to experimental results. Adding to the results shown in the TPA discussion of the previous section, this section will present combustion parameters that were calculated by the UM HCCI model such as CA50, burn duration and combustion efficiency. The conditions used for the forward simulation were the same as those used for TPA and were displayed in Table 3.2. The scope behind forward simulation of the boosted HCCI experiment was to identify potential weaknesses of the model and to calibrate the DLT and Bx parameters (shown in Chapter 2) so that experimental results are accurately represented. The following simulation curves include tuning of these two parameters and are directly compared to the experimental ones.

Figure 3.43 and Figure 3.44 show gross IMEP and gross indicated efficiency as functions of fueling rate and exhibit very good agreement between the calibrated model and the experiment. As observed from TPA results, agreement was best at low and medium loads; at high load levels the simulation calculated lower efficiency than what was measured. However, the difference in IMEPg and gross indicated efficiencies was always lower than 6 % which was considered satisfactory. Good closed cycle performance calculations verified the choice of HCCI Woschni as the most appropriate correlation for boosted HCCI simulation.

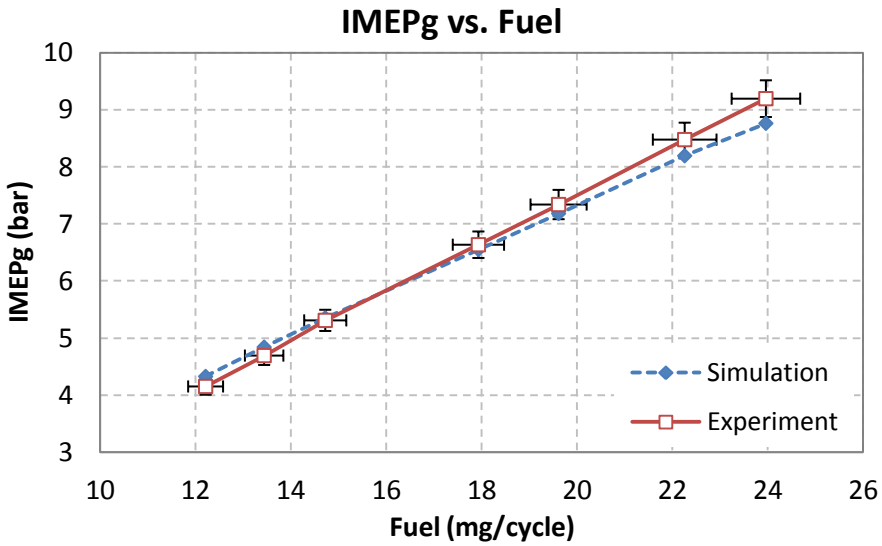

Figure 3.43 – Gross IMEP as a function of fueling rate from forward simulation of the GM boosted engine experiment.

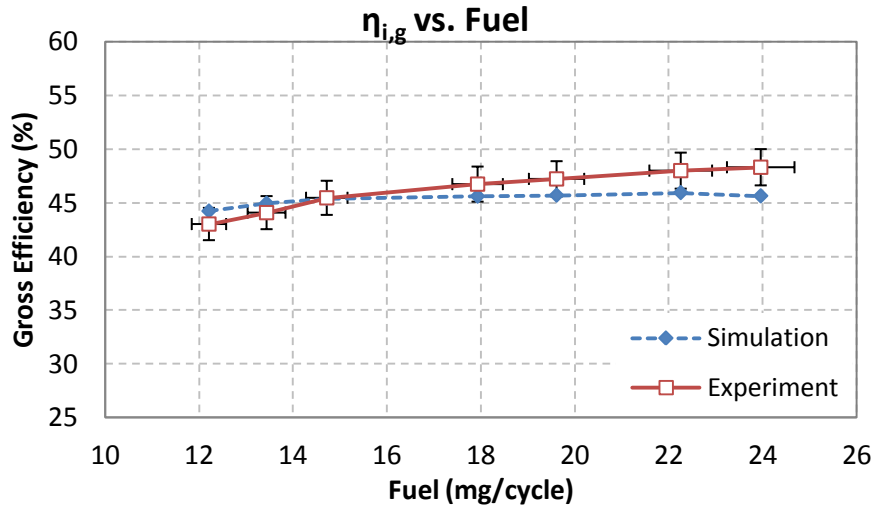

Figure 3.44 – Gross indicated efficiency as a function of fueling rate from forward simulation of the GM boosted engine experiment.

Three pressure analysis showed that the engine model was very good at calculating the gas exchange process which was confirmed by the results of the forward simulation. Figure 3.45 and Figure 3.46 show net IMEP and PMEP as functions of fueling rate and it can be observed that the calibrated model was very good at calculating pumping work and net performance parameters. Pumping work was always higher in the model but the difference never exceeded 0.15 bar. The increased pumping work in the

model can be attributed to discharge coefficients that simulated more restrictive valves that the actual ones. Good calculation of net performance parameters was confirmed by net specific fuel consumption which is shown in Figure 3.47. The increased PMEP calculated by the model resulted in higher NSFC values that then experiment but the agreement was overall good.

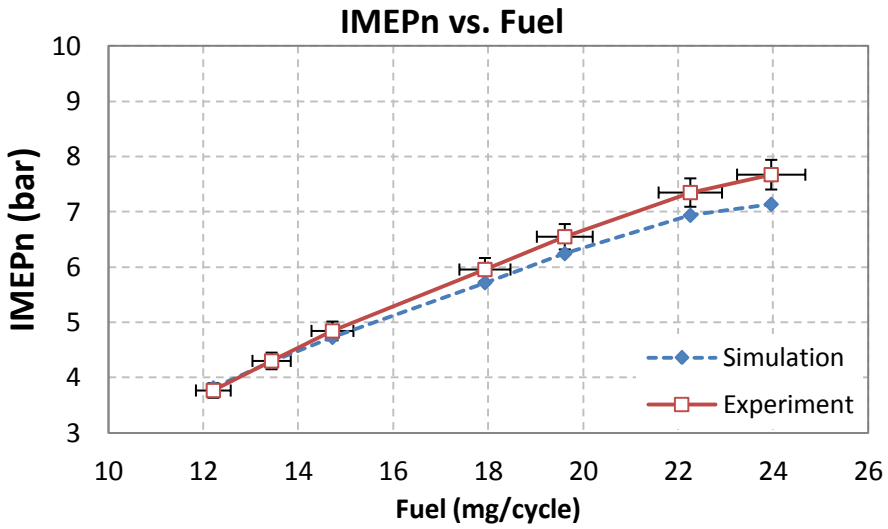

Figure 3.45 – Net IMEP as a function of fueling rate from forward simulation of the GM boosted engine experiment.

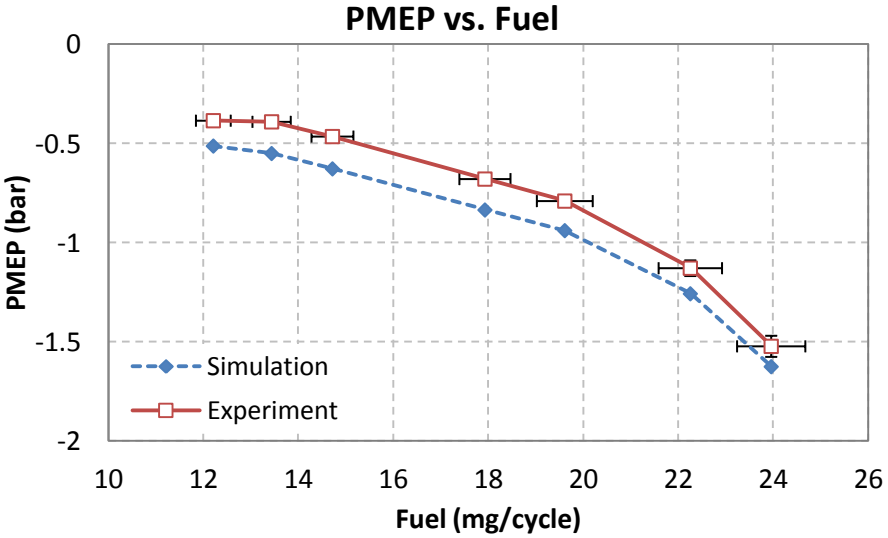

Figure 3.46 – Net IMEP as a function of fueling rate from forward simulation of the GM boosted engine experiment.

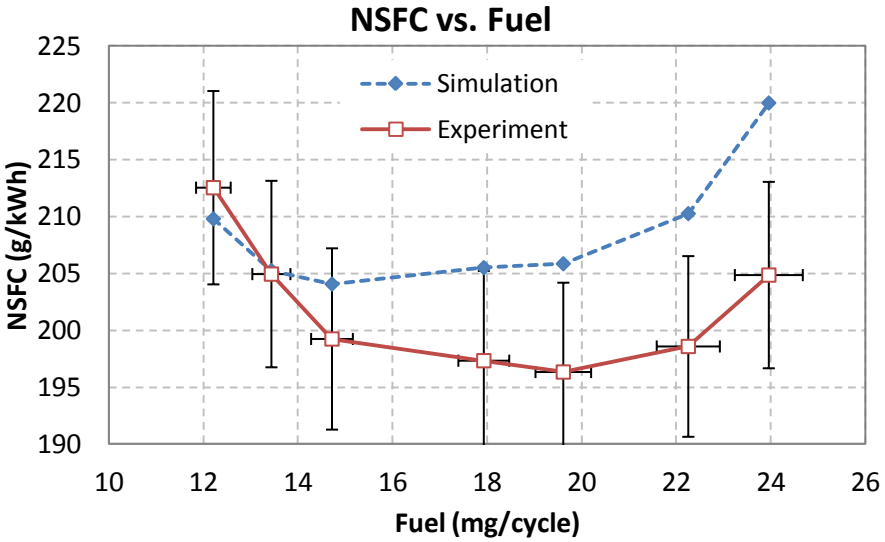

Figure 3.47 – Net ISFC as a function of fueling rate from forward simulation of the GM boosted engine experiment.

Good calculation of net performance parameters would not be possible without accurate calculation of cylinder trapped total and air masses. Figure 3.48 and Figure 3.49 display the excellent agreement on trapped total and air masses between the simulation and the experiment.

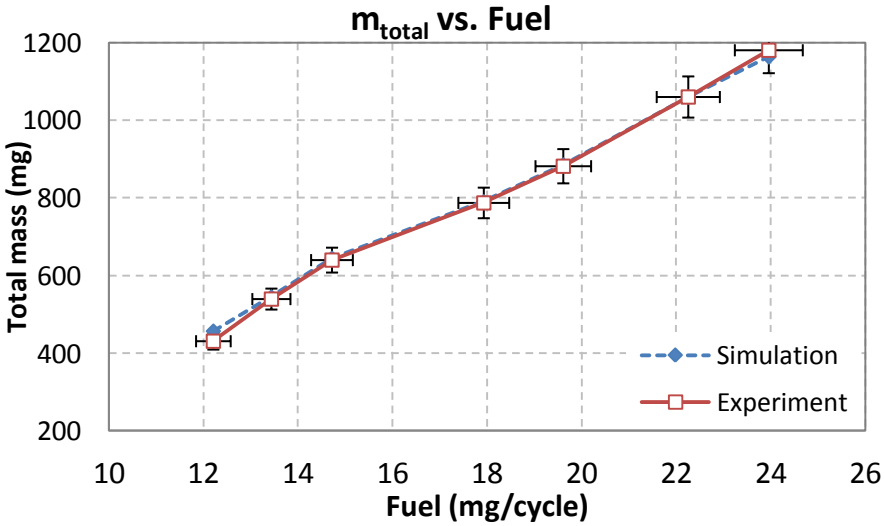

Figure 3.48 – Trapped total mass as a function of fueling rate from forward simulation of the GM boosted engine experiment.

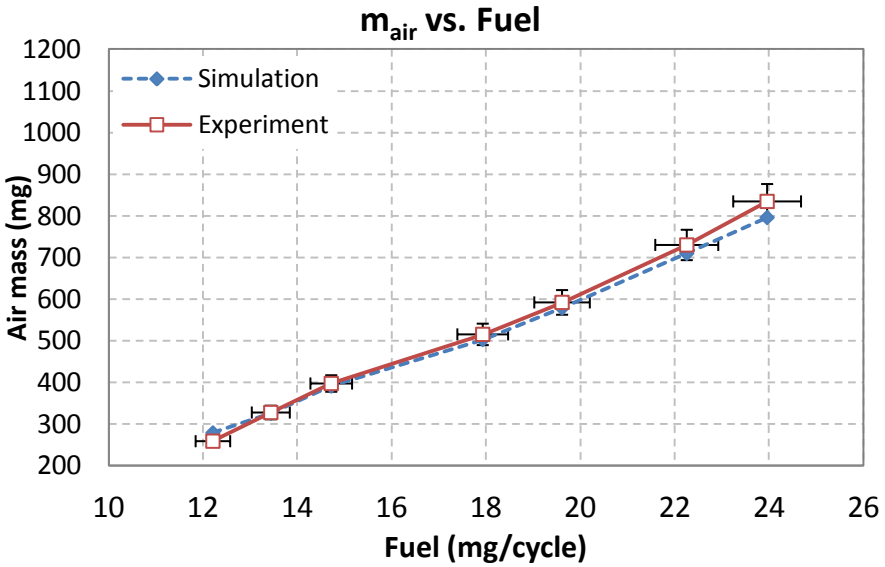

Figure 3.49 – Trapped air mass as a function of fueling rate from forward simulation of the GM boosted engine experiment.

Residual gas fraction was also calculated satisfactorily and it is shown in Figure 3.50. Since the simulated trapped total and air masses were very close to those measured, RGF followed the same trend. Good agreement was also observed in the equivalence ratio and effective equivalence ratio shown in Figure 3.51 and Figure 3.52. Good agreement on Φ' ensured accurate calculation of ignition timing and burn rates from the model.

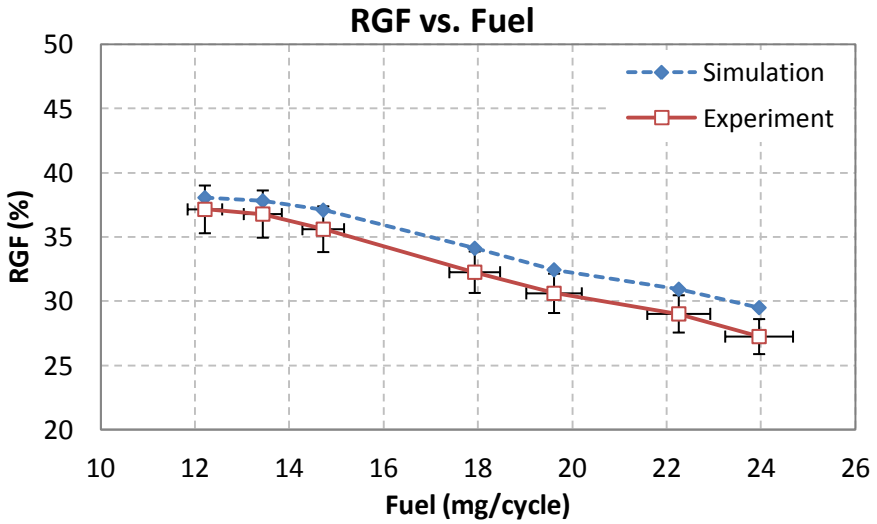

Figure 3.50 – Residual gas fraction as a function of fueling rate from forward simulation of the GM boosted engine experiment.

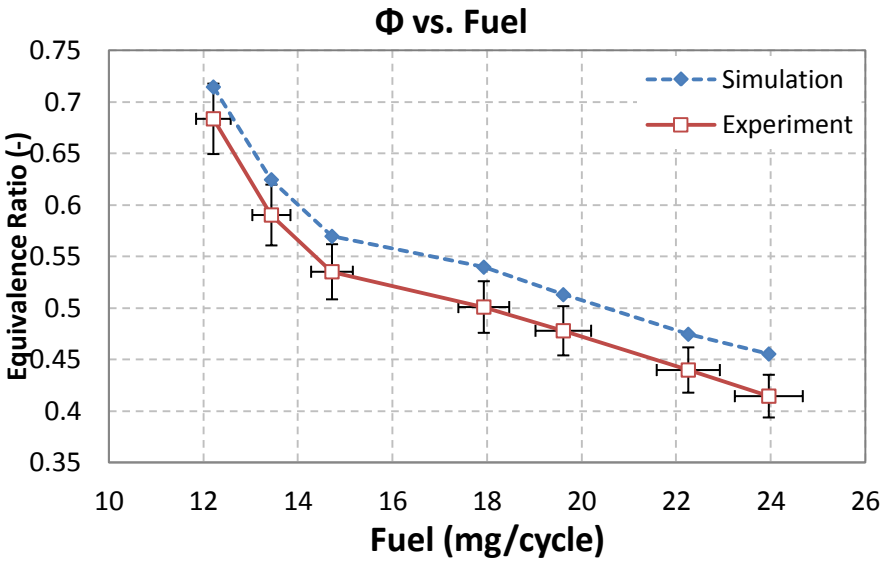

Figure 3.51 – Equivalence ratio as a function of fueling rate from forward simulation of the GM boosted engine experiment.

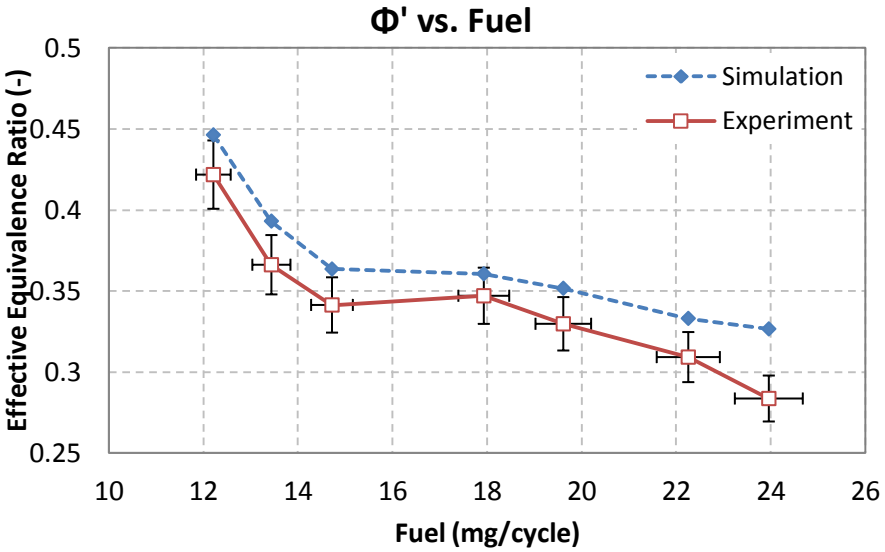

Figure 3.52 – Effective equivalence ratio as a function of fueling rate from forward simulation of the GM boosted engine experiment.

Figure 3.53 and Figure 3.54 show two combustion parameters that were critical in the assessment of the combustion model; crank angle of 50 % burn and burn duration as functions of fueling rate. Calibrating the combustion model by tuning the DLT and Bx parameters was based on experimentally derived CA50 and burn duration values. DLT calibration aimed at accurate calculation of ignition timing, while Bx calibration aimed at

accurate calculation of burn duration. The calibration process was successful since the calculated CA50 and CA10-90 values were very close to those observed in the experiment. The autoignition correlation seemed to calculate later ignition timing at low and medium loads but that effect was mitigated as load increased. The end result was good calculation of CA50 location and very good calculation of burn duration across the load range. It should be highlighted that as intake pressure and load increased, autoignition chemistry was accelerated which had to be reflected in the autoignition correlation of the model. The literature has not shown any dependence of burn duration on intake pressure but it has shown strong dependence on ignition timing and stratification phenomena in the cylinder. The absence of any stratification description in the model required calibration of Bx so that burn duration could be calculated accurately. Figure 3.54 shows that accurate calculation of burn duration was possible although the model lacked detailed physical description of the combustion chamber. Analysis of the combustion events suggested that CA50 occurred between 9 and 13 CAD aTDC across the load range and burn duration ranged from 10 to 12 CAD.

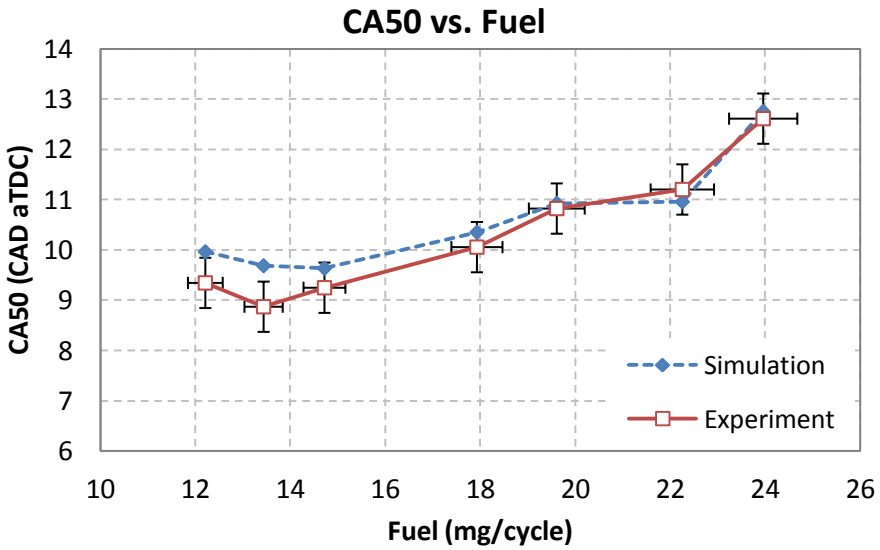

Figure 3.53 – CA50 location as a function of fueling rate from forward simulation of the GM boosted engine experiment.

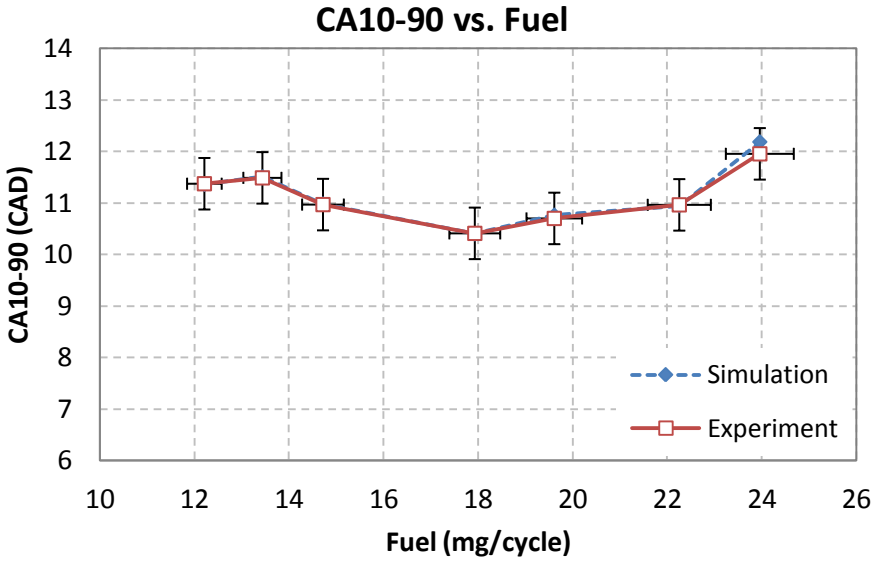

Figure 3.54 – Burn duration as a function of fueling rate from forward simulation of the GM boosted engine experiment.

As a consequence of accurate ignition timing and burn duration calculations, the pressure rise rates and peak pressures in the cylinder were also accurately calculated. The result was good agreement on ringing intensity as seen in Figure 3.55. Ringing intensity in the simulation was somewhat lower that the one derived from the experiments but the model was able to capture the trend of reduced R.I. with later and longer combustion events. On the other hand, the agreement on NO_x emissions was not that good, which was also observed in the FFVA forward simulation. Figure 3.56 shows NO_x emissions index as a function of fueling rate and it can be seen that the simulated NO_x was significantly lower that the measured one. It should be noted that in the experiment, maximum load at naturally aspirated conditions was constrained by NO_x emissions. The first experimental point in Figure 3.56 exceeded the 1 g/kg fuel limit posed by the US-2010 emissions regulations, but the model could not calculate that level of NO_x formation. Boosted operation drastically reduced NOx formation due to increasing dilution levels of the charge and lower cylinder temperatures.

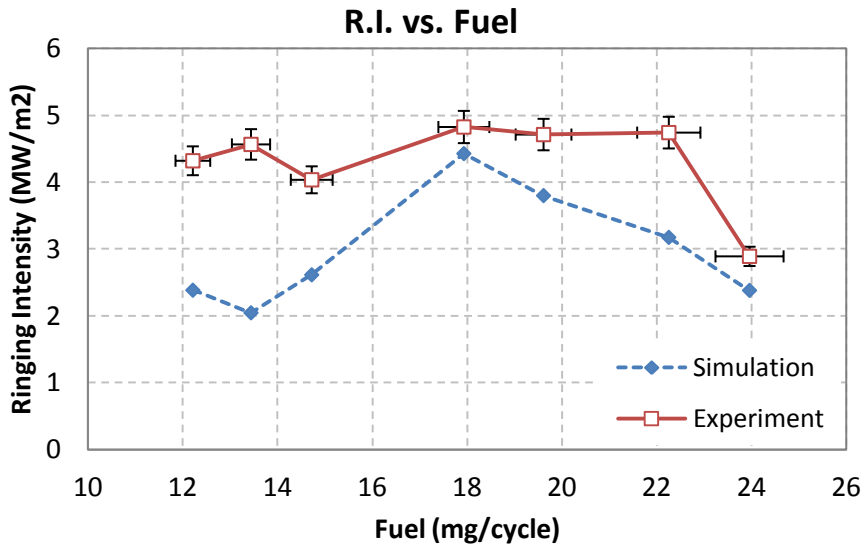

Figure 3.55 – Ringing Intensity as a function of fueling rate from forward simulation of the GM boosted engine experiment.

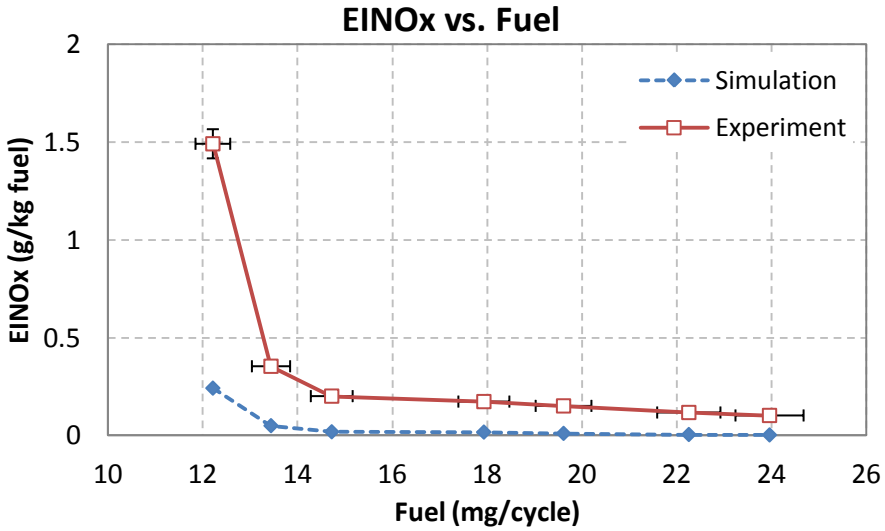

Figure 3.56 – NO_x emissions index as a function of fueling rate from forward simulation of the GM boosted engine experiment.

The last combustion parameter that was involved in the comparison of the forward simulations to experimental results was combustion efficiency and it is shown in Figure 3.57. It should be highlighted that the two curves shown in this plot represent two different combustion efficiency definitions. The experimentally measured one was derived from the exhaust gas composition and was always higher the simulated one, which was a calculation of in-cylinder combustion efficiency. As such, the exhaust

measurement included residual gas trapped in the cylinder which had a second chance to burn; that explains the higher combustion efficiency values. Limited conclusions can be drawn about the accuracy of the model; however, increased dilution levels with boost and load resulted in reduced combustion efficiency which agrees with results reported in the literature.

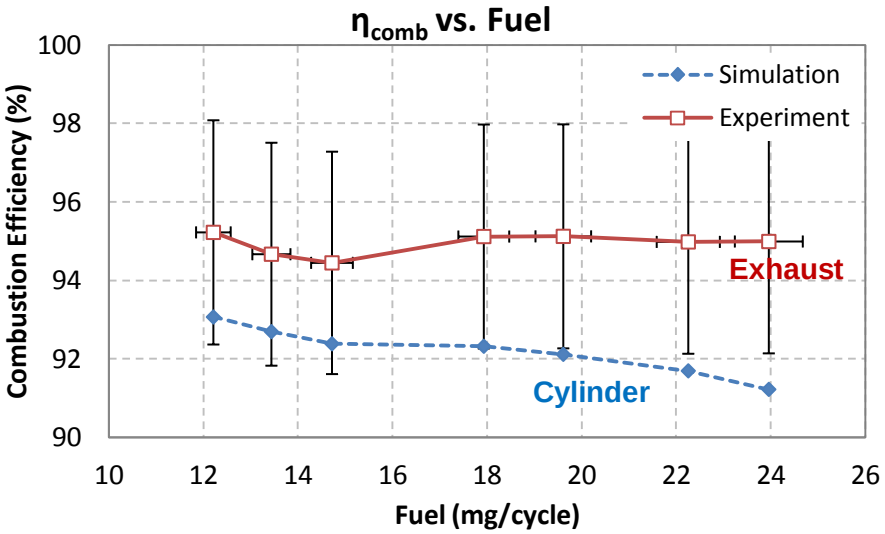

Figure 3.57 – Combustion efficiency as a function of fueling rate from forward simulation of the GM boosted engine experiment.

The following four plots compare experimental and simulated pressure traces at two operating points; 3.8 bar IMEPn and 6 bar IMEPn during the combustion and recompression events. Figure 3.58 shows pressure traces for the 3.8 bar IMEPn case during the main compression, combustion and expansion events. It can be observed that the calibrated model produced a pressure trace that was very close to the experimental one albeit certain discrepancies can be identified. Peak cylinder pressure was 3 bar higher in the simulation and post-compression pressures were 0.6 bar lower. The former can be attributed to higher burn rates calculated by the model; the latter can be attributed to pre-ignition reactions that could not be captured by the model.

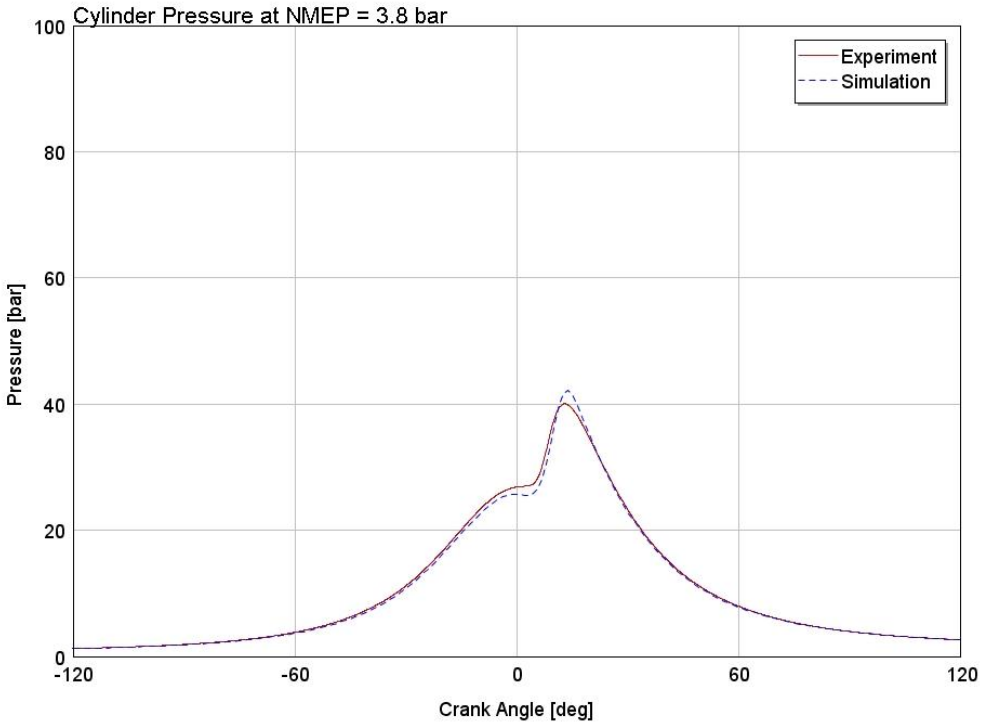

Figure 3.58 – Cylinder pressures during combustion at 3.8 bar IMEPn for the GM boosted engine experiment and simulation.

Figure 3.59 compares pressure traces for the same operating point during the recompression period. As observed in the FFVA engine simulation, the experimental pressure trace was higher than the simulated one during recompression, which can be attributed to heat release which could not be captured by the model.

Figure 3.60 and Figure 3.61 show the same pressure traces for a higher load operating point, at 6 bar IMEPn. The differences between the pressure traces remain as those seen in the previous plots but they were more pronounced because of increased charge mass and enhanced autoignition kinetics with pressure. Therefore, the difference in post-compression pressure was increased and so was the difference in peak pressure. During the recompression period, the experimental pressure was again higher than the simulated one confirming the hypothesis that heat release phenomena were occurring in the GM boosted engine.

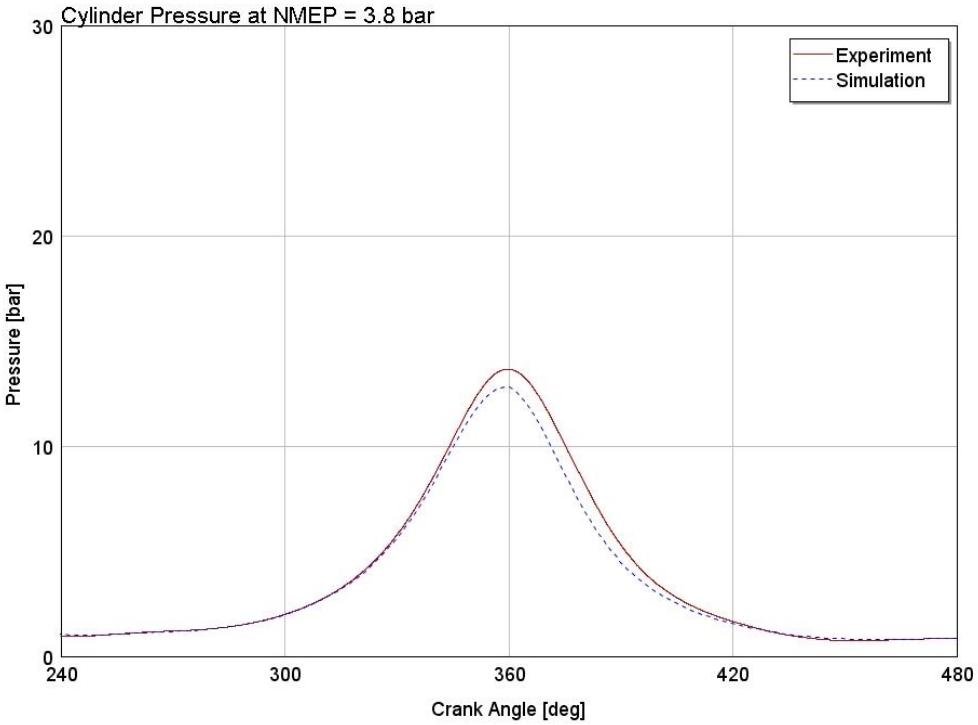

Figure 3.59 – Cylinder pressures during recompression at 3.8 bar IMEPn for the GM boosted engine experiment and simulation.

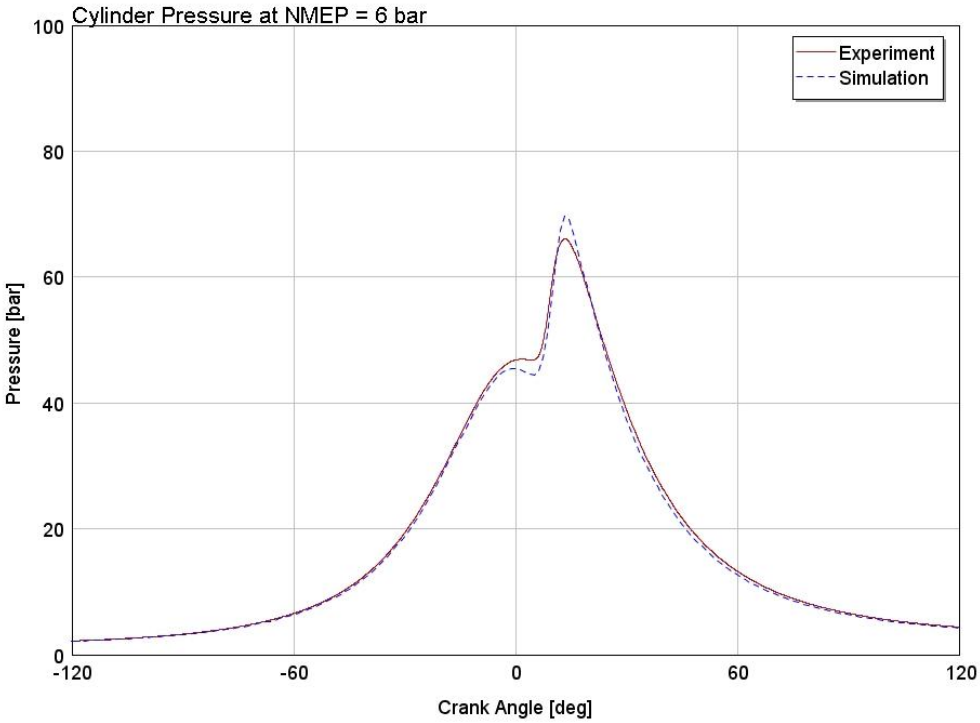

Figure 3.60 – Cylinder pressures during combustion at 6 bar IMEPn for the GM boosted engine experiment and simulation.

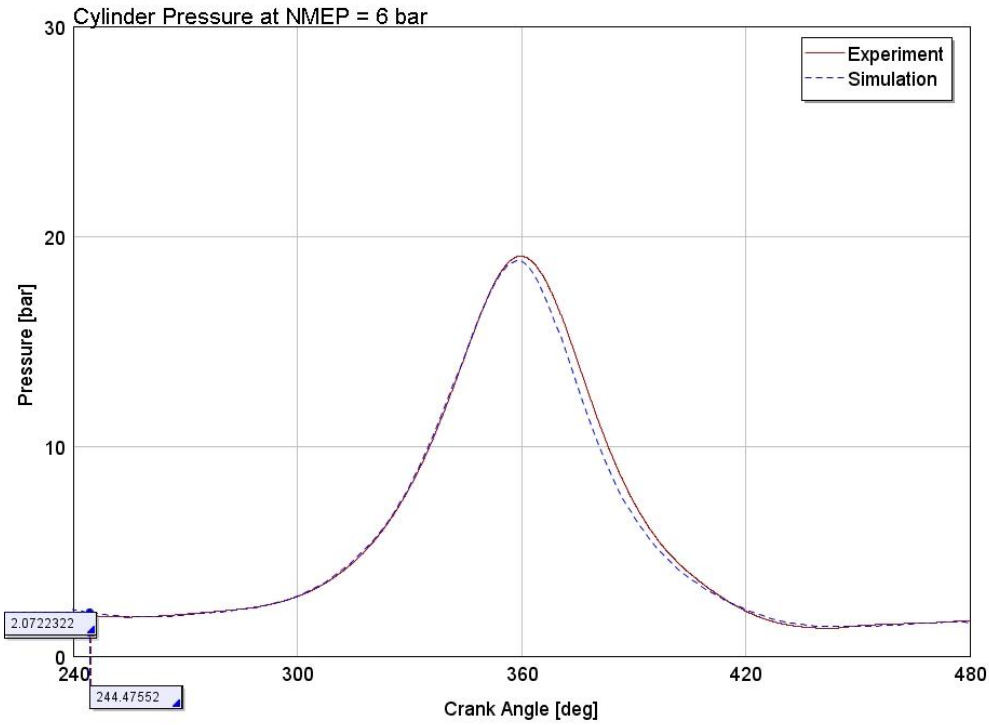

Figure 3.61 – Cylinder pressures during recompression at 6 bar IMEPn for the GM boosted engine experiment and simulation.

In conclusion, the combustion model had to be calibrated in order to be able to capture the ignition timing and burn duration effects of boosted HCCI operation. The calibration included reduction of the DLT parameter in order to account for enhanced autoignition kinetics with boost and adjustment of the Bx parameter to account for changes in burn duration that occurred with boost and reduced NVO. Overall, the calibrated model aided by the HCCI Woschni heat transfer correlation performed well and calculated the experimental operating points satisfactorily. The following section will present the third and last set of experimental results that were used for model performance evaluation and were sourced from Sandia National Laboratories.

3.3 Model Performance Evaluation against Sandia Engine Results

The first two experiments that were presented in the previous sections (FFVA and GM boosted engines) were utilized in order to assess the performance of the UM combustion model in simulating HCCI combustion in light-duty automotive engines using negative valve overlap. Publications from Sandia National Laboratories have presented studies on boosted HCCI operation in a medium-duty engine that features positive valve overlap and a more robust engine structure [5]. The Sandia experiments did not involve variable valve actuation or residual gas trapping for charge temperature and composition control. They accomplished HCCI combustion by regulating intake temperature for ignition control and used external EGR to control combustion phasing and burn rates. The outcome was what researchers often refer to as "pure HCCI", meaning that there was minimal residual gas trapped in the cylinder from cycle to cycle, thus altering charge composition compared to NVO engines. In addition, the Sandia engine featured compression ratio of 14 which created more favorable TDC conditions for autoignition compared to the FFVA and GM boosted engines. Therefore, it was deemed necessary to evaluate the performance of the burn model against the Sandia experiment in order to identify potential limits and drawbacks. The experiment consisted of a simultaneous intake pressure and load sweep and the boundary conditions are shown in Table 3.3. Intake pressure spanned a wider range compared to the GM boosted engine experiment but backpressure was only 2 kPa higher than the intake in all cases [5]. The authors employed external EGR when intake pressure reached 1.8 bar and EGR was increased as boost and load increased further.

Simulation of the Sandia experiment started from three pressure analysis (TPA) and proceeded with forward simulations. The latter revealed some weaknesses of the autoignition correlation which will be analyzed in the following.

Table 3.3 – Sandia engine intake pressure and load sweep operating conditions

Intake Pressure (bar)	1	1.3	1.6	1.8	2	2.4	2.8	3.25
Exhaust Pressure (bar)	1.02	1.32	1.62	1.82	2.02	2.42	2.82	3.27
Intake Temperature (K)	485.1	489.9	493.7	501	510.5	514.2	509.8	507.6
PVO (CAD)	7	7	7	7	7	7	7	7
Fuel (mg/cycle)	27	35.1	44.5	52.1	50.9	70.6	75	79.3
η_{comb} (%)	93.2	93.2	93.1	93	93	92.8	92.4	91.4

3.3.1 Sandia Experiment Three Pressure Analysis

Three pressure analysis was the starting point for the Sandia engine simulation in the same way as the FFVA and GM boosted experiments were approached. Inputs to the model included instantaneous intake, exhaust and cylinder pressures, intake temperature, valve events, fueling rate and combustion efficiency. The following plots will compare experimental and TPA curves for performance and composition parameters. Figure 3.62 shows gross IMEP as a function of fueling rate and displays very good agreement between the experiment and three pressure analysis. Attainable load spanned a wider range compared to the GM boosted engine experiment.

Figure 3.63 shows net specific fuel consumption as a function of fueling rate which confirmed the good agreement between experiment and TPA as seen from the IMEPg curves. IMEPn or PMEP values were not provided by the authors but the net ISFC curves revealed that the simulated pumping work would be very close to the actual. Use of minimal positive valve overlap in this engine and virtually no backpressure translated to minimal pumping work across the load range, in contrast to the NVO engines examined in the previous sections.

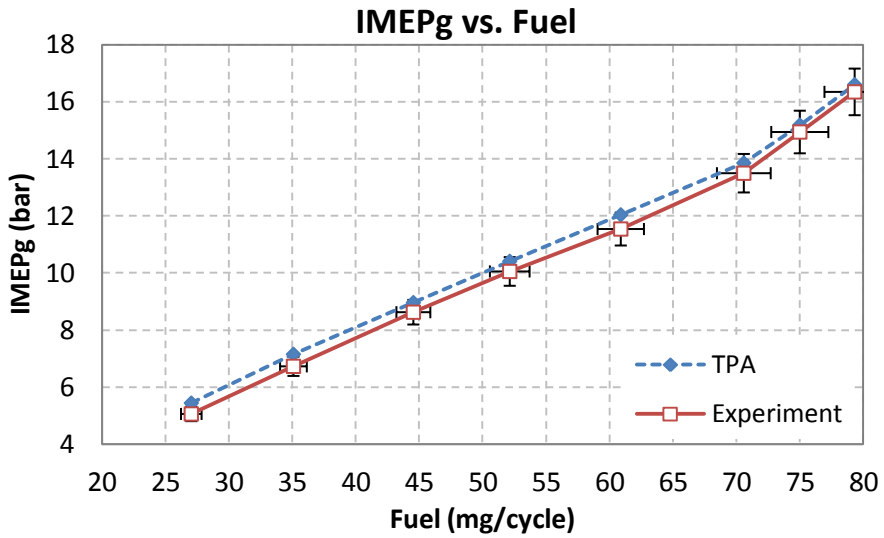

Figure 3.62 – Gross IMEP as a function of fueling rate from TPA of the Sandia engine experiment.

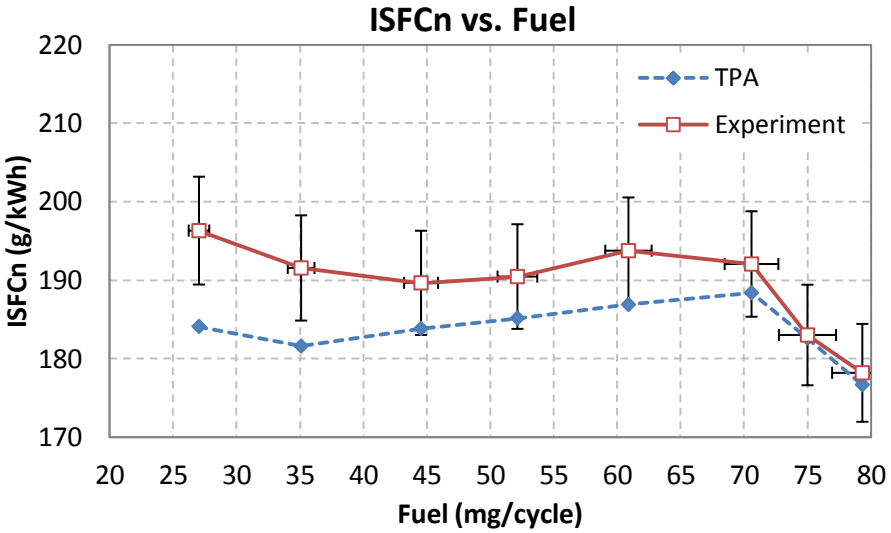

Figure 3.63 – Net specific fuel consumption as a function of fueling rate from TPA of the Sandia engine experiment.

Figure 3.64 and Figure 3.65 compare trapped total and air masses between the experiment and TPA. It was observed that trapped total and air masses were always higher in the three pressure analysis with a maximum difference of 11 %. The difference can be attributed to discharge coefficients that made the valves less restrictive that the actual ones, allowing more air and exhaust gas to flow into and out of the cylinder. It

should be noted that trapped air mass peaked at 1.6 bar intake pressure (44.5 mg/cycle of fuel) and reduced as external EGR was used to displace fresh air in the cylinder.

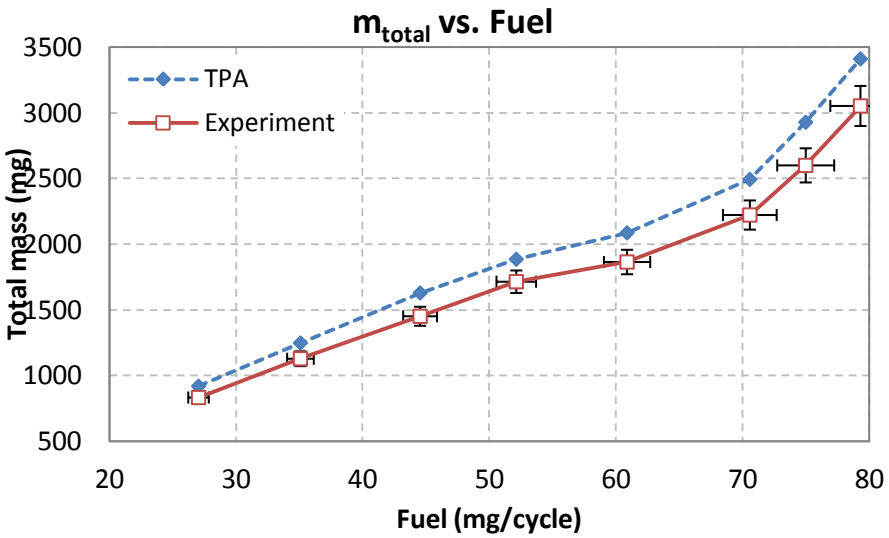

Figure 3.64 – Trapped air mass as a function of fueling rate from TPA of the Sandia engine experiment.

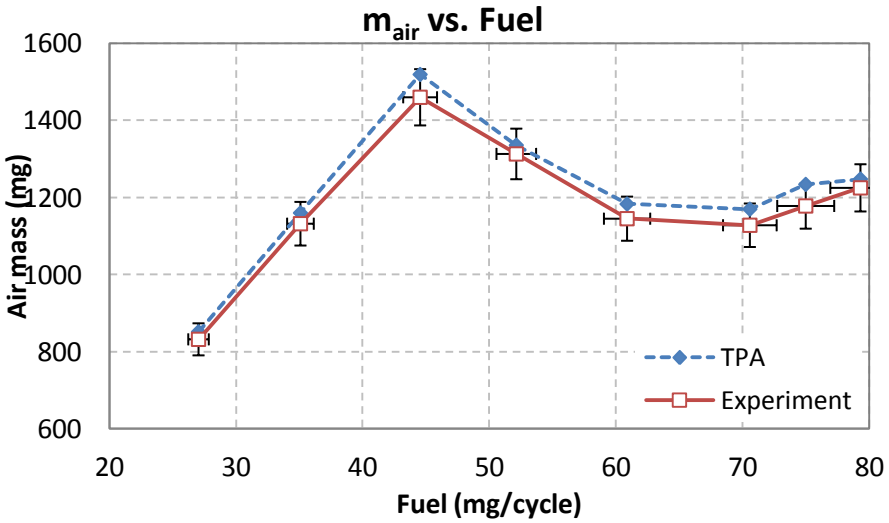

Figure 3.65 – Trapped air mass as a function of fueling rate from TPA of the Sandia engine experiment.

Figure 3.66 and Figure 3.67 show equivalence ratio and effective equivalence ratio as functions of fueling rate for the experiment and TPA. Both plots show that three pressure analysis was very good at simulating mass flows into and out of the cylinder, resulting in very good description of the actual composition. The fact that Φ in TPA deviated from the measured one after 1.6 bar intake pressure, indicates that simulated EGR trapped in the cylinder was more than that measured in the experiment.

Figure 3.68 shows gross indicated efficiency as a function of fueling rate and it confirms the very good agreement for the closed portion of the cycle as seen from the IMEPg curves previously. It should be noted that the heat transfer correlation used for TPA was the classic Woschni as described in previous sections and aided accurate simulation of the closed portion of the cycle.

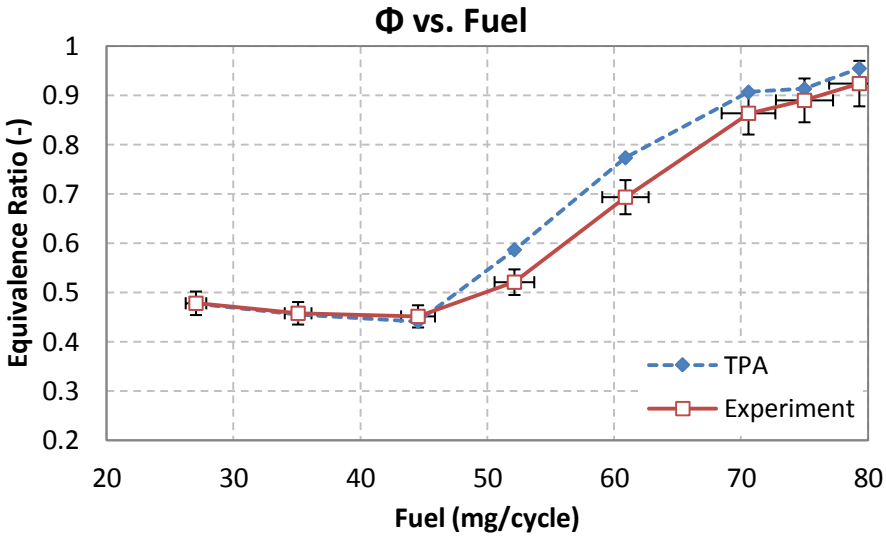

Figure 3.66 – Equivalence ratio as a function of fueling rate from TPA of the Sandia engine experiment.

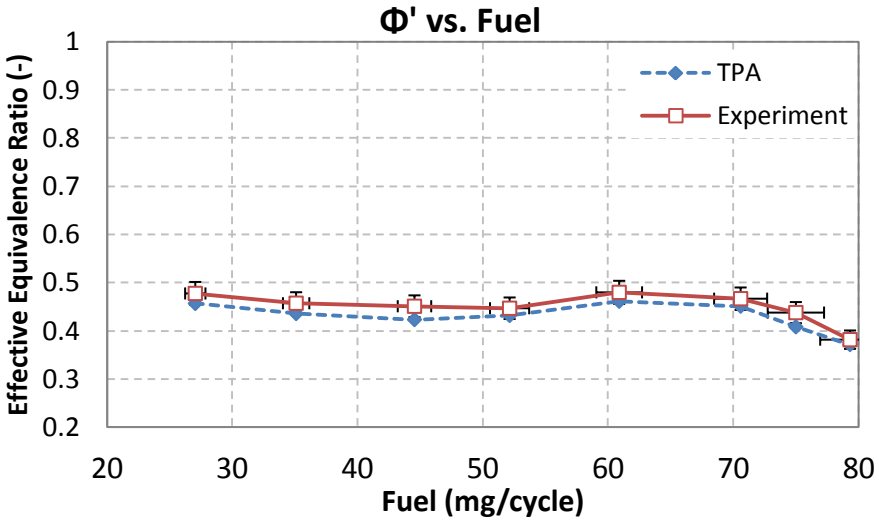

Figure 3.67 – Effective equivalence ratio as a function of fueling rate from TPA of the Sandia engine experiment.

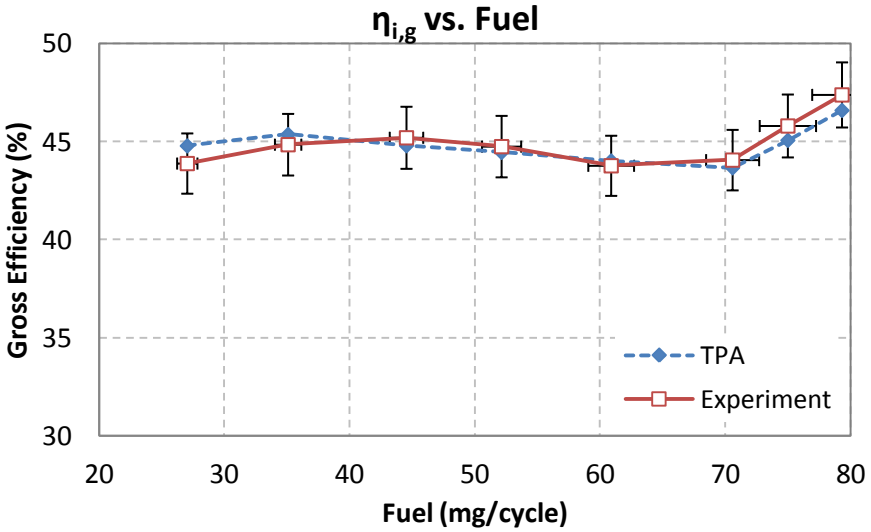

Figure 3.68 – Gross indicated efficiency as a function of fueling rate from TPA of the Sandia engine experiment.

Figure 3.69 and Figure 3.70 compare experimental and TPA pressure traces for two operating points, at 6.7 bar IMEPg and 15 bar IMEPg. For the first operating point, agreement was excellent. For the second operating point (2.4 bar intake pressure), post-compression pressures were lower in the simulation which was attributed to the reported low temperature heat release (LTHR) occurring at elevated intake pressures.

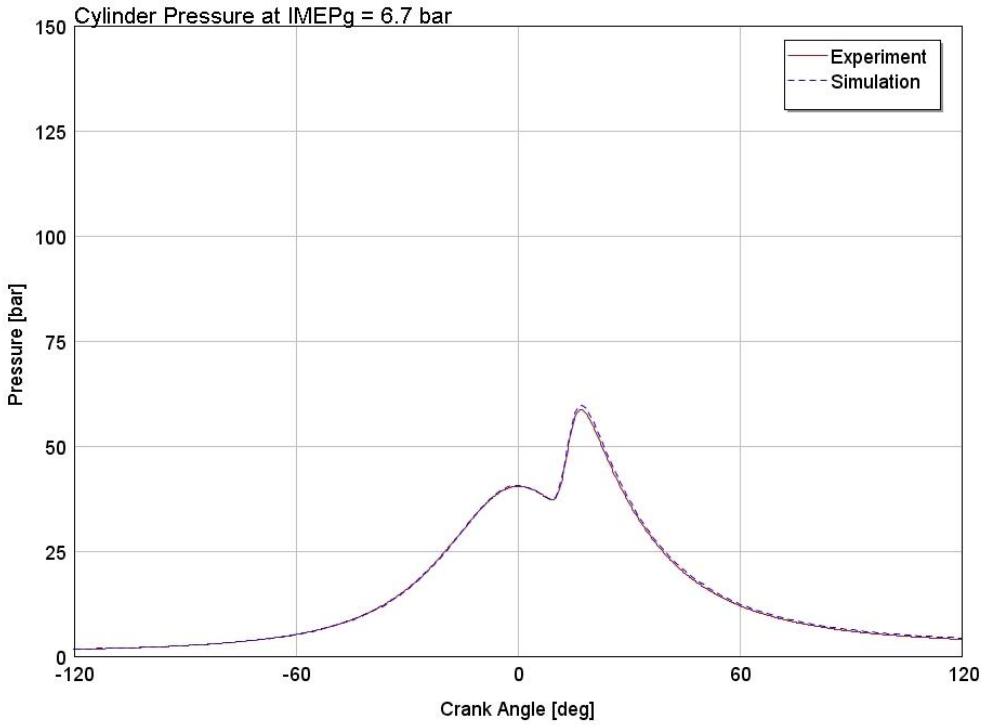

Figure 3.69 – Cylinder pressures during combustion at 6.7 bar IMEPg from TPA of the Sandia engine experiment.

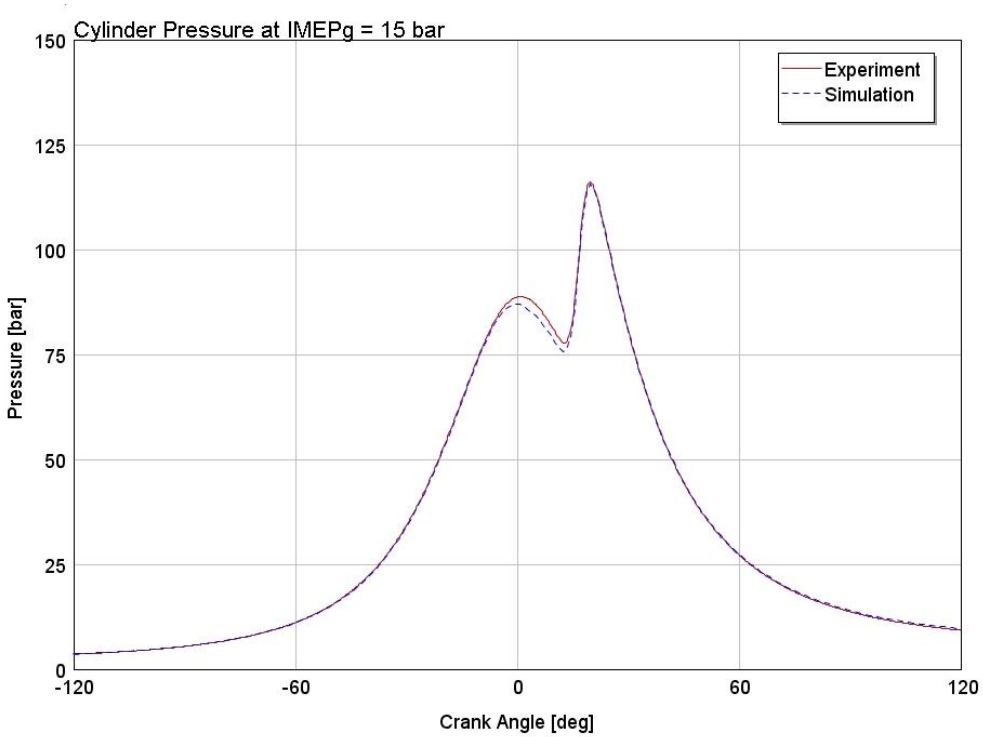

Figure 3.70 – Cylinder pressures during combustion at 15 bar IMEPg from TPA of the Sandia engine experiment.

The fact that trapped masses, composition and heat transfer were accurately captured by three pressure analysis paved the way for successful forward simulation of the Sandia boosted experiment. However, attempting the forward simulation revealed some weaknesses of the model which will be discussed in the following section.

3.3.2 Sandia Experiment Forward Simulation

Accurate forward simulation of boosted HCCI operation is primarily based on successful calculation of ignition timing. The previous section showed that the UM HCCI combustion model can successfully describe naturally aspirated and boosted operation of HCCI engines operating with NVO. However, the model proved unable to calculate ignition and combustion for the Sandia experiment. The reason was inaccurate description of the autoignition process for the high pressure conditions of the specific experiment.

The autoignition correlation used in the forward model was developed by He et al. and described isooctane ignition delay times under HCCI conditions [10]. Figure 3.71 shows a collection of isooctane ignition delay times from three different studies in the literature [8, 9, 10]. The three straight lines denoted as 5.5 atm UM RCF, 10 atm UM RCF and 15 atm UM RCF represent the correlation used in the forward model. The sloped lines recorded by Fieweger et al. and Davidson et al. represent data taken for higher pressures, at 40 atm and 53 atm respectively. The difference between the straight and the sloped lines lies in the Negative Temperature Coefficient (NTC) behavior observed at high pressures and facilitating ignition of the charge at highly boosted conditions. The autoignition correlation used in the model was not developed for highly boosted conditions; therefore it could not capture the NTC behavior required for accurate simulation of the Sandia experiment. The combination of high compression ratio and high intake pressure in the experiment meant that post compression pressures were in the

zone where NTC behavior occurs. Dec et al. described pre-ignition reactions as Low Temperature Heat Release (LTHR) and stated that LTHR played a key role in highly boosted conditions and when combustion was phased late in the cycle. Figure 3.72 shows a collection of shock tube data and detailed chemical kinetics simulations and reveals the NTC behavior of gasoline fuels at high pressure conditions. It should be noted that as post-compression pressures increase, NTC behavior becomes more pronounced thus reducing ignition delay times.

The lack of NTC behavior description from the autoignition correlation used in the model resulted in inability to calculate ignition for the Sandia boosted HCCI experiment. In fact, that problem was more pronounced as intake pressure increased. Addition of external EGR at high load intensified the problem by reducing the oxygen concentration in the cylinder.

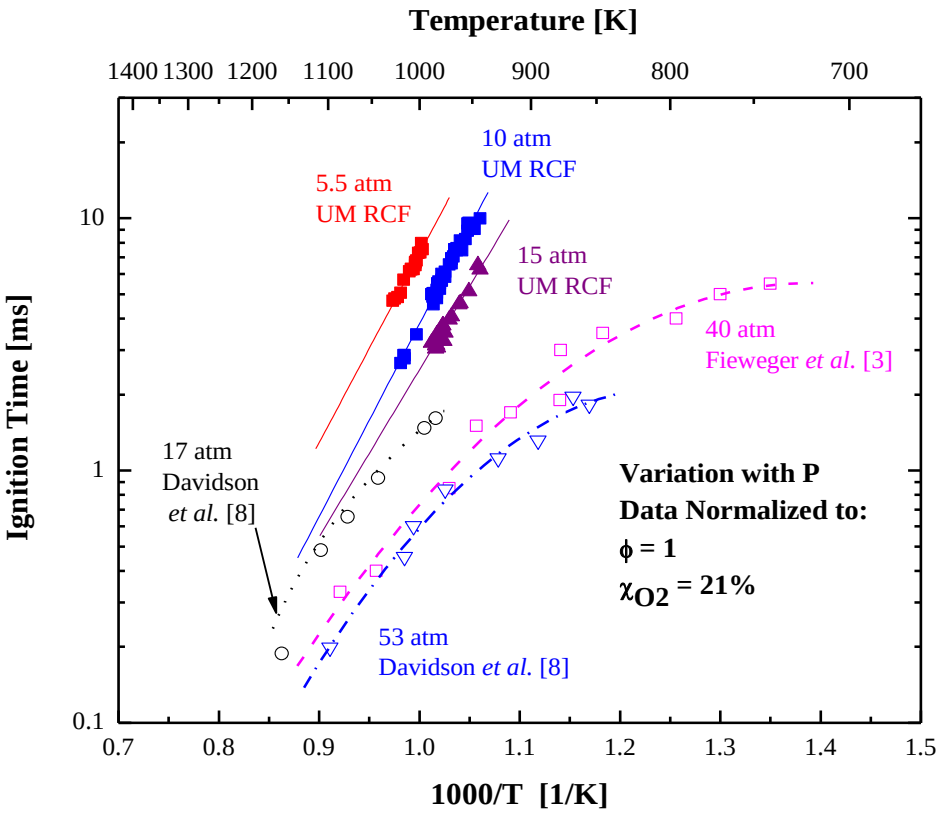

Figure 3.71 – Collection of isooctane ignition delay times from three different studies.

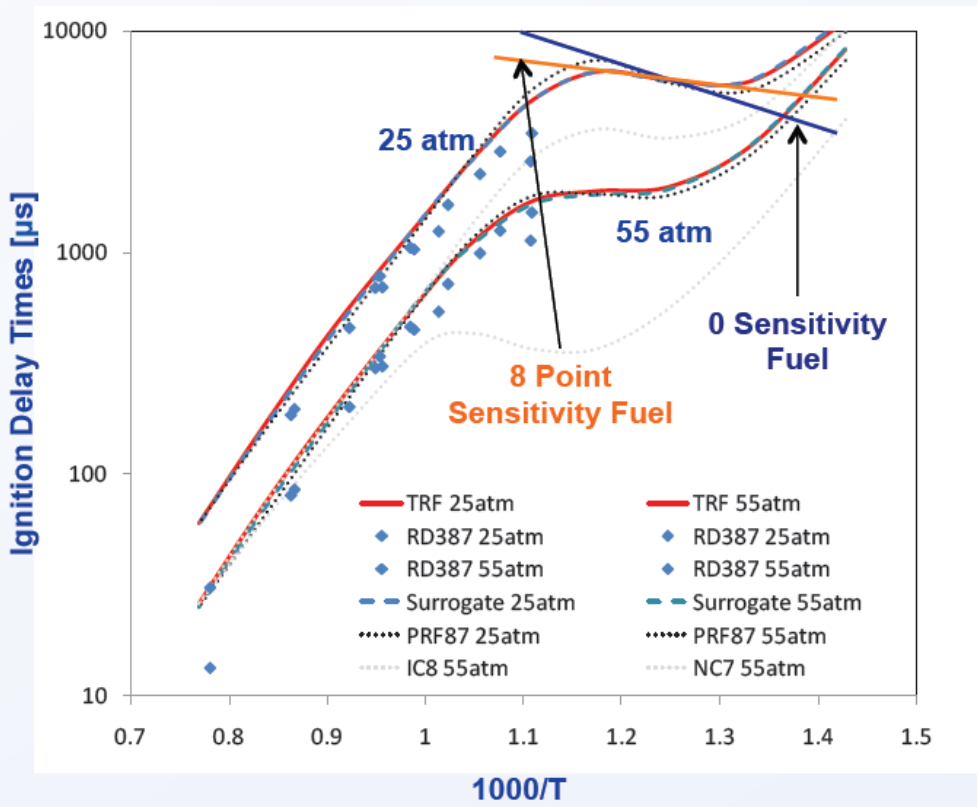

Figure 3.72 – Collection of ignition delay times for full-blend and surrogate fuel mixtures [11].

The lack of NTC behavior description was not the only reason behind unsuccessful calculation of the Sandia experimental points. The GM boosted experiment exhibited high post-compression pressures as well but the forward model was successful at simulating it even without the appropriate NTC description. The cause can be identified at TDC temperature which was higher for the NVO engines and increased with NVO as well. Figure 3.73 displays a comparison of the TDC temperatures between the three experiments. TDC temperature is shown as a function of load; it can be readily observed that for the GM boosted experiment TDC temperature reduced with load since dilution levels increased and RGF was reduced. The same happened at the Sandia experiment as well, but the reason was introduction of external EGR which was increased with load. Higher TDC temperatures at the NVO engines seemed to be the primary factor affecting ignition, resulting in accurate ignition calculations from the model. On the other

hand, the high post-compression pressures encountered in the Sandia engine promoted NTC behavior, resulting in shorter ignition delay times than what calculated by the autoignition correlation.

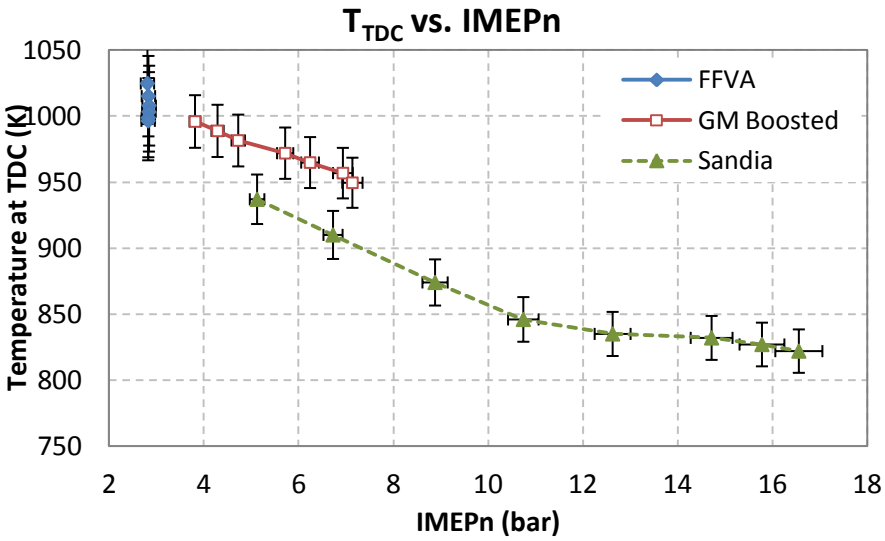

Figure 3.73 – TDC temperature comparison for the FFVA, GM Boosted and Sandia experiments.

The second factor affecting autoignition calculations in the model was oxygen concentration and it is displayed in Figure 3.74 as a function of load for the three engines. For the GM boosted engine, oxygen concentration increased with load since dilution levels increased as explained earlier. However, oxygen concentration in the Sandia engine decreased with load since more external EGR was introduced as load increased.

Negative temperature coefficient behavior and oxygen concentration were the two factors that resulted in misfiring phenomena when the Sandia engine experiment was simulated. The primary factor was NTC behavior and it has been well documented in the literature. Improvement of the combustion model would require adoption of an autoignition correlation that can describe NTC behavior for different fuels and calculate accurate ignition delay times for a wide range of post-compression pressures.

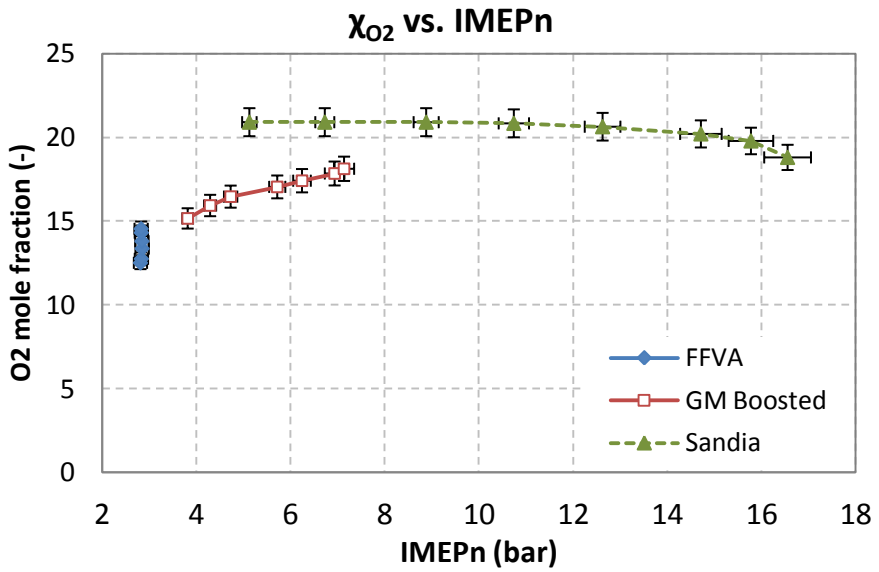

Figure 3.74 – Oxygen mole fraction comparison for the FFVA, GM Boosted and Sandia experiments.

3.4 Errors and Uncertainty Analysis

The engine submodels presented and used in this dissertation were evaluated based on three different sets of experimental data, as shown in the previous sections. For that reason, it was deemed necessary to establish the errors occurring in the experimental data and the resulting uncertainty in several derived quantities.

3.4.1 Experimental Uncertainty

Experimental measurements are typically accompanied by measurement errors, which can be divided into two components: random error and systematic error. Random error is always present in a measurement and it is a result of inherently unpredictable fluctuations in the readings of an instrument or in the interpretation of an instrument reading. Random errors appear as discrepancies in the results of the same repeated measurement. For that reason, they can be estimated by comparing multiple measurements, and reduced by averaging them. A typical example of random error reduction is the averaging of cylinder pressure traces. In all the experimental results that

were presented in the previous sections, pressure traces and other crank-angle resolved quantities were averaged over 300 cycles in order to reduce random error in measurements.

On the other hand, systematic errors are biases in measurements which result in the situation where the mean of multiple measurements differs from the actual value of the measured quantity. Sources of systematic error may be imperfect calibration of the measurement instruments, changes in the environment that interfere with the measurement process, or incorrect methods of observation. Unlike random errors, systematic errors cannot be discovered by repeated measurements, since they would always bias the results towards the same direction. In addition, the fact that systematic errors are present in measurements of raw engine quantities (e.g. cylinder pressure, mass) means that they will be present in the calculation of derived quantities (e.g. mean effective pressure). The most effective way to reduce systematic errors is appropriate calibration of the measurement instruments.

W. Northrop showed that uncertainty of experimental results can be established based on systematic error (u_0), uncertainty based on single test repeatability (u_m) and uncertainty based on three tests per operating condition of the engine (u_r) [13]. Figliola and Beasley used the root-sum-squares method (RSS) to estimate overall uncertainty (u_t) [14]:

$$u_t = \sqrt{u_0^2 + u_m^2 + u_r^2} \tag{3.3}$$

The authors highlighted that the RSS method assumes that the variations of an error over repeated measurements follow a Gaussian distribution, which appears to be confirmed by experimental observation and experience. The following table summarizes overall uncertainty in several experimental measurements [7]:

Table 3.4 – Instrument uncertainty of key engine variables

Measurement	Uncertainty
Pressure – Transducer (kPa)	4
Temperature – Thermocouple (K)	2.2
Brake Torque – Dynamometer (N-m)	1.7
Engine Speed – Dynamometer (RPM)	5
Fuel flow – Flow meter (mg/s)	0.5
Combustion noise – Noise meter (dB)	1
NOx – Emissions analyzer (ppm)	1
THC – Emissions analyzer (ppm)	5
CO – Emissions analyzer (ppm)	15
CO_2 – Emissions analyzer (ppm)	200
O2 – Emissions analyzer (ppm)	800

Figliola and Beasley presented the method of sequential perturbation for calculation of uncertainty in derived quantities; for engine applications these can be variables such as mean effective pressure, specific fuel consumption, efficiency and emissions index [14]. The method consists of a finite difference approach to obtaining approximate solutions to partial differential equations and it is summarized in the following steps:

- Calculation of the average set of each variable, x_i and their relative uncertainties u_{xi} (relative uncertainties can be calculated as twice the standard deviation, $u_{xi} = 2\sigma$).
- Calculation of the target result, R_0, using the found average values: $R_0 = f(x_1, x_2, ..., x_n)$

- Increase of the independent variables by their respective uncertainties and recalculation of the target result:

  $R_1^+ = f(x_1 + u_{x1}, x_2, ..., x_n)$

  $R_2^+ = f(x_1, x_2 + u_{x2}, ..., x_n)$

  …

  $R_1^+ = f(x_1, x_2, ..., x_n + u_{xn})$

- Decrease of the independent variables by their respective uncertainties and recalculation of the target result R_i^- in a similar manner.
- Calculation of the differences $\delta R_i^+, \delta R_i^- \forall i$:

  $\delta R_i^+ = R_i^+ - R_0$

  $\delta R_i^- = R_i^- - R_0$

- Evaluation of the approximate uncertainty contribution from every variable:

  $$\delta R_i = \frac{\delta R_i^+ - \delta R_i^=}{2}$$

- Evaluation of uncertainty as the sum of squares of every contribution:

  $$u_m = \left[\sum_{i=1}^{n} (\delta R_i)^2 \right]^{1/2}$$

The uncertainty in modeling and experimental results discussed in the following was obtained from the type of analysis summarized above; uncertainty values from Table 3.4 were used in the process displayed. However, limited availability of error data in certain cases hindered uncertainty calculations. It should also be noted that variables obtained from heat release analysis of experimental results contained propagated errors, resulting from use of multiple measured quantities in mathematical equations. These were estimated since details of the heat release analysis were not available.

3.4.2 Simulation Uncertainty

As described in the previous section, experimental measurements are accompanied by random and systematic errors. However, simulation is devoid of random errors and accompanied only by systematic errors. Incomplete knowledge about the state of a system and the governing physical processes are often sources of systematic errors in simulations. Furthermore, the highly non-linear nature of many physical processes pertinent to internal combustion engines can result in amplification of even small uncertainties in the input variables.

The models used in the present work describe the in-cylinder processes of an engine by solving mass, momentum and energy conservation equations to the best accuracy allowed by the assumptions involved. However, the same set of equations does not necessarily exhibit the same performance for all kind of engines. Individual hardware may require different parameters, which is another factor that introduces uncertainties in simulations. The engine models presented in Chapter 2 and used in the present work aimed at describing three main processes in engine operation: gas exchange, combustion and heat transfer. The importance of these three processes stems from the fact that they directly affect useful work production and efficiency levels of engine systems. Therefore, it was deemed necessary to understand the uncertainties involved in these processes.

The gas exchange process was simulated by solving 1-D compressible flow equations in GT-Power [15]. The primary parameter that affected this process was valve discharge coefficients; they were essential for accurate calculation of flow through the valves and thus cylinder trapped mass. Discharge coefficients are obtained experimentally by flow testing of cylinder heads and are subsequently used in simulations. The uncertainty involved in obtaining the discharge coefficients was not a known parameter and therefore cannot be reported in this study.

Combustion description was the most challenging task for simulating boosted HCCI engines. The UM combustion model that was detailed in Chapter 2 consisted of two modules, the autoignition correlation and the burn rate correlation. The autoignition expression was proposed by He et al. in 2005 [10] and describes isooctane ignition delay times under HCCI conditions. Equation (2.3) of the previous chapter showed that ignition delay times depend on cylinder pressure, fuel to oxygen equivalence ratio, oxygen mole fraction and cylinder temperature. The authors claimed that extensive error analysis was conducted in order to identify the uncertainty in the results of their study [10]. They noted that primary sources of uncertainty in τ_{ign} were due to uncertainties in the mixture composition (which yields uncertainty of ± 0.65 % in determining mixture equivalence ratio and oxygen mole fraction), uncertainties in the pressure measurements (due to accuracy of pressure transducer and charge amplifier) and corresponding uncertainties in their calculated effective temperature. Overall, the authors reported that maximum uncertainty in their study was ± 12 % and the average uncertainty was ± 6 %. The second module of the UM combustion model relied on effective equivalence ratio (Φ') and engine speed, as presented in equations (2.5) and (2.6) of the previous chapter. Uncertainty in the measurement of engine speed in the experiment was ± 0.25 % and it was replicated to the best accuracy in the simulation. Uncertainty in the calculation of cylinder residual gas fraction can be attributed to systematic errors in the simulation but it was not exactly known. RGF calculation is directly affected by NVO and trapped air mass, with uncertainty for NVO measurements being ± 3.5 %. As stated in Chapter 2, experimental RGF was an outcome of heat release analysis which makes it harder to estimate the uncertainty since details of the analysis were not known. It should be noted that interpretive errors may occur when experimental and modeling results are compared, which is another factor of potential uncertainty. Engine experimental conditions can never be matched exactly in simulation which indicates that systematic errors are present

and hard to identify. However, the likelihood of multiple errors being present at the same time is rather small since simulation only suffers from such systematic errors.

Heat transfer is also a physical process that is hard to model in boosted HCCI engines. The present work utilized the classic Woschni heat transfer correlation that provides the heat transfer coefficient by making use of the average charge temperature. From equations (3.1) and (3.2) it can be deduced that the uncertainty in heat transfer calculation results from uncertainty in the estimation of cylinder pressure (± 0.1 %), cylinder temperature (± 0.5 %) and mean piston speed (± 0.25 %).

By considering the uncertainties involved in the experimental measurements and simulations, it can be concluded that the variables likely to include the highest uncertainty are valve overlap, residual gas fraction, ignition timing and burn rate. The following section will discuss the sensitivity of simulating engine processes on certain inputs provided to the models.

3.4.3 Simulation Sensitivity Analysis

The UM HCCI combustion model that was presented in Chapter 2 was used for forward calculations of the combustion event. In specific, it calculated ignition timing and burn rate based on several inputs. These inputs were presented in detail in Chapter 2; however, the forward calculation nature of the model highlighted the need for a one-way sensitivity analysis to its inputs. Such an analysis allows the researcher to assess the impact that changes in certain parameters will have on the results of these models, and thus determine which parameters are key drivers of the model's results.

The following table summarizes a sensitivity analysis of ignition delay time (He et al, 2005 [10]) to the inputs of the correlation: fuel to oxygen equivalence ratio, cylinder pressure, oxygen mole fraction and cylinder temperature. Representative in-cylinder conditions were set at 0.5 F/O equivalence ratio, 30 atm cylinder pressure, 15 % oxygen

mole fraction and 950 K cylinder temperature at TDC. Subsequently, each one of these inputs was sequentially increased by 5 % and the effect on the calculated ignition delay time was recorded. It was observed that cylinder temperature was the key driver for the ignition delay calculation, since a 5 % increase in temperature resulted in 27 % reduction in ignition delay. This observation agrees with the analysis of the previous sections, where the misfiring problems for the Sandia engine simulation were analyzed. The strong effect of temperature on ignition delay can be attributed to the exponential dependence derived from He et al. and their experiments. Ignition delay times exhibited approximately linear dependence on changes in equivalence ratio and cylinder pressure. This behavior was also justified by equation (2.3) and the exponents involved in the correlation. Increased oxygen mole fraction appeared to have the least effect on reducing ignition delay; it was also the variable that showed the least variation across the sweeps examined in the three experimental datasets. The strong dependence of ignition delay times in TDC temperature renders this variable as the key factor in establishing good agreement with experimental results.

Table 3.5 – Sensitivity of ignition timing on correlation inputs

Input perturbed by 5 %	**τ_{ign} change**
Equivalence ratio, F/O (-)	-6 %
Pressure (atm)	-4 %
O_2 mole fraction (-)	-1.5 %
Temperature (K)	-27%

It should be noted that the burn rate correlation depended on effective equivalence ratio (Φ') and engine speed, as presented in Chapter 2. Similar perturbations in these parameters revealed that burn rate was not very sensitive to changes in engine speed; a 5

% increment in engine speed resulted in only 0.5 % increment in burn rate. However, the dependence on Φ' was much more pronounced; 5 % higher Φ' resulted in 7.5 % increased burn rate. Ignition timing had a direct effect on cylinder pressure rise rate since it was governing when the high burn rates will appear in the cycle. Based on the current sensitivity analysis as well as the autoignition discussion presented in the previous section, it can be concluded that autoignition modeling is the key element in accurately describing combustion in HCCI engines. Ignition timing appears to change significantly across the load range while burn rate does not. The last observation was also supported by experimental results from the GM boosted engine setup which showed that burn duration (CA10-90) ranged between 10 and 12 CAD across the load range (Figure 3.54).

Uncertainty and sensitivity analyses showed that particular attention needs to be paid to the interpretation of experimental results, as well as accurate modeling of in-cylinder processes. Nevertheless, it needs to be highlighted that the current dissertation focused on thermodynamic analysis of HPLB engines, which was consistent while taking into account the uncertainties involved.

3.5 Assessment of Gas Exchange and Heat Transfer Models

The model performance evaluation process presented in the previous three sections was approached in two steps; three pressure analysis and forward simulations using the UM combustion model. The three pressure analysis utilized experimentally measured pressure traces and allowed the isolation of gas exchange and heat transfer processes from the combustion process. TPA results from all three engine simulations showed that the 1-D gas dynamics model is very good at calculating mass flows into and out of the cylinder, as well as pumping work. The critical factor for accurate pumping work calculation appeared to be the set of discharge coefficients used to model flow through the valves. For the GM boosted and Sandia engines, the used set of discharge

coefficients allowed the model to calculate trapped masses within experimental error. However, inappropriate discharge coefficients for the trapezoidal valve events of the FFVA engine resulted in inaccurate flow description. Therefore, the pumping work calculated for the FFVA experiment was more than 50 % higher than the actual at all cases, thus affecting the calculation of net performance parameters. The solution can certainly be sought in experimentally obtaining discharge coefficients for the specific valve configuration. Overall, the gas exchange model proved to be very good at calculating mass flows and pumping work.

Heat transfer description in LTC engines is a topic that has not received great attention from the research community, but it is currently an active research field. The classic Woschni correlation that was developed a few decades ago based on diesel engine experiments, remains the correlation of choice for quasi-dimensional of even multi-dimensional simulations. In 2004, Chang et al. proposed a modified form of the Woschni correlation based on HCCI heat flux measurements which was initially incorporated into the UM HCCI combustion model [6]. However, the model performance evaluation process showed that this modified Woschni correlation might not be appropriate for quasi-dimensional simulations, since it overcalculates heat transfer before combustion and during the recompression phase in NVO engines. Therefore, the classic Woschni correlation was used for the simulations presented in the previous sections. Calculated gross indicated efficiency was at the limit of experimental error but the differences from the experimental values were less than 6 % which was satisfactory. Nevertheless, the difference in trends between experiment and simulation indicated that heat transfer for boosted HCCI may not have been accurately captured by the existing correlations. It should be noted though, that the present research work did not aim at investigating heat transfer phenomena in LTC engines; therefore, no solid conclusions can be drawn from the use of current correlations. It is possible that the correlations are calibrated in order to match experimental data; however, new heat transfer models may be required for

accurate forward simulations. The need for improved heat transfer models paves the way for exciting future research work.

3.6 Assessment of Combustion Model

By completing three pressure analysis, the ability to model gas exchange was assessed and found to be very good. The next logical step was to engage the forward combustion model in order to assess its capacity to calculate ignition timing and burn rates for a wide range of naturally aspirated and boosted HCCI conditions. The experimental data required for that wide range came from the three different engines described in the previous sections. They included a combustion phasing sweep at naturally aspirated conditions and two intake pressure and load sweeps. The performance evaluation process showed that the UM HCCI model is very good at calculating ignition and burn duration for naturally aspirated conditions. Combustion variables such as CA50 and burn duration were calculated within the experimental error. In addition, the model offered robust combustion description for boosted conditions provided that post-compression temperatures are high enough to offset the effect of negative temperature coefficient behavior (higher that 950 K). That would be the case for an engine such as the GM boosted one which employed NVO and compression ratio of 12.5 On the other hand, the model failed to calculate ignition for cases that NTC behavior was the dominant factor (temperature at TDC lower than 950 K). The autoignition correlation employed in the model was not developed for high pressure conditions and it was therefore unable to calculate accurate ignition delay times for engines like the Sandia one. For that engine, the combination of high boost, high compression ratio with the absence of NVO resulted in higher TDC pressures (up to 100 bar) but lower TDC temperatures that the first two engines (820 – 940 K). The result was pronounced NTC behavior which shortened ignition delay times at these conditions and aided high load HCCI operation. The

combustion model was not able to capture that behavior thus resulting in misfiring phenomena.

Accurate calculation of ignition timing appeared to be the primary factor for successful boosted HCCI simulations. Intake pressure affected ignition kinetics and that effect needed to be captured in an accurate fashion. Burn rates depend heavily upon ignition timing but the literature has shown that they are not greatly affected by cylinder pressure [5, 11]. Therefore, the key to successful forward simulations appears to be accurate ignition delay calculations. For that reason, autoignition correlations that capture NTC behavior will need to be employed.

3.7 Summary

Model performance evaluation and calibration was an essential step in the process of successfully simulating high pressure lean burn engines. Performance evaluation was accomplished by utilizing three experimental datasets originating from the FFVA and GM boosted engines at the University of Michigan and from a boosted HCCI engine at Sandia National Laboratories. Among the three experiments, the GM boosted was the one that provided the most comprehensive input set for the engine model due to higher fidelity of several parameters (e.g. valve discharge coefficients). Comparison of modeling and experimental results showed that the calibrated model can successfully describe the gas exchange process and the burn rates. Calculated values for cylinder trapped air and total masses were within the experimental error. As a result, the model could accurately calculate mixture composition. Calculated values of performance variables such as IMEP and indicated efficiency were at the limit of experimental error but the differences from the experimental values were less than 6 % which was satisfactory. Furthermore, combustion variables such as CA50 and burn duration were calculated within the experimental error as well. However, the model was not as successful in calculating

ringing intensity and NO_x emissions index. Even though the trends of both variables were captured, calculated values were lower in the ringing intensity case (10 – 40 %) and significantly lower in the NOx emissions case (one order of magnitude).

Although calculated gross indicated efficiency was less than 6 % different from the experimental one, it was observed that this difference increased with intake pressure and load. This behavior indicated that heat transfer may not have been accurately captured in the model. Elevated pressure and high dilution levels seemed to incur effects on heat transfer that require further investigation.

The UM HCCI combustion model presented in the previous chapter is a combination of an ignition delay expression and burn rate correlations. It was able to successfully calculate ignition for NVO engines where post-compression pressures were lower than 70 bar and cylinder temperature was the dominant factor affecting ignition (higher than 950 K). However, the combustion model did not succeed in calculating ignition for the Sandia engine experiment were TDC pressures were up to 100 bar and temperatures were lower than 940 K. The reason was insufficient description of the negative temperature coefficient behavior which was the dominant factor affecting ignition delay times. Despite these drawbacks, the combustion model proved to be suitable for light-duty HCCI engine simulations. The combination of robust gas exchange and combustion description created a suitable framework for the purpose of thermodynamic analysis of HPLB engines.

3.8 References

1. Manofsky, L., Vavra, J., Assanis, D. and Babajimopoulos, A., "Bridging the Gap between HCCI and SI: Spark-Assisted Compression Ignition," SAE Paper 2011-01-1179, 2011

2. Yun, H.J. and Mirsky, W., "Schlieren-Streak Measurements of Instantaneous Exhaust Gas Velocities from a Spark-Ignition Engine," SAE Paper 741015, 1974

3. Fitzgerald, R. P., Steeper, R. R., Snyder, J. A., Hanson, R. K. and Hessel, R. P., "Determination of Cycle Temperatures and Residual Gas Fraction for HCCI Negative Valve Overlap Operation," SAE Paper 2010-01-0343, 2010

4. Ortiz-Soto, E. A, Vavra, J. and Babajimopoulos, A., "Assessment of Residual Mass Estimation Methods for Cylinder Pressure Heat Release Analysis of HCCI Engines with Negative Valve Overlap," Proceedings of the ASME 2011 Internal Combustion Engine Division Fall Technical Conference, ICEF2011-60167, 2011

5. Dec. J. and Yang. Y., "Boosted HCCI for High Power without Engine Knock and Ultra-Low NO_x Emissions using a Conventional Fuel," SAE Paper 2010-01-1086, 2010

6. Chang, J., Guralp, O., Filipi, Z., Assanis, D., Kuo, T., Najt, P. M. and Rask, R., "New Heat Transfer Correlation for an HCCI Engine Derived from Measurements of Instantaneous Surface Heat Flux", SAE Paper 2004-01-2996, 2004

7. Stefan Klinkert, personal communication, May 2012

8. Davidson, D.F., Oehlschlaeger, M.A., Herbon, J.T., and Hanson, R.K. (2002) "Shock Tube Measurements of Iso-Octane Ignition Times and OH Concentration Time Histories," Proceedings of the Combustion Institute 29: 1295–1304

9. Fieweger, K., Blumenthal, R., and Adomeit, G.(1997) "Self-Ignition of S.I. Engine Model Fuels: A Shock Tube Investigation at High Pressure," Combustion and Flame 109: 599–619

10. He, X., Donovan, M.T., Zigler, B.T., Palmer, T.R., Walton, S.M., Wooldridge, M.S. and Atreya, A., 2005, "An Experimental and Modeling Study of Iso-octane Ignition Delay Times at Homogeneous Charge Compression Ignition Conditions," *Combustion and Flame,* **142**(3), pp. 266-275

11. Mehl, M., Pitz, W. J and Westbrook, C. K., "Detailed Kinetic Modeling of Boosted HCCI Combustion with Gasoline," AEC and HCCI Working Group Meeting, Sandia National Laboratories, 23-25 February 2010

12. Wikipedia.org

13. Northrop, W.F., "Particulate and Gas Phase Hydrocarbon Emissions from Partially Premixed Low Temperature Compression Ignition Combustion of Biodiesel," Ph.D. Thesis, University of Michigan, 2010

14. Figliola, R., and Beasley, D., Theory and Design of Mechanical Measurements (3rd edition), New York, 2000

15. Gamma Technologies, Inc. http://www.gtisoft.com/

CHAPTER 4

MULTI-CYLINDER HCCI ENGINE SIMULATION

As stated in Chapter 2, the objective of the present research work was to investigate the interactions between advanced combustion, boosting and variable valve actuation for high pressure lean burn gasoline engines. In order to reach that goal, extensive multi-cylinder engine simulations were performed that focused on gas exchange and thermodynamics of high pressure lean burn engines. The simulations were targeted towards investigating high load boosted HCCI operation and proved to be very good at providing insight into the interactions of the in-cylinder environment with the external engine subsystems. High load HCCI operation requires high mass for sufficient work output, high intake temperature for ignition and high dilution levels for control of pressure rise rates. Multi-cylinder simulations played a key role in describing the trade-offs involved in HPLB engines featuring high compression ratio, boosting, VVA and external EGR, and in identifying effective combinations of those features in order to achieve the desired operating conditions.

The following sections will describe the multi-cylinder engine models that were developed and utilized. They will also present a number of studies that produced key results in the effort to examine HPLB engines. These studies characterized the effects of intake preheating, boosting, variable valve actuation, elevated compression ratio and external EGR use on high load HCCI operation and allowed an integrated view of potential strategies. The reported results were obtained from HCCI engine simulations,

but the majority of the conclusions drawn apply to HPLB engines in general regardless of their dependence on spark or compression for ignition of the charge.

4.1 Engine System Model Formulation

In order to perform meaningful multi-cylinder engine simulations, the engine system had to be modeled as a collection of robust submodels. As such, the accuracy of every engine model described in this dissertation could not exceed the accuracy of its best submodel. Multi-cylinder models were built based on a single-cylinder one of the GM boosted HCCI engine at the University of Michigan. Cylinder geometry and dimensions of valves and ports were specified for the single-cylinder model which was subsequently appended to form a four-cylinder model with total displaced volume of 2.2 L.

4.1.1 Combustion and Heat Transfer Models

The transition to multi-cylinder models was based on the fact that the only difference between single-cylinder and multi-cylinder engines is associated with charging. Single-cylinder and multi-cylinder engines have the same combustion, heat transfer and work production characteristics. Firing order and valve timings are responsible for manifold gas dynamics phenomena that introduce variation of trapped masses between the cylinders. Differences in trapped masses result in what is known as cylinder to cylinder variation. It should be noted that the model was very good at capturing these phenomena and that NVO engines did not seem to suffer any cylinder to cylinder variation. The reason was that valve events never intersected, thus the manifolds exchanged mass with the cylinders individually. There was no purging of the cylinder gases and very limited backflow phenomena when negative valve overlap was employed. That common nature of single-cylinder and multi-cylinder engines allowed utilization of

the gas exchange, combustion and heat transfer models that were assessed against different experiments as presented in the previous chapter.

Following the performance evaluation process presented in detail in Chapter 3, multi-cylinder models utilized the calibrated combustion model combined with the HCCI Woschni heat transfer correlation. The combination of the two offered the best calculations of closed cycle parameters when the GM boosted experiment was modeled and provided robustness in multi-cylinder simulations.

4.1.2 Variable Valve Actuation

All of the four-cylinder models that will be presented in this dissertation shared a common cylinder block and employed one or both of the following valve strategies; a low-lift negative valve overlap strategy or a high-lift positive valve overlap one.

Figure 4.1 displays the valve lifts for the NVO strategy as functions of crank angle. Peak valve lift was 5 mm and duration was 145 CAD for both intake and exhaust events. As will be analyzed in the following sections, NVO was critical for low and medium load HCCI operation since it accomplished simultaneous control of mixture composition and temperature through residual gas trapping. However, as seen from experimental results in the previous chapter, NVO operation was associated with increased pumping work and high cylinder temperatures.

Figure 4.2 displays the valve lifts for the PVO strategy as functions of crank angle. Peak valve lift in this case was 10 mm and duration was 258 CAD for both intake and exhaust valves. The PVO valve strategy was derived directly from SI engine applications and offered very different gas exchange characteristics to the four-cylinder engine compared to the NVO strategy. These characteristics will be described in the following sections and stem from the fact that there was no direct mechanism for residual gas trapping or heating of the charge on a cycle basis.

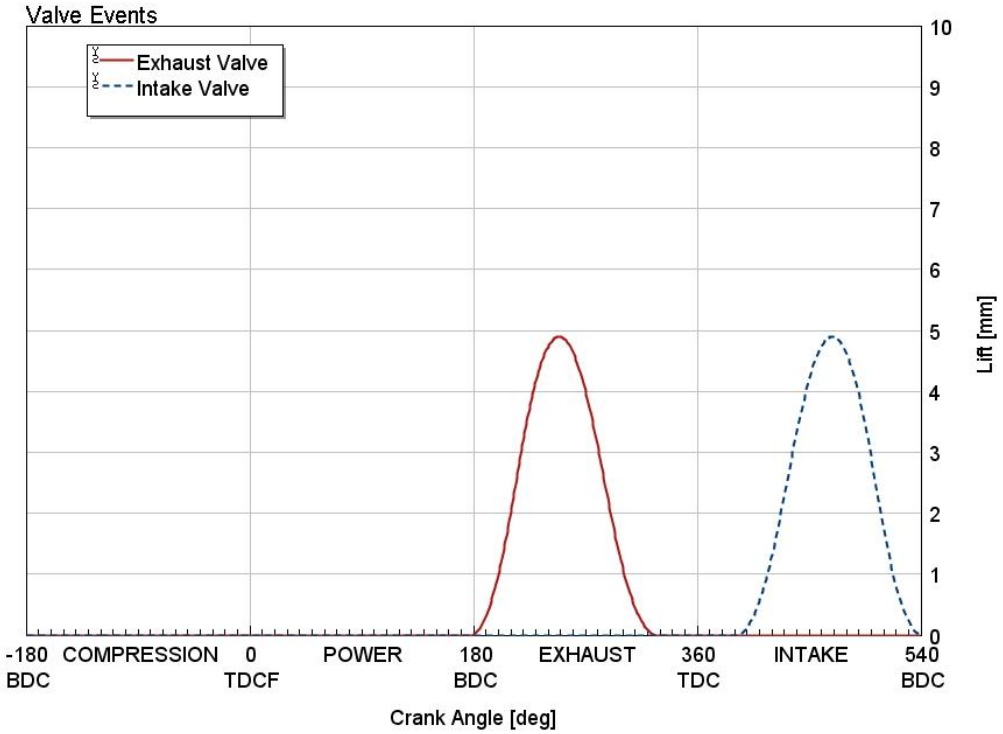

Figure 4.1 – 5 mm valve events forming negative overlap

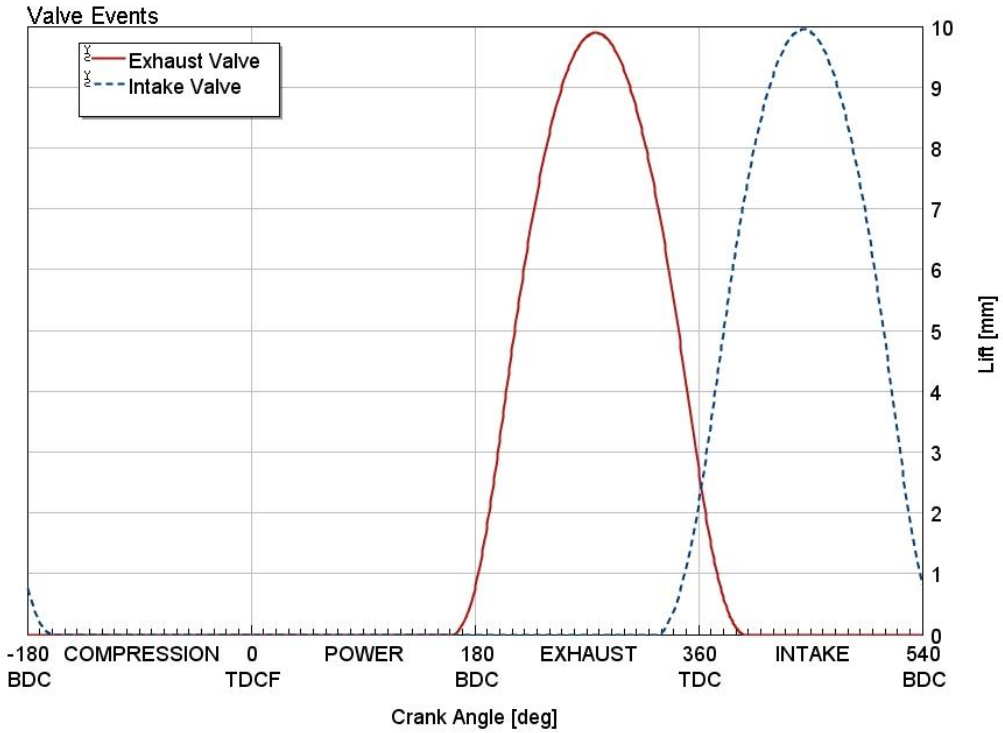

Figure 4.2 – 10 mm valve events forming positive overlap

4.1.3 Boosting Systems

Elevated intake pressure was an essential parameter for high load HCCI operation and it was achieved by utilizing a few different boosting systems. As discussed in Chapter 1, turbocharging technology has played a key role in the widespread adoption of downsized boosted SI engines; therefore, it has the potential to provide solutions for HPLB engines as well. The current research work made use of three different devices, two turbochargers and a supercharger. The turbochargers were of different size and were used individually in two of the engine systems that will be described in the following. In addition, the larger turbocharger was used in series with the supercharger to form an advanced boosting system that offered significant flexibility.

The first turbocharger used was a small unit produced by IHI and designed for use in SI engines displacing 0.6 – 1 L. As such, it could not handle wide ranges of mass flow rates but it was very well suited to the 2.2 L HCCI engine model since it could provide high pressure ratios at low mass flow rates. The following Figure 4.3 and Figure 4.4 show the IHI compressor and turbine performance maps respectively. The IHI turbocharger was combined with NVO to form the first engine system that will be described in the following sections.

The second boosting system used was comprised of a larger turbocharger supplied by BorgWarner and sized for SI engines displacing about 2 L. It differed from the IHI turbocharger primarily because it could accommodate a wider range of mass flow rates and pressure ratios. The turbine also featured variable geometry (VGT) which offered additional flexibility for controlling the boundary conditions in boosted HCCI. The BorgWarner turbocharger was coupled to a switchable NVO/PVO valve strategy to form the second engine system of interest. NVO was employed at low loads in order to trap the required residual gas for ignition control; it was switched to PVO at medium and high loads in order to reduce pumping losses, cylinder temperatures and aid efficiency as will

be shown in the following sections. Figure 4.5 shows the compressor performance map and Figure 4.6 shows the turbine performance map for the BorgWarner turbocharger. The turbine map shows the VGT in two of its settings used.

The third boosting system used in this study employed the BorgWarner turbocharger in series with a TVS-R410 supercharger supplied by Eaton. The map of the latter is shown in Figure 4.7. The supercharger was connected directly to the engine crankshaft and the gear ratio could be selected according to the intake pressure requirements of the application. The combination of VGT and supercharger resulted in a very flexible boosting system that provided high intake pressure and allowed good control of exhaust backpressure. The two-stage boosting system was used in conjunction with the switchable NVO/PVO valve strategy and proved to be very effective in providing the boundary conditions needed for high load boosted HCCI.

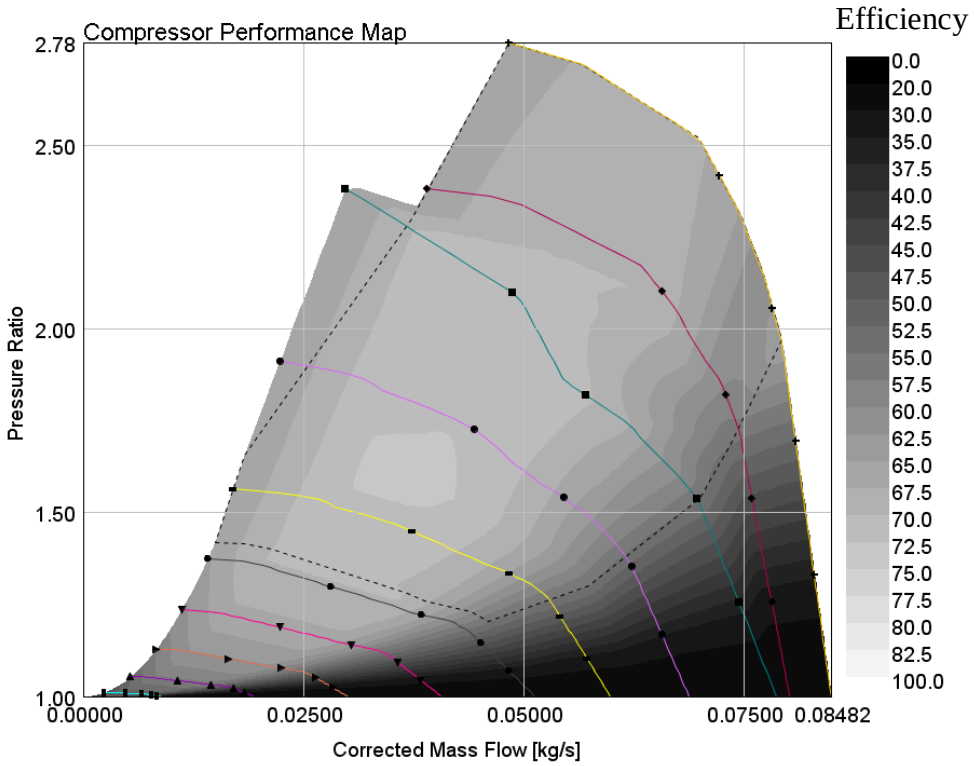

Figure 4.3 – IHI compressor performance map

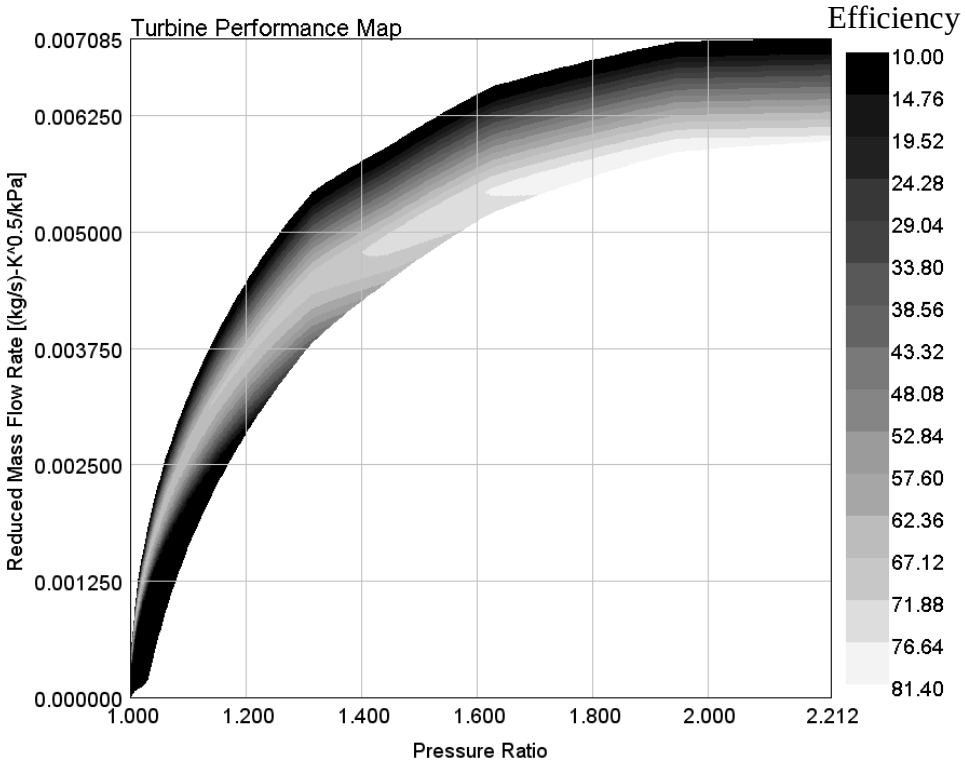

Figure 4.4 – IHI turbine performance map

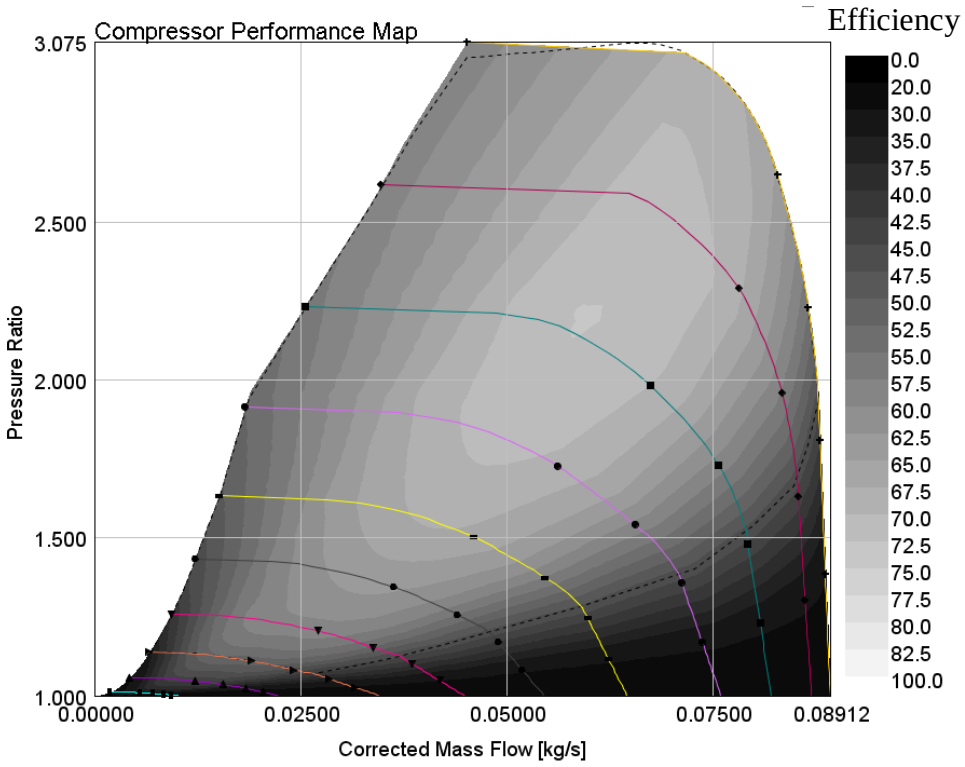

Figure 4.5 – BorgWarner compressor performance map

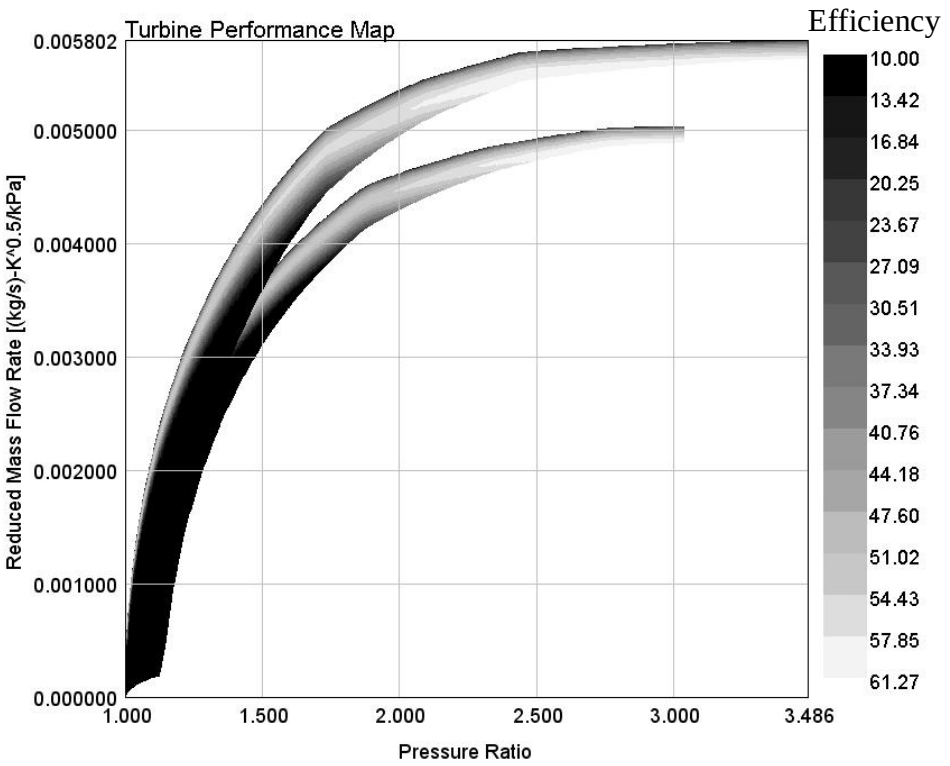

Figure 4.6 – BorgWarner turbine performance map

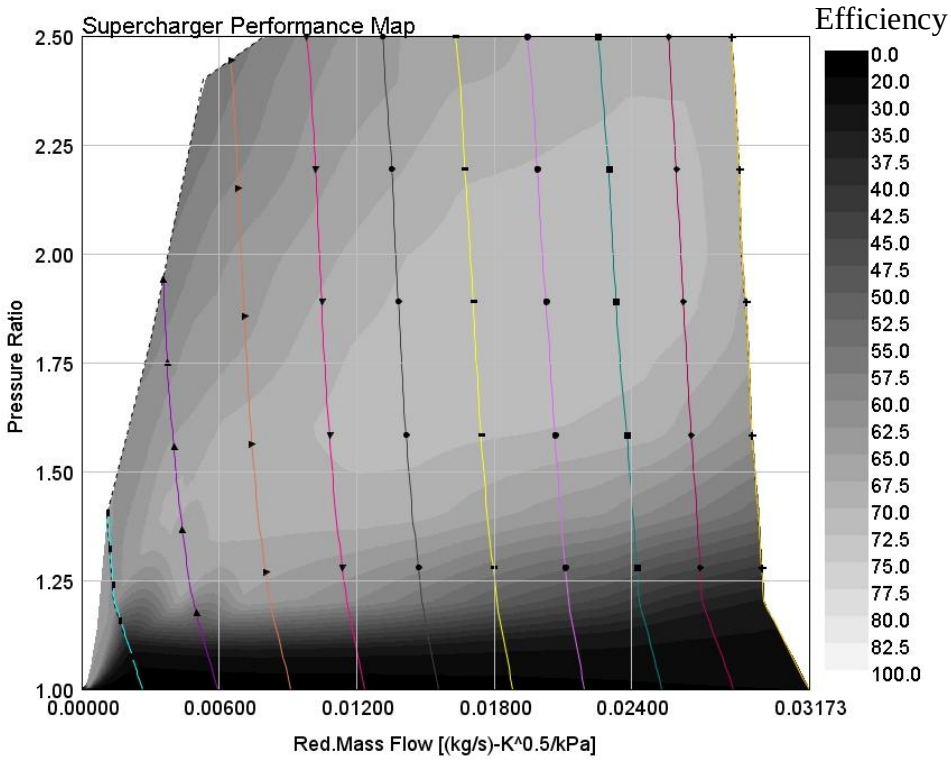

Figure 4.7 – Eaton supercharger performance map

4.1.4 Additional Subsystems and Features

In addition to the boosting system and valvetrain configurations described above, the engine models presented in this dissertation included two more subsystems that were critical for HPLB operation. The first one is an aftercooler positioned downstream of the boosting system and enabled good control of intake temperature. The second one is a low-pressure EGR loop which enabled external EGR use.

Multi-cylinder boosted HCCI simulations were greatly enhanced by a new methodology which aimed at using the engine model the same way as experimental engines are used. This methodology led to a novel model configuration which will be referred to as "virtual dyno". Through this configuration, the model was run interactively and the user could change several engine parameters such as combustion mode, fueling rate, valve overlap and engine speed during runtime. The virtual dyno configuration proved very effective in providing the ability to adjust engine parameters for attaining the optimum operating points.

Model operation was subject to several constraints imposed by combustion and hardware limitations. These constraints included maximum cylinder pressure, maximum Ringing Intensity (R.I.), maximum Coefficient of Variance (CoV) of IMEP and maximum $EINO_x$. The maximum acceptable cylinder pressure was set at 120 bar in order to discard operating points that would result in extreme mechanical stresses in an actual SI engine structure. Ringing intensity was constrained at 6 MW/m^2 in order to ensure reasonable pressure rise rates during heat release. Cyclic variability is indicative of combustion instability and bi-stable phenomena in HCCI engines. A constraint that accounts for maximum CoV of IMEP was used to ensure low cycle to cycle variation and was set at 5 %. As discussed in chapter 2, the constraint imposed for the NO_x emissions index is 1 g NO_x/ kg fuel which is representative of the US-2010 emissions standards.

The following sections will present studies performed with the multi-cylinder engine models and aimed at examining key effects of high load boosted HCCI operation. Emphasis was given to the interactions of engine subsystems with the combustion mode from a thermodynamics point of view. From that aspect, the effect of intake temperature on high load boosted HCCI will be investigated and the interactions between boosting systems and valve strategies will be characterized. Furthermore, the effects of compression ratio on high load operation will be displayed and potential use of external EGR will be examined. Conclusions will be drawn based on overall efficiency considerations, and techniques that enable HPLB operation will be proposed.

4.2 Effect of Intake Temperature on High Load Boosted HCCI Operation

Since HCCI combustion was first achieved in experimental engines, intake preheating has been one of the primary control parameters for achieving ignition and for phasing combustion in the cycle. Dec et al. reported that intake temperature spanned a wide range (45 – 146 °C) in their boosted HCCI experiment that achieved maximum load of 16.3 bar IMEPg [1]. As discussed in chapters 1 and 3, variable valve actuation eliminated the need for intake preheating by introducing methods of trapping hot residual gas in the cylinder and accomplishing charge heating on a cycle basis. Manofsky et al. compared intake preheating with internal residual on an NVO engine as methods of achieving charge heating and reported that intake preheating resulted in consistently higher heat release rates [4]. The authors attributed that to higher oxygen concentration when high amounts of air were used and enhanced thermal stratification when high amounts of NVO were used. It should be noted though that the engine utilized high NVO even when the intake air was preheated.

Multi-cylinder simulations revealed a new operating approach that utilized the hot intake air exiting the compressor to displace some of the residual gas in the cylinder for

charge heating. Intake temperature was retained at high levels by means of bypassing the intercooler, thus the engine was operated with hot intake air. The elevated air temperature in turn required less RGF for ignition and because of that less NVO. The combination of these parameters meant that less exhaust gas was retained in the cylinder and more exhaust gas was directed to the turbine, thus improving its efficiency and increasing the work offered to the compressor. Increased compressor work resulted in higher intake pressures which provided the necessary dilution levels for increased fueling rates without ringing. The increased dilution also allowed for combustion to be phased slightly earlier in the cycle for improved thermal efficiency without sacrificing exhaust gas temperature. As load was increased, NVO was reduced further and turbocharger pressure ratios were increased accordingly, thus allowing further improvements in load and efficiency. This operating loop enabled good control of the intake conditions via the exhaust conditions and proved to be characteristic of turbocharged engines.

The following figures will display some performance, composition and combustion parameters for one of the engine systems, which employed the smaller IHI turbocharger and purely NVO as the valve strategy. The engine operated at 2000 rpm on hot intake air and exhibited significant benefits in upper load limit and efficiency.

Figure 4.8 displays IMEPn and BMEP as functions of the fueling rate for the single turbocharged engine using only NVO. Operation with hot intake air allowed this engine to reach 9 bar IMEPn and the limit was posed by the ability of the turbocharger to provide even higher pressure ratios. Figure 4.9 shows net and brake specific fuel consumption as functions of net and brake MEP respectively. For every load level, combustion was phased as early as possible in the cycle in order to maximize expansion ratio and improve thermal efficiency. The limit for early combustion phasing was set by ringing intensity and for that reason the engine was operated just below the ringing intensity constraint. It can be seen from Figure 4.9 that maximum indicated efficiency was reached at 7 bar NMEP; excessive pumping work at higher loads acted to reduce

efficiency. While indicated efficiency remained fairly constant at lower loads, brake efficiency was reduced since friction was a larger fraction of the engine useful work at low loads.

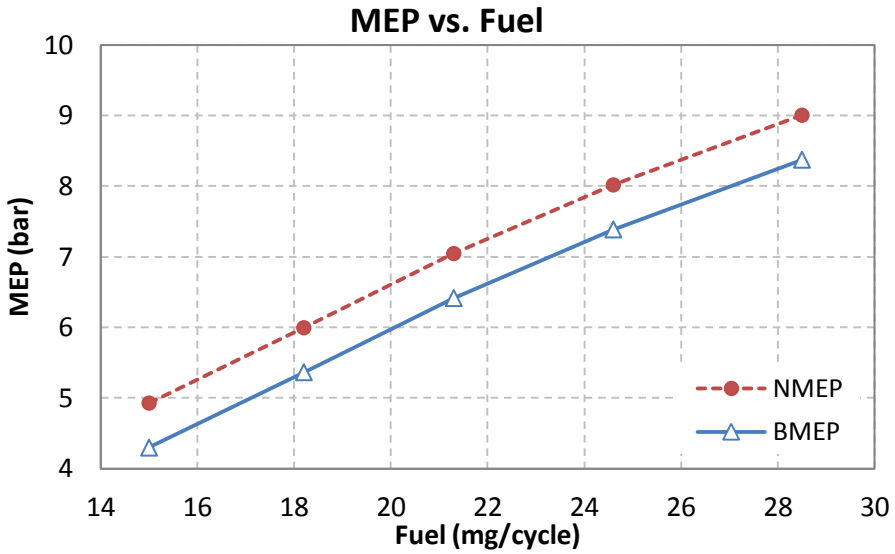

Figure 4.8 – Load range for a single turbocharged HCCI engine using NVO

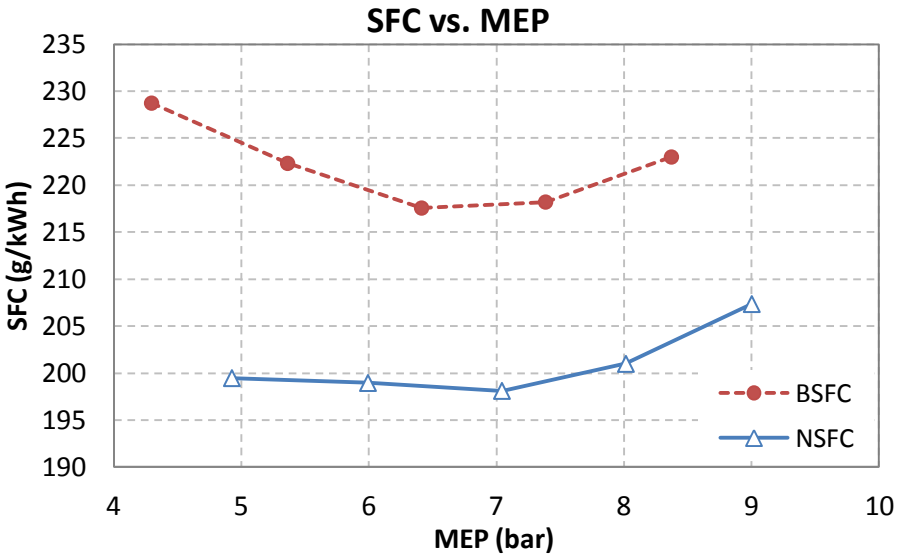

Figure 4.9 – Specific fuel consumption for a single turbocharged HCCI engine using NVO

Intake pressure was the main enabler of high load HCCI operation and it is shown in Figure 4.10 along with exhaust pressure as functions of IMEPn. As discussed in Chapter 1, recent literature has shown exhaust backpressure to be a problem when HCCI engines are coupled with turbochargers. The reason stems from low temperature combustion and the resulting low enthalpy exhaust stream directed to the turbine. While low exhaust temperature is characteristic of the combustion mode, backpressure development is highly dependent on the hardware used. Turbo matching is one important factor involved and the operating strategy of the engine is another one. As seen in the same figure, backpressure was not a problem in this engine when hot intake air was utilized. In addition, appropriate turbo matching in this case meant that engine operation at 2000 rpm was appropriately suited to the turbocharger mass flow rate characteristics. A key effect was that operation with hot intake air allowed more exhaust gas to be directed to the turbine. The outcome was high turbine pressure ratio and efficiency which translated to high compressor pressure ratio. Exhaust pressure was always higher than the intake thus contributing to the negative pumping loop, but it was not a significant problem.

The low valve lifts of the NVO strategy were primarily responsible for the high values of PMEP shown in Figure 4.11. Pumping work increased with load, since intake and exhaust mass flow rates increased accordingly. The high pumping work encountered in this simulation was an indication that boosting and low valve lifts is not the most efficient combination for achieving high load HCCI. It also suggested that if external compression is sufficient to bring Intake Valve Closing (IVC) temperature to the high levels required for ignition, NVO and high RGF are not required. The last point led to the study of a combined valve strategy that features NVO to PVO switching that will be demonstrated in the following sections. Figure 4.11 also shows intake temperature as a function of load and one can see that it follows a trend similar to that of intake pressure

shown in Figure 4.10. This similarity was expected since intake air temperature is raised by compression in the turbocharger and then governed by the intercooler.

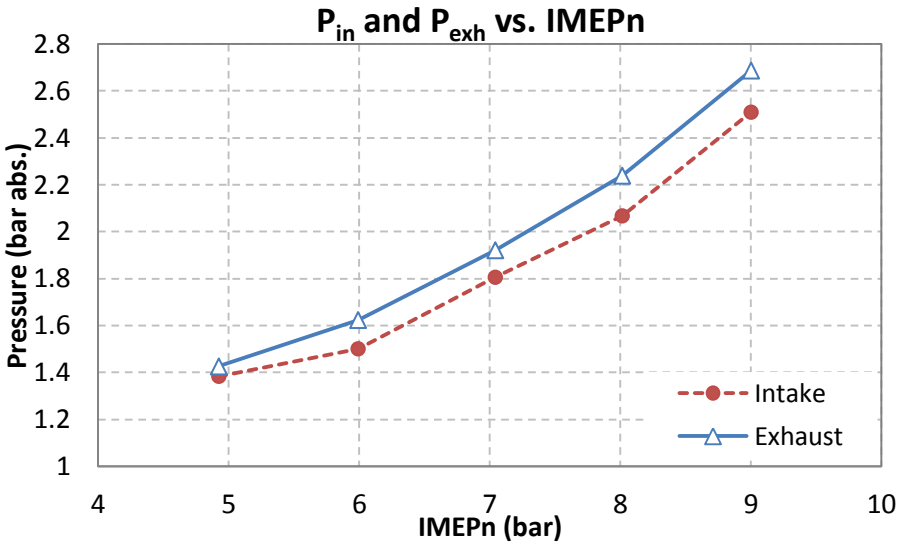

Figure 4.10 – Intake and exhaust pressures for a single turbocharged HCCI engine using NVO

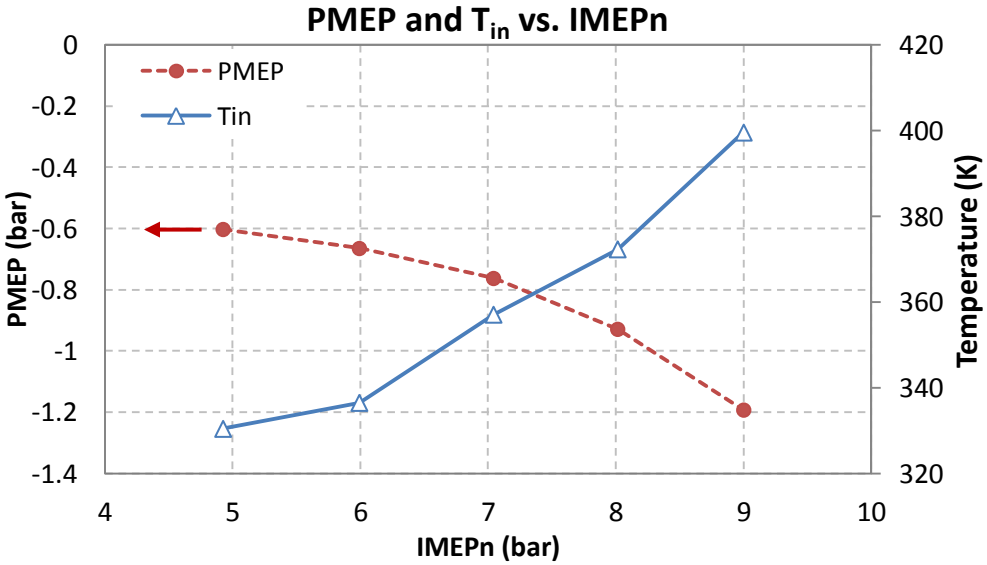

Figure 4.11 – PMEP and intake temperature for a single turbocharged HCCI engine using NVO

Figure 4.12 displays the use of NVO and RGF for mixture preparation as load was increased. RGF followed a similar trend to NVO since it was primarily controlled by it. The other control parameter for RGF was exhaust backpressure which did not play a significant role in this simulation since it was not much higher that the intake one. Required NVO ranged from 138 CAD at 5 bar IMEPn to 30 CAD at 9 bar IMEPn and as a result RGF ranged from 40 % at 5 bar IMEPn to 12 % at 9 bar IMEPn. The wide ranges observed were due to the fact that intake pressure and temperature increased significantly with load, thus necessitating reduced RGF levels. Hot intake air successfully displaced RGF allowing for increased fueling rates and increased exhaust flow to the turbine. Figure 4.13 shows equivalence ratio and effective equivalence ratio as functions of load. The latter one was defined as $\Phi' = \Phi(1\text{-RGF})$, taking into account the amount of residual gas in the cylinder and was a measure of the energy content of the charge. It can be seen that Φ reduced as load increased which suggests that the amount of air increased more rapidly than the amount of fuel. This relationship between air and fuel was one of the key enabling mechanisms of high load HCCI, since increased dilution levels allowed for higher fueling rates. On the other hand, Φ' increased with load which shows that the relative energy content of the charge increased with load. Mixture preparation in this simulation was achieved through intake air, residual gas and fueling rate. Fuel injection timing was held constant and was placed during NVO to provide for a homogeneous mixture, so fuel stratification was not a parameter. As mentioned earlier in the text, attainable load was limited by the ability of the boosting system to provide higher intake pressure. By providing even higher pressures at the intake, dilution levels could have been increased allowing for higher fueling rates as well. The second factor that limited maximum load was pumping work which increased significantly as mass flow rates through the engine increased. Both of these limits prompted investigation of more advanced boosting systems that would provide solutions to these problems.

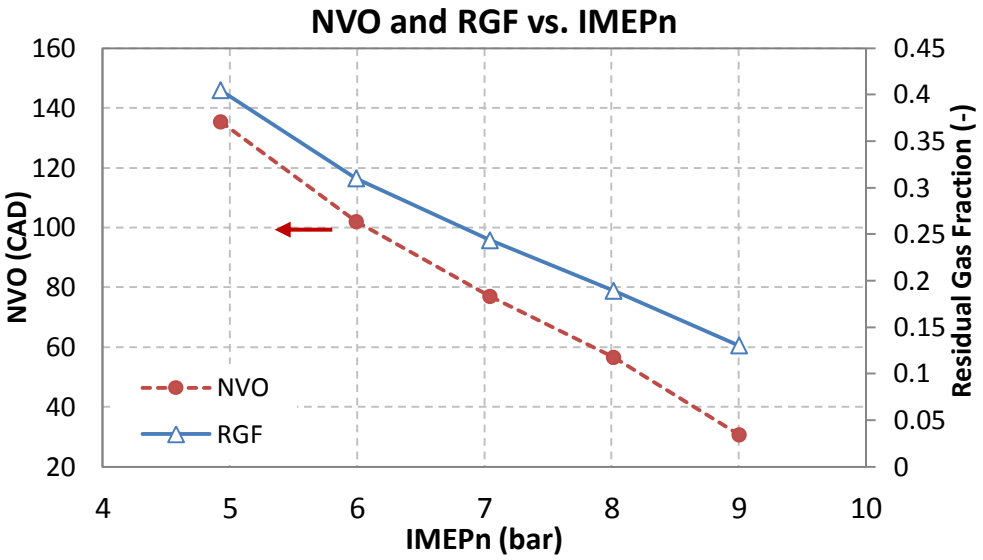

Figure 4.12 – NVO and residual gas fraction for a single turbocharged HCCI engine using NVO

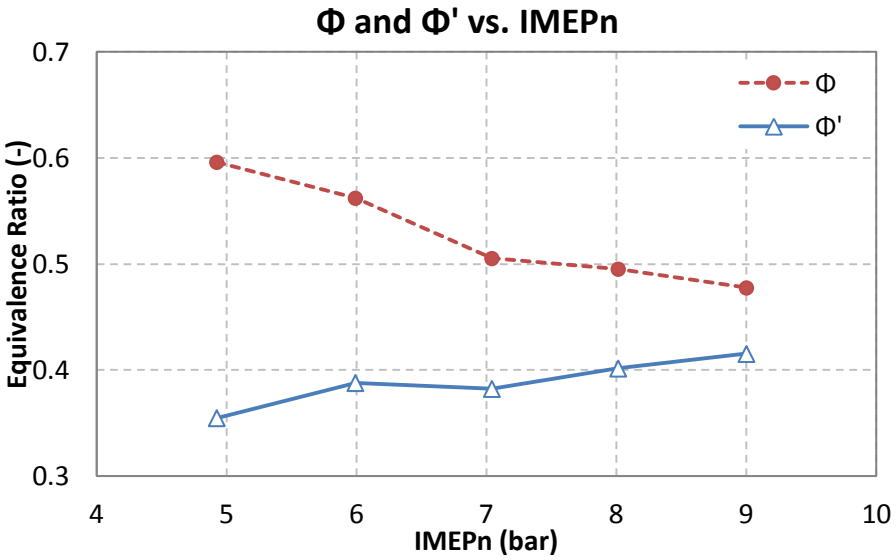

Figure 4.13 – Equivalence ratio and effective equivalence ratio for a single turbocharged HCCI engine using NVO

Figure 4.14 shows engine behavior relative to operational constraints discussed earlier. It displays R.I. and $EINO_x$ as functions of load and it is readily apparent that NO_x emissions were never an issue for boosted HCCI. High levels of dilution and the resulting low peak cylinder temperatures ensured that NO_x formation stayed well below the US

2010 standards. Ringing intensity however obtained high values which were close to the 6 MW/m^2 limit. That was a result of intentional engine operation at early combustion phasing which increased R.I. values but also allowed for higher expansion ratio and thermal efficiency. Figure 4.15 shows Peak Cylinder Pressure (PCP) and Crank Angle of 50 % burn (CA50) as functions of load. High intake pressure and dilution levels translated to relatively low PCP across the load range. At maximum load, PCP was 85 bar which was comfortably below the peak pressures that current SI engines can withstand. The simulated four-cylinder engine exhibited slight cylinder to cylinder variation; the CA50 values shown below were the maximum values between the four cylinders at every load point. CA50 values ranged from 7 to 16 which can be justified by the fact that load was almost doubled across the range. As load increased, combustion needed to be phased later in the cycle to accommodate high pressure rise rates. At maximum load of 9 bar NMEP, combustion had to be centered at 16 CAD after TDC. Similar CA50 values have also been experimentally observed [2].

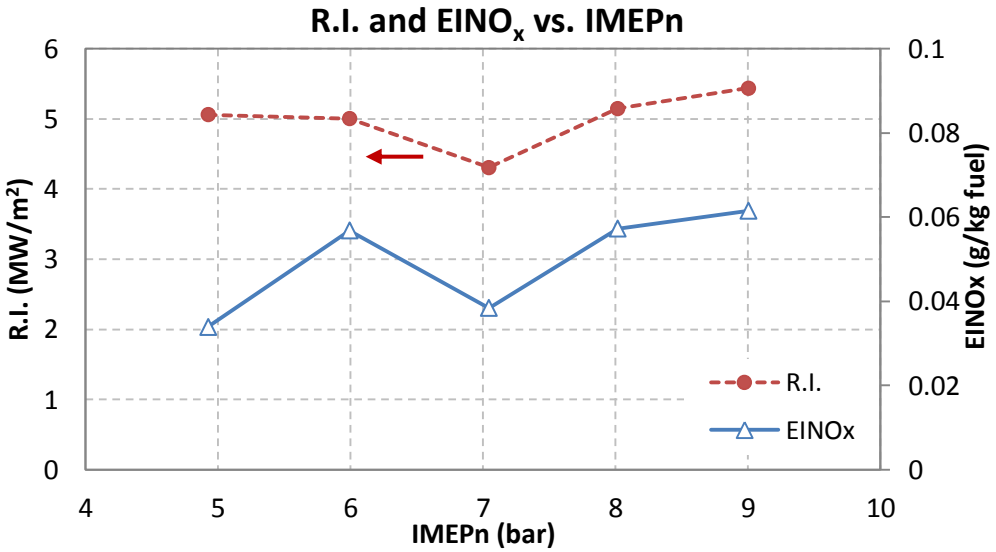

Figure 4.14 – Ringing intensity and NOx emissions index for a single turbocharged HCCI engine using NVO

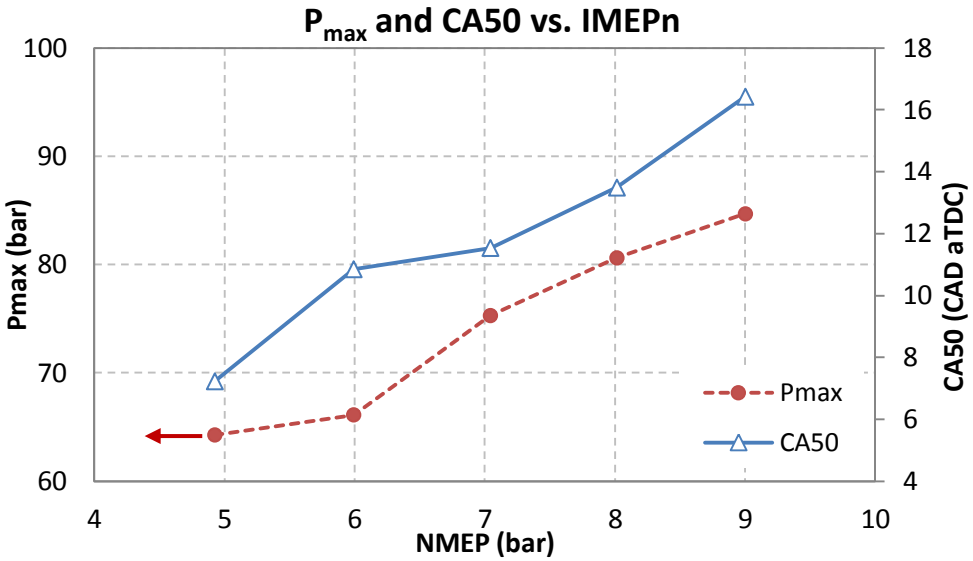

Figure 4.15 – Peak cylinder pressure and CA50 for a single turbocharged HCCI engine using NVO

The hot intake air operating strategy allowed for full exploitation of the small turbocharger attached to this engine. Hot intake air reduced the need for residual gas, so by reducing NVO more exhaust gas was sent to the turbine. Higher exhaust mass flow rates improved turbocharger performance which resulted in higher intake pressures. Figure 4.16 and Figure 4.17 show the compressor and turbine performance maps respectively with the operating points of the three highest load cases (7, 8 and 9 bar NMEP) being superimposed on the plots. The three operating points appear to lie on a straight line on the compressor map, which runs through the highest efficiency contours. The last point for 9 bar NMEP had a pressure ratio of 2.51, which was the value of absolute intake pressure at maximum load. In a similar way, the three points lie on the most favorable region on the turbine map as well. However, the maximum load point pushed the turbine at its flow capacity limit and the compressor close to its pressure ratio limit, thus not allowing for higher intake pressures. As noted earlier, this was the load limiting factor for the engine. Turbo matching for this engine model proved to be successful for operation at 2000 rpm. The small size of the turbocharger allowed for high intake pressure even when exhaust gas enthalpy from HCCI combustion was low.

Operation above 9 bar NMEP and above 2000 rpm was limited by the turbocharger though. Accommodating higher exhaust mass flow rates while maintaining similar intake pressure ratios seemed essential for high load boosted HCCI operation and prompted the exploration of a more advanced boosting system that will be presented in the following sections.

The combination of turbocharging and NVO was found to be favorable for elevating charge temperature but it came with a pumping work penalty. In addition, the limits of the turbocharger itself dominated the upper load limit of the engine. These two shortcomings could be addressed by using different boosting systems and by employing NVO/PVO cam switching as will be shown in the following sections. Different boosting systems have the potential to supply higher intake pressure if needed and the dual NVO/PVO valve strategy can aid gas exchange efficiency.

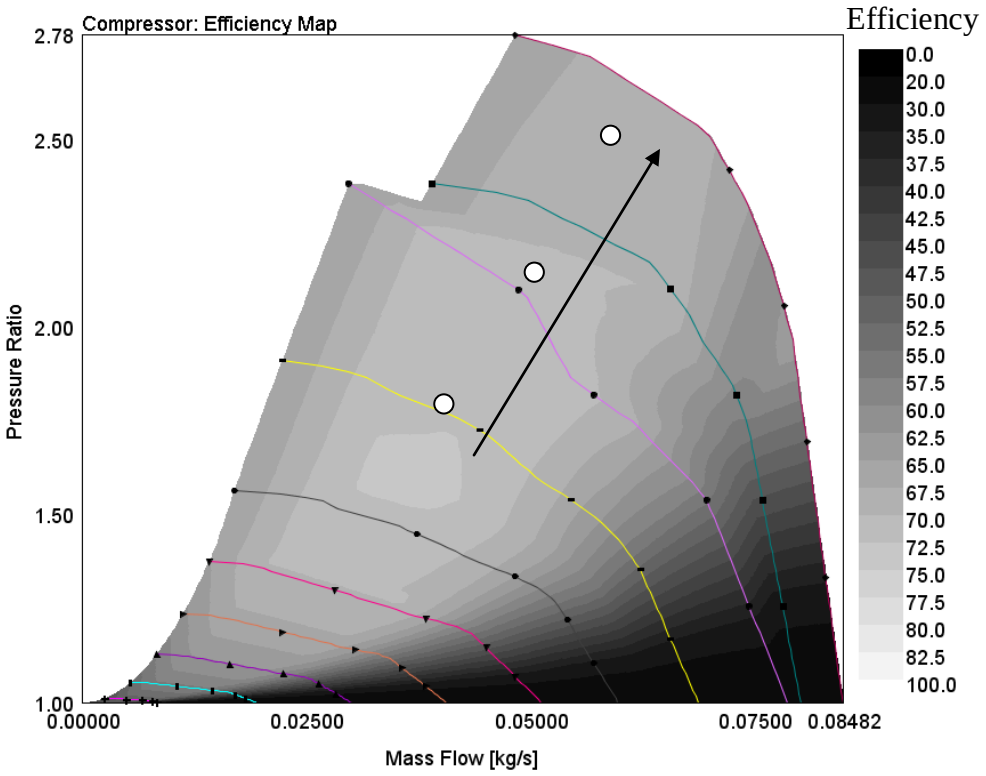

Figure 4.16 – Compressor performance map and three operating points for a single turbocharged HCCI engine using NVO

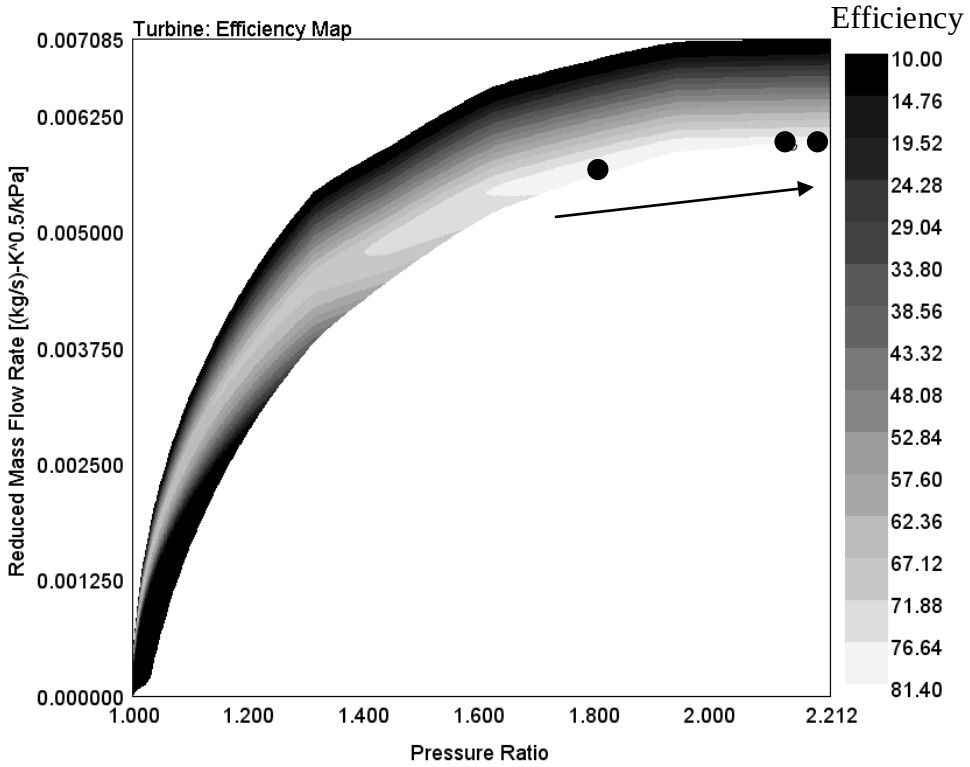

Figure 4.17 – Turbine performance map and three operating points for a single turbocharged HCCI engine using NVO

Overall, this section showed that elevated intake temperature can be successfully used to replace residual gas for charge heating on a cycle basis. The combination of intake heating and VVA showed that dilution levels were improved and thermal efficiency increased as well. By utilizing hot intake air and directing more exhaust gas to the turbocharger, charge heating was performed externally to the cylinder, at the intake system. In conclusion, heating of the charge using the intake system appears to be more efficient than heating it using the valve strategy. The findings indicated that elevated intake temperature may enable the use of high lift, PVO valve strategies that do not involve any direct mechanism for residual gas trapping. The following section will introduce a switchable NVO/PVO valve strategy combined with advanced boosting systems and will attempt to explain the trade-offs involved.

4.3 Advanced Valve Strategies and Boosting Systems for High Load HCCI

4.3.1 Positive Valve Overlap and Turbocharging

The investigation of a turbocharged HCCI engine with negative valve overlap demonstrated that hot intake air can be effectively used for high load operation. It was found that performing charge heating outside of the cylinder was more efficient that performing it inside the cylinder. The benefits were associated with the performance of the boosting system and its ability to provide high pressure at the intake side. In addition, thermal efficiency was increased by air dilution. Two issues were identified that prompted further investigation; the first one was significant pumping work at high loads due to NVO. The second one was limited mass flow rate capacity of the turbocharger at high engine loads. This section will try to address both of them by introducing a different boosting system as well as a different valve strategy. The larger BorgWarner turbocharger that featured variable geometry turbine was used in conjunction with the PVO high-lift valve strategy. The hypothesis that intake preheating by the boosting system was adequate to ensure ignition of the charge when PVO was used was confirmed. The results are presented and discussed in the following in a similar manner to that of the previous section.

Figure 4.18 shows the load range for this engine starting from 5 bar IMEPn. IMEPn and BMEP are shown as functions of fueling rate and one can see that the maximum attainable load was increased by 1 bar compared to the NVO engine seen in the previous section. As described earlier in this chapter, the combination of NVO and PVO offered significant advantages in boosted HCCI operation. NVO was used at low loads since the intake pressure and temperature supplied from the turbocharger were not enough to provide sufficient heating of the charge for ignition. When intake pressure and temperature were sufficient for ignition the valve events were switched to PVO. PVO use offered pumping work benefits and lower cylinder temperatures. Both of these effects

will be discussed in the following. NVO/PVO switching occurred at 7 bar NMEP and that point is highlighted in Figure 4.18.

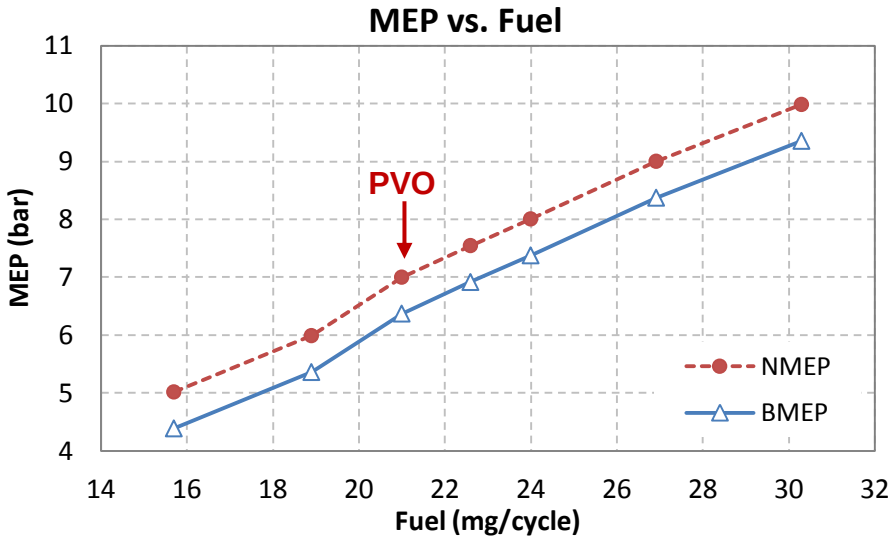

Figure 4.18 – Load range for a VGT turbocharged HCCI engine using NVO/PVO

Figure 4.19 shows NSFC and BSFC as functions of NMEP and BMEP respectively. The effect of PVO on improving engine efficiency is evident from the SFC variation with load. NVO use at low loads suffered from high pumping work which hindered engine efficiency. After the valve strategy was switched to PVO though, efficiency improved markedly. PVO acted to reduce pumping work thus improving gas exchange and net indicated efficiency. In addition, it lowered cylinder temperatures by trapping cooler residual gas and mixing of hot and cold gases during valve intersection. Lower cylinder temperatures increased γ and thermal efficiency. The combination of increased thermal and gas exchange efficiencies with PVO allowed for high values of indicated and brake efficiencies. Peak indicated efficiency was 41.7 % at 9 bar NMEP and brake efficiency at the same point was 38.8 %.

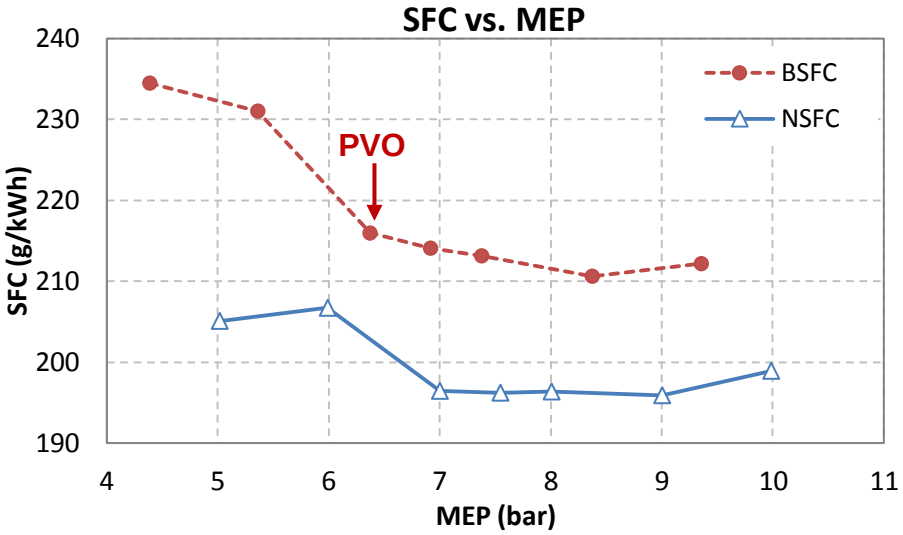

Figure 4.19 – Specific fuel consumption for a VGT turbocharged HCCI engine using NVO/PVO

It should be noted that improved indicated efficiency was achieved despite the fact that intake pressures were lower than those observed in the NVO engine earlier. Figure 4.20 shows intake and exhaust pressures as functions of load. The reason behind lower intake pressures was inferior turbo matching at 2000 rpm. Turbocharger operation also resulted in higher ΔP values across this engine compared to the NVO engine.

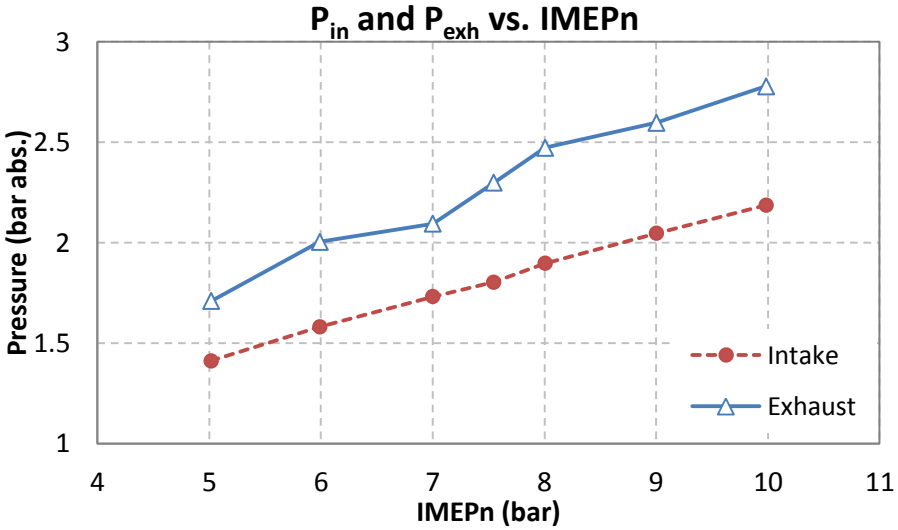

Figure 4.20 – Intake and exhaust pressures for a VGT turbocharged HCCI engine using NVO/PVO

PMEP and intake temperature are shown in Figure 4.21 as functions of load. The significant decrease of PMEP when PVO was used resulted from the absence of recompression and from higher valve lifts that mitigated throttling losses across the valves. As load increased beyond 7 bar NMEP, the advantage of variable geometry combined with PVO allowed pumping work to be kept fairly constant from 8 to 10 bar NMEP which was highly beneficial for indicated efficiency. Intake temperature followed a similar trend to intake pressure since heating occurred due to compression in the turbocharger. It is interesting to note that PVO operation was allowed when intake temperature exceeded 350 K and intake pressure exceeded 1.7 bar abs.

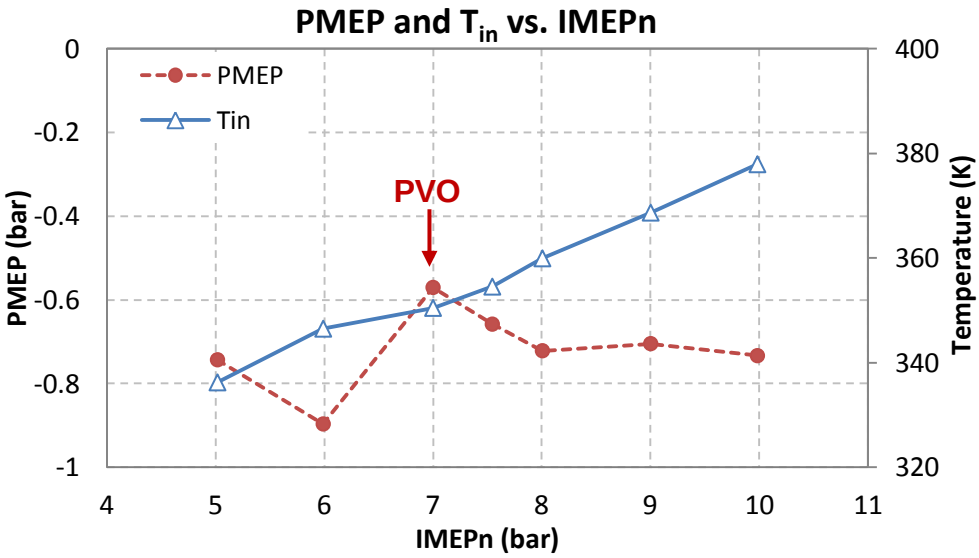

Figure 4.21 – PMEP and intake temperature for a VGT turbocharged HCCI engine using NVO/PVO

Figure 4.22 displays NVO and residual gas fraction as function of load. PVO is shown as negative NVO in this plot. As indicated in the previous figures, NVO/PVO switching occurred between 6 and 7 bar NMEP. After the switching occurred, the engine exhibited increased need for residual gas which was attributed to the fact that residual gas from PVO was cooler that residual gas from NVO. The main mechanism for retaining exhaust gas in the cylinder with PVO was the effect of backpressure; therefore, exhaust

gas was not trapped in the cylinder but transferred to the exhaust ports and then reinducted when cylinder pressure dropped below exhaust pressure. As load increased PVO was reduced, allowing less time for gas exchange and resulting in less residual gas in the cylinder. At the same time, increased exhaust flow to the turbine helped to improve turbocharger performance and provide higher intake pressure as load increased. It should be noted that when PVO was used, residual gas did not have the same heating ability as when NVO was used. Therefore, use of PVO meant that external heating of the charge was essential for HCCI combustion.

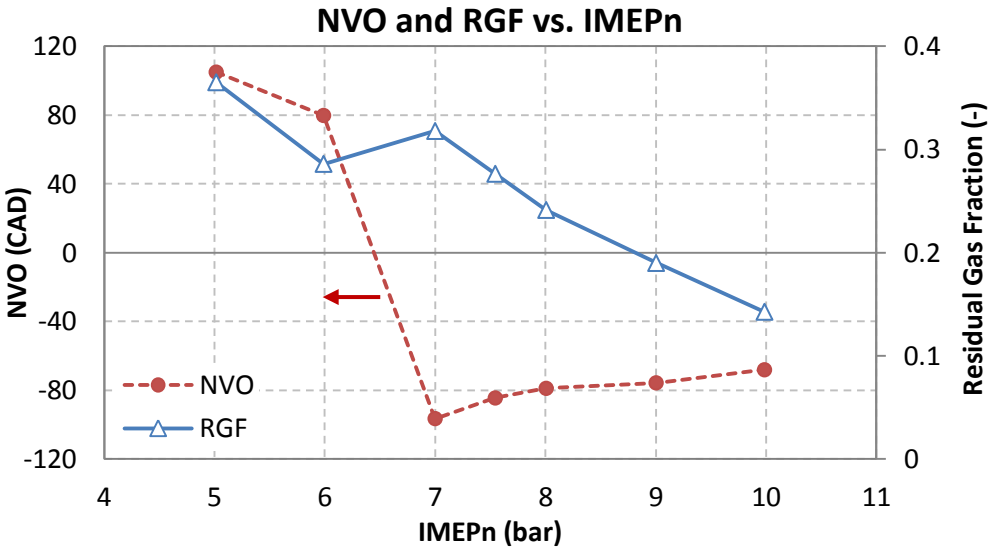

Figure 4.22 – NVO and residual gas fraction for a VGT turbocharged HCCI engine using NVO/PVO

Figure 4.23 shows Φ and Φ' as functions of load. Equivalence ratio generally decreased with load but not monotonically. NVO to PVO switching at 7 bar NMEP caused a slight increase in Φ; RGF was increased too thus displacing fresh air in the mixture. As load increased further, Φ decreased and reached 0.49 at maximum load. Effective equivalence ratio increased with load and verified that the energy content of the charge increased accordingly. As discussed earlier, the key mechanism behind

turbocharged HCCI operation was the increasing dilution levels with load which allowed tight control of pressure rise rates during heat release.

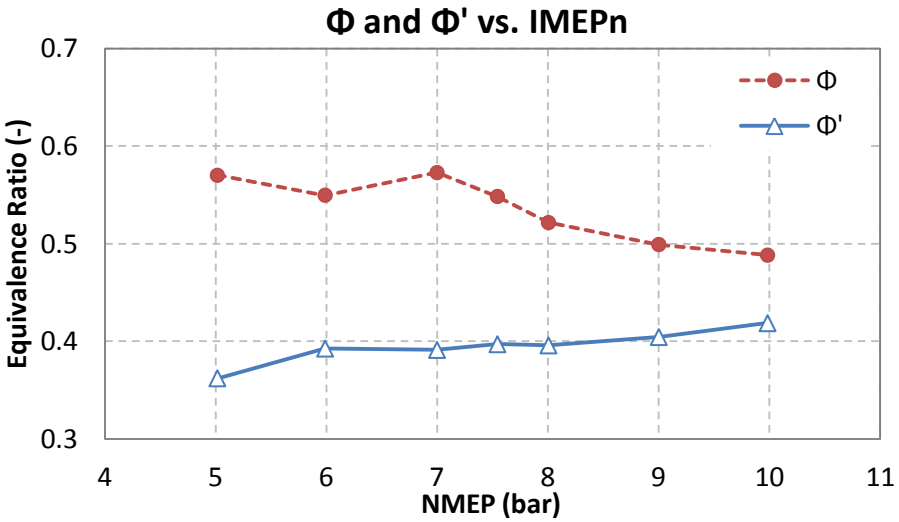

Figure 4.23 – Equivalence ratio and effective equivalence ratio for a VGT turbocharged HCCI engine using NVO/PVO

Figure 4.24 displays ringing intensity and NOx emissions index as functions of load. Combustion phasing was adjusted so that every operating point was close to the ringing limit in order to maximize expansion ratio and thermal efficiency. It is interesting to observe that after NVO/PVO switching occurred, both R.I. and EINOx were reduced even though load was increased. Cooler residual gas and lower overall cylinder temperatures acted to phase combustion later in the cycle thus reducing pressure rise rates. NO_x emissions were not an issue at any load level, since dilution was always sufficient for peak cylinder temperatures below the NO_x formation threshold.

Figure 4.25 shows peak cylinder pressure and CA50 as functions of load. It can be seen that peak cylinder pressure increased monotonically with load up to 9 bar NMEP, but its slope changed when NVO was switched to PVO. The reason was that combustion could be phased earlier in the cycle in order to improve thermal efficiency. CA50 values verified the earlier combustion phasing potential when PVO was used which was primarily enabled by reduced cylinder temperatures. Peak cylinder pressure was less than

84 bar which was comfortably below the limit for SI engine structures. CA50 values spanned a wide range from 10 to 18 CAD aTDC. The later end of that range has not been observed experimentally for this engine type, but the model was able to calculate stable combustion even at these late timings.

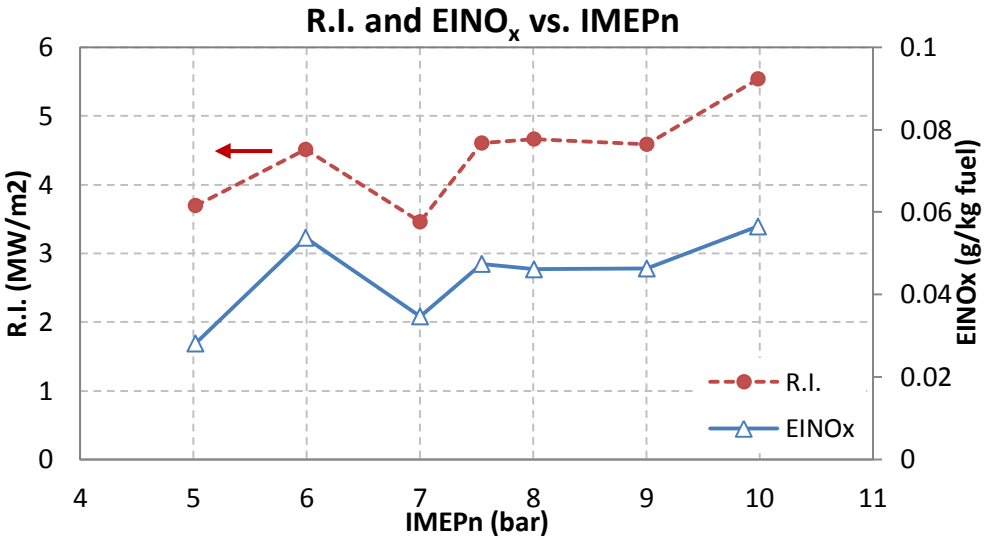

Figure 4.24 – Ringing intensity and NOx emissions index for a VGT turbocharged HCCI engine using NVO/PVO

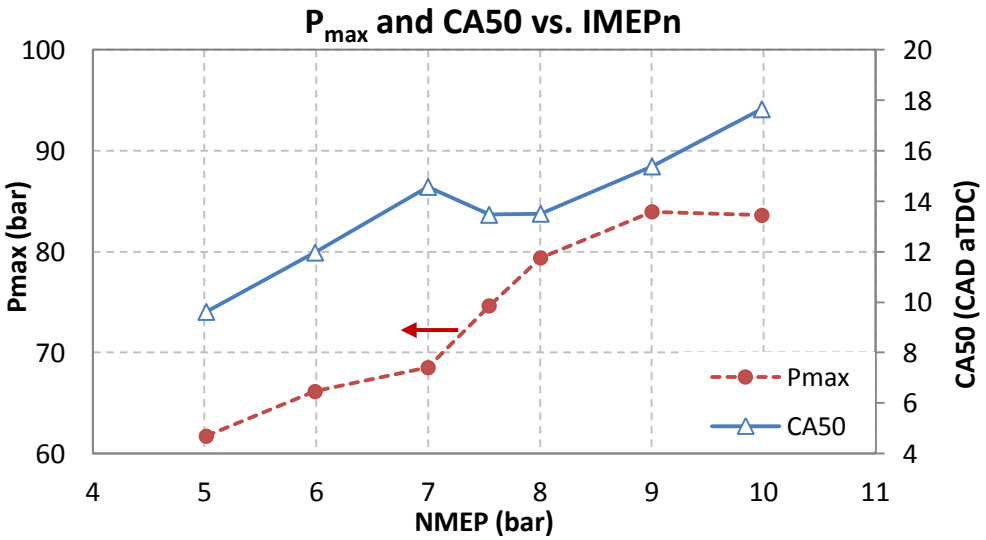

Figure 4.25 – Peak cylinder pressure and CA50 for a VGT turbocharged HCCI engine using NVO/PVO

Figure 4.26 and Figure 4.27 show the compressor and turbine performance maps respectively, with the three highest load points superimposed. Figure 4.27 includes the maps from three different settings of the variable geometry turbine which correspond to different rack positions for the three operating points. It is readily apparent that the three highest engine operating points (8, 9 and 10 bar IMEPn) occurred in high efficiency regions of both the compressor and turbine maps which resulted in good overall turbocharger efficiency and favorable boundary conditions for the cylinders. Advanced boosting features like the variable geometry turbine proved to be very helpful for controlling backpressure which simultaneously affected residual gas and pumping work. Similarly to what was observed in the previous section, the load limiting factor appeared to be intake pressure ratio which dictated dilution levels and pressure rise rates.

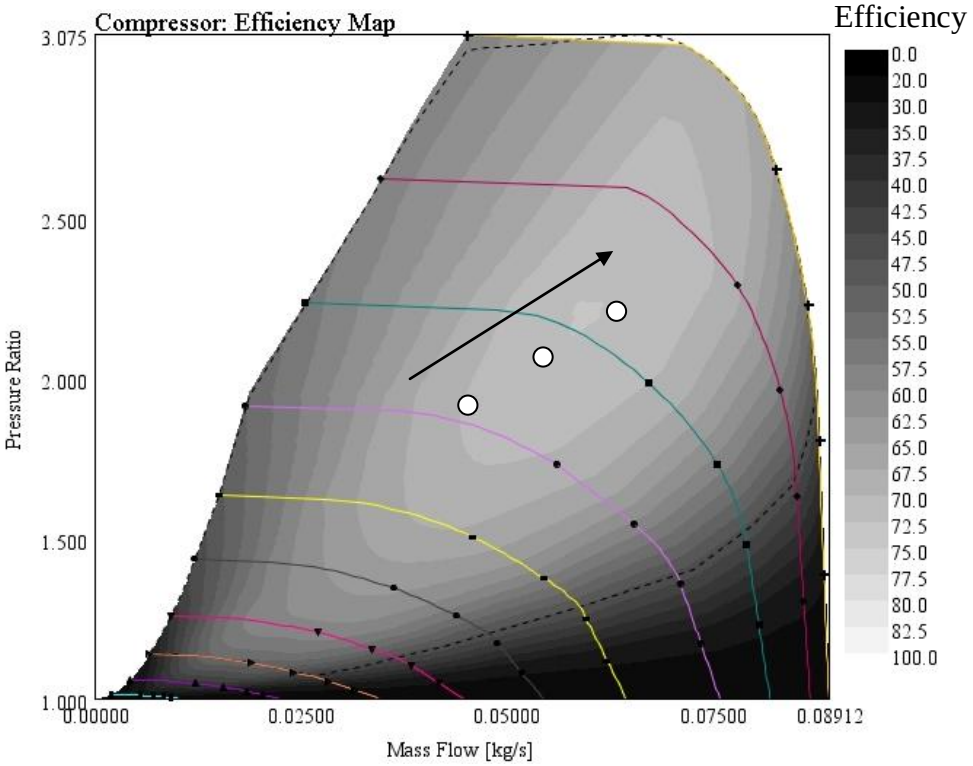

Figure 4.26 – Compressor performance map and three operating points for a VGT turbocharged HCCI engine using NVO/PVO

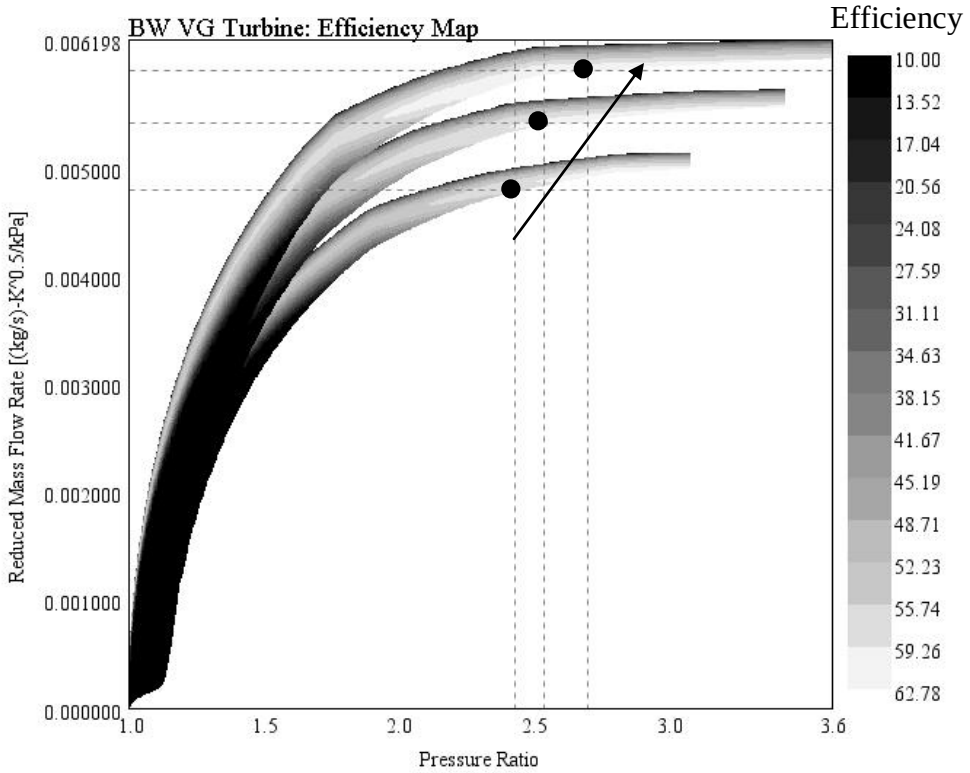

Figure 4.27 – Turbine performance map and three operating points for a VGT turbocharged HCCI engine using NVO/PVO

In conclusion, the hypothesis that PVO valve events could promote high load boosted HCCI operation was confirmed by multi-cylinder simulations. The engine model employed NVO/PVO cam switching and variable geometry turbocharging and was used to explore the trade-offs between boosting and VVA for mixture preparation. It was found that low load operation could not be achieved without the use of NVO for residual gas trapping. However, as load increased and intake temperature rose, PVO could be employed with multiple benefits on reducing pumping work and cylinder temperatures. The result was high indicated efficiency across a wider load range in an engine setup that closely resembles currently available downsized boosted SI engines. The load limiting factor appeared to be intake pressure which dictated dilution levels and allowable fueling rates. In order to further explore that limit, a two-stage boosting system was deemed necessary. That system in conjunction with the beneficial NVO/PVO valve strategy will be presented and discussed in the following section.

4.3.2 An Advanced System Combining Two-Stage Boosting and VVA

The two previous sections demonstrated that elevated intake temperature can be used as an effective means of charge heating in boosted HCCI engines and resulted in significant efficiency benefits. When NVO was employed, hot intake air was used to displace residual gas from the cylinder and improve boosting performance. However, the recompression event was associated with increased pumping work and hindered efficient engine operation. Subsequently, PVO proved to be beneficial for efficiency by significantly reducing pumping work and also by reducing cylinder temperatures. The effect of the latter was to improve thermal efficiency and reduce ringing propensity during combustion as well. Therefore, the combination of NVO and PVO in a switchable valve strategy offered considerable flexibility and allowed for wide HCCI load range. The investigation of two different turbocharging systems revealed that available pressure ratio at the intake side is a load limiting factor since it directly controls dilution levels. Therefore, application of an advanced boosting system was investigated in order to examine the hypothesis that higher pressure ratios can lead to higher attainable load.

Advanced boosting featured the VGT turbocharger shown previously in series with a supercharger, thus forming a two-stage system. Intelligent use of the supercharger was made by means of bypassing it at low loads and by adjusting its gear ratio to the engine crankshaft. Both methods were used as ways to minimize the mechanical work penalty of the supercharger and ensure maximum brake efficiency of the system. It should be noted that even though variable gear ratio superchargers face practical constraints, the ratio range used for this study was narrow (2.5 - 3). The supercharger was bypassed at low loads (5 and 6 bar NMEP) since the intake pressure supplied by the turbocharger was sufficient for the dilution levels required. Bypassing the supercharger helped maintain high levels of brake efficiency, since the mechanical work required was a large fraction of the engine useful work at low loads.

The following figures present the results obtained from the simulation of advanced boosting combined with the NVO/PVO valve strategy, in the same way as those presented in the two previous sections. Figure 4.28 shows NMEP and BMEP as functions of fueling rate. It is readily apparent that the addition of supercharging to the system resulted in extension of the upper load limit to 11 bar NMEP. The reasons behind the load extension will be discussed in the following. Brake work did not seem to suffer from supercharger use since the gear ratio was intentionally kept low.

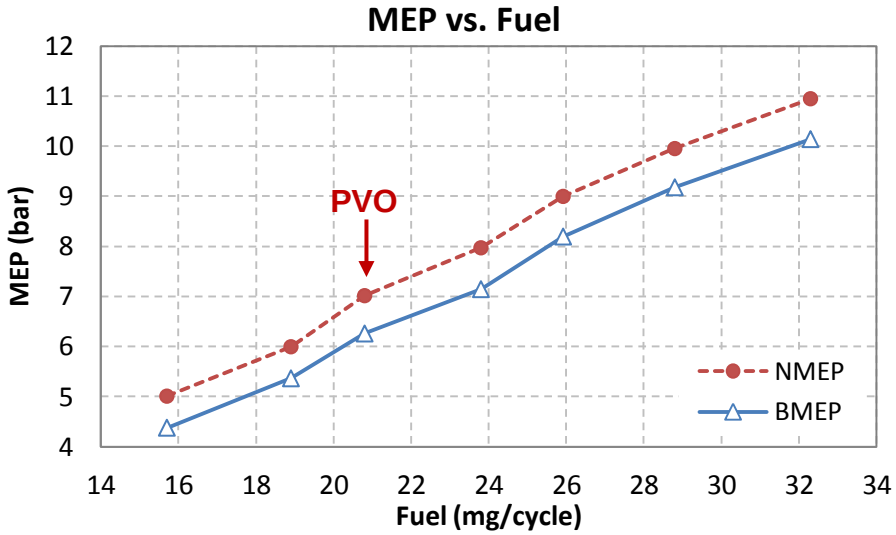

Figure 4.28 – Load range for a two-stage boosted HCCI engine using NVO/PVO

Figure 4.29 shows indicated and brake specific fuel consumption as functions of NMEP and BMEP respectively. It can be seen that the addition of supercharging led to efficiency benefits compared to the single-stage systems described in the previous sections. The efficiency benefit was primarily attributed to higher intake pressures supplied by the combined boosting system, which allowed for even higher dilution levels and further improvements in thermal efficiency. Engaging the supercharger after 6 bar NMEP and at the same time switching from NVO to PVO, resulted in significant gains in efficiency as can be seen from the SFC curves. High load operation reached levels of efficiency comparable to those of diesel engines.

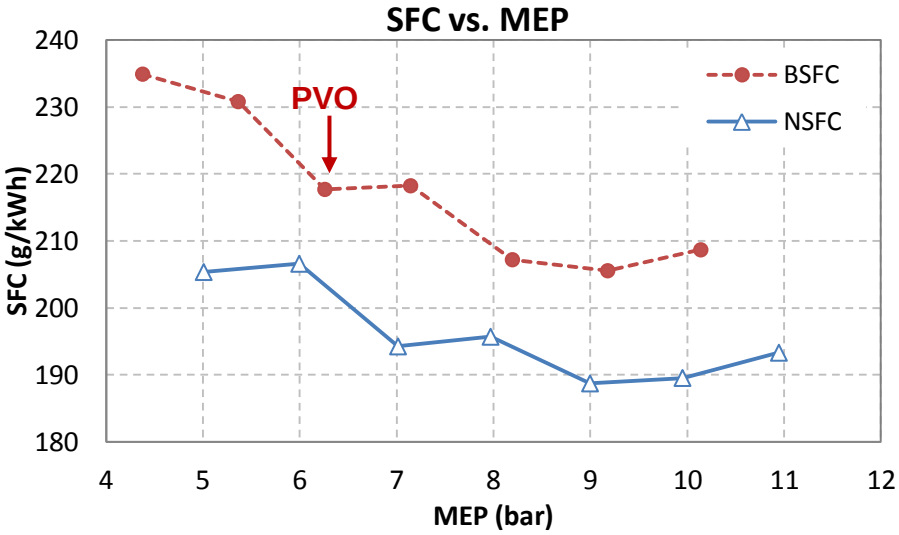

Figure 4.29 – Specific fuel consumption for a two-stage boosted HCCI engine using NVO/PVO

Figure 4.30 shows the variation of intake and exhaust pressures with load. When the supercharger was engaged intake pressure increased significantly, resulting in high dilution levels and low PRR during heat release. These factors allowed for higher thermal efficiency while the improved breathing through PVO allowed for higher gas exchange efficiency. The fact that intake pressure increased significantly meant that ΔP across the engine was less adverse as load increased, which was another factor that contributed to improved gas exchange efficiency. The outcome was high indicated and brake efficiencies.

High intake pressure resulted in high intake temperature as seen in Figure 4.31, thus facilitating engine operation with hot intake air and PVO. Beyond 8 bar NMEP, dilution levels were sufficient for high load HCCI. Intake temperature kept rising, allowing for less RGF thus more exhaust gas was directed to the turbocharger. As load increased turbocharger performance was improved, and the contribution of supercharging enabled controlled backpressure through variable geometry. The result was reduced pumping work as shown in Figure 4.31. Backpressure control managed to keep PMEP fairly constant from 7 to 11 bar NMEP by reducing flow restriction through the turbine.

However, intake pressure did not increase much, because the amount of work done by the compressor remained almost constant. The combination of dilution, combustion phasing and pumping work at medium loads lead to high levels of indicated and brake efficiency. Peak intake pressure observed for this engine system was close to 2.3 bar abs. which was somewhat lower than that observed from the single turbocharged engine operating on NVO alone. Intake pressure appeared to be the dominant factor affecting attainable load but gas exchange was critical in order to ensure high efficiency levels.

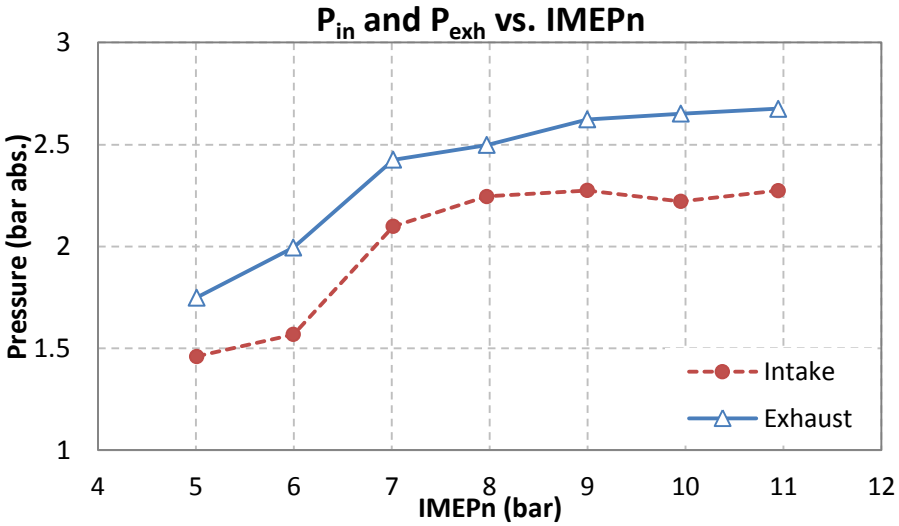

Figure 4.30 – Intake and exhaust pressures for a two-stage boosted HCCI engine using NVO/PVO

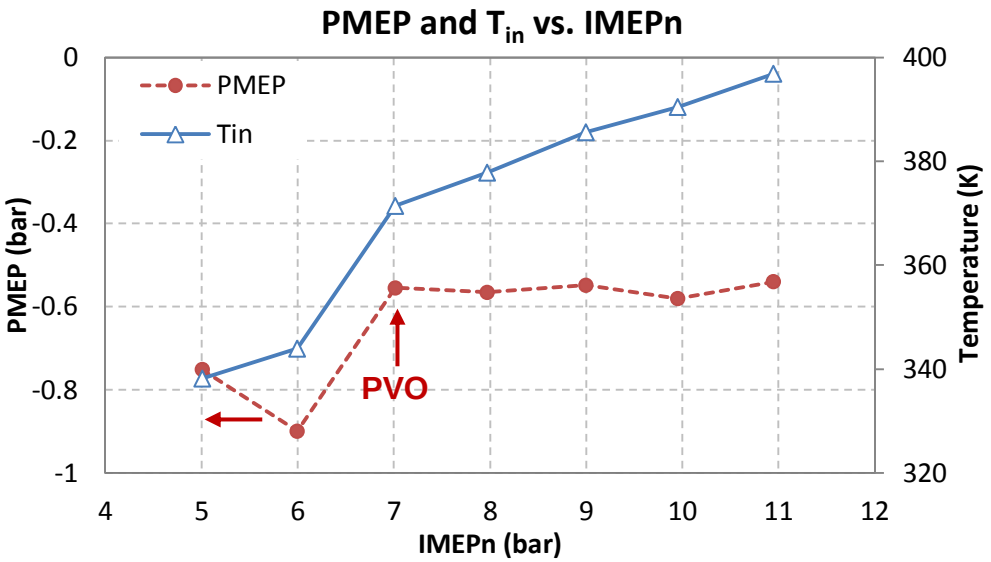

Figure 4.31 – PMEP and intake temperature for a two-stage boosted HCCI engine using NVO/PVO

Figure 4.32 displays the NVO/PVO cam switching and its effect on cylinder residual gas fraction. As mentioned above, 7 bar NMEP was the NVO/PVO switching point as well as the point where the supercharger was engaged. The introduction of high amounts of positive overlap (100 CAD) led to a slight increase in RGF, since there was ample time for gas exchange and for backpressure to push exhaust gases back into the cylinder. As load increased beyond 8 bar NMEP, RGF kept reducing. It should again be noted that trapped residual gas when PVO was used, was of lower temperature that when NVO was used. The reason was different trapping mechanisms as explained in the previous section. At maximum load, the engine required only 9 % of residual gas which is close to the values observed in the Sandia experiment shown in Chapter 3. The contribution of supercharging at 7 bar NMEP acted to increase dilution levels, as shown in Figure 4.33 . Equivalence ratio was reduced from 0.55 to 0.45, but Φ' was reduced as well, indicating a reduction in the energy content of the charge. Above 7 bar NMEP, the combination of fairly constant intake pressure and increasing intake temperature resulted in approximately constant Φ. On the other hand, Φ' kept increasing since the amount of RGF was decreasing with load and fueling rate was increasing. Results from the three

engine systems displayed so far indicated that equivalence ratio approached values of 0.5 or less at maximum load which were critical in order to control pressure rise rates during heat release.

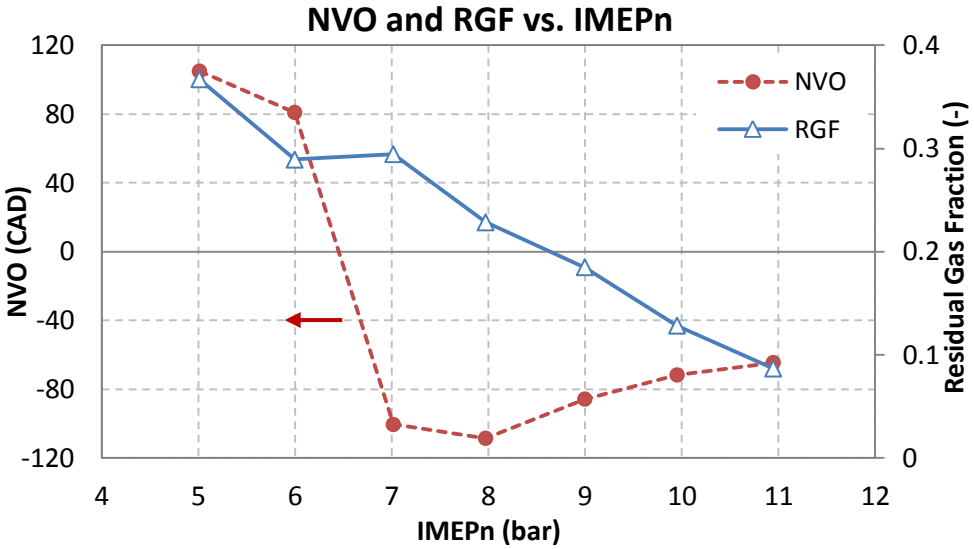

Figure 4.32 – NVO and residual gas for a two-stage boosted HCCI engine using NVO/PVO

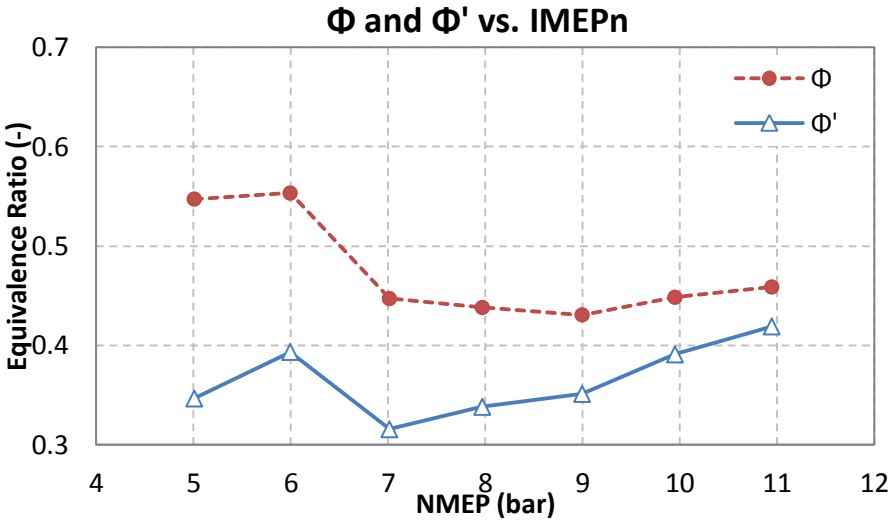

Figure 4.33 – Equivalence ratio and effective equivalence ratio for a two-stage boosted HCCI engine using NVO/PVO

The high levels of dilution resulting from the combination of PVO and supercharging, allowed for low PRR and low cylinder temperatures during the combustion process. At medium loads (7, 8 bar NMEP) the low effective equivalence ratio allowed for very low ringing intensity and NO_x formation as seen on Figure 4.34. The effectiveness of dilution is evident from the steep decrease of both R.I. and $EINO_x$ when the engine switched from NVO to PVO at 7 bar NMEP and the supercharger was engaged. As expected, increasing the fueling rate to obtain higher loads, led to higher PRR and higher values of R.I. At the same time, NO_x emissions were kept very low, which was the case for the two previous boosted HCCI engines presented as well. It is interesting to note that the ringing intensity and NOx curves have similar shapes, which verified their strong dependence on dilution levels.

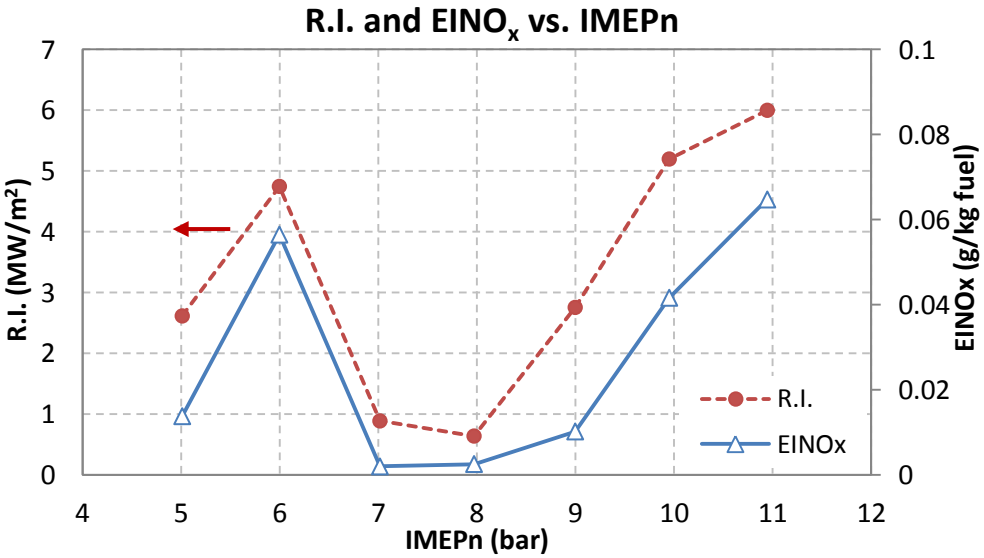

Figure 4.34 – Ringing intensity and NOx emissions index for a two-stage boosted HCCI engine using NVO/PVO

In order to avoid excessive PRR, combustion was phased later in the cycle as load increased. CA50 and peak cylinder pressure are shown in Figure 4.35. Although advanced combustion phasing would allow for increased thermal efficiency, only a small amount of advancing could be obtained for loads higher than 8 bar NMEP. High PRR

rates needed to be mitigated, but also reducing RGF through backpressure led to significant gains in PMEP as shown earlier. Peak cylinder pressure did not exceed the limits of current SI engines, but combustion needed to be significantly retarded at maximum load, since PCP could approach 110 bar.

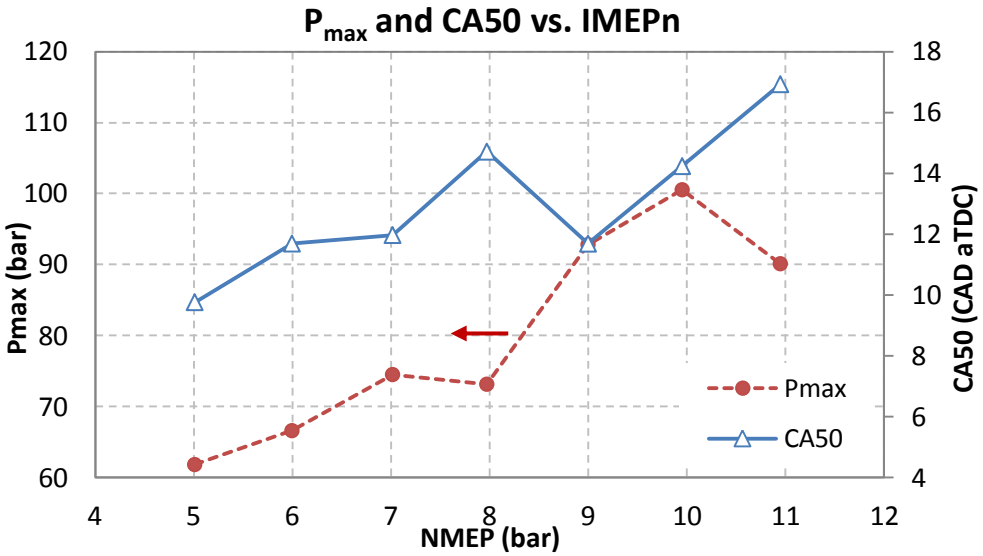

Figure 4.35 – Peak cylinder pressure and CA50 for a two-stage boosted HCCI engine using NVO/PVO

The presence of two boosting devices at the intake side was beneficial for intake pressure but only the turbocharger operated at high efficiency levels. Supercharger operation was somewhat hindered by the low gear ratio which resulted in low rotor speeds. However, operation with hot intake air enabled good use of both devices. Figure 4.36 and Figure 4.37 present the compressor and turbine maps of the VGT with the three highest load points superimposed on them (9, 10, 11 bar NMEP). The turbocharger operated at roughly constant pressure ratio on both the exhaust and intake side at these three load levels. The outcome was low backpressure development but no real increase of intake pressure from the compressor. The contribution of supercharging was to provide the additional pressure ratio needed for high dilution levels and that contribution was adjusted by its gear ratio to the engine crankshaft. Figure 4.38 shows the supercharger

performance map. The same high load operating points are shown on the lower left side of the map, at low pressure ratio and mass flow rate levels. The performance of the turbomachines suggested that a smaller supercharger be equally effective while further reducing the associated mechanical work. It also suggested that the use of a VGT be beneficial in a dual stage supercharging and turbocharging configuration. The variable geometry of the turbine provided an additional control knob for reducing backpressure, improving gas exchange efficiency and adjusting cylinder residual gas levels.

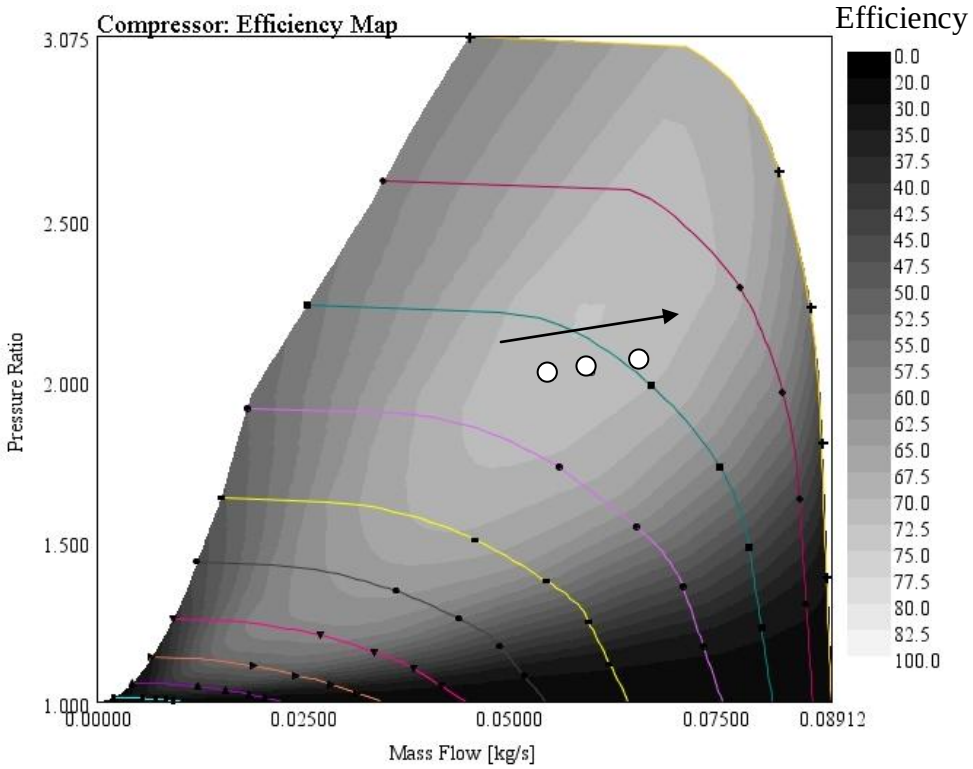

Figure 4.36 – Compressor performance map a two-stage boosted HCCI engine using NVO/PVO

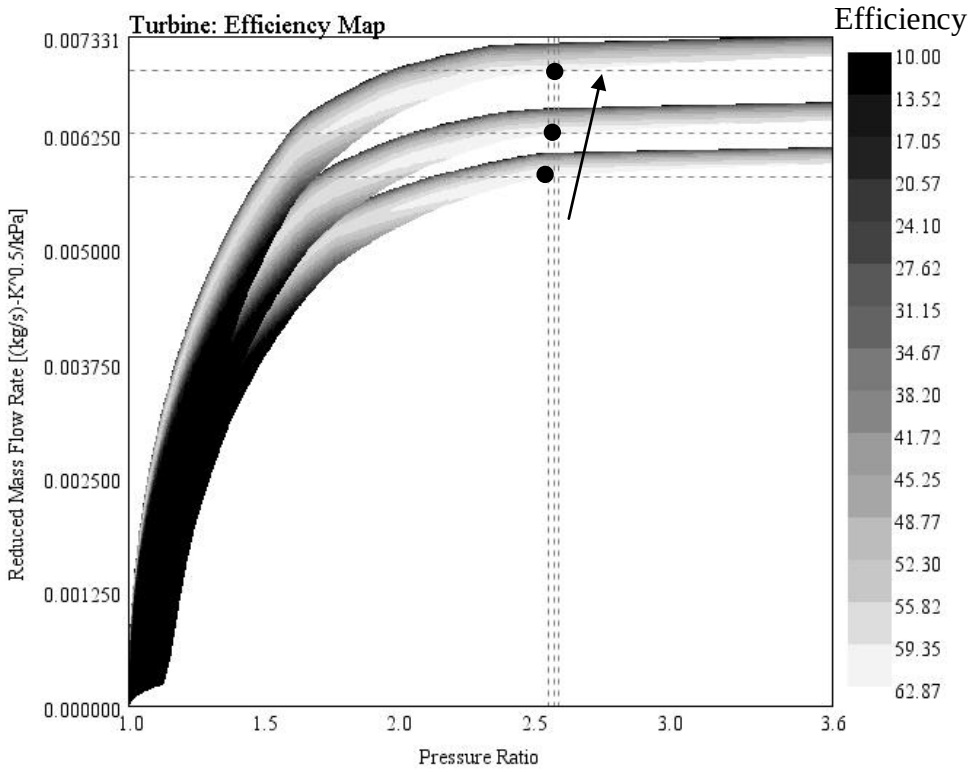

Figure 4.37 – Turbine performance map for a two-stage boosted HCCI engine using NVO/PVO

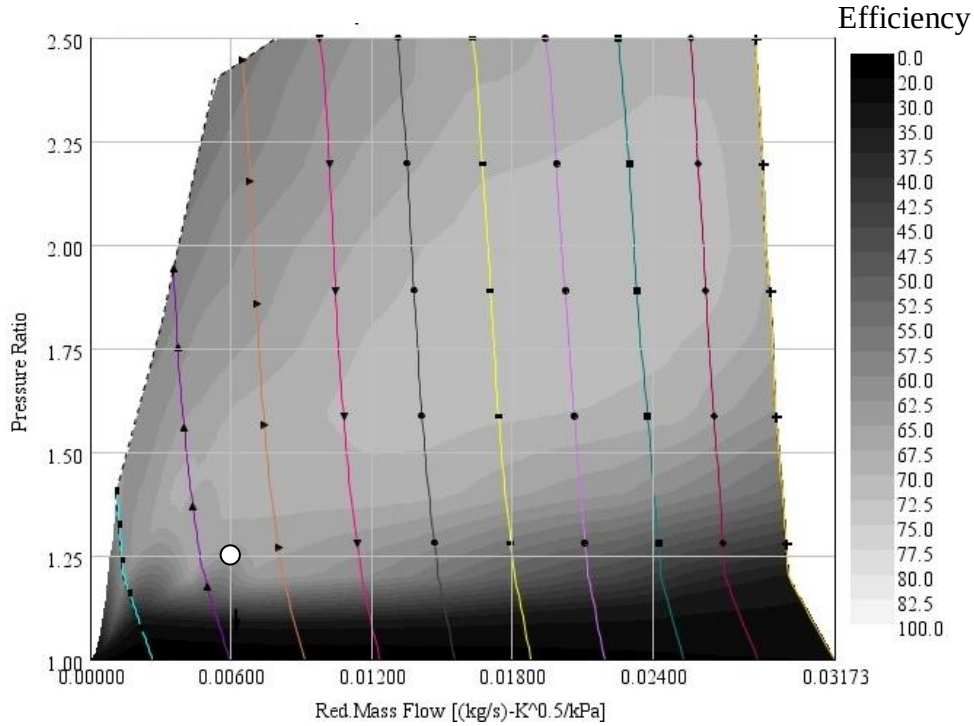

Figure 4.38 – Supercharger performance map for a two-stage boosted HCCI engine using NVO/PVO

Overall, results from the two-stage boosted HCCI simulation supported the hypothesis that elevated intake pressures can lead to higher attainable load. The primary mechanism was improved dilution levels which resulted both in lower pressures rise rates and lower cylinder temperatures. The former directly affected the engine's ringing propensity while the latter was associated with NOx formation. Both factors also helped to improve thermal efficiency. The combination of advanced boosting with a flexible valve strategy proved to be highly beneficial for gas exchange efficiency. The primary reason was enabling the use of high-lift valve events without recompression. In addition, variable geometry assisted with backpressure and RGF control. Intelligent use of the supercharger ensured that mechanical work penalty was minimal thus aiding mechanical efficiency. In summary, elevated pressure and dilution levels led to increased engine thermal efficiency; high-lift valve events let to increased gas exchange efficiency, and intelligent supercharger use led to increased mechanical efficiency. The combination of these factors resulted in indicated and brake efficiency levels comparable to those of diesel engines.

The three previous sections presented multi-cylinder HCCI simulations that involved three different boosting systems in conjunction with two VVA strategies. The results showed that boosting and VVA can be used to provide the charge compositional and thermal characteristics that enable high load HCCI operation. The three engine models operated on compression ratio of 12.5 and it was demonstrated that boosted HCCI can be accomplished with currently available boosting and VVA technology. The next section is going to investigate the effect of compression ratio on boosted HCCI operation as seen so far. Increased compression ratio is associated with thermal efficiency benefits, but lower compression ratio would enable HCCI operation in currently available downsized boosted SI engines. Therefore, the hypothesis that compression and heating performed outside of the cylinder can enable lower compression ratio needs to be examined and discussed.

4.4 Effect of Compression Ratio on Boosted HCCI Operation

A wide range of compression ratios (CR) for HCCI engines has been explored in the literature, based on the strong dependence of ignition kinetics on the compression process. Experiments and simulations that involve SI engine derivatives have investigated compression ratio settings from 10 to 14 [5, 6, 7, 8, 9], whereas diesel engine derivatives have featured higher compression ratios ranging from 14 to 17 [1, 10, 11, 12, 13]. On one hand, engines with lower compression ratios have exhibited the need for higher intake temperature for ignition control and potentially increased RGF levels but have also exhibited lower peak cylinder pressures. On the other hand, engines with higher compression ratios have displayed less dependence on intake temperature and residuals but higher peak cylinder pressures that require diesel-engine level of robustness.

This section will attempt to investigate the effect of compression ratio on boosted HCCI operation by examining load sweeps at different compression ratio levels. The engine system used was the advanced one presented in the previous section and employed a two-stage boosting system with switchable NVO/PVO valve strategy. The following figures will display several performance variables for four compression ratio levels, 11, 11.75, 12.5 and 14.

Figure 4.39 shows the load range for each one of the compression ratio levels. For all cases, minimum load was set at 5 bar NMEP and maximum load was explored. It can be readily observed that maximum attainable load was the same (up to 11 bar NMEP) for compression ratios of 11, 11.75 and 12.5 albeit with different efficiencies. Using CR = 14 allowed for further increase of the upper load limit to 12 bar NMEP. The reasons behind these benefits are associated with intake, exhaust conditions and dilution levels and are going to be addressed in the following. The switchable NVO/PVO valve strategy was exploited by using NVO for low load engine operation and PVO for medium and high load operation as shown previously. At low loads, residual gas trapping was necessary

since the intake pressure and temperature supplied from the turbocharger (supercharger was bypassed) were low and insufficient for ignition. When intake pressure and temperature were sufficient for ignition, the valve events were switched to PVO which offered reduced pumping work, higher dilution levels and lower cylinder temperatures. The IVC temperature requirement for ignition was reduced as compression ratio increased. This requirement had a direct impact on the valve strategy, since at lower compression ratios there was increased need for residual gas trapping and thus NVO use. In order to satisfy that requirement and seek optimum efficiency across the load range, the NVO/PVO switching point had to be moved higher in the load range as compression ratio was reduced.

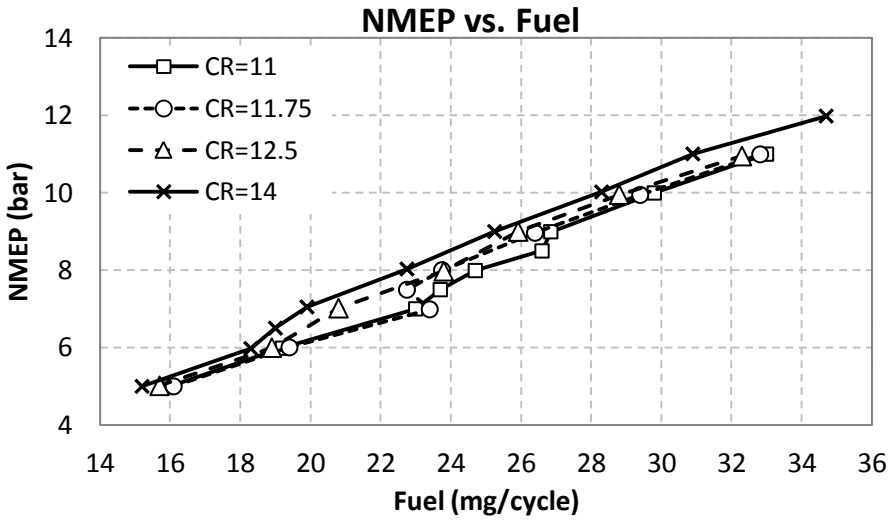

Figure 4.39 – Load range for a two-stage boosted HCCI engine using NVO/PVO at four compression ratio levels

Figure 4.40 shows BSFC as a function of BMEP and one can see that changing compression ratio had a pronounced effect on engine efficiency. Studies from the literature have shown that high load HCCI efficiency is comparable to diesel engines [9]. The highest compression ratio (14) led to the highest improvements in efficiency at medium and high loads. The BSFC vs. BMEP curves exhibited certain sudden changes

from point to point which were caused by engaging the supercharger and by NVO/PVO switching as load increased. The combination of high intake pressures for high dilution levels, PVO valve events for low pumping work and compression ratio of 14 for high thermal efficiency, managed to bring BSFC close to the 200 g/kWh mark. That level of efficiency represents a considerable improvement compared to what has been shown so far and it signifies the importance of compression ratio, boosting system and valve strategy synergies for high pressure lean burn engines. The maximum indicated efficiency observed was 44.5 % and it was achieved with CR = 14 at 9 bar NMEP.

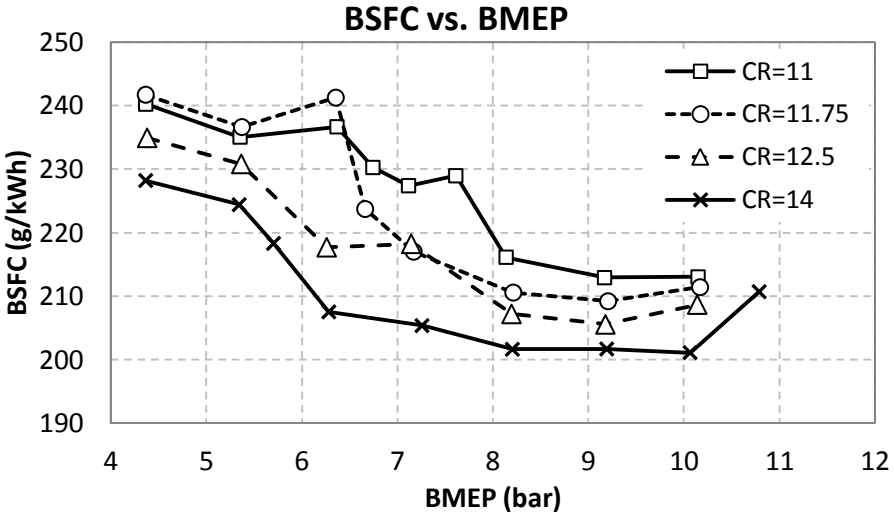

Figure 4.40 – Specific fuel consumption for a two-stage boosted HCCI engine using NVO/PVO at four compression ratio levels

Figure 4.41 and Figure 4.42 show the variation of intake and exhaust pressures with load for all four compression ratio settings. It is interesting to note that as compression ratio increased, intake pressure at medium and high loads decreased. The same behavior was observed for exhaust pressure as well and it can be explained by considering expansion ratio and intake pressure requirements. Expansion ratio increased with compression ratio resulting in lower exhaust energy available for the turbine. Lower energy directed to the turbine meant that there was lower boost available on the intake

side. The second reason behind the intake pressure behavior was related to supercharger operation. The supercharger gear ratio was adjusted so that intake pressure was appropriate for every load level approached. As compression ratio increased there was reduced need for intake pressure and temperature for ignition. Therefore, the supercharger was used less as compression ratio increased. Less use of the supercharger led to reduced intake pressure but that effect was outweighed by increased compression in the cylinder and improved mechanical efficiency. Exhaust pressure was affected by one more parameter of the system; the variable turbine geometry. Since intake pressure became less critical as compression ratio increased, the turbine rack could be opened more and backpressure could be reduced. The combination of low supercharger use, high compression in the cylinder and relatively open turbine position resulted in very good brake efficiency at medium and high loads. The important trade-off encountered in this engine was associated with intake air compression. By raising the compression ratio, one can take advantage of the thermodynamic benefits on efficiency, but at the same time adjust the boosting system in such a way that gas exchange efficiency is improved as well. It should be noted that pumping work was significantly reduced when NVO was switched to PVO, since there was no recompression event in the cycle and larger lifts reduced throttling losses across the valves. As shown previously, NVO/PVO switching occurred at lower loads as compression ratio increased and this explained the sharp changes of intake and exhaust pressure trends.

The benefits of PVO operation on pumping work are evident in Figure 4.43 which shows PMEP as a function of load. For all compression ratio settings PMEP increased at first, since operation at low to medium loads relied on NVO. After the point where NVO/PVO switching occurred – which happened earlier as CR increased – PMEP was reduced considerably. The reader may observe that PMEP was roughly constant from the switching point and above. Increased mass flow rates with load would lead one to expect increased PMEP as well, but use of the variable geometry turbine allowed good

backpressure control and resulted in pumping work benefits. Turbine rack was opened more as load and compression ratio increased since intake pressure requirements from the compressor did not change.

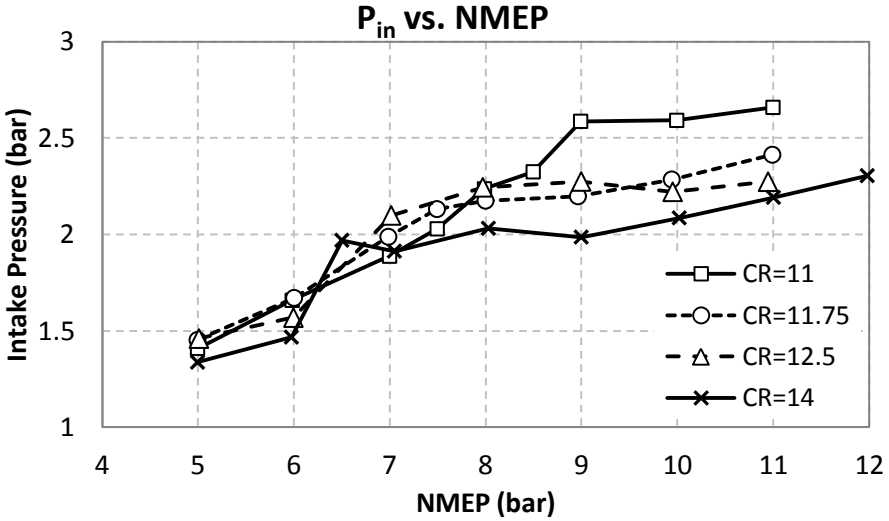

Figure 4.41 – Intake pressure for a two-stage boosted HCCI engine using NVO/PVO at four compression ratio levels

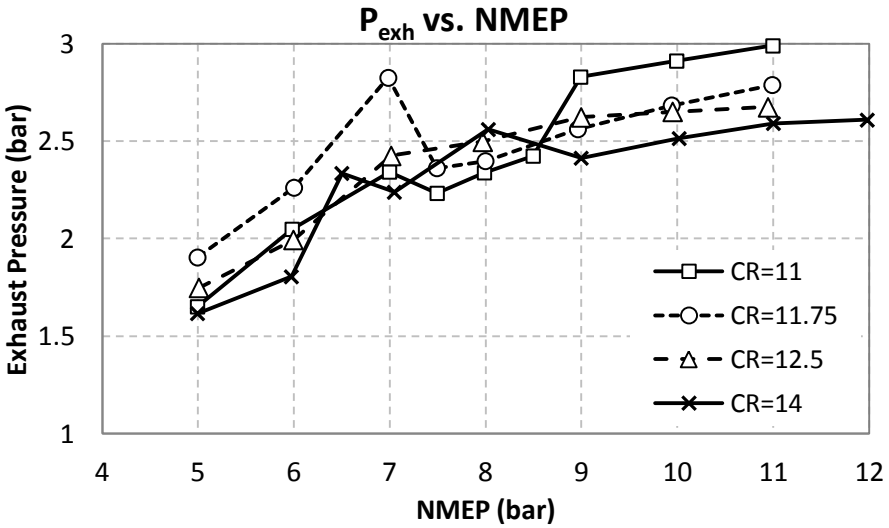

Figure 4.42 – Exhaust pressure for a two-stage boosted HCCI engine using NVO/PVO at four compression ratio levels

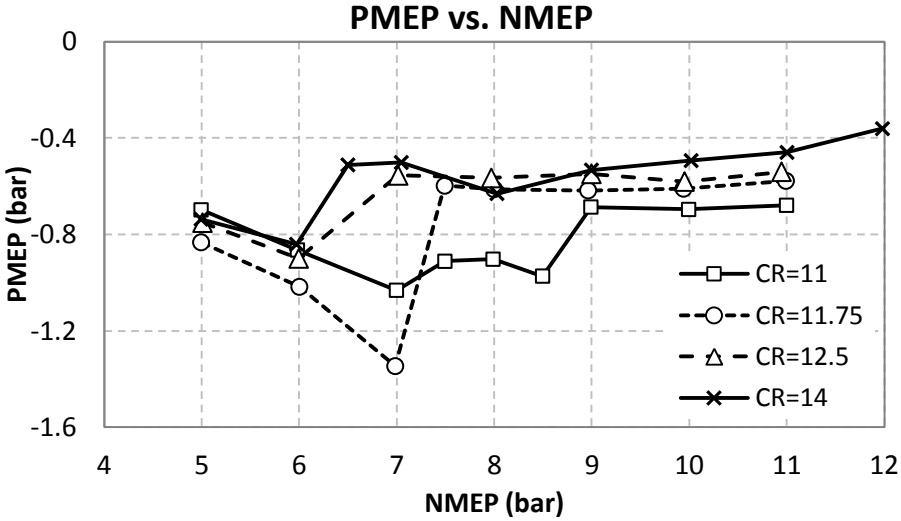

Figure 4.43 – PMEP for a two-stage boosted HCCI engine using NVO/PVO at four compression ratio levels

The strategy that allowed high load HCCI operation for both engines utilized hot intake air as described in detail in the previous sections. Figure 4.44 shows intake temperature as a function of load for the four compression ratio levels. Intake temperature increased with load since compression from the boosting system became more vigorous and it helped to reduce dependence on residual gas for ignition. As expected, the engine exhibited the need for higher intake temperature when compression ratio was set to the lowest setting of 11. There was also increased need for hot intake air when CR was 14 and NVO was switched to PVO at 6.5 bar NMEP. At the two highest load points for CR = 14, intake temperature had to be reduced though; combined heating from the intake and from piston compression was more than needed thus resulting in early ignition and ringing phenomena if not reduced. Overall, the hot intake air operating strategy proved to be beneficial for high load HCCI regardless of compression ratio level. Differences in compression ratio required shifting of the cam switching point but did not affect the overall operating approach.

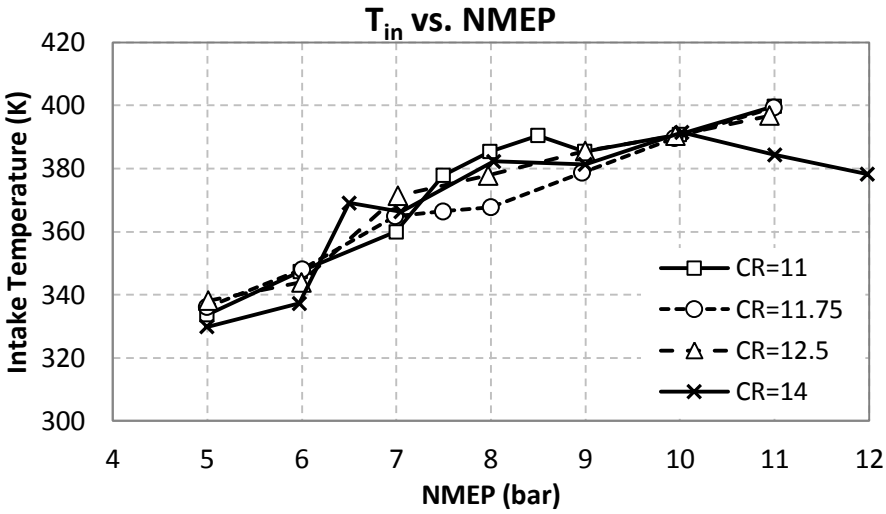

Figure 4.44 – Intake temperature for a two-stage boosted HCCI engine using NVO/PVO at four compression ratio levels

Cam switching is displayed in Figure 4.45 which shows NVO as a function of load. It should be noted that PVO is shown as negative NVO in this plot. Starting from CR = 11, one can see that NVO was necessary until 8.5 bar NMEP where cam switching occurred. The switching point occurred at 7 bar NMEP for CR = 11.75, and at 6 bar NMEP for CR = 12.5 and 14. NVO ranged between 60 and 130 CAD and PVO ranged between 30 and 120 CAD. These broad ranges indicate that a flexible cam phasing system would be necessary for this kind of application. Figure 4.46 displays residual gas fraction variation with load. It is interesting to note that after every cam switching point RGF in the cylinder increased. That was a result of mixture preparation requirements for ignition control. When NVO was replaced by PVO, residual gas temperature was lower. Residual gases were not trapped in the cylinder through the valve events, but expelled to the exhaust manifold and then reinducted into the cylinder by adverse pressure gradient. Heat transfer to the exhaust valves, ports and manifold and mixing with the fresh incoming charge acted to reduce the temperature of residual gas when PVO was used. Reduced temperature meant that RGF had to be increased in order to accomplish charge heating for ignition. As load increased further, intake pressure and temperature increased

as well thus necessitating less PVO and RGF. As noted earlier, higher compression ratios allowed lower RGF and this dependence can be clearly observed at high loads in Figure 4.46. For 11 bar NMEP, RGF was 18.5 % for CR = 11, but only 8.5 % for CR = 12.5.

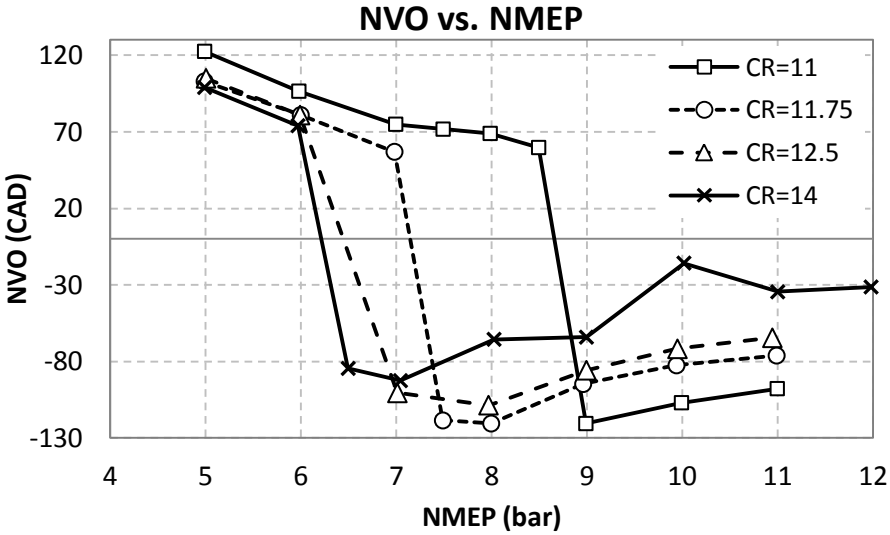

Figure 4.45 – Negative valve overlap for a two-stage boosted HCCI engine using NVO/PVO at four compression ratio levels

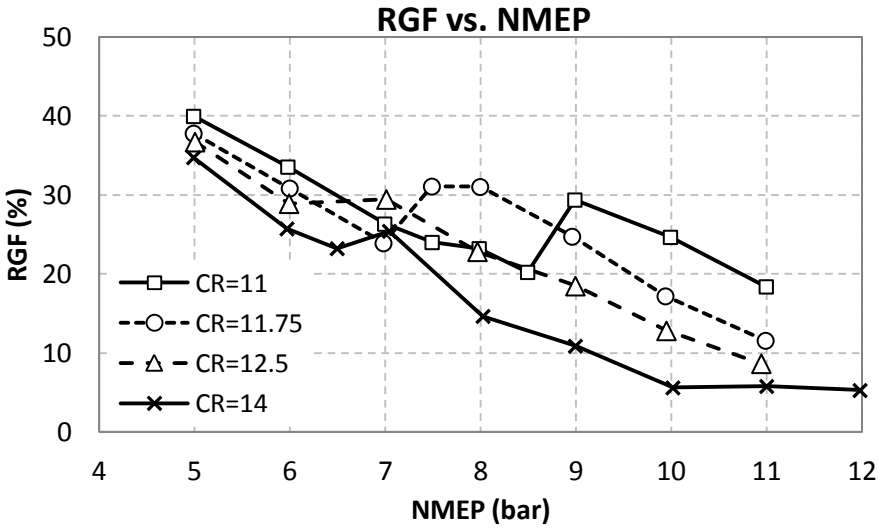

Figure 4.46 – Residual gas fraction for a two-stage boosted HCCI engine using NVO/PVO at four compression ratio levels

Figure 4.47 shows equivalence ratio (Φ) as a function of load for all compression ratio levels. Equivalence ratio was affected by air mass, residual gas mass and fueling rate; the combination of these parameters acted to generally reduce Φ as load increased. Reducing Φ was the essential mechanism behind high load HCCI operation, since it directly decreased pressure rise rates and ringing propensity. RGF use that was shown above was responsible for the discrepancies between different compression ratio levels. Lower compression ratio necessitated more residual gas trapping for ignition control thus increasing equivalence ratio levels. It is interesting to note that engaging the supercharger led to significant reduction of Φ, which is more evident in the CR = 12.5 and CR = 14 cases. The additional air mass provided by supercharger operation resulted directly in leaner mixtures and reduced pressure rise rates during combustion. After the NVO/PVO switching point, equivalence ratio was held roughly constant with the exception of CR = 14, where Φ followed an increasing trend from medium to maximum load.

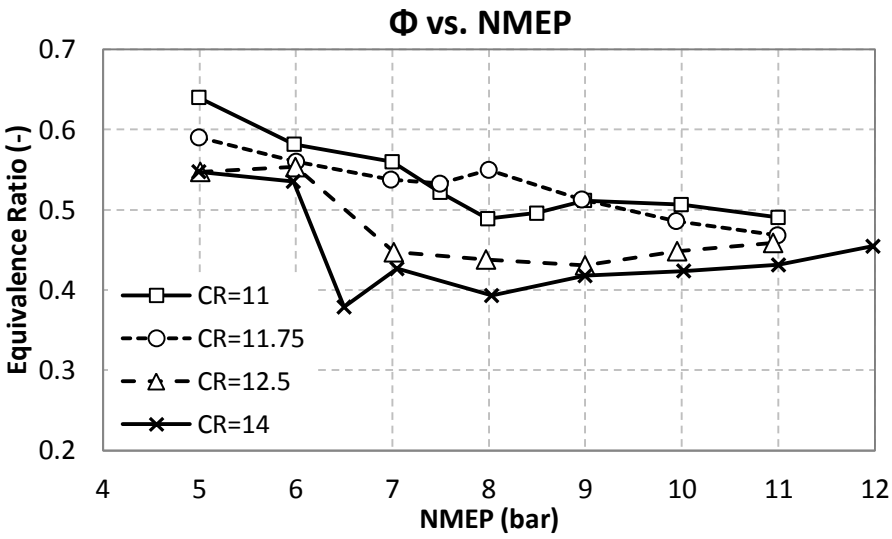

Figure 4.47 – Equivalence ratio for a two-stage boosted HCCI engine using NVO/PVO at four compression ratio levels

As load increased, combustion had to be phased later in the cycle in order to accommodate increased pressure rise rates. The combination of later ignition and lower equivalence ratios acted to prolong burn duration resulting in later CA50 values at high load. Figure 4.48 displays CA50 as a function of load for all compression ratio settings. For every CR case, CA50 followed an increasing trend at first when NVO was used. After NVO was switched to PVO, CA50 decreased in all cases. The effect of PVO on lowering cylinder temperatures allowed for earlier combustion phasing compared to NVO points without hitting ringing constraints. Therefore, using PVO resulted in thermal efficiency benefits from earlier combustion phasing; it also resulted in gas exchange efficiency benefits from eliminating the recompression loop and reducing throttling losses though the valves. It is interesting to note that at the highest compression ratio, CA50 spanned that widest range of values. On the lower load side, high compression from the piston combined with NVO meant that ignition was possible earlier that the rest of the cases. On the upper load side, CR = 14 allowed for 1 bar increase (12 bar NMEP maximum) and that was achieved by further retardation of the combustion event.

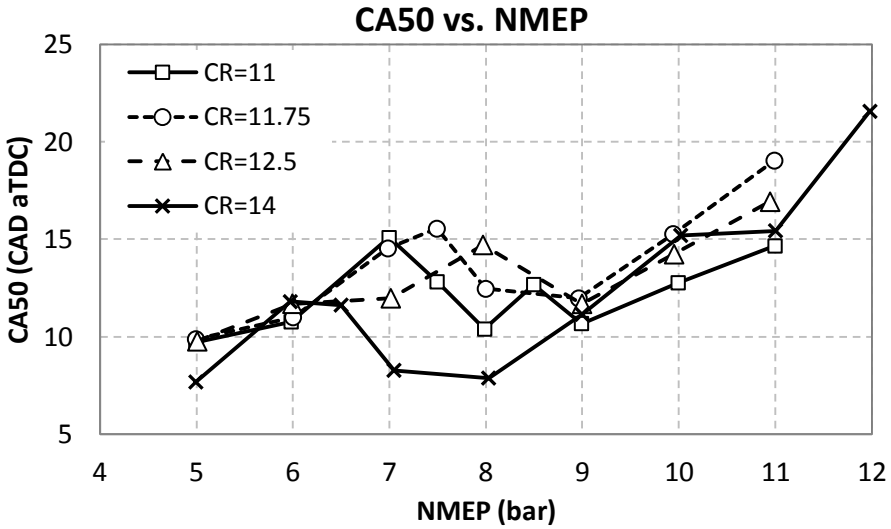

Figure 4.48 – CA50 for a two-stage boosted HCCI engine using NVO/PVO at four compression ratio levels

The effects of compression ratio, boosting and NVO/PVO switching on equivalence ratio and cylinder temperature that were discussed so far can be also portrayed through the ringing intensity variation shown in Figure 4.49. For all cases simulated, combustion was phased as close to TDC as possible in order to maximize thermal efficiency, provided that the R.I. limits were not exceeded. Operation with NVO at lower loads resulted in high R.I. despite the fact that CA50 was kept relatively late at these points. That behavior was due to elevated cylinder temperatures resulting from hot residual gases trapped during the recompression event. For every compression ratio level, a drop in R.I. was observed after NVO/PVO switching occurred. As explained earlier, PVO resulted in reduced cylinder temperatures and leaner mixtures; these two features where key enablers of high load HCCI since they significantly reduced PRR during combustion. As load increased to medium and high levels, R.I. was again increased, quickly reaching or exceeding the 6 MW/m^2 limit. It is widely accepted that cylinder temperature is the governing factor of NO_x emissions formation. For all boosted HCCI cases that were simulated, cylinder temperature was below the NO_x formation threshold, resulting in minimal NO_x emissions across the load range. Figure 4.50 shows NO_x emissions index ($EINO_x$) as a function of load. As seen for all boosted HCCI simulations, $EINO_x$ values were always well below the US 2010 regulations.

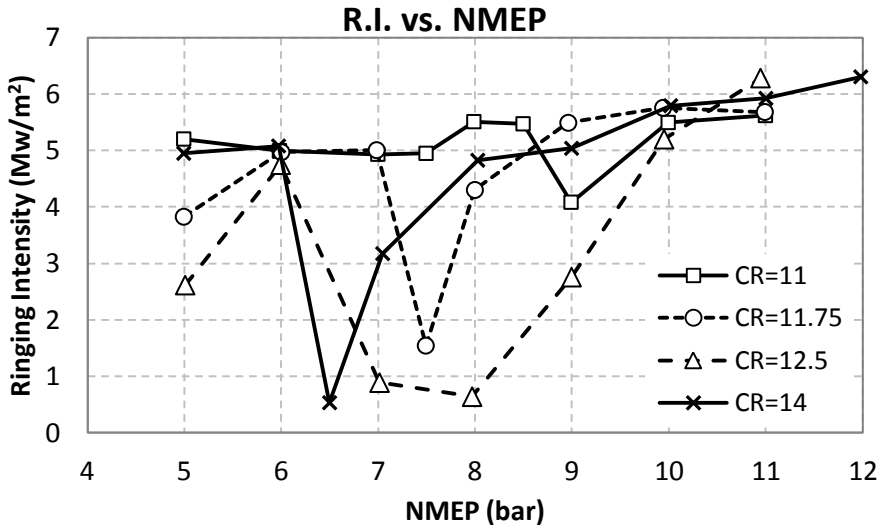

Figure 4.49 – Ringing intensity for a two-stage boosted HCCI engine using NVO/PVO at four compression ratio levels

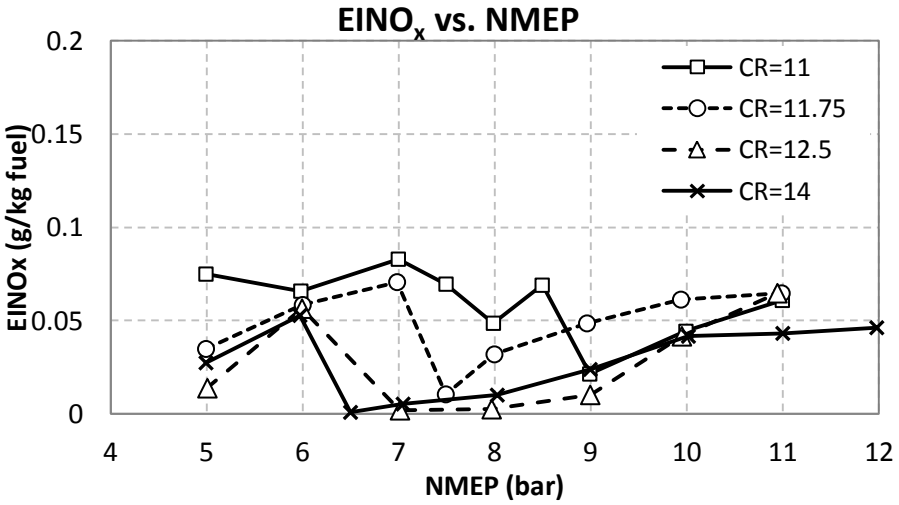

Figure 4.50 – NOx emissions index for a two-stage boosted HCCI engine using NVO/PVO at four compression ratio levels

Peak cylinder pressure is one of the major concerns in boosted HCCI operation and it is directly related to compression ratio. Figure 4.51 shows the variation of peak cylinder pressure with load for all CR levels. It appears that CR = 14 was the only setting that resulted in peak cylinder pressures that would challenge an SI engine structure. At medium and high loads PCP was between 100 and 110 bar which were close to the limit of what SI engines can tolerate. Therefore, boosted HCCI operation at CR = 14 would

require a slightly more robust cylinder structure compared to currently available SI engines.

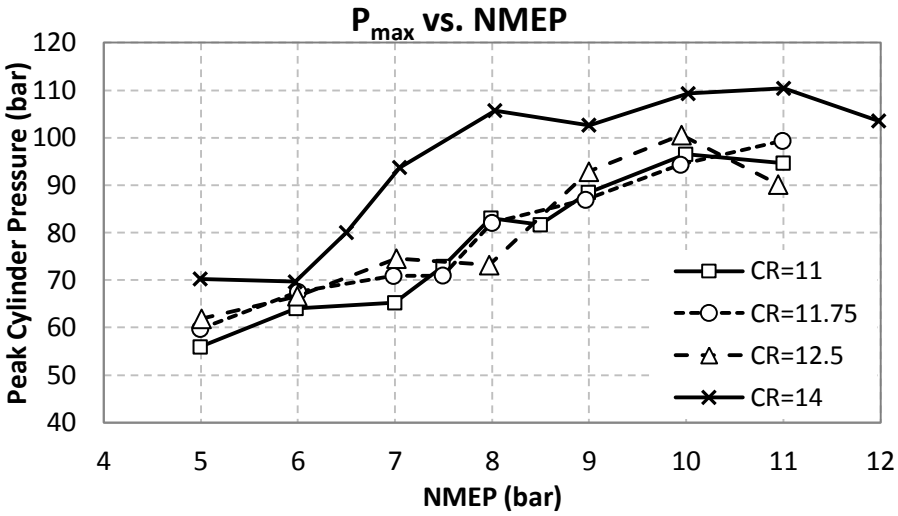

Figure 4.51 – Peak cylinder pressure for a two-stage boosted HCCI engine using NVO/PVO at four compression ratio levels

As highlighted throughout this dissertation, boosting performance is crucial for creating the in-cylinder conditions required for high load HCCI operation. The key factor is intake pressure which is inherently dependent on exhaust conditions and turbocharger performance. Figure 4.52, Figure 4.53 and Figure 4.54 show performance maps for the compressor, turbine and supercharger respectively. On Figure 4.52 three lines are superimposed on the compressor map. They represent three compression ratio levels – CR = 11, 11.75 and 12.5 – at the three highest load points, 9, 10 and 11 bar NMEP. All nine operating points are located on high efficiency regions of the map, which confirmed that the compressor was well suited to the engine mass flow rate characteristics at 2000 rpm and high load. However, as compressor ratio increased, the operating points moved to lower pressure ratios on the map. That trend can be explained by the increasing

expansion ratio and resulting reduced exhaust energy that was directed to the turbine and converted to compressor work.

Figure 4.53 shows the VGT performance maps for CR = 11.75 and for the three highest load points, 9, 10 and 11 bar NMEP. The turbine rack position is also showed and displays how this device can be manipulated in order to achieve the desired exhaust conditions. At 9 bar NMEP the rack is 10 % open, but at 11 bar NMEP is 47 % open. The variability of the turbine allowed backpressure to be reduced with associated pumping work benefits, as shown previously.

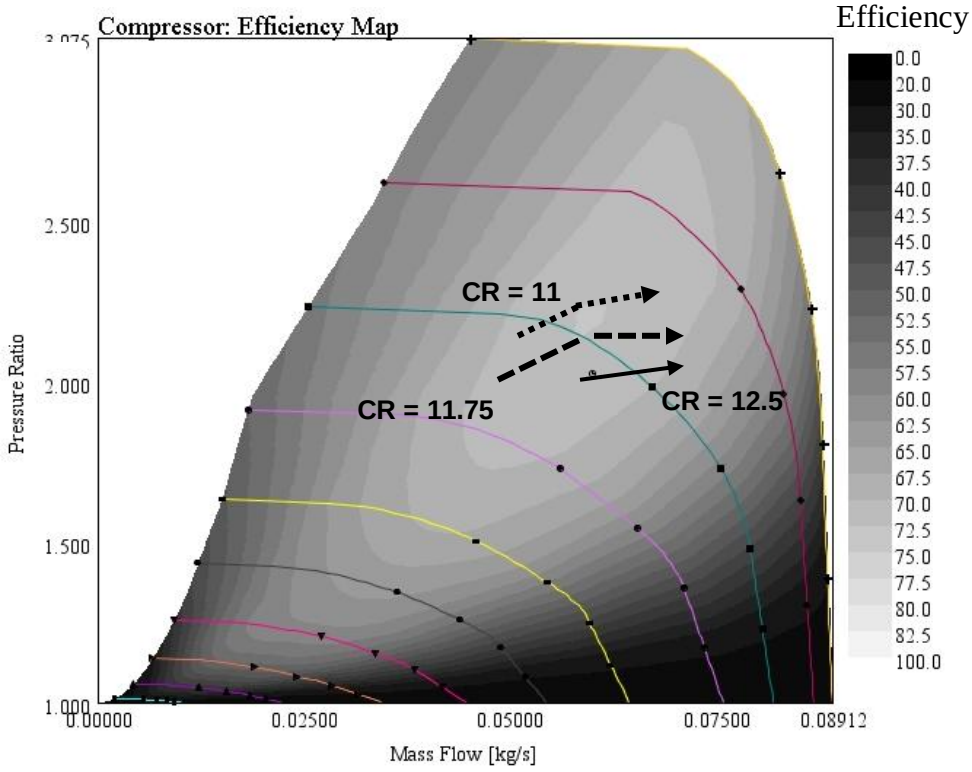

Figure 4.52 – Compressor performance map for a two-stage boosted HCCI engine using NVO/PVO at three compression ratio levels

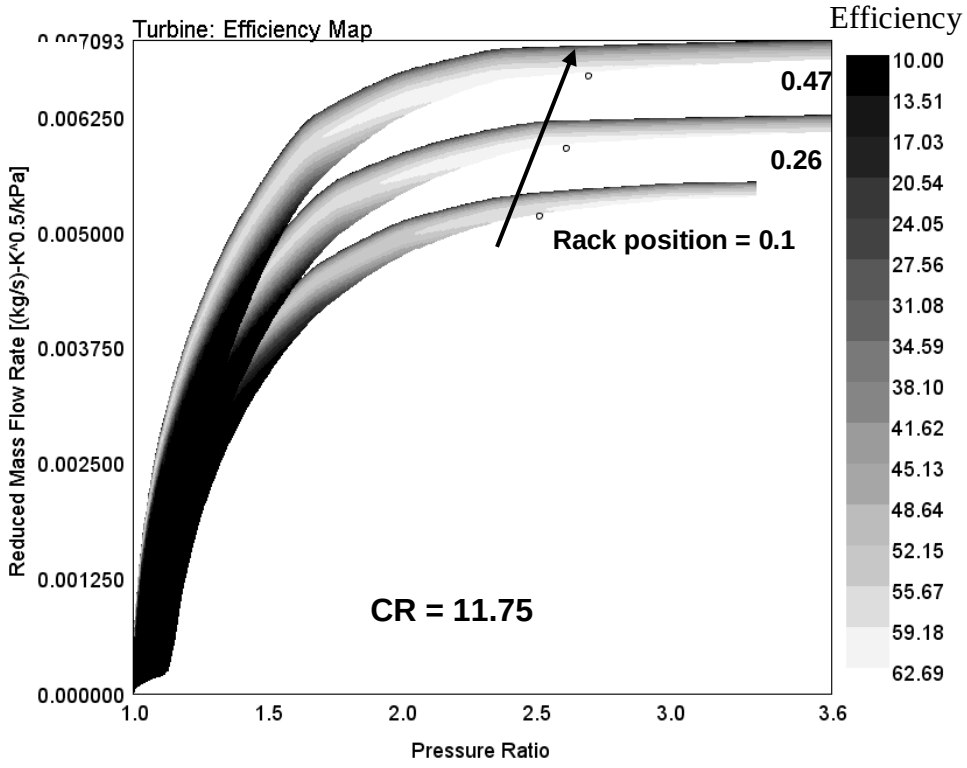

Figure 4.53 – Turbine performance map for a two-stage boosted HCCI engine using NVO/PVO at compression ratio of 11.75

Finally, the supercharger performance map is shown in Figure 4.54. Even though the contribution of supercharging was essential for delivering the desired intake pressure, one can see that the device did not operate at its optimum pressure ratio and efficiency levels. The reason was the adjustable gear ratio which was chosen in order to provide moderate additional pressure ratio while requiring minimal mechanical work. Both of the boosting devices used with this engine are currently available hardware and not specifically designed for boosted HCCI operation. Advancements in turbocharging and supercharging technology can certainly help increase intake pressure levels and high load potential with improved performance characteristics and overall system efficiency.

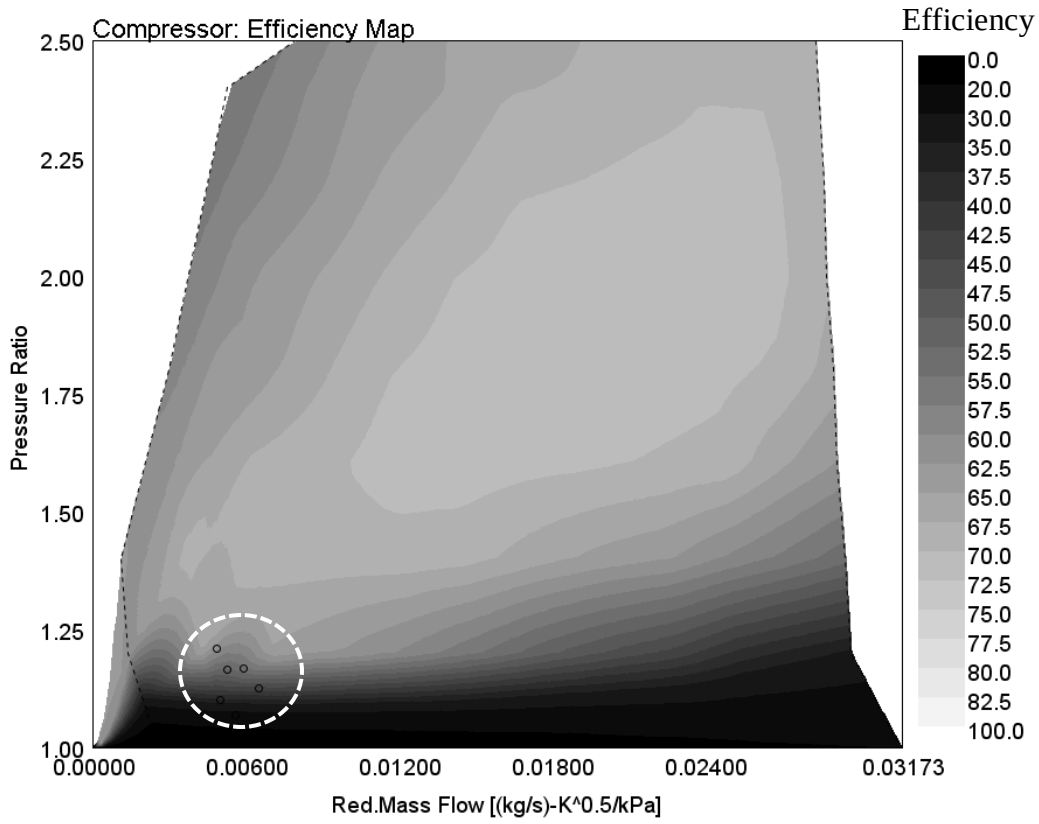

Figure 4.54 – Supercharger performance map for a two-stage boosted HCCI engine using NVO/PVO at compression ratio of 11.75

The previous sections displayed boosted HCCI simulations and confirmed the hypothesis that hot intake air can be used to aid boosted HCCI operation in terms of attainable load and efficiency. It was also demonstrated that NVO strategies are not essential for boosted HCCI operation, provided that charge heating can be accomplished externally to the cylinder. In fact, it was shown than regular SI high-lift cams can be used and resulted in a multitude of benefits in thermal and gas exchange efficiencies. The current section made use of all the previous findings in order to investigate the hypothesis that operation with hot intake air can alleviate the need for elevated compression ratio, thus bringing HCCI engines closer to currently available SI engines. The results supported this hypothesis and showed that high load boosted HCCI operation can be achieved with compression ratios as low as 11. However, efficiency levels decreased at lower compression ratios which reduced the benefits of HCCI combustion. In addition,

reduced compression ratios increased IVC temperature requirements which translated to either increased need for boosting performance or use of NVO strategies. It was shown that when using a switchable NVO/PVO valve strategy, the cam switching point moved to higher loads as CR is reduced. Therefore, benefits from reduced pumping work and cylinder temperatures were limited. Overall, even though the hypothesis was confirmed, it appears that in order to enjoy the efficiency benefits of HCCI combustion, compression ratio needed to be set at 12 or above.

The studies presented so far examined the required interactions between combustion and engine subsystems for HPLB engines and reached interesting and meaningful conclusions. The following section will present the last study linking combustion and system level aspects, which is the use of external EGR. The hypothesis that external EGR can be used to improve engine efficiency will be examined and discussed.

4.5 Effect of Exhaust Gas Recirculation on Boosted HCCI Operation

Exhaust Gas Recirculation (EGR) is a widely established technique in modern diesel engines which is used to introduce inert gases of high heat capacity into the combustion chamber thus reducing peak cylinder temperatures and NO_x formation. It has also been used in SI engines but not at the same extent. In the last decade, the engine research community has identified EGR use as an enabler of HCCI combustion. Several research groups have employed EGR to control ignition timing and burn rates and have shown that it can be used to extend the upper load limit of HCCI engines [1, 2, 4 and 13]. As discussed in Chapter 3, a recent experimental study by Dec et al. showed that inert gases can be successfully used to increase ignition delay times in boosted HCCI engines thus lowering pressure rise rates during heat release [1]. In fact, the authors showed that EGR was essential in their effort to increase attainable load. Analyzing the effects of

external EGR use for high load HCCI combustion is an active research topic. Several research groups have claimed that presence of EGR in the cylinder does not directly affect burn rates; however, EGR introduces stratification in the cylinder which in turn affects the burn rates.

Despite the fact that EGR is considered as an HCCI combustion enabler, the single-cylinder experimental studies presented in the literature have focused on combustion often neglecting overall engine operation with EGR. The current section will attempt to investigate boosted HCCI operation when making use of external EGR and focus on performance and system level effects. It should be noted that the combustion model was not able to capture thermal or compositional stratification effects on burn rates so this modeling study could not have focused on the combustion event. However, the model was very good at capturing the temperature effect and providing boundary conditions needed for engine simulations. Therefore, this section will examine the hypothesis that external EGR can be used to control heat release rates and increase attainable load. The engine used was the single turbocharged HCCI engine operating with NVO on compression ratio of 12.5 that was presented in the beginning of this chapter. The fact that NVO operation ensured high temperatures at IVC rendered this engine system appropriate for studying the effects of EGR. EGR was introduced via a low-pressure loop that extracted exhaust gas downstream of the turbine and introduced it upstream of the compressor. Consequently, exhaust gas ran through the compressor in the same way as in a modern diesel engine.

The following figures will present performance and combustion variables for this engine when operating with and without external EGR. The amount of EGR was regulated based on the need to retard combustion phasing and reduced PRR. However, air dilution levels increased with load and boost so EGR levels reduced as load increased. That trend was the opposite of what has been observed in experimental studies where generally EGR is increased with load.

Figure 4.55 shows the engine load range with and without EGR use. One can observe that attainable load was roughly the same for both cases. In fact, EGR use led to lower maximum load for a few reasons that will be discussed in the following. The primary reason was increased intake temperature when EGR was employed that necessitated later combustion phasing thus reducing effective expansion ratio.

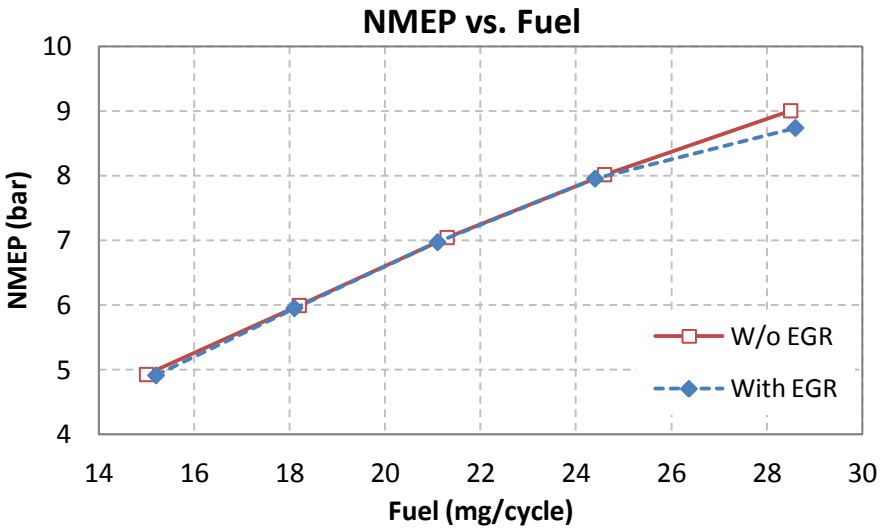

Figure 4.55 – Load range for a turbocharged HCCI engine using NVO with and without EGR

Figure 4.56 shows brake specific fuel consumption as a function of BMEP. Addition of EGR resulted in inferior efficiency across the load range which can be attributed to the lower ratio of specific heats. It should be noted that even without EGR, diluents were combinations of intake air and residual gas trapped during recompression. The addition of EGR increased the amount of exhaust gas in the cylinder and at the same increased intake temperature as will be seen in the following. Both of these factors acted to reduce the ratio of specific heats thus reducing thermal efficiency. The superiority of air dilution for efficiency was also identified by Lavoie et al. in their thermodynamic sweet spot analysis [14]. The authors claimed that air dilution was superior for efficiency but EGR dilution was superior for NO_x formation suppression in boosted HCCI engines,

which was confirmed by the forward calculations in multi-cylinder models presented here.

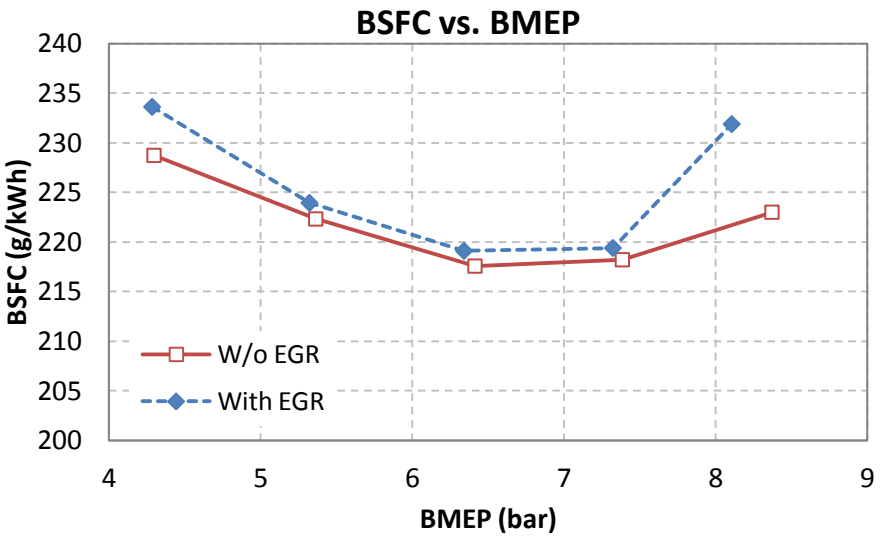

Figure 4.56 – Brake specific fuel consumption for a turbocharged HCCI engine using NVO with and without EGR

Figure 4.57 and Figure 4.58 show intake and exhaust pressures as function of load respectively. The hot intake air operating strategy that was analyzed in the previous section and found to be highly beneficial for boosted HCCI operation was implemented in this study as well. Figure 4.57 shows that in order to increase attainable load by a factor of two, intake pressure had to be increased by a similar factor. The reasons behind the importance of elevated intake pressure have been extensively analyzed in this chapter and are associated with increased dilution levels for controlling pressure rise rates. Low-pressure driven EGR meant that exhaust gas ran through the compressor but that did not seem to affect its pressure ratio. In the same way, EGR use did not seem to affect exhaust conditions and turbine performance either. Therefore, turbocharger operation was similar when EGR was used which resulted in similar intake and exhaust pressures with the case of no EGR.

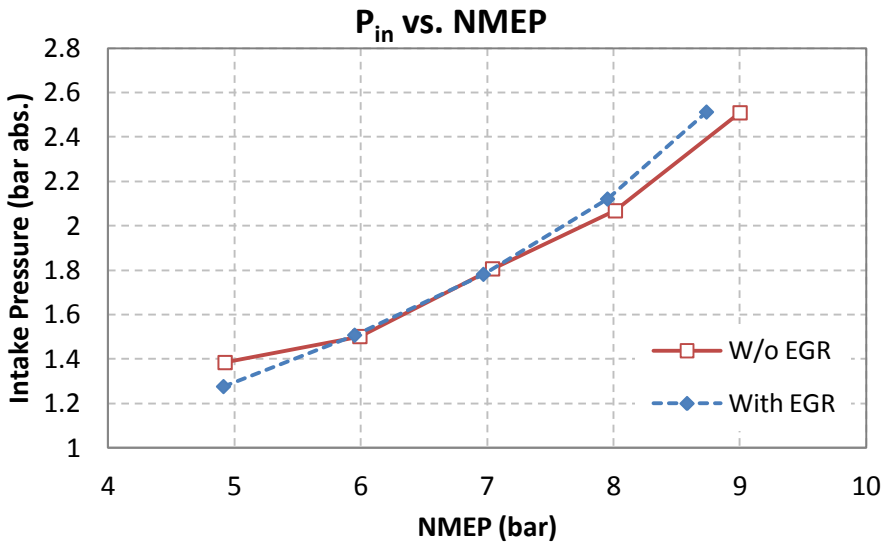

Figure 4.57 – Intake pressure for a turbocharged HCCI engine using NVO with and without EGR

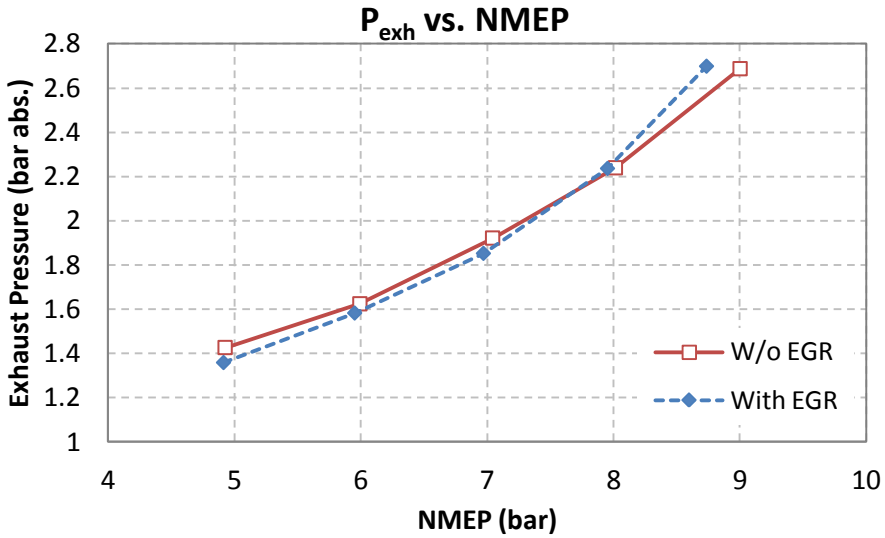

Figure 4.58 – Exhaust pressure for a turbocharged HCCI engine using NVO with and without EGR

A key parameter for implementing the hot intake air strategy was intake temperature and it is displayed in Figure 4.59 as a function of load. EGR use meant that hot exhaust gas was introduced upstream of the compressor; therefore, compressor outlet temperature was higher when exhaust gas was recirculated. Higher intake temperature resulted in lower NVO as seen previously and more exhaust gas directed to the turbine.

The additional exhaust gas diluent present at the intake side could potentially replace some of the residual gas trapped during recompression thus allowing further reduction in NVO and pumping work.

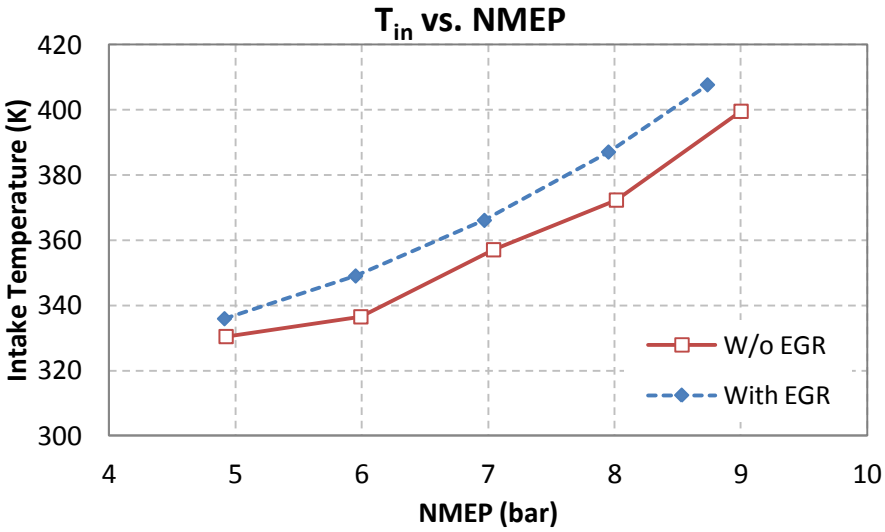

Figure 4.59 – Intake temperature for a turbocharged HCCI engine using NVO with and without EGR

However, that was not verified by the simulation since pumping work at high load seemed to be slightly worse when EGR was employed. Figure 4.60 shows PMEP as a function of load. PMEP was equal to that of the case without EGR except from the highest load case. The reason can be identified at the slightly increased backpressure, since NVO was actually lower for the EGR simulations. NVO is shown in Figure 4.61 and it can be readily observed that increased intake temperature and EGR alleviated the need for residual gas. As a result, NVO could be reduced across the load range. The resulting total residual gas fraction is shown in Figure 4.62 along with EGR fraction as a function of load. Total residual gas was higher in the case of EGR use which indicated that the amount of external EGR could not replace the same amount of internal residual gas. The reason was that the temperatures of the two were very different. Therefore, when external EGR was employed, the engine operated at higher levels of residual gas

and at higher intake temperature. Both of these factors had an accelerating effect on ignition kinetics which lowered ignition delay times. However, they were both compensated by the presence of external EGR.

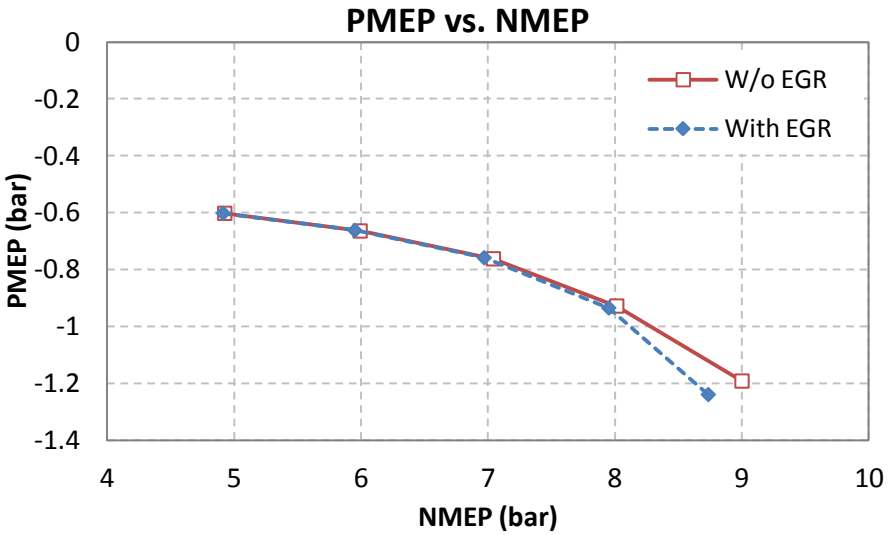

Figure 4.60 – PMEP for a turbocharged HCCI engine using NVO with and without EGR

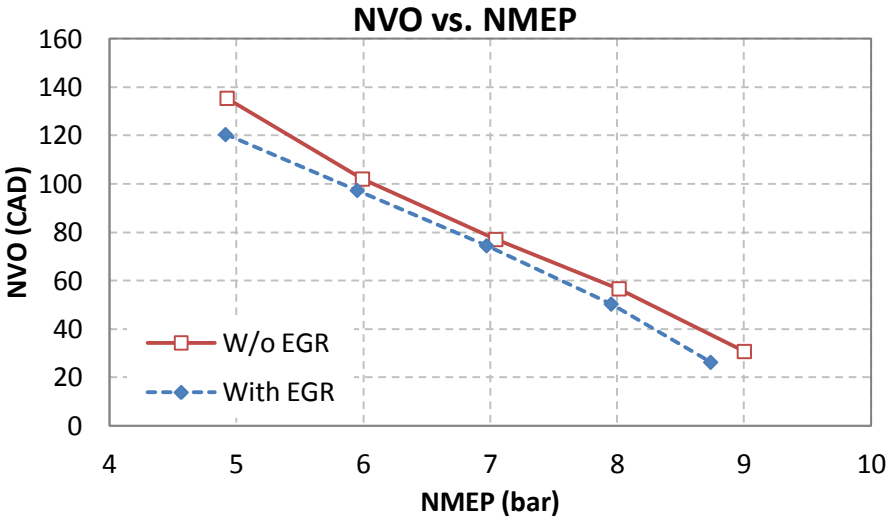

Figure 4.61 – Negative valve overlap for a turbocharged HCCI engine using NVO with and without EGR

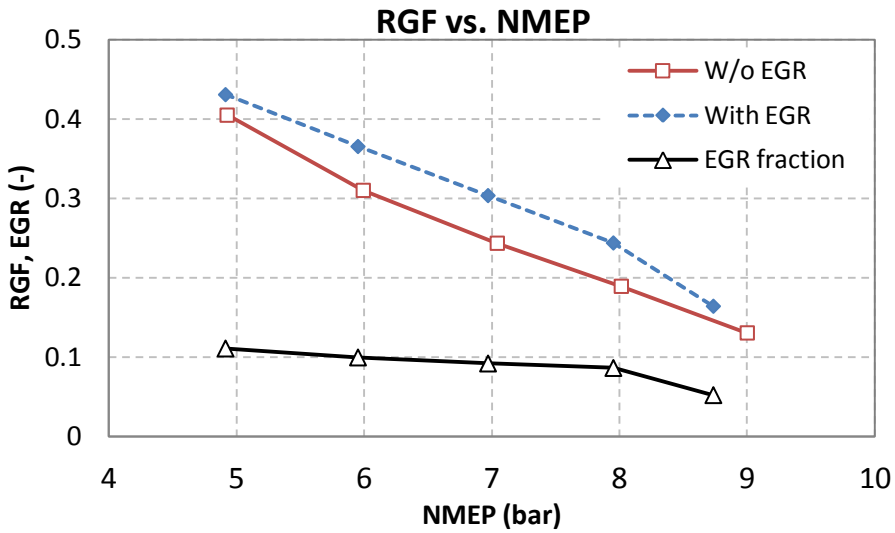

Figure 4.62 – EGR and total residual gas fraction for a turbocharged HCCI engine using NVO with and without EGR

Increased levels of residual gas in the cylinder resulted in higher equivalence ratios as seen in Figure 4.63. The difference was more pronounced at low loads since the amount of external EGR introduced to the cylinder reduced with load. Utilizing external EGR led to different mixture composition and temperature. Some of the residual gas in the charge was replaced by external EGR of lower temperature but the intake air was of higher temperature as seen previously. The combination of these factors resulted in higher CA50 values when EGR was used especially at the lower and upper end of the load range. The fact that combustion was phased later in the cycle when EGR was used indicated that the simulation was primarily affected by increased intake temperatures. The heating capacity effect on decelerating ignition kinetics seemed to be secondary. The combinations of all these factors revealed that although external EGR can be a combustion enabler, it might not necessarily be as desirable from a system level standpoint.

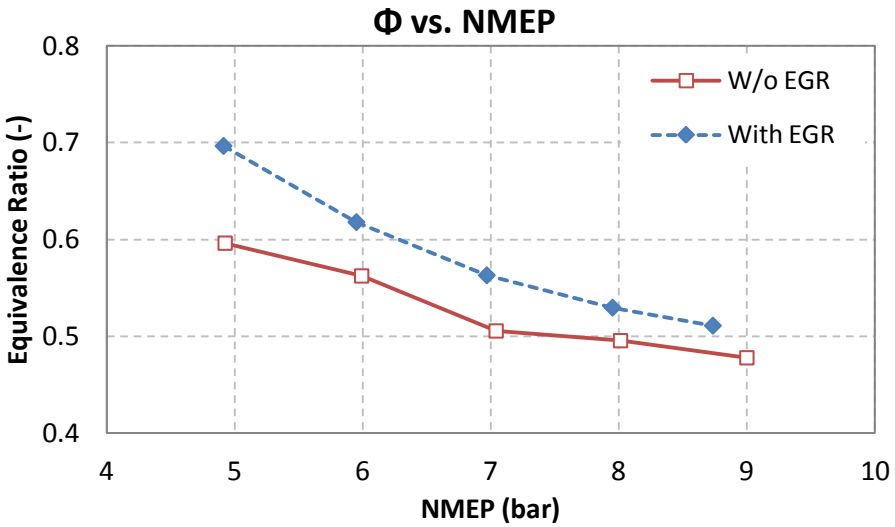

Figure 4.63 – Equivalence ratio for a turbocharged HCCI engine using NVO with and without EGR

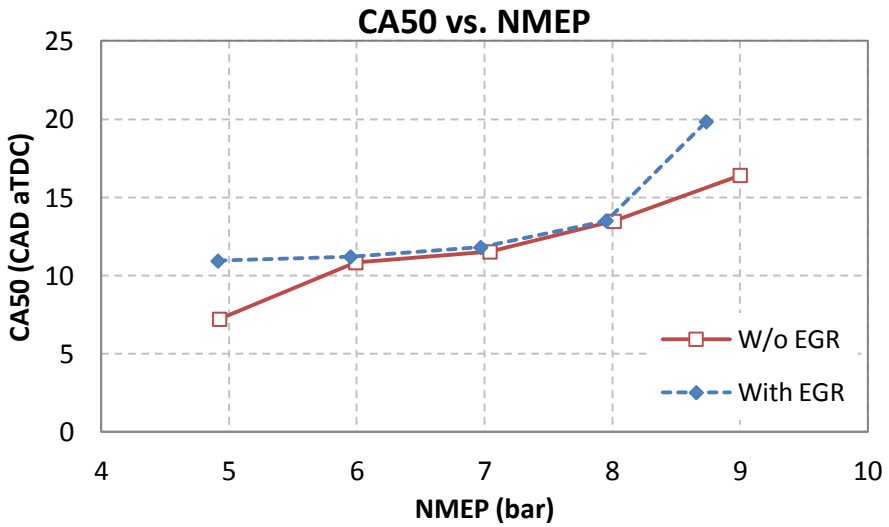

Figure 4.64 – CA50 for a turbocharged HCCI engine using NVO with and without EGR

Figure 4.65 and Figure 4.66 show ringing intensity and NO_x emissions index as functions of load respectively. The simulation was run in such a way as to ensure maximum engine efficiency for every operating point. Combustion was phased as early in the cycle as possible, resulting in operation close to the ringing intensity limit as shown in Figure 4.65. External EGR did not affect the ability to phase combustion earlier since the final level of combustion phasing was done through varying NVO. NO_x emissions

were never a problem in all boosted HCCI simulations that have been presented in this dissertation and that was the case here as well. NO_x emissions were comparable to those observed without EGR use. The thermal effect of EGR certainly acts to lower cylinder temperatures and NO_x formation, but dilution levels in these simulations were always more than enough to ensure cylinder temperatures below the NO_x formation threshold.

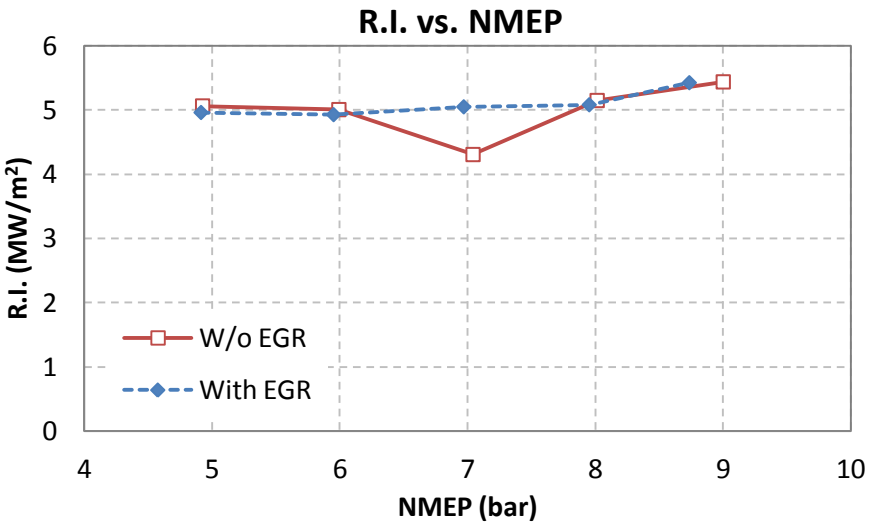

Figure 4.65 – Ringing intensity for a turbocharged HCCI engine using NVO with and without EGR

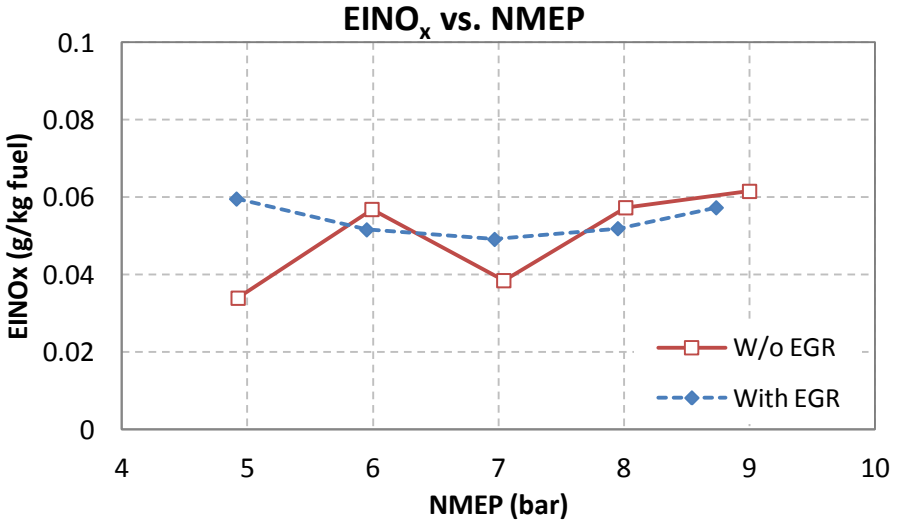

Figure 4.66 – NOx emissions index for a turbocharged HCCI engine using NVO with and without EGR

This section displayed use of external EGR for boosted HCCI operation. Results showed that although EGR is considered as a combustion enabler, it is not necessarily desirable from an engine system point of view. Introducing hot EGR upstream of the compressor resulted in increased intake temperatures that allowed lower NVO and efficient operation. However, higher amount of exhaust gas and higher intake temperatures resulted in reduced γ and thermal efficiency when EGR was used. Overall, the hypothesis that external EGR can be used to control heat release rates and increase attainable load cannot be supported based on the results presented in this section. Experimental studies in the literature have supported this hypothesis, but the system level implications of using EGR may render it unattractive for HPLB engines.

4.6 Summary

This chapter presented multi-cylinder boosted HCCI simulations that aimed at investigating and quantifying the interactions between compression ratio, boosting, VVA and EGR use. By using different VVA strategies and boosting systems, it was demonstrated that the combination of elevated pressure and negative valve overlap is not beneficial for high load HCCI operation. Exploiting hot intake air for charge heating within the intake system alleviated the dependence on residual gas and NVO for mixture preparation thus aiding turbocharger performance and engine efficiency. In addition, it was shown that heating the charge at the intake system enabled use of high-lift valve events that formed positive valve overlap and acted to significantly reduce pumping work and cylinder temperatures. The combination of boosting and PVO offered multiple benefits on the thermal and gas exchange efficiencies of the engine. Furthermore, it was found that wide range boosted HCCI operation can be accomplished with compression ratios as low as 11 which bring HPLB engines closer to currently available SI powertrains. However, lowering the compression ratio resulted in increased need of

intake air boosting and heating which places additional emphasis on the development of appropriate boosting systems. The combination of high compression ratio (14), advanced boosting and dual NVO/PVO valve strategies proved to offer HCCI engines efficiency levels comparable to or better than those of diesel engines. Last, external EGR use which is known to be a combustion enabler, proved not to be very beneficial from an engine efficiency point of view. Therefore, when combustion does not require external EGR use it can be avoided in favor of efficient engine operation.

The next chapter will attempt to augment the present thermodynamic analysis by examining HPLB operation from a 2^{nd} law perspective. Availability analysis of boosted HCCI engines will be presented and findings will be discussed.

4.7 References

1. Dec. J. and Yang. Y., "Boosted HCCI for High Power without Engine Knock and Ultra-Low NO_x Emissions using a Conventional Fuel," SAE Paper 2010-01-1086, 2010

2. Stefan Klinkert, personal communication, May 2012

3. Babajimopoulos, A., Challa, V.S.S.P., Lavoie, G.A. and Assanis, D.N., 2009, "Model-Based Assessment of Two Variable Cam Timing Strategies for HCCI Engines: Recompression vs. Rebreathing," ICES2009-76103, Proceedings of the ASME Internal Combustion Engine Division Spring Technical Conference, Milwaukee, WI

4. Manofsky, L., Vavra, J., Assanis, D. and Babajimopoulos, A., "Internal Residual vs. Elevated Intake Temperature: How the Method of Charge Preheating Affects the Phasing Limitations of HCCI Combustion," ICES2012-81127, Proceedings of the ASME Internal Combustion Engine Division Spring Technical Conference, May 6-9, 2012, Torino, Piemonte, Italy

5. Martins M. and Zhao H., 4-Stroke Multi-Cylinder Gasoline Engine with Controlled Auto-Ignition (CAI) Combustion: a comparison between Naturally Aspirated and Turbocharged Operation, SAE paper 2008-36-0305, 2008

6. Johansson, T., Johansson, B., Tunestal, P. and Aulin, H., HCCI Operating Range in a Turbocharged Multi Cylinder Engine with VVT and Spray-Guided DI, SAE paper 2009-01-0494, 2009

7. Mamalis, S., Nair, V., Andruskiewicz, P., Assanis, D., Babajimopoulos, A., Wermuth, N., and Najt, P. M. Comparison of Different Boosting Strategies for Homogeneous Charge Compression Ignition Engines – A Modeling Study, *SAE Int. J. Engines* **3**(1): 296-308, 2010

8. Kulzer, A., Nier, T. and Karrelmeyer, R., A Thermodynamic Study on Boosted HCCI: Experimental Results, SAE Paper 2011-01-0905, 2011

9. Mamalis, S., Babajimopoulos, A., Guralp, O. and Najt, P. M., Optimal Use of Boosting Configurations and Valve Strategies for High Load HCCI – A Modeling Study, SAE paper 2012-01-1101, 2012

10. Christensen M., Johansson B., Amneus P., and Mauss F., Supercharged Homogeneous Charge Compression Ignition, SAE paper 980787, 1998

11. Olsson J., Tunestal P., Haraldsson G., and Johansson B., A Turbo Charged Dual Fuel HCCI Engine, SAE paper 2001-01-1896, 2001

12. Dec. J. E., Yang. Y. and Dronniou, N., Boosted HCCI – Controlling Pressure Rise Rates for Performance Improvements using Partial Fuel Stratification with Conventional Gasoline, SAE paper 2011-01-0897, 2011

13. Saxena, S., Chen, J-Y and Dibble, R., Maximizing Power Output in an Automotive Scale Multi-Cylinder Homogeneous Charge Compression Ignition (HCCI) Engine, SAE paper 2011-01-0907, 2011

14. Assanis, D.N., Lavoie, G. L. and Ortiz-Soto, E., "Thermodynamic Sweet Spot Under Highly Dilute and Boosted Gasoline Engine Conditions", SAE 2011 High Efficiency IC Engines Symposium, April 10-11, 2011, Detroit, MI

CHAPTER 5

AVAILABILITY ANALYSIS OF LTC ENGINES

Chapter 4 presented a thermodynamic analysis of multi-cylinder boosted HCCI engines and discussed the interactions of system features such as boosting and VVA with the ignition and combustion events. The current chapter will attempt to augment this thermodynamic analysis by examining LTC (and HPLB) engines from a 2^{nd} law perspective. The energy concept will be replaced by availability or exergy and the two latter terms will be used interchangeably in the following text.

Availability analysis was performed using the framework presented in Chapter 2 in conjunction with multi-cylinder engine simulations such as those discussed in Chapter 4. Boosted HCCI engine processes were analyzed based on useful work extraction potential and not energy terms, and the associated enabling technologies were assessed based on exergy loss and destruction criteria. The following sections will present results from the 2^{nd} law analysis and attempt to assess boosting and VVA techniques for high load operation from an exergy perspective. The effects of high pressure lean burn operation on engine irreversibilities will be investigated and efficiency limits will be discussed. Overall, availability analysis will attempt to quantify the effects of design and thermodynamic parameters on exergy destruction and losses, and identify processes that can mitigate them in favor of engine efficiency.

5.1 2nd Law Analysis of Boosted HCCI

Results from the thermodynamic analysis of multi-cylinder boosted HCCI engines in Chapter 4 highlighted certain techniques and processes that enabled high load efficient operation. The following sections will display these techniques from a 2nd law perspective and attempt to identify characteristics that are not observable from a traditional 1st law point of view. For that reason, two of the engine systems that were examined in Chapter 4 will be revisited; the turbocharged engine with NVO and the two-stage boosted engine operating on the combined NVO/PVO valve strategy.

It should be noted that 2nd law analysis was performed as post-processing of the results obtained from 1st law analysis as presented in Chapter 4. The major assumptions of the analysis were associated with the 2-zone nature of the combustion model and the adiabatic treatment of turbomachines. In addition, the fuel was considered to be sulfur-free and non-preheated; exergy calculations were performed using the fuel's lower heating value at the dead state temperature which was 25 °C.

5.1.1 Turbocharged HCCI with NVO

One of the major findings of the multi-cylinder simulations that were presented and analyzed in Chapter 4 was that combining boosting and negative valve overlap is not beneficial for high load HCCI. The reason stems from the combination of high engine mass flow rates, low valve lifts and recompression which acted to significantly increase pumping work at medium and high loads. An additional factor was high cylinder temperatures which let to ringing and could not be effectively reduced without cooling of the intake stream. As a result, high load HCCI operation could be achieved but pumping work hindered the potential for greater efficiency and higher load levels.

The following figures will display instantaneous and mean exergy variables that were obtained from 2nd law analysis of a turbocharged HCCI engine with NVO. As

shown in Chapter 4, the load range examined was 5 – 9 bar NMEP with 9 bar NMEP being the maximum attainable load of the engine. Figure 5.1 shows the development of cumulative in-cylinder availability terms during an engine cycle at maximum load. It should be noted that the cumulative terms shown below were obtained by time integration of the respective instantaneous availability terms over an engine cycle. As presented in Chapter 2, the cumulative availability values were subsequently used in the cylinder availability balance equation in order to calculate the entropy generation. Steady-state operation would require that cylinder availability be:

$$\int_{0}^{720} \frac{dA_{cyl}}{d\theta} d\theta = 0 \tag{5.1}$$

Figure 5.1 shows the variation of total cylinder availability over an engine cycle, as well as work, heat transfer, fuel, exhaust flow, intake flow and irreversibilities. Prior to ignition, total cylinder availability was increased through work offered by the piston during the compression stroke. Ignition after TDC meant that cylinder availability remained constant around TDC or even dropped slightly at cases due to heat transfer to the walls. After ignition occurred, pressure and temperature rise acted to increase cylinder availability, irreversibilities and heat transfer. The sudden change in cylinder availability and irreversibilities resulted from the short burn duration of HCCI combustion. The work term increased significantly during the expansion stroke and until BDC when the piston reversed and the exhaust stroke began. Indicated work production caused a simultaneous decrease in the availability of the working fluid. Negative valve overlap resulted in EVO timing after BDC and this was the point where exhaust flow availability started to increase. The recompression event around gas exchange TDC resulted in significant reduction of indicated work which was only minimally recovered as availability of the working fluid; the major part of the recompression work was destroyed and lost to heat transfer. Cylinder availability reached its minimum after the exhaust valve opened and

remained there until the end of the cycle when the working fluid returned to its initial state.

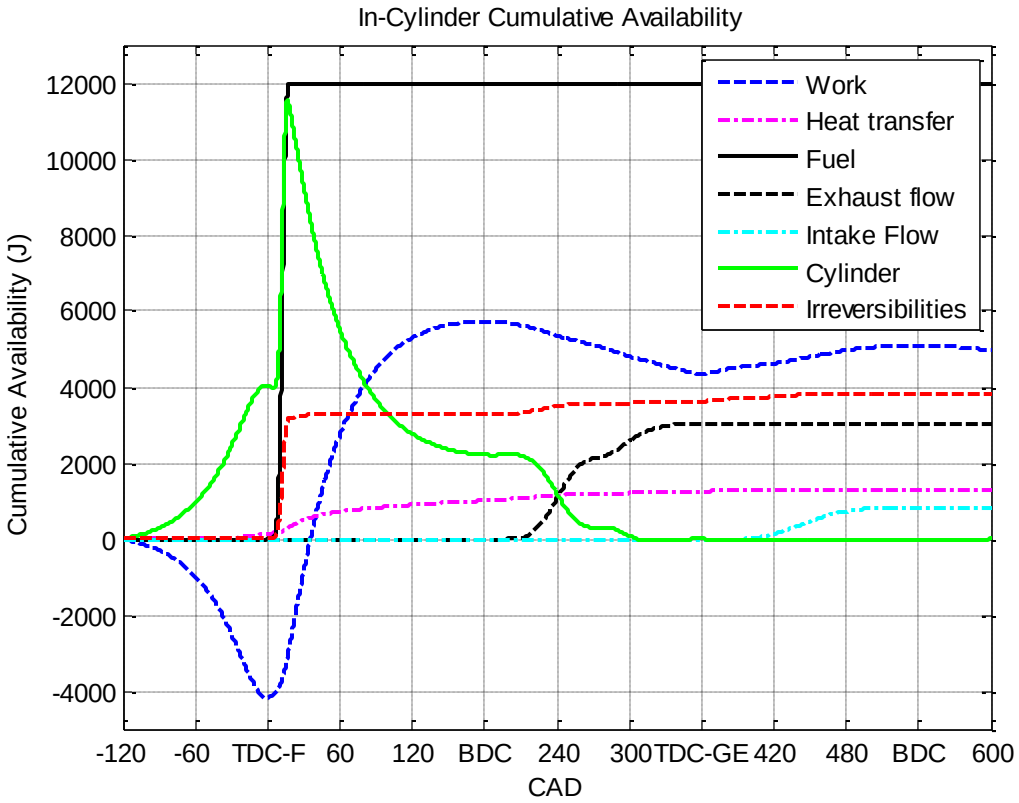

Figure 5.1 – Cumulative in-cylinder availability terms during a cycle for a turbocharged HCCI engine with NVO at 9 bar NMEP

Examination of the in-cylinder availability terms indicated that negative valve overlap is by itself a burden on the production of useful work. Work offered by the piston to the working fluid during recompression was destroyed or lost to heat transfer and not recovered when the recompressed working fluid expanded after gas exchange TDC. In addition, the significant pumping work caused by low valve lifts and the recompression loop rendered NVO as an unattractive valve strategy for efficient engine operation. Figure 5.1 presented results for a turbocharged HCCI engine. It should be noted though, that when a supercharger was employed in the boosting system, the mechanical work

required to drive the supercharger was included in the work and availability calculations of the cylinder.

Table 5.1 shows fuel energy and exergy distributions for the turbocharged HCCI engine with NVO at maximum load. Indicated work fractions were about the same but heat transfer was about 32 % lower in exergy terms; the difference was an indication that availability transfer due to heat transfer to the walls was less significant from a 2nd law perspective. Exhaust flow was the major term of discrepancy though; 1st law analysis indicated that it contained about 42 % of the fuel energy but 2nd law indicated that it accounted for only 20 % of the fuel exergy. This difference revealed that less than half of the exhaust energy was available to produce useful work. Irreversibilities accounted for almost 28 % of the fuel exergy and they occurred almost entirely during combustion. Farrell et al. have reported similar values of combustion irreversibilities [2]. It should be noted that fuel chemical exergy is 6.38 % higher than the fuel lower heating value. This difference explains the fact that friction was a slightly smaller fraction of fuel exergy than fuel energy.

Table 5.1 – Fuel energy and exergy distribution for a turbocharged HCCI engine with NVO operating at 9 bar NMEP

	Energy (%)	Exergy (%)
Indicated Work	41.87	41.79
Heat Transfer	15.79	10.57
Exhaust Flow	42.34	20.01
Irreversibilities	-	27.63
Friction	3.29	3.09

The vast majority of 2nd law studies in the literature have focused on diesel engines. Primus et al. [1] studied a six-cylinder turbocharged and aftercooled medium-duty diesel engine operating at 224 kW and 2100 RPM and reported the fuel energy and exergy distribution shown in Table 5.2.

Table 5.2 – Fuel energy and exergy distribution for a medium-duty diesel engine [1]

	Energy (%)	Exergy (%)
Indicated Work	40.54	39.21
Heat Transfer	17.23	13.98
Exhaust Flow	31.31	12.73
Irreversibilities	-	21.20
Friction	4.67	4.52

The authors reported that the diesel engine operated at 70 % load; it appeared to be less efficient than the turbocharged HCCI engine simulation since both energy and exergy fractions of indicated work were lower. Heat transfer was also lower in the HCCI engine both in terms of energy and exergy. The low temperature nature of HCCI combustion resulted in reduced heat transfer to the walls compared to a traditional diesel engine such as the one Primus et al. studied. Exhaust flow was a larger portion of fuel energy or fuel exergy in the HCCI simulation compared to the diesel engine. However, the available portion of exhaust energy was less than 50 % for the diesel engine as well. The fact that exhaust flow exergy was a larger portion of fuel exergy in the HCCI engine indicated that exergy saved from reduced heat transfer was not converted into useful work but transferred out of the cylinder in the exhaust flow. Therefore, manipulation of the engine operating characteristics could direct more exergy to the exhaust flow in favor

of turbocharger performance. Irreversibilities were also higher for the HCCI engine which was a result of low temperature combustion.

The load levels examined in the simulation are shown in Figure 5.2. Load ranged from 5 bar NMEP which was considered the starting point of boosted operation, to 9 bar NMEP which was the maximum attainable load by this engine. Maximum load corresponded to 30.7 kW (41.2 hp) of brake power and 5 bar NMEP corresponded to 16 kW (21.5 hp). The load range will be shown as a percentage of maximum load in the following figures.

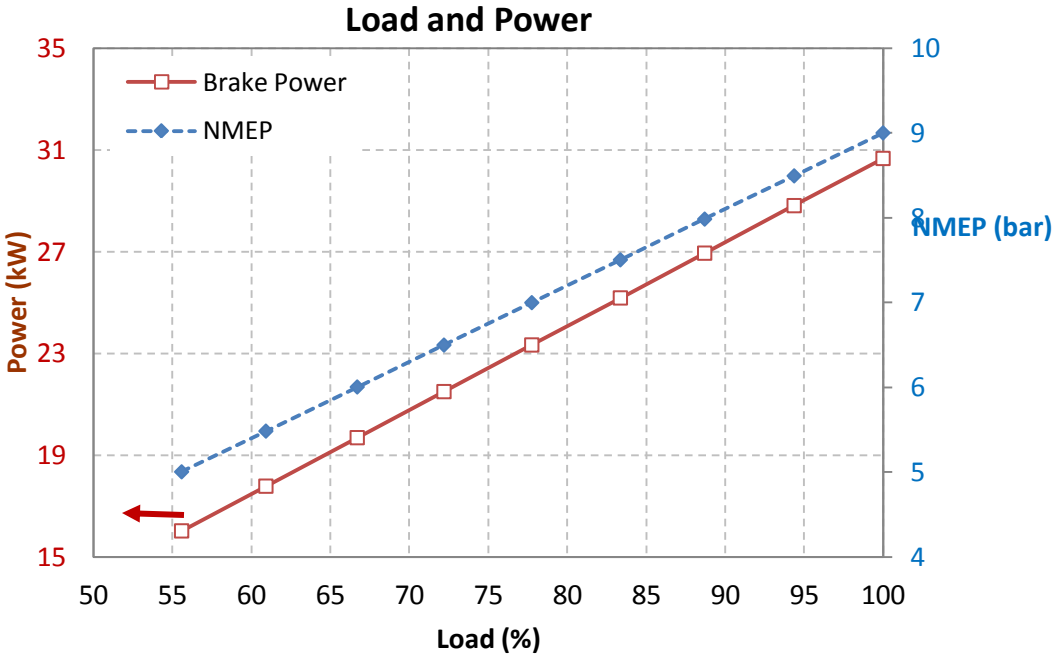

Figure 5.2 – Load and brake power for a turbocharged HCCI engine with NVO

Figure 5.3 shows availability distribution as a function of load for the turbocharged HCCI engine with NVO. Peak engine exergy efficiency was 36.2 % at 78 % load and friction losses were about constant at 3.09 % as shown in Table 5.1. Combustion irreversibilities ranged from 28 to 30 % and increased with load. The increasing trend was attributed to increasing dilution levels with load which kept cylinder temperatures low and significantly increased charge mass; the latter greatly affected

irreversibilities. Lower cylinder temperatures compared to traditional SI or diesel engines resulted in higher fractions of fuel availability destroyed due to entropy generation. Availability transfer due to heat transfer ranged from 13 to 10 % and slightly decreased with load which was a result of increased dilution levels as well. On the other hand, exhaust flow exergy losses increased considerably with load and ranged from 14.9 to 21.3 %. The increase in exhaust flow exergy with load explained the improved turbine performance as load increased.

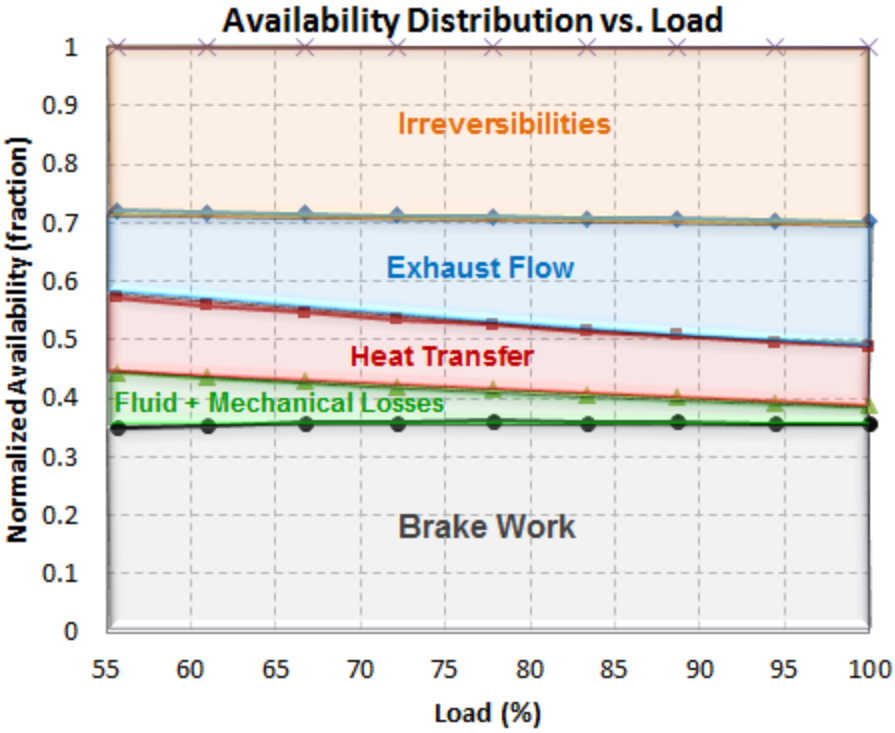

Figure 5.3 – Availability distribution for a turbocharged HCCI engine with NVO

Combustion irreversibilities are known to be a strong function of peak cylinder temperature and mass. In order to examine that dependence, specific irreversibilities were defined as irreversibilities per unit load. Figure 5.4 shows specific irreversibilities and peak cylinder temperature as a function of load for the turbocharged HCCI engine simulation. It can be readily observed that both peak cylinder temperatures and

irreversibilities increased with load, which revealed that exergy destruction was affected more by increased mass than increased cylinder temperature. The reason can be identified in the small variation of peak cylinder temperature with load. At 55 % load peak cylinder temperature was 1820 K which increased to 1880 K at maximum load, an increment of 3.3 %. On the other hand, charge mass more than doubled across the load range which was the dominant factor behind increased cylinder irreversibilities.

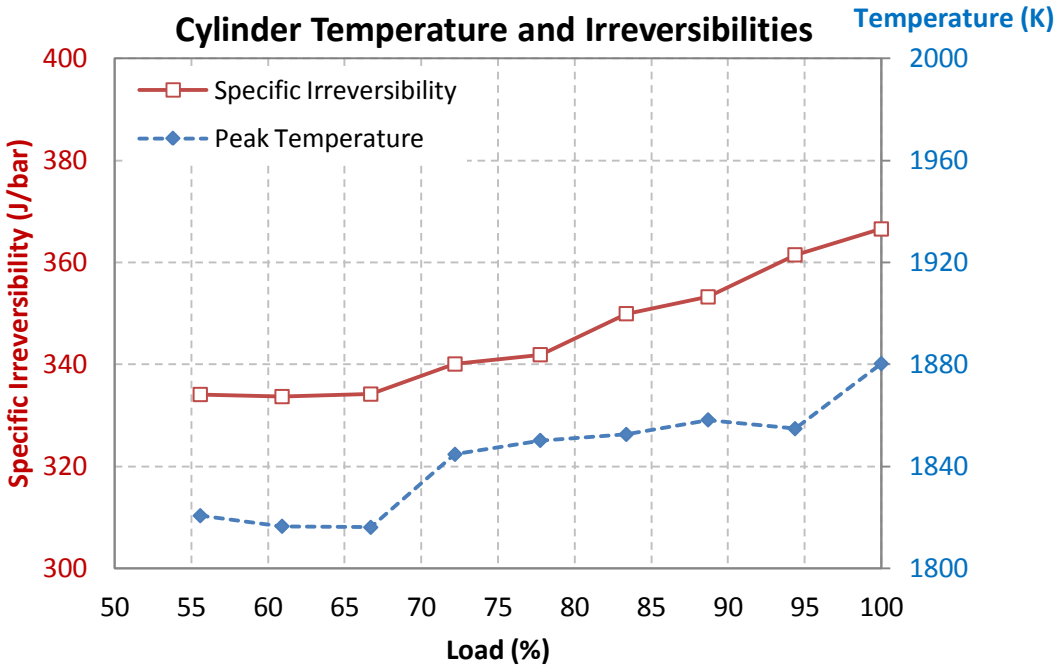

Figure 5.4 – Cylinder temperature and specific irreversibilities for a turbocharged HCCI engine with NVO

Figure 5.5 displays 1st and 2nd law engine efficiencies as functions of load. Brake efficiency is the known metric also discussed in Chapter 4, while exergy efficiency takes into account brake work and fuel availability input as defined in Chapter 2. Total exergy efficiency takes into account exhaust gas availability as well, which can be harnessed for useful work production, e.g. with a compound turbine. It can be observed that brake efficiency and exergy efficiency follow the same trend which can be explained by the fact that both of them are based on brake work. However, exergy efficiency exhibited lower

values than brake efficiency because fuel availability was 6.38 % higher than the fuel lower heating value as noted previously. Total exergy efficiency obtained the highest values since it included the potential of exhaust gases to produce useful work. It is interesting to note that total exergy efficiency increased monotonically with load which resulted from increasing exhaust flow availability with load as seen in Figure 5.3.

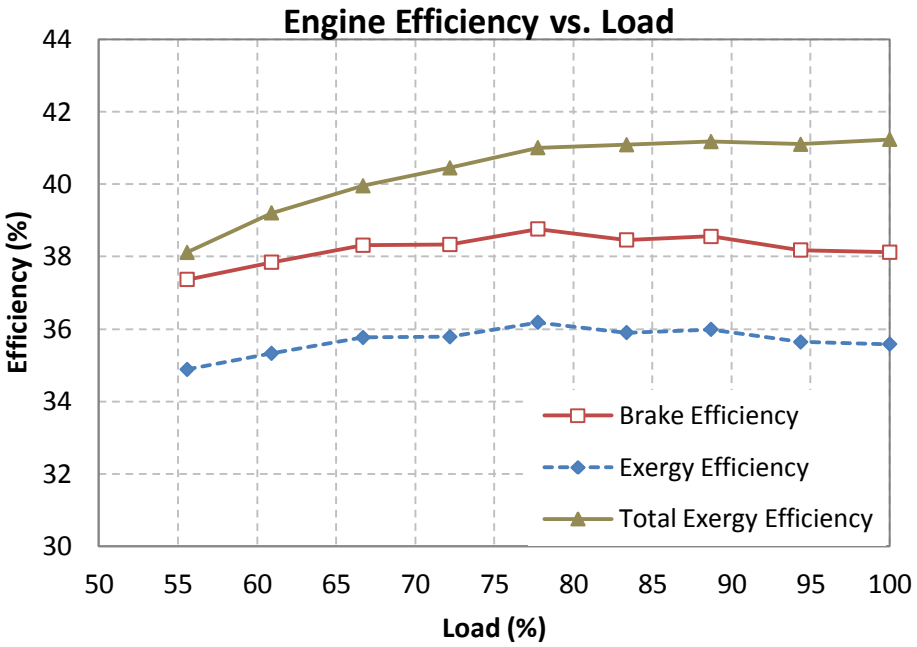

Figure 5.5 – Engine brake and exergy efficiencies for a turbocharged HCCI engine with NVO

The multi-cylinder simulation results presented in Chapter 4 highlighted the importance of boosting performance for HPLB engines; 2nd law analysis can provide additional insight into processes that can improve boosting and engine efficiency. Figure 5.6 shows exhaust flow available power (in kW) as a function of load at four locations in the engine exhaust system; exhaust ports, turbine inlet, turbine and turbine discharge. It is interesting to note that while engine load was approximately doubled across the load range, flow availability at the exhaust ports increased by a factor of four. Availability decreased as the working fluid moved away from the exhaust ports and toward the

turbine due to heat transfer to the exhaust manifold walls. The process of converting exhaust gas exergy into shaft work at the turbine included exergy destruction as well. The resulting turbine power was less than 50 % of available power at the exhaust ports and that fraction decreased as load decreased. In addition, poor turbine performance at low loads meant that exhaust exergy escaping the turbine was higher than turbine useful work and that relationship was reversed only after 70 % load. It should be noted that the turbine power shown is the difference between pre-turbine and post-turbine

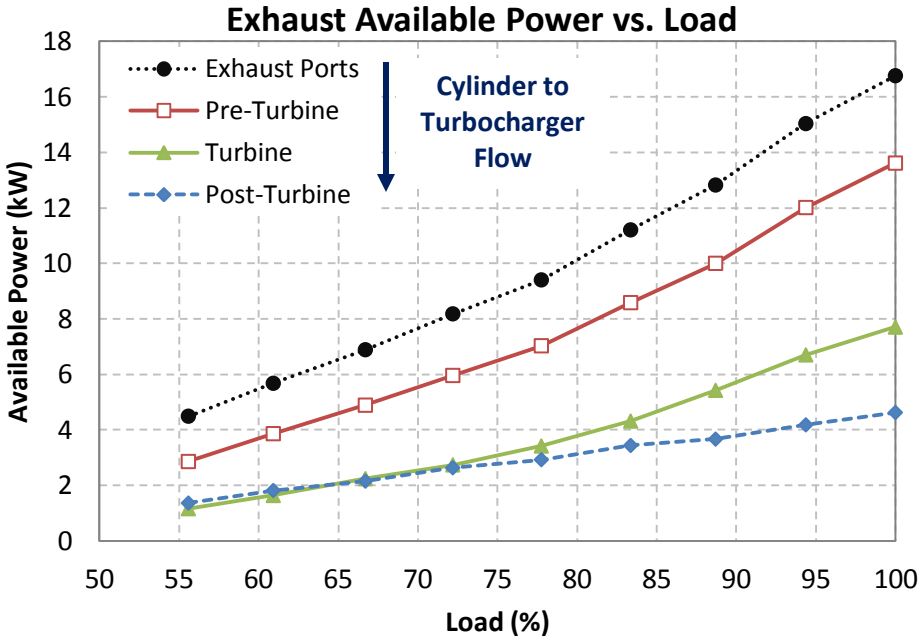

Figure 5.6 – Exhaust available power for a turbocharged HCCI engine with NVO

Increasing turbine power with load was a result of improved isentropic and exergy efficiencies as shown in Figure 5.7. Both isentropic and exergy efficiencies increased with load indicating improved boosting performance. It should be noted that isentropic and exergy efficiencies are connected but they are not the same. Isentropic efficiency compared the actual expansion process in the turbine with the isentropic one; exergy efficiency was a measure of how well exhaust gas exergy was converted into useful work at the turbine shaft. The specific turbine used was very well matched to the engine mass

flow rates at 2000 rpm thus exergy efficiency reached 86 % at high loads. Compressor performance was satisfactory as well given the fact that its peak isentropic efficiency was lower than that of the turbine. Nevertheless, compressor exergy efficiency was above 75 % across the load range, indicating that shaft work provided by the turbine was effectively converted into intake flow availability.

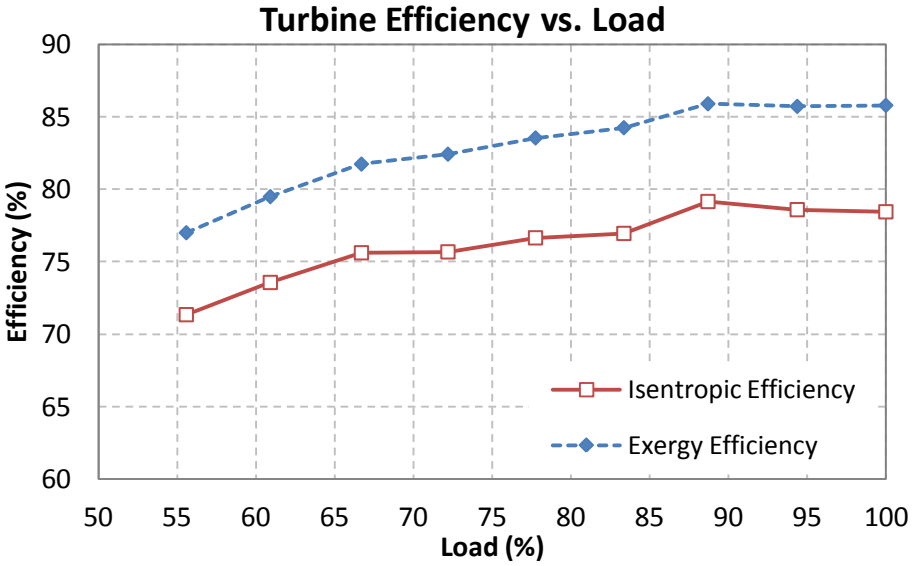

Figure 5.7 – Turbine efficiencies for a turbocharged HCCI engine with NVO

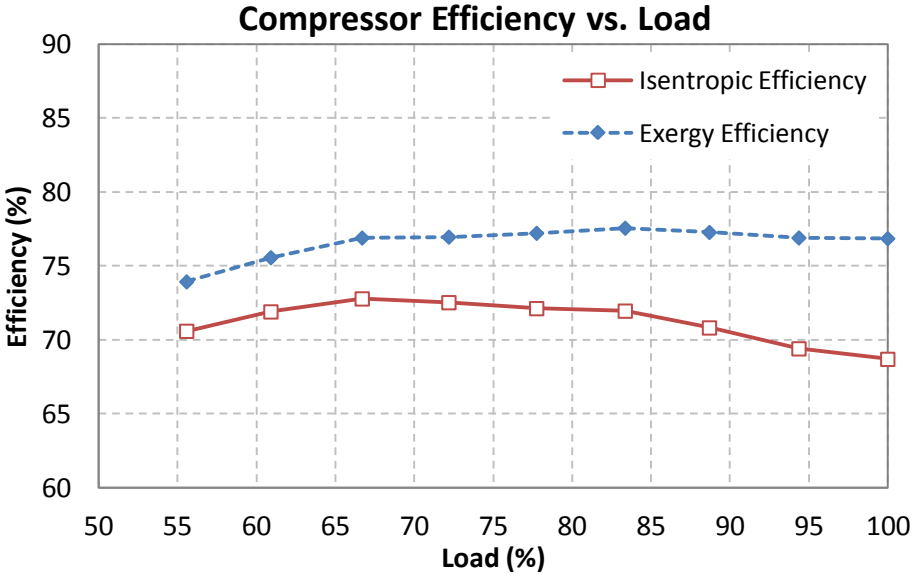

Figure 5.8 – Compressor efficiencies for a turbocharged HCCI engine with NVO

Availability analysis of a turbocharged HCCI engine using NVO illuminated interesting aspects of HPLB operation. It confirmed the observation made in Chapter 4 that the combination of boosting and negative valve overlap is not beneficial for high load HCCI. The reduction in indicated work during recompression was split between irreversibilities and heat transfer and was never recovered. In addition, low-valve lifts exacerbated fluid flow losses during gas exchange which contributed to the high pumping losses shown in Chapter 4. Low temperature combustion was associated with higher cylinder irreversibilities compared to traditional SI or diesel engines that stemmed from high dilution levels and low cylinder temperatures. However, reduced exergy transfer due to heat transfer to the walls mitigated the irreversibilities drawback. HPLB operation was associated with further irreversibilities increase since dilution levels were greater. Irreversibilities were primarily affected by charge mass since cylinder temperatures were comparable across the load range.

Exergy analysis of the exhaust system revealed that turbine useful work was always lower that 50 % of the available energy at the exhaust ports, indicating that low heat rejection manifolds could drastically improve boosting performance. Furthermore, engine total exergy efficiency indicated that significant efficiency gains can be achieved by exploiting the availability of exhaust gases with additional devices. In fact, efficiency gains would be more pronounced at higher loads.

The following section will present a similar 2^{nd} law analysis for the advanced, two-stage boosted HCCI with switchable NVO/PVO valve strategy. It will attempt to explore the implications of advanced boosting and PVO on exergy losses and transfers and to verify the observations made in Chapter 4 from a 2^{nd} law perspective.

5.1.2 Two-stage Boosted HCCI with NVO/PVO

The multi-cylinder engine simulations presented in Chapter 4 revealed that boosted HCCI operation can be markedly improved by utilizing intake air to heat the charge instead of using large amounts of residual gas through NVO. Subsequently, certain hypotheses pertaining to the interaction of engine subsystems with the combustion event were stated and confirmed. The first of these hypotheses stated that reduced dependence on residual gas for charge heating could enable use of PVO valve events in order to improve gas exchange efficiency. The hypothesis was confirmed by boosted HCCI simulations; additional benefits of PVO were also identified, such as reduced cylinder temperatures which resulted in less ringing propensity and improved thermal efficiency. It was found that a major limiting factor for maximum attainable load was intake pressure ratio. Therefore, the second hypothesis stated that higher pressure ratio at the intake side could help the engine achieve further increments in attainable load. This hypothesis was also verified by introducing an advanced boosting system that featured variable geometry turbocharging and supercharging in series. The two-stage boosting system operated in tandem with a switchable NVO/PVO valve strategy that ensured adequate charge heating at low loads and improved efficiency at high loads.

This section will present a 2nd law analysis on that advanced engine system and will attempt to assess the associated benefits from an exergy perspective. The following figures will present 2nd law analysis results in the same way as those shows in the previous section.

Figure 5.9 shows the variation of total cylinder availability over an engine cycle, as well as work, heat transfer, fuel, exhaust flow, intake flow and irreversibilities. All cumulative availability terms followed similar trends to those seen in Figure 5.1 for the NVO engine. However, indicated work decreased less around gas exchange TDC since there was no recompression loop. Exhaust flow cumulative availability increased since

PVO allowed higher amounts of exhaust gases to exit the cylinder. Also, the absence of recompression prevented heat transfer from increasing around gas exchange TDC. Irreversibilities were comparable to those of the NVO engine; in both cases, exergy was primarily destroyed during combustion. Irreversibilities exhibited slight increase after EVO and IVO, which was attributed to the efflux and influx of gases, mixing and decrease of cylinder temperature. The operating point shown was at 9.5 bar NMEP which was comparable to the one shown in Figure 5.1. Combustion irreversibilities where slightly increased at lower loads where PVO resulted in reduced cylinder temperatures compared to the NVO simulations.

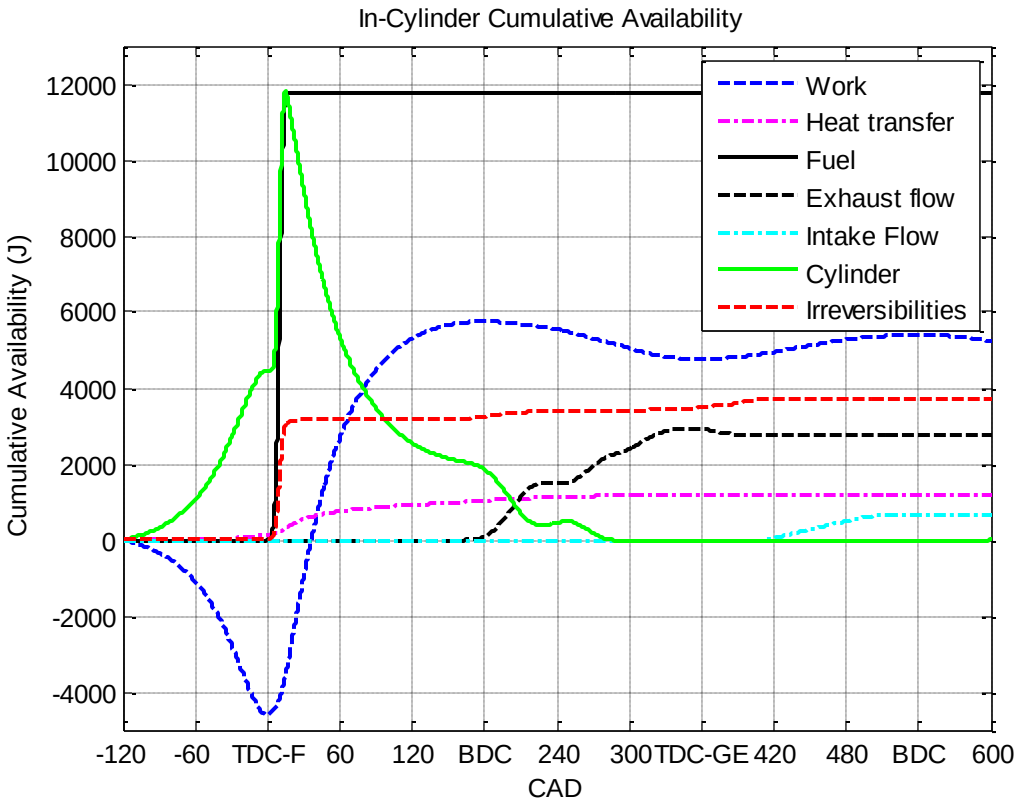

Figure 5.9 – Cumulative in-cylinder availability terms during a cycle for a two-stage boosted HCCI engine with NVO/PVO at 9.5 bar NMEP

The load range achieved from the combination of advanced boosting and VVA with HCCI combustion is shown in Figure 5.10. The starting point for all simulations was

5 bar NMEP and maximum attainable load increased to 11 bar NMEP compared to the engine presented in the previous section. Maximum load corresponded to 36.2 kW (48.5 hp) of brake power and 5 bar NMEP corresponded to 16 kW (21.5 hp). Load will be shown as a percentage of maximum load in the following figures ranging from 45 to 100 %.

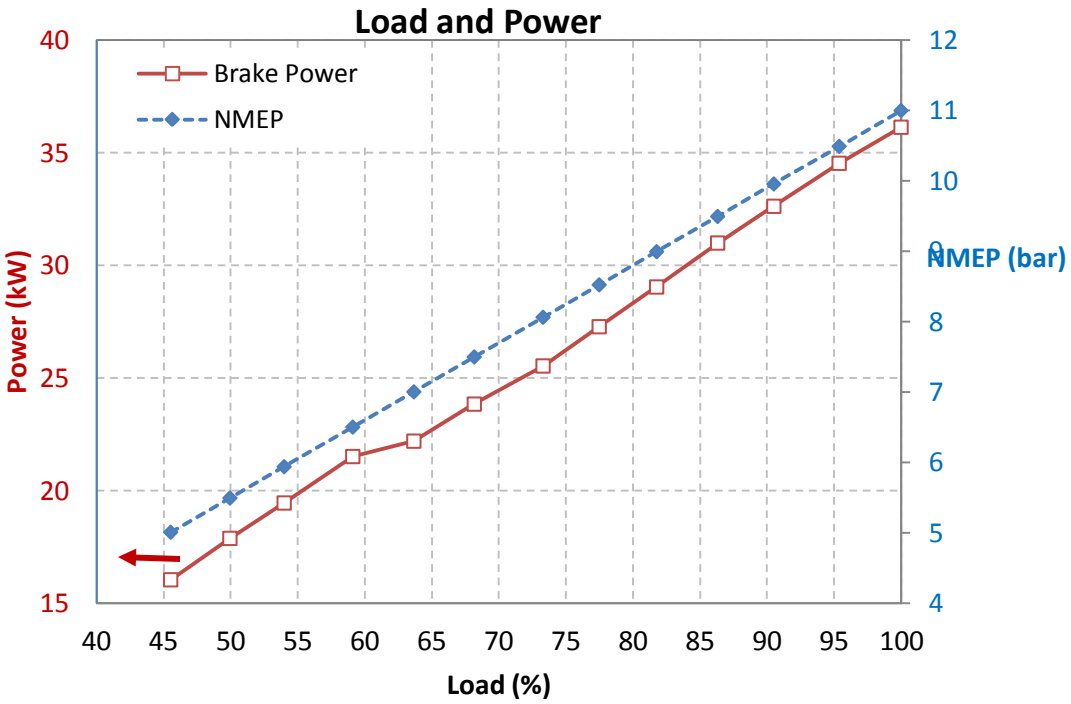

Figure 5.10 – Load and brake power for a two-stage boosted HCCI engine with NVO/PVO

Figure 5.11 shows availability distribution as a function of load for the two-stage boosted HCCI engine with NVO/PVO. Peak engine exergy efficiency was 36.6 % at 90 % load which was marginally increased compared to the engine of the previous section. Combustion irreversibilities ranged from 28 to 30 % and increased with load as shown in the previous section as well. The increasing trend was attributed to increasing dilution levels with load which kept cylinder temperatures low and significantly increased charge mass which greatly affected irreversibilities. Introduction of PVO further reduced

cylinder temperatures thus contributing to increased irreversibilities with load. On the other hand, lower cylinder temperatures with PVO restrained exergy loss due to heat transfer. Exergy loss to the walls ranged from 13 to 9 % and decreased with load. Exhaust flow exergy losses increased at low loads (16.5 to 20.5 %) when NVO was used but switching to PVO decreased exhaust flow exergy primarily because of reduced exhaust gas temperature. It should be noted that PVO use resulted in lower fluid flow losses across the load range but supercharging was responsible for slightly increased friction losses when engaged. In total, fluid and mechanical losses were lower than those seen in the previous section across the load range.

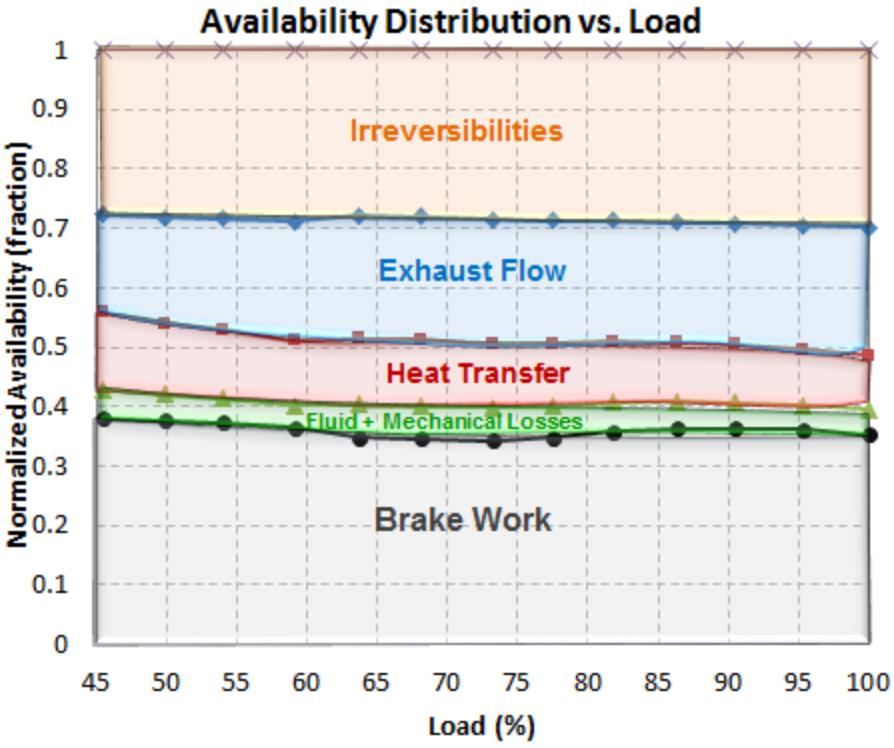

Figure 5.11 – Availability distribution for a two-stage boosted HCCI engine with NVO/PVO

As discussed previously, combustion irreversibilities were a strong function of peak cylinder temperature and mass. Specific irreversibilities (per unit load) were calculated for completeness and are shown in Figure 5.12 as a function of load along with

peak cylinder temperature. Specific irreversibilities increased linearly with load when NVO was used and the supercharger was bypassed (up to 60 % load) which was attributed to the dominant effect of increasing charge mass. Beyond 60 % load the supercharger was engaged and NVO was switched to PVO which resulted in considerable reduction of peak cylinder temperature due to increased dilution. Absolute irreversibilities increased due to reduced temperatures during combustion; however, specific irreversibilities decreased at that point because there was a clear increase in engine load. Specific irreversibilities kept increasing as load increased further up to 11 bar NMEP. The increasing trend was associated with increased charge mass with load which offset the effect of increasing peak cylinder temperature. It should be highlighted that utilizing high-lift valve events resulted in significant decrease in cylinder temperatures as shown in Figure 5.12. NVO use led to peak cylinder temperatures up to 1880 K but the combination of supercharging and PVO reduced them to 1723 K at the following operating point (~ 65 % load). Reduced cylinder temperatures were responsible for increased irreversibilities during combustion, but reduced pumping work and improved thermal efficiency were able to counterbalanced them; the end result was a slight improvement in exergy efficiency compared to the combination of turbocharging and NVO.

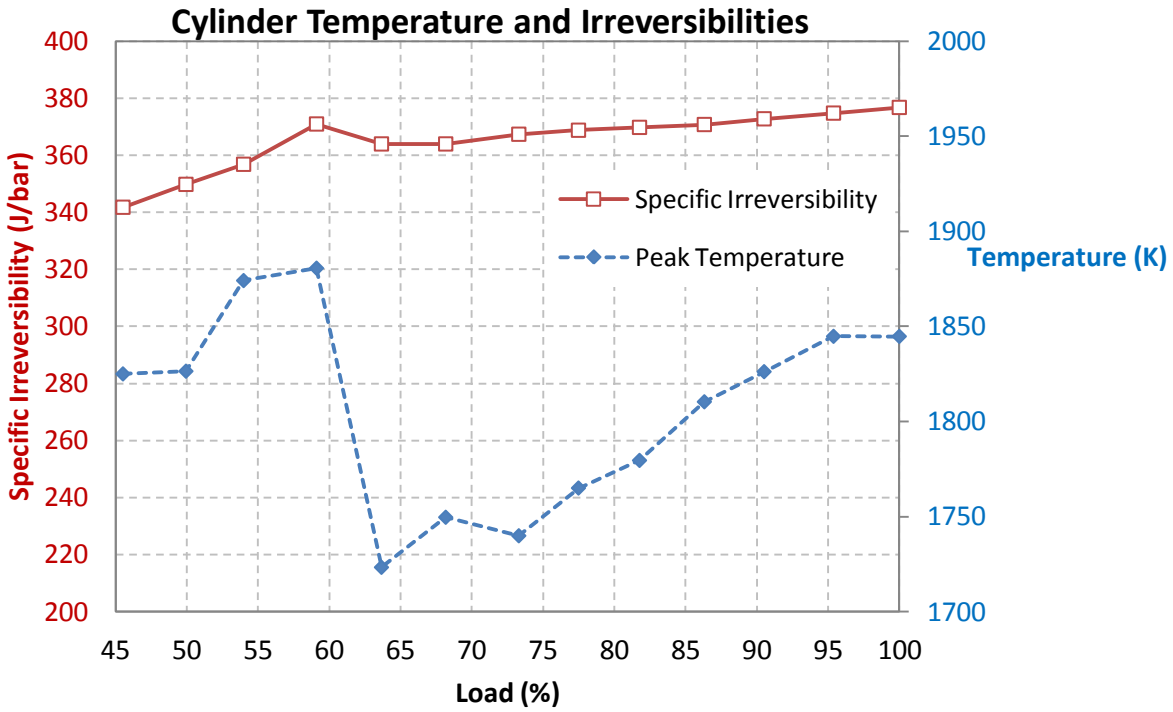

Figure 5.12 – Peak cylinder temperature and specific irreversibilities for a two-stage boosted HCCI engine with NVO/PVO

Figure 5.13 shows 1st and 2nd law engine efficiencies as functions of load for the two-stage boosted engine using NVO/PVO. Brake efficiency and exergy efficiency appear to follow the same trend which can be explained by the fact that both of them were based on brake work. As discussed in the previous section, exergy efficiency exhibited lower values than brake efficiency because fuel availability was higher than the fuel lower heating value. It can be readily observed that when the supercharger was engaged and NVO was switched to PVO (at 60 % load), there was considerable improvement in brake and exergy efficiencies. That improvement was a combined result of increased gas exchange and thermal efficiencies. However, total exergy efficiency decreased at 60 % load because increased levels of dilution acted to reduce exhaust gas temperature and therefore exhaust availability. Beyond 60 % load, brake and exergy efficiencies increased and reached a plateau at 80 % load. However, total exergy

efficiency kept increasing since an increasing fraction of fuel exergy was transferred to the exhaust flow.

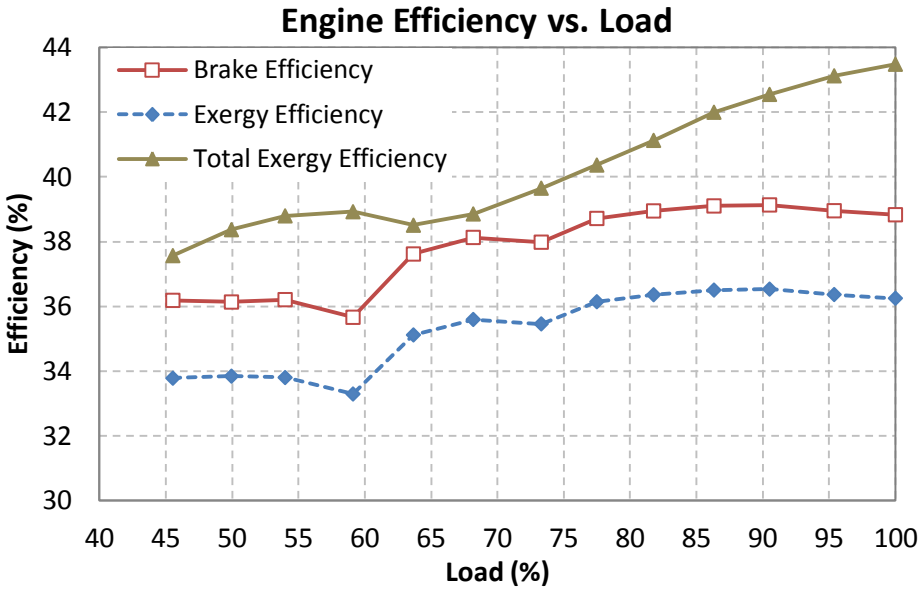

Figure 5.13 – Engine brake and exergy efficiencies for a two-stage boosted HCCI engine with NVO/PVO

Exhaust flow available power is shown in Figure 5.14 as a function of load, at four locations in the engine exhaust system; exhaust ports, turbine inlet, turbine and turbine discharge. The combination of turbocharging and NVO presented in the previous section resulted in load that was approximately doubled across the load range, but in flow availability at the exhaust ports that was increased by a factor of four. Advanced boosting and PVO altered that ratio of exhaust availability to engine load. Figure 5.14 shows that load was increased by a factor of 2.2, but exergy at the exhaust ports was increased by a factor of 3.2 across the load range. Reduced exhaust port exergy compared to the previous engine was a direct result of reduced cylinder temperatures and consequently reduced exhaust gas temperatures with PVO. Turbine power was again less than 50 % of available power at the exhaust ports and that fraction was only approached at high load. However, work extraction at the turbine was markedly improved after 60 % load; that

was a direct result of high-lift valve events that did not retain hot exhaust gas in the cylinder but allowed it to be transferred to the exhaust manifold.

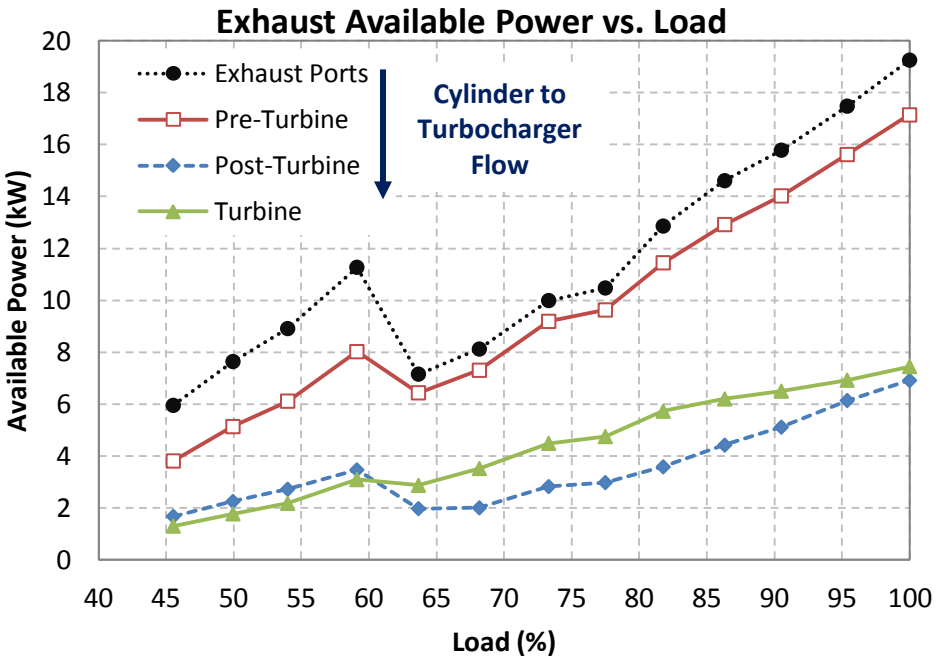

Figure 5.14 – Exhaust available power for a two-stage boosted HCCI engine with NVO/PVO

Increasing turbine power after 60 % load was a result of improved isentropic and exergy efficiencies as shown in Figure 5.15. Both isentropic and exergy efficiencies increased with load indicating improved boosting performance. However, engaging the supercharger and switching from NVO to PVO at 60 % load reduced exhaust gas temperature and degraded turbine performance. In addition, manipulation of the turbine variable geometry at high loads allowed a reduction in exhaust pressure and pumping work but kept exergy efficiency constant. Compressor performance was satisfactory and high levels of exergy efficiency were achieved across the load range. The compressor was linked to exhaust conditions only through turbine work, but that was not sufficient to cause a drop in performance at 60 % load. Compressor exergy efficiency peaked at 85 %

load since altering the turbine geometry at high loads caused the compressor operating points to move away from the optimal efficiency islands (also shown in Chapter 4).

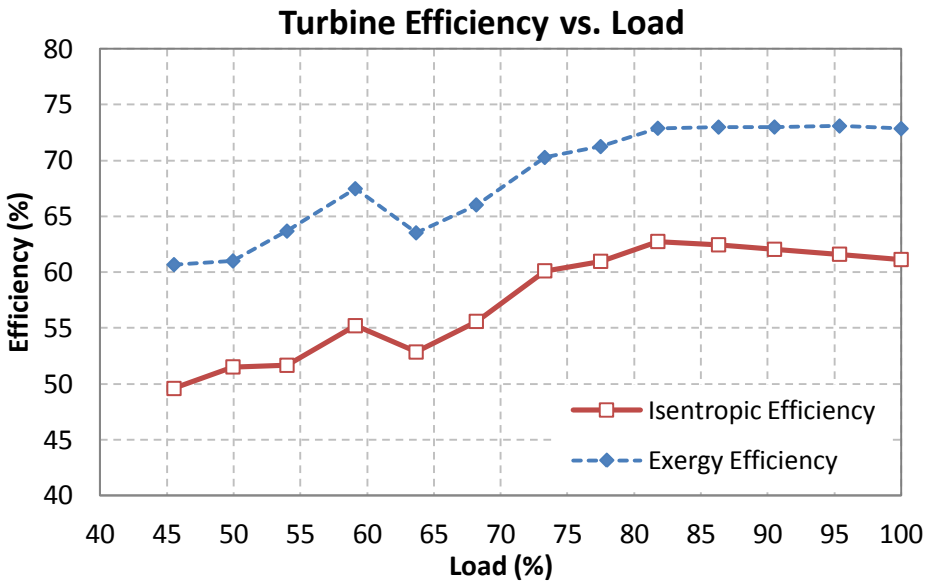

Figure 5.15 – Turbine efficiencies for a two-stage boosted HCCI engine with NVO/PVO

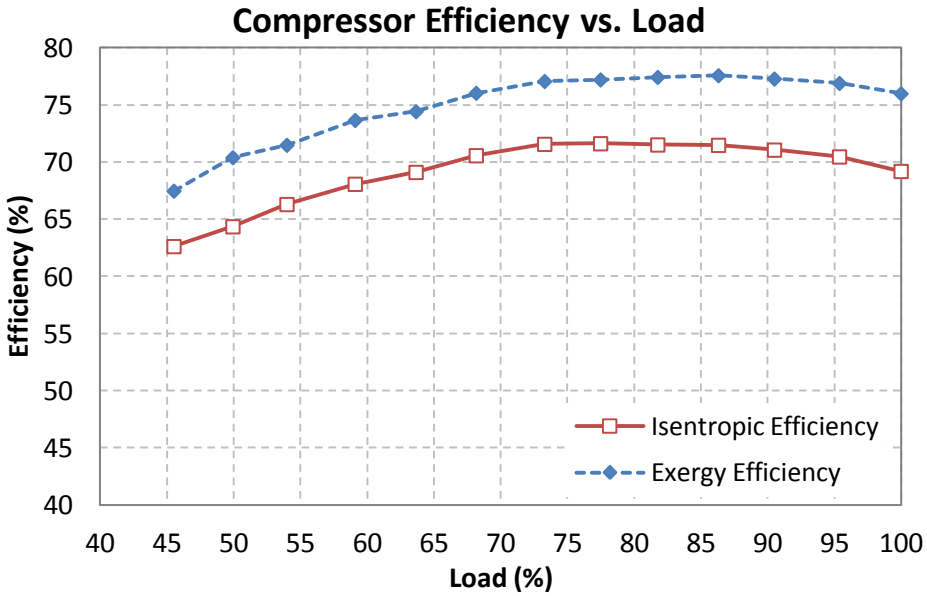

Figure 5.16 – Compressor efficiencies for a two-stage boosted HCCI engine with NVO/PVO

2nd law analysis of the two-stage boosted HCCI engine with NVO/PVO revealed some interesting trade-offs that could not be adequately described by traditional 1st law analysis. It was shown in Chapter 4 that increased pressure ratio at the intake side in conjunction with high lift valve events enabled efficient high load operation. That was achieved by improving gas exchange and thermal efficiencies as well as reducing pressure rise rates during combustion. Reducing cylinder temperatures was expected to be harmful from an exergy perspective since cylinder irreversibilities would increase. However, reduced exergy losses to the walls mitigated the effect of exergy destruction. Furthermore, it was found that increasing dilution levels with load reduced exhaust availability and hindered efficient turbine operation at medium loads. Results from the previous section indicated that NVO offered limited benefits because it reduced indicated work production. The current section displayed that PVO was beneficial for indicated work production but was associated with increased irreversibilities and lower exhaust flow availability. Nevertheless, the benefits resulting from improved gas exchange and thermal efficiencies were dominant and offset the shortcomings of high dilution levels. Overall, high dilution levels proved to be very beneficial for work production despite the fact that resulted in reduced exhaust flow exergy. The desired high dilution levels can be achieved by an advanced boosting system in conjunction with high lift valve events.

5.2 Effect of Boosting on Engine Irreversibilities and Efficiency

The previous section presented 2nd law analysis of two multi-cylinder boosted HCCI engines which featured different boosting systems and valve strategies. The difference between the two boosting systems was effectively the available pressure ratio at the intake side. Elevated pressure was found to be the main enabler of high load HCCI operation because it allowed ignition of lean mixtures and at the same time ensured high dilution levels and low pressure rise rates during combustion. Therefore, boosting

systems that can provide the highest possible pressure ratios at the intake side are desirable for HPLB engines.

However, availability analysis of LTC engines revealed that high dilution levels were associated with high irreversibilities during combustion. The literature has shown that turbocharged diesel engines destroyed 20 – 22 % of fuel exergy during combustion, but boosted HCCI results showed that combustion irreversibilities were 28 – 30 % of fuel exergy [1]. In addition, combustion irreversibilities did not seem to decrease with load and peak temperature. On the contrary, irreversibilities increased because boosting increased dilution levels with load and also increased charge mass proportionally to intake pressure. Therefore, it can be concluded that boosted LTC engines suffer from increased combustion irreversibilities and increasing boost can potentially increase them further.

Despite the fact that cylinder irreversibilities increased with load (and boost), it was found that work output increased faster than fuel exergy input. The end result was improved exergy efficiency with boost and load. The reasons stem from improved thermal efficiency with boost and reduced pumping work when high lift valve events were employed. Furthermore, results from the boosted simulations showed that high dilution levels resulted in low exergy losses to the walls through heat transfer which aided work production as well. The combination of these factors led to the conclusion that boosting LTC engines may exacerbate cylinder irreversibilities but the benefits of thermal efficiency, heat transfer and pumping work are enough to offset them and offer higher cylinder exergy efficiency.

Figure 5.3 displayed that exhaust flow availability was increased with load, since exergy saved from reduced heat transfer was not converted into useful work but transferred out of the cylinder with exhaust gases. That observation agrees with low heat rejection diesel engine studies from the literature. Turbocharging was critical since it enabled harvesting of exhaust flow exergy and was by itself sufficient to bring engine

exergy efficiency above 36 %. That efficiency level is comparable to those of medium-duty turbocharged diesel engines examined in the literature and about 12 % higher than naturally aspirated LTC engines [1, 2]. Therefore, boosting is certainly a desirable technique in the effort to increase engine exergy efficiency. Researchers have claimed that the existence of a turbine restriction in the exhaust manifold may inhibit exhaust flow, thus exerting backpressure on the cylinders and increasing irreversibilities in the exhaust manifold. However, exhaust irreversibilities were always a very small fraction of fuel exergy. Furthermore, the present work has shown that adoption of an advanced boosting system allowed significant flexibility in the control of backpressure and other boundary conditions.

Overall, boosting LTC engines appears to be slightly harmful for cylinder irreversibilities but very beneficial for engine exergy efficiency. Cylinder irreversibilities may increase due to higher levels of dilution with boosting, and potentially increased fluid flow irreversibilities due to higher mass flow rates and backpressure. However, these drawbacks are greatly offset by benefits in heat transfer, thermal efficiency and gas exchange efficiency. In addition, extraction of useful work from exhaust flow availability proved to be able to raise engine exergy efficiency to values comparable to or higher than those of diesel engines.

5.3 Comparison of NVO and PVO for HPLB Engines

Traditional 1st law analysis that was presented in Chapter 4 verified the hypothesis that high lift valve events can be used when air heating from the intake system can satisfy HCCI autoignition requirements. Medium to high load operation was shown to bring intake pressure and temperature to high levels that facilitated ignition without the need of heating from residual gases. Therefore, PVO valve strategy was used and it was found to be highly beneficial for pumping work and thermal efficiency. In addition, it was found

that PVO lowered cylinder temperatures because there was no direct trapping of hot burned gases. The outcome was reduced pressure rise rates during heat release and reduced ringing propensity that allowed higher fueling rates.

Availability analysis that was presented in the previous sections demonstrated that use of high lift valve events had a negative impact on combustion irreversibilities due to reduced cylinder temperatures. That was primarily the case at medium (6.5 – 7.5 bar NMEP) loads where peak cylinder temperatures were in the vicinity of 1750 K. Beyond 8 bar NMEP, peak cylinder temperatures were comparable to those of NVO engines thus combustion irreversibilities were similar. In fact, recompression of burned gases induced additional irreversibilities and exergy loss due to heat transfer. Figure 5.14 also showed that lower exhaust gas temperatures resulted in reduced exhaust flow availability. However, higher mass flow rates allowed for increased turbine work and therefore improved exergy harvesting in the exhaust system compared to NVO operation. In addition, high valve lifts were beneficial to fluid flow losses which were shown to be reduced compared to NVO operation.

Autoignition occurring in HCCI engines placed the most significant requirement on mixture preparation strategies. Temperature at 60 CAD before firing TDC needed to be above a certain threshold in order to enable autoignition of the charge. That threshold was about 620 K for naturally aspirated operation. As load and boost increased the temperature threshold decreased and reached 560 K at maximum load (11 bar NMEP). Therefore, it was shown that NVO use was required at low loads for charge heating, but it could be replaced by PVO at medium and high loads in order to improve engine efficiency.

As described in Chapter 1, high pressure lean burn engines include but are not limited to boosted HCCI. Spark Assisted Compression Ignition (SACI) is a combustion mode that has been gaining interest among the research community and can be applied to the same engine as HCCI with intelligent use of the spark plug. In a spark assisted or

spark ignition environment the intake temperature requirement would be of minor importance. The two remaining requirements for high load operation would be high charge mass for high work output and high dilution levels for low pressure rise rates during combustion. Therefore, operation with hot intake air and high lift valve events would be easier to implement for improving engine efficiency.

Overall, multi-cylinder simulations and 2nd law analysis of boosted HCCI engines showed that PVO valve strategy can be successfully used to enable medium and high load HCCI operation. The combination of boosting and PVO proved to be highly beneficial for pumping work and thermal efficiency. From an availability viewpoint, use of PVO was responsible for increased irreversibilities at medium loads due to lower cylinder temperatures and reduced exhaust flow exergy. However, higher mass flow rates resulted in more useful work extraction at the turbine and lower cylinder temperatures resulted in reduced exergy losses from heat transfer. Low load HCCI operation requires residual gas trapping with NVO because air heating from the intake system is not sufficient for ignition. Nevertheless, a switchable NVO/PVO valve strategy can be implemented which would be very beneficial to engine efficiency, and would also bring HCCI combustion closer to SI combustion in a dual mode (or multi-mode) engine.

5.4 Low Heat Rejection HCCI

Availability analysis of boosted HCCI engines revealed that a considerable amount of fuel exergy was lost to exhaust flow and that amount increased with engine load. It was also found that heat transfer slightly decreased with load and it accounted for 9 – 13 % of fuel exergy. The low temperature nature of HCCI combustion resulted in low exhaust gas exergy; therefore, it was concluded that by increasing exhaust flow exergy, benefits in boosting performance and intake pressure could be realized. Exhaust flow exergy can be increased by utilizing Low Heat Rejection (LHR) techniques. The LHR

concept originated from diesel engines and studies have been presented in the literature for more than thirty years [4]. Numerous experimental investigations on single-cylinder and multi-cylinder engines have shown that low heat rejection can aid thermal efficiency, increase exhaust availability and reduce emissions in diesel engines. Overall, various researchers concluded that exergy saved from reduced heat transfer to the walls was not converted into useful work on the piston but transferred to the exhaust flow. A recent thermodynamic study by Tuner on low heat rejection HCCI concluded that gross indicated thermal efficiency has the potential to reach 60 % [5]. However, the author observed that reduced heat transfer had an accelerating effect on ignition timing and pressure rise rates which needed to be appropriately controlled.

Increased exhaust flow availability has the potential to improve boosting performance which was shown to be crucial for high load HCCI operation. Therefore, the hypothesis that low heat rejection can improve high load HCCI operation was investigated through multi-cylinder simulations. The engine used was the two-stage boosted one featuring NVO/PVO switching at medium loads. In order to simulate LHR, heat transfer in the cylinder and exhaust manifold was reduced by 40 %. The entire load range was explored starting from 5 bar NMEP and the results are presented in the following.

Figure 5.17 shows the load range for the standard and LHR engines as a function of fueling rate. It can be readily observed that the low heat rejection engine was more efficient, since it required less fuel across the load range. The reason was not increased indicated work due to reduced heat transfer; it was higher intake pressure due to improved boosting performance. Increased exhaust flow availability allowed the turbine to extract more useful work and the compressor to operate at higher pressure ratios at the intake side. The outcome was improved dilution levels which allowed for earlier combustion phasing and increased thermal efficiency. The interaction between exhaust

availability and boosting shown here is an indication that boosting efficiency is equally important to cylinder efficiency for HPLB engines.

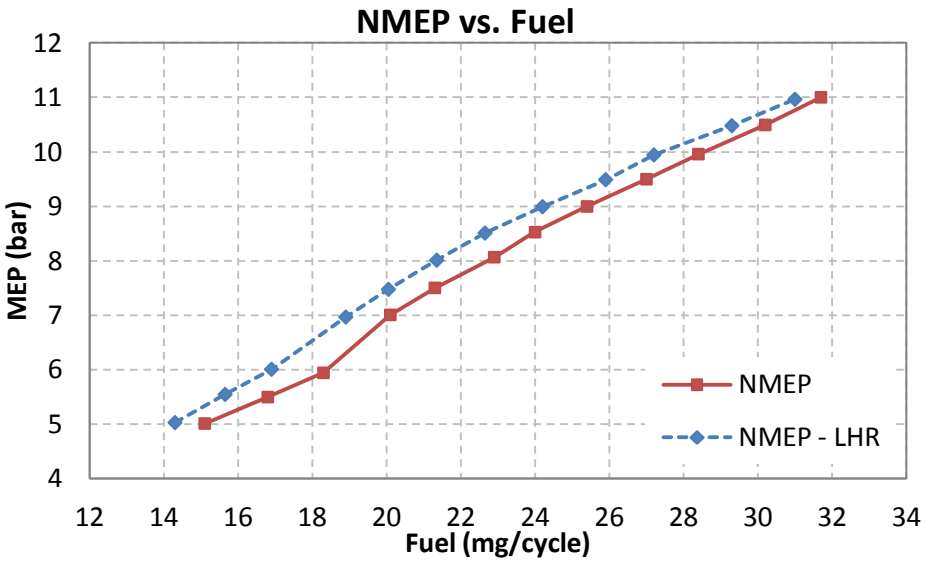

Figure 5.17 – Load range for the standard and low heat rejection engines

The efficiency difference can be also seen in Figure 5.18 which shows brake specific fuel consumption as a function of BMEP for both engines. The low heat rejection engine was clearly more efficiency across the load range with the largest difference occurring at 8 – 9 bar BMEP. Maximum brake efficiency for the standard engine was 39.2 % and occurred at 9 bar NMEP. That was increased to 42.5 % for the LHR engine and occurred slightly higher at 10 bar NMEP. As mentioned above, improved thermal efficiency due to increased dilution was one the reasons behind the efficiency difference. Gas exchange efficiency in the LHR engine was improved as well, since higher exhaust exergy allowed for improved backpressure control through the variable geometry turbine. Furthermore, mechanical efficiency was also slightly improved at the LHR engine. The reason was that intake pressure requirements were met by the turbocharger thus allowing for minimal supercharger use.

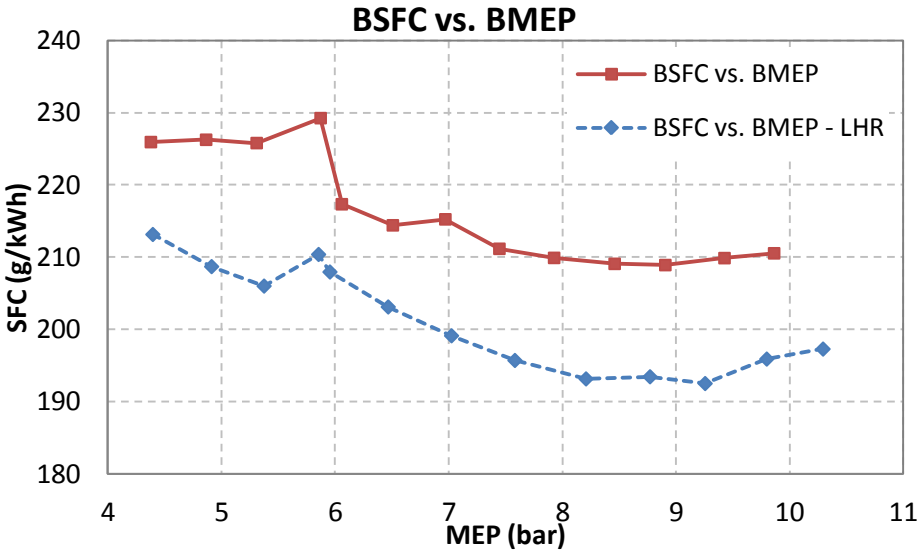

Figure 5.18 – Specific fuel consumption for the standard and low heat rejection engines

Figure 5.19 shows fuel exergy distribution as a function of load for the low heat rejection engine. By comparing it to Figure 5.11, it can be observed that heat transfer was significantly reduced across the load range. The standard engine lost 9 – 13 % of its fuel exergy to the walls through heat transfer; that fraction was reduced to 5 – 7 % for the LHR engine. Similarly to what has been reported in the literature of diesel engines, most of the exergy saved from heat transfer was transferred out of the cylinder with exhaust flow. The standard engine transferred 16.5 – 21.5 % of its fuel exergy to the exhaust flow; the LHR engine though transferred 20 – 25 % to the exhaust flow. Increased exhaust flow exergy had a more pronounced effect at low and medium loads where the standard engine could not develop high intake pressure without the contribution of supercharging. The outcome was higher intake pressure at low and medium loads regardless of NVO or PVO use. Higher boost resulted in higher dilution levels which offered lower pressure rise rates and higher thermal efficiency. Cylinder irreversibilities were equal among the standard and LHR engines and accounted for 28 – 30 % of fuel availability.

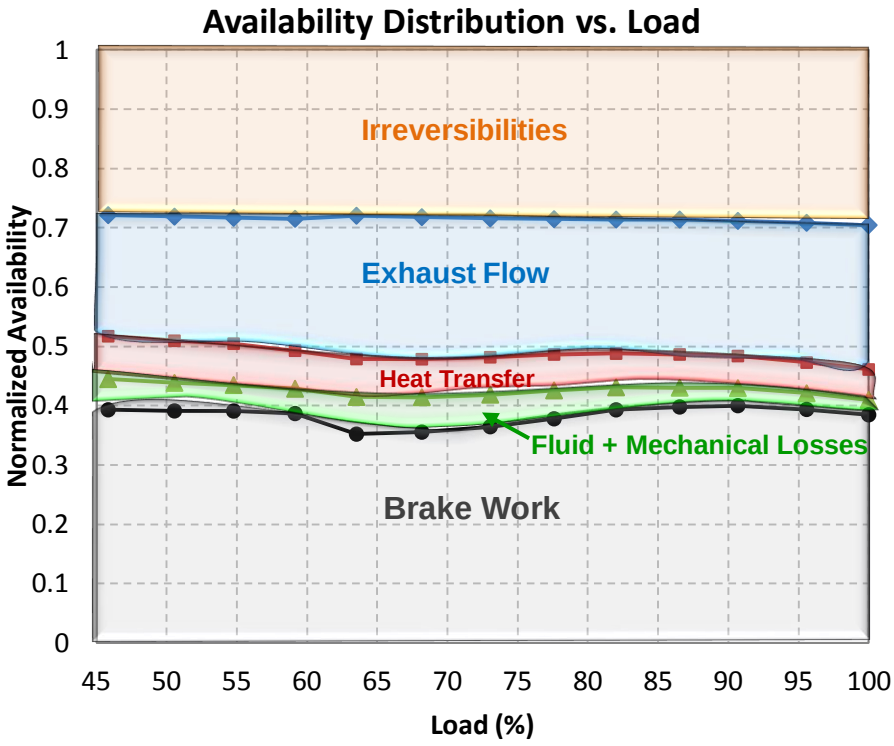

Figure 5.19 – Fuel availability distribution for the low heat rejection engine

Although the LHR engine exhibited significantly lower heat transfer, peak cylinder temperatures were lower than the standard engine as can be seen in Figure 5.20. The reason was increased intake pressure and dilution levels for the low heat rejection engine. Equivalence ratio is shown in Figure 5.21 for both engines and the effect of increased intake pressure is evident. Φ was significantly lower at low and medium loads where boosting performance was benefited the most by increased exhaust availability. The combination of high boost and NVO/PVO switching at 7 bar NMEP resulted in equivalence ratio of 0.33 and peak cylinder temperature of 1603 K which were highly beneficial for thermal efficiency and ringing. Both peak cylinder temperature and equivalence ratio curves converged for the two engines as load increased above 7 bar NMEP. The effect of increased exhaust availability on boosting was less pronounced since turbocharger performance was adequate in both cases. In fact, the LHR engine operated slightly richer at maximum load. That was a result of manipulating the variable

geometry turbine for reducing backpressure which limited boost at the intake side and reduced RGF.

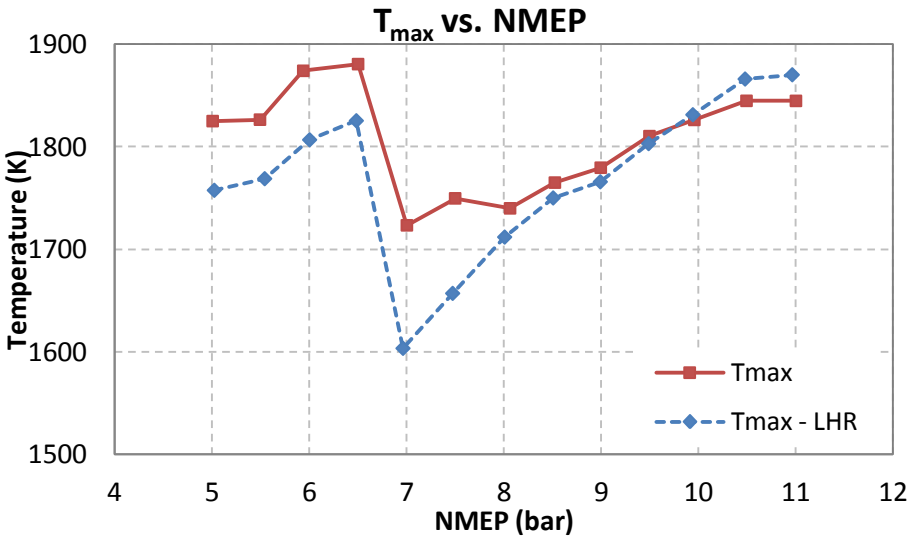

Figure 5.20 – Peak cylinder temperature for the standard and low heat rejection engines

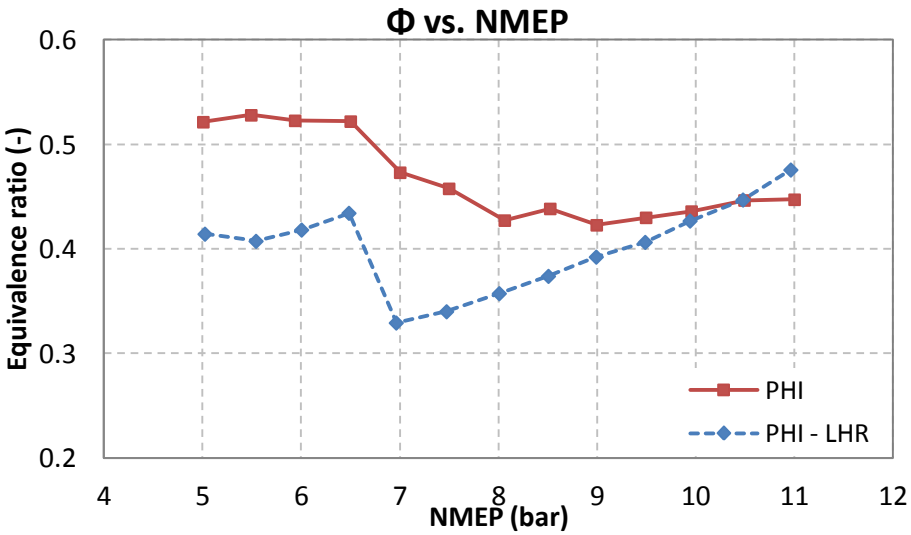

Figure 5.21 – Equivalence ratio for the standard and low heat rejection engines

The essence of improving efficiency from low heat rejection can be summarized in Figure 5.22, which shows exhaust available power and turbine power as functions of load for both engines. Available power at the exhaust ports was significantly increased across the load range as a result of 40 % reduced in-cylinder heat transfer. Heat transfer

was reduced in the exhaust manifold as well; the combination of the two allowed the turbine to extract more exergy from the exhaust gas across the load range thus improving boosting performance. The benefit from higher exhaust exergy was maximized in the 60 - 80 % load range. In fact, after NVO/PVO switching at 64 % load, exhaust available power was 53 % higher and turbine power at the same point was almost doubled. The difference in turbine power between the two engines decreased at higher loads but the LHR engine provided higher exergy to the turbine across the load range. It should be noted however, that even though heat transfer in the cylinder and exhaust manifold was significantly reduced, turbine useful work was always lower than 50 % of the available power at the exhaust ports. The same observation was made in the previous sections and agreed with several studies presented in the literature. Turbine work approached 50 % of the available exhaust power at 64 % load.

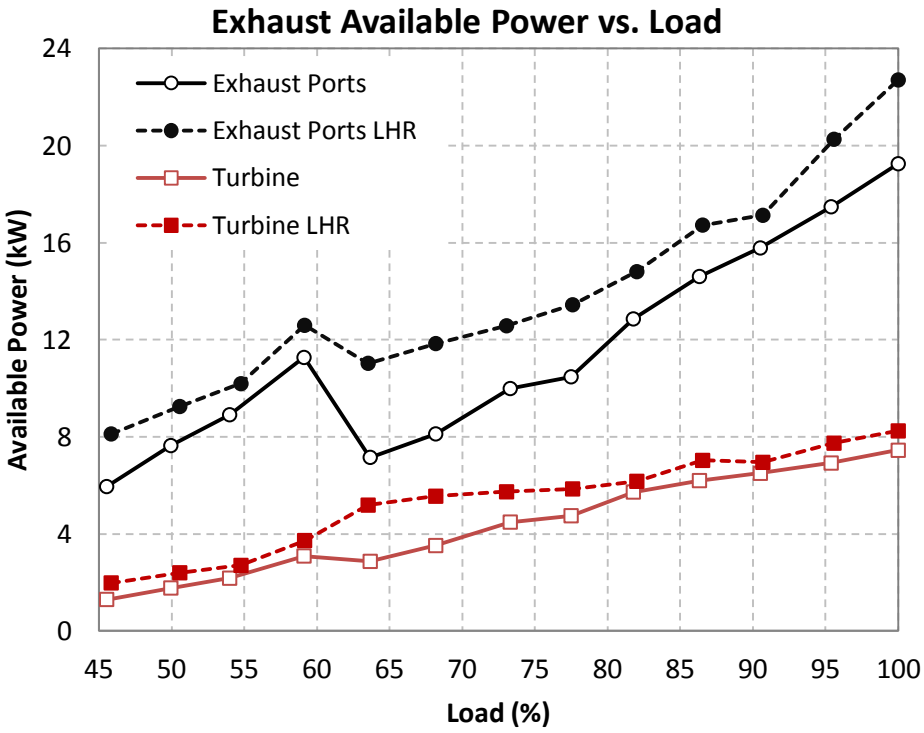

Figure 5.22 – Exhaust flow available power for the standard and low heat rejection engines

Improved turbine performance is displayed in Figure 5.23 as well, which shows turbine exergy efficiency as a function of load for the standard and LHR engines. As discussed in the previous sections, switching from NVO to PVO at 64 % load reduced cylinder temperatures and exhaust flow exergy. The resulting decrease in turbine power shown in Figure 5.23 compromised boosting performance and intake pressure. However, increased exhaust exergy in the LHR case, allowed for monotonically increasing turbine useful work and exergy efficiency with engine load. Peak turbine exergy efficiency was 75 %, which was not very different than that of the standard engine. However, turbine exergy efficiencies were very different at medium load (65 – 75 %) which offered the desired intake pressure benefits.

Increased turbine exergy efficiency resulted in increased compressor exergy efficiency as shown in Figure 5.24. Compressor exergy efficiency was always higher than in the standard engine, resulting in elevated intake pressures. In fact it was higher than 78 % for a wide range of loads (64 – 100 %) which ensured excellent boosting performance and high dilution levels.

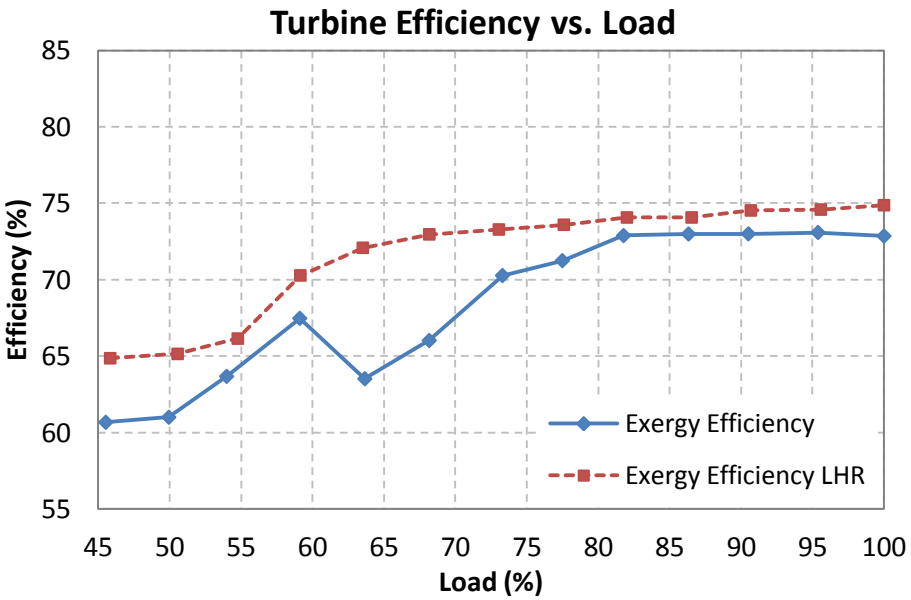

Figure 5.23 – Turbine exergy efficiency for the standard and low heat rejection engines

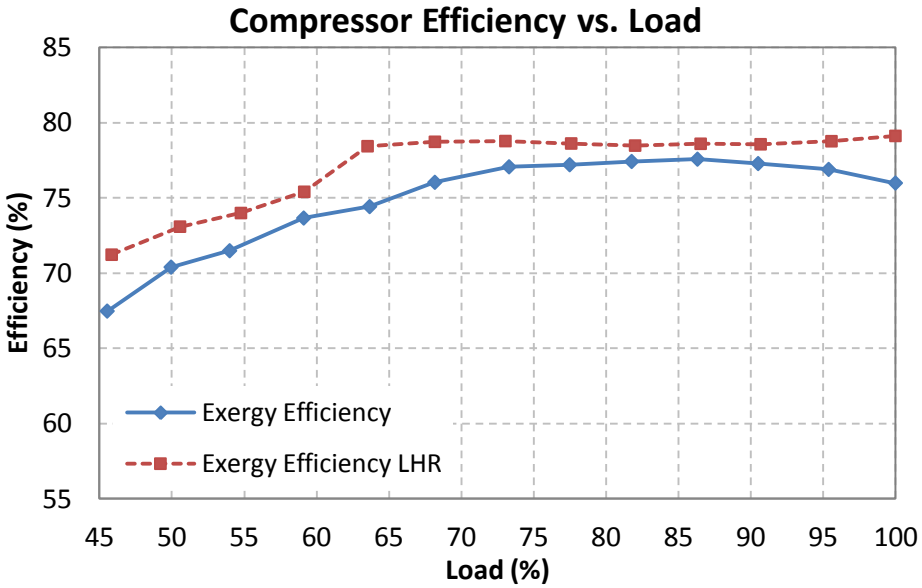

Figure 5.24 – Compressor exergy efficiency for the standard and low heat rejection engines

High intake pressure and dilution levels resulted in high engine exergy efficiency across the load range as shown in Figure 5.25. Exergy efficiency was based on brake work and for the LHR engine it was 6 – 11 % higher than that of the standard engine. Peak exergy efficiency was 39.7 % (corresponding to 42.5 % brake efficiency) and occurred at 90 % load (10 bar NMEP). The reasons behind improved exergy efficiency were increased dilution levels which benefited thermal efficiency, and reduced pumping work through intelligent use of the boosting system. Reduced heat transfer in the cylinder and exhaust manifold raised exhaust gas temperature and thus exhaust flow exergy. Although turbine work was greatly benefited from higher exergy, exhaust gases leaving the turbine had some remaining potential to do work. That potential was accounted for in total exergy efficiency shown in Figure 5.25. Total exergy efficiency was 10 – 16 % higher than the standard engine when low heat rejection was implemented. The decrease shown at 64 % load resulted from NVO to PVO switching which reduced exhaust temperature.

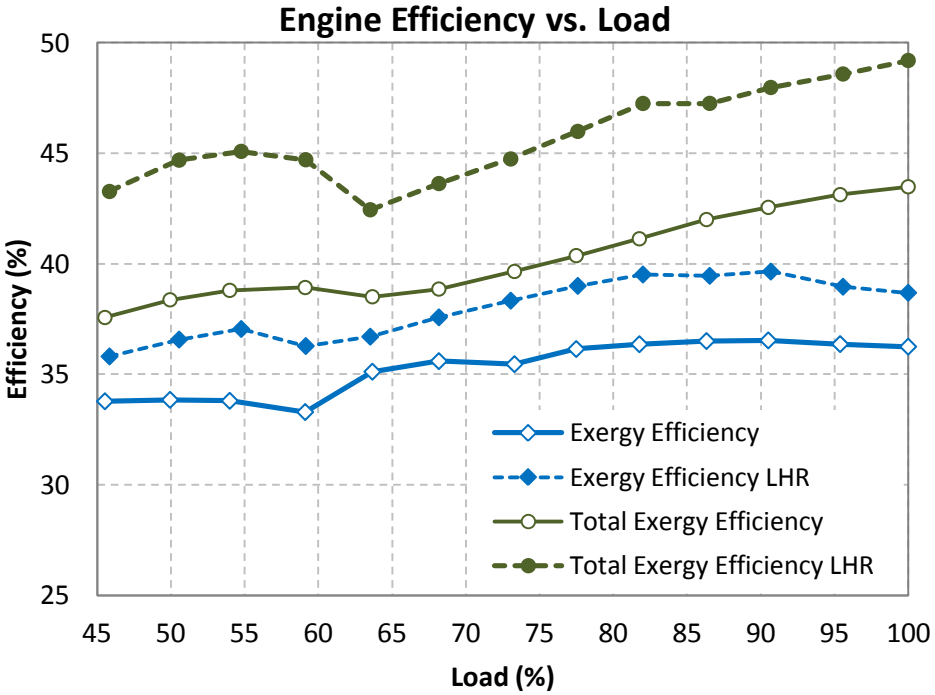

Figure 5.25 – Engine exergy efficiency and total exergy efficiency for the standard and low heat rejection engines

Overall, multi-cylinder simulations of low heat rejection boosted HCCI showed that reduced heat transfer in the cylinder and exhaust manifold can lead to significant efficiency improvements, thus the starting hypothesis was confirmed. LHR resulted in increased exhaust flow exergy which allowed improved boosting performance and intake pressure. Dilution levels increased according to intake pressure and offered thermal efficiency benefits as well as low pressure rise rates during heat release. In addition, excellent boosting performance enabled good control of backpressure through variable geometry thus improving gas exchange efficiency. The combination of these factors resulted in higher engine exergy efficiency and improved control of mixture preparation for HCCI combustion. Low heat rejection simulations demonstrated that boosting efficiency is equally important to cylinder efficiency for HPLB engines, and that in-cylinder phenomena can be manipulated for the benefit of system efficiency.

5.5 Summary

An availability analysis framework was developed and integrated with multi-cylinder engine models for the simulation of high pressure lean burn engines. By utilizing that framework, two different boosted HCCI engines were simulated and analyzed. The engine models featured single-stage and two-stage boosting systems combined with NVO and PVO valve strategies as seen in Chapter 4 as well. Instantaneous and mean exergy variables were calculated in order to quantify exergy transfers and irreversibilities of the engines. Assumptions in the 2^{nd} law analysis framework were associated with the 2-zone nature of the combustion model employed and the adiabatic treatment of turbomachines. Furthermore, fuel was considered to be sulfur-free and non-preheated, and its lower heating value at 25 °C was used for availability calculations.

Results showed that LTC engines suffer from increased cylinder irreversibilities compared to traditional SI or diesel engines, due to lower cylinder temperatures. In fact, it was found that boosted operation may further increase cylinder irreversibilities because it is primarily accomplished by increasing dilution levels as well as charge mass. However, this drawback was greatly offset by benefits in heat transfer, thermal efficiency and gas exchange efficiency. The fraction of fuel exergy destroyed in the cylinder was roughly constant with load, but exergy loss due to heat transfer decreased with load. Boosting performance was dependent on exhaust flow exergy fraction which was considerably increased with load.

Engine exergy efficiency was calculated based on brake work and it was found to increase with load. The two-stage boosted engine with NVO/PVO reached peak exergy efficiency of 36.5 % at 9.5 bar BMEP. By accounting for the potential of exhaust gases to produce useful work, peak exergy efficiency increased to 43.5 %. Use of high-lift valve events was found to lower cylinder temperatures and increase irreversibilities. However,

PVO greatly benefited pumping work which was the dominating factor behind improved exergy efficiency.

Exhaust available power was critical for boosting performance but it was found that the turbine could extract less than 50 % of it at all cases. Low heat rejection simulations were performed in order to investigate the effect of increased exhaust flow exergy on boosted HCCI operation. It was found that LHR was highly beneficial for high load HCCI by improving boosting performance and offering very high dilution levels at low and medium loads. When LHR was implemented, engine exergy efficiency peaked at 39.7 %; by accounting for the potential of exhaust gas to produce useful work, total exergy efficiency peaked at 49.2 %.

System level simulations combined with availability analysis provided a very useful tool for thermodynamic analysis of high pressure lean burn engines. However, it should be noted that availability analysis does not provide new insight into the processes that lead to efficient work production in internal combustion engines. Instead, it provides a different perspective on these processes and highlights the relative importance of availability transfers across the system boundaries. As a result, exergy analysis can be a very useful tool for engineers. By using that framework, the effects of boosting, variable valve actuation, external EGR and compression ratio on high load LTC operation can be explored and quantified. Their synergies can be leveraged in order to achieve optimum combustion, thermal, gas exchange and mechanical efficiencies. The combination of high intake pressure and temperature with high valve lifts was shown to be very beneficial for high load operation both from energy and exergy efficiency standpoints. The combination of these features has the potential to bring HCCI engines very close to currently available downsized boosted DISI engines.

5.6 References

1. Primus, R. J. and Flynn, P. F., "The Assessment of Losses in Diesel Engines using Second Law Analysis," ASME WA Meeting, Anaheim, CA. Proceedings of the AES; 1986, pp. 61-68

2. Farrell, J. T., Stevens, J. G. and Weissman, W., "A Second Law Analysis of High Efficiency Low Emission Gasoline Engine Concepts", SAE Paper 2006-01-0491, 2006

3. Rakopoulos, C. D. and Giakoumis, E. G., "Second-law analyses applied to internal combustion engines operation", *Progress in Energy and Combustion Science*, 32 (2006) 2-47, 2006

4. Jaichandar, S. and Tamilporai, P., "The Status of Experimental Investigations on Low Heat Rejection Engines," SAE Paper 2004-01-1453, 2004

5. Tuner, M. "Studying the Potential Efficiency of Low Heat Rejection HCCI Engines with a Stochastic Reactor Model," SAE Paper, 2009-24-0032, 2004

CHAPTER 6

CONCLUSIONS AND RECOMMENDATIONS

This dissertation presented simulations and detailed thermodynamic analysis of high pressure lean burn engine systems. Simulations focused on multi-cylinder boosted HCCI engines using combustion and heat transfer submodels that were assessed against different sets of experimental data. The models were used to investigate the effects of boosting, variable valve actuation, EGR and compression ratio level on high load HCCI operation. Interactions between engine subsystems and in-cylinder processes were explored and analyzed. Thermodynamic investigation was augmented by 2^{nd} law analysis, and techniques that can bring low temperature combustion engines closer to currently available powertrains were discussed. The major conclusions and recommendations for future work are summarized in the following.

6.1 Synopsis and Conclusions

High load HCCI operation requires the combination of high charge mass for high work production, high dilution levels for control of pressure rise rates, and sufficient temperature for autoignition of the charge. Detailed thermodynamic analysis of boosted HCCI engines confirmed that elevated intake pressure has the potential to enable high load operation and indicated that unconventional techniques may be required to achieve that. Appropriate techniques were identified by system level simulations that featured boosting based on actual turbomachine maps, variable valve actuation and exhaust gas recirculation. It was found that for the same load level, intake pressure boosting acts to

increase dilution levels in the combustion chamber through additional air mass and at the same time accelerates autoignition kinetics. Its effect on HCCI combustion is twofold; increased dilution levels offer lower pressure rise rates during heat release but elevated pressure enhances autoignition in dilute mixtures. Therefore, higher fueling rates can be accommodated without ringing and high load levels can be attained.

In order to perform meaningful multi-cylinder simulations, the combustion and heat transfer submodels were evaluated based on experimental data. Three sets of data were used that originated from three different single cylinder engines; the single-cylinder FFVA and GM boosted HCCI engines present at the University of Michigan, and a single cylinder HCCI engine present at Sandia National Laboratories. The first two datasets represented naturally aspirated and boosted operation with negative valve overlap, while the third one represented boosted operation with positive valve overlap events. All three datasets obtained from single-cylinder engines were used for calibration of single-cylinder engine models.

The combustion model was the critical part in simulating boosted HCCI and it consisted of ignition delay and burn rate correlations. The performance evaluation process revealed that the model was very good at determining burn rates provided that ignition timing was accurately calculated. The latter proved to be problematic at high pressure and low temperature conditions, such as those encountered in the Sandia engine that promoted negative temperature coefficient behavior. However, the combustion event was described well for the FFVA and GM boosted engines and performance variables were accurately calculated. Heat transfer description was originally based on the modified Woschni expression, but it was shown that heat flux was overcalculated. Therefore, the classic Woschni model was used for description of the average heat flux from the working fluid to the cylinder walls. Nevertheless, modeling results indicated the need for a dedicated heat transfer model for high pressure lean burn engines.

Single-cylinder engines are directly related to multi-cylinder ones since they only differ in cylinder charging. Therefore, the UM forward calculation combustion model was used in multi-cylinder simulations in order to explore the synergies between advanced combustion, boosting, VVA, EGR and different compression ratio levels.

The most important contribution of the present research work was the investigation of two-way interactions between combustion and engine subsystems and their quantification on the basis of energy and exergy efficiency. By combining boosting and VVA it was demonstrated that mixture dilution can be improved by using hot intake air to replace residual gas in the cylinder. In engines employing negative valve overlap, operation with hot intake air resulted in reduced NVO levels, thus both thermal and gas exchange efficiencies were improved. Furthermore, it was shown that NVO can be completely eliminated and replaced by PVO when heating from the intake system is sufficient to ensure autoignition of the charge. It was found that high lift valve events improved gas exchange efficiency considerably while reducing cylinder temperatures which were critical for ringing avoidance and high thermal efficiency. However, low load operation necessitated NVO use for adequate charge heating on a cycle basis. Boosting systems that featured two-stage compression and variable geometry were combined with NVO/PVO cam switching. That combination enabled wide range boosted HCCI operation at efficiency levels that matched or exceeded those of diesel engines. By employing hot intake air for mixture preparation it was shown that it is more efficient to heat the charge using the intake system than using residual gas trapping through VVA.

External EGR is considered to be a combustion enabler for HPLB engines but system level simulations showed that it is not necessarily beneficial for engine efficiency. In addition, it was found that using EGR may degrade boosting performance which is absolutely critical for boosted HCCI.

One of the common features of advanced engine concepts that have been shown in the literature is elevated compression ratio compared to SI engines. Boosted HCCI was

simulated at different compression ratios in order to explore the interactions between in-cylinder compression and external compression from the boosting system. It was found that compression from the boosting system can successfully replace in-cylinder compression while maintaining high engine efficiency levels. Therefore, boosted HCCI can potentially operate at compression ratios closer to that of modern DISI engines albeit with certain efficiency penalty. Higher compression ratio was found to be beneficial for high load and thermal efficiency while not hindering boosting performance. The only drawback appeared to be elevated cylinder pressures which might require more robust engine structures.

Thermodynamic investigation of HPLB engines was augmented by 2^{nd} law analysis and provided insight into the exergy destruction and transfer processes. It was found that LTC engines suffer from greater cylinder irreversibilities compared to traditional SI or diesel engines due to low cylinder temperatures and high dilution levels. Further increase in dilution levels with boosting resulted in further increase in cylinder irreversibilities; however, improvements in thermal and gas exchange efficiencies greatly offset that drawback. Combining boosting and high lift valve events mitigated exergy losses due to heat transfer and fluid flow losses. Exhaust flow exergy was identified as a critical factor for HPLB operation due to its direct effect on boosting performance. Therefore, low heat rejection was investigated as a technique that can offer exhaust flow exergy and boosting performance benefits. It was shown that LHR allowed increased intake pressure and dilution levels which improved thermal efficiency and lowered pressure rise rates during heat release. Engine exergy efficiency was significantly improved across the load range and intake temperature requirements of HCCI were easier to meet.

Overall, simulation and thermodynamic analysis of boosted HCCI engines showed that wide load range and high efficiency can be achieved by employing currently available hardware and combining them in an unconventional manner. Combining

boosting and high lift valve events has the potential to bring HPLB engines closer to currently available powertrains and offer efficiency levels that match or exceed those of diesel engines.

6.2 Suggestions for Future Work

Research work presented in this dissertation aimed at performing a detailed thermodynamic analysis of high pressure lean burn engines. In addition, it aimed at providing insight into the interactions of the combustion event with key engine subsystems and settings. The current engine model and availability analysis framework is a collection of submodels which can be further improved and modified in order to perform different simulations. As such, there is room for improvement in the following three areas:

- Description of the autoignition process in the combustion model. High pressure lean combustion in gasoline engines promotes negative temperature coefficient behavior before combustion starts, as seen from the Sandia experiments. Therefore, it is critical that NTC behavior be captured by the ignition delay correlation, which is currently not the case. Accurate ignition calculation will facilitate accurate burn rate calculations from the combustion model. This way, the forward calculation model will be made more robust thus allowing exploration of wider operating regimes.
- Description of stratification effects on burn duration. The forward calculation burn model used in this dissertation is a single zone model which was based on detailed CFD simulations. However, it lacks explicit description of thermal or compositional stratification of the charge. Both of these factors can affect the rate of heat release; therefore, they are considered to be crucial for

determining HCCI burn duration and would add robustness to the forward calculation model.

- Heat transfer description in HPLB engines. The model performance evaluation process revealed that the major discrepancies between experiments and simulations occurred in the closed part of the cycle. That was an indication that heat transfer may not have been accurately described by the submodel employed. The existence of thick boundary layers in HCCI engines may alter the heat transfer phenomena described by currently available correlations. In addition, boosting and unconventional valve events may introduce Reynolds number discrepancies compared to SI or diesel engines. Therefore, development of a dedicated heat transfer model may prove highly beneficial for accurate HPLB engine simulations.

The current engine model and 2nd law analysis framework can be used for exploration and thermodynamic assessment of novel technologies and combustion modes, provided that the appropriate submodels exist. For instance, a combustion model that can describe spark assisted compression ignition combustion can be implemented and used in the same way as the HCCI forward calculation model was used. Such a modeling tool would allow simulation of multi-cylinder multi-mode engines that can capture advanced combustion regimes ranging from very lean HCCI to stoichiometric SI. Furthermore, the transient nature of the cycle simulation software paves the way for transient HCCI studies provided the appropriate combustion models are implemented. Transient simulation could describe behavior related to SI/HCCI mode switching, spark assist, NVO/PVO cam switching and transient behavior of advanced boosting systems.

Overall, the cycle simulation and 2nd law analysis framework provides a useful tool for thermodynamic analysis of HPLB engines, and investigation of the techniques and technologies that will bring such engines closer to production.